

Contents

Preface.....	viii
Introduction	viii
Learning objectives:.....	ix
Positioning	ix
1 Hydrography.....	1
1.1 Physical Oceanography	1
1.1.1 The Atmosphere.....	2
1.1.2 The Air/Sea Interface.....	3
1.1.3 The Water Column	3
1.1.4 Physical Properties of Sea Water	5
1.1.5 Temperature – Salinity Relationship	14
1.1.6 Acoustic Ambient Noise.....	17
1.1.7 Freezing and Sea Ice	17
1.1.8 Coefficient of Thermal Expansion	17
1.1.9 Dynamical Processes, Surface Gravity Wind Waves.....	18
1.2 The Ocean.....	19
1.2.1 The Ekman Spiral.....	20
1.2.2 Seabed Effects.....	21
1.2.3 Upwelling	21
1.2.4 Typical Patterns of Ocean Circulation	22
2 Sound Theory	26
2.1 Sound Velocity	26
2.2 Pulse Length.....	27
2.3 Intensity and Power	27
2.4 The Decibel and Absolute Reference Level	28
2.5 Multiple Paths.....	28
2.6 Typical Vertical Profiles of Sound Velocity and Corresponding Conditions of Sound Propagation.....	29
2.6.1 Underwater Sound Channel (USC).....	30
2.6.2 Surface Sound Channel	33
2.6.3 Antiwaveguide Propagation.....	34
2.7 Deformation of underwater acoustic signals – Doppler Effect	35
2.8 Underwater Acoustic Noise	36
2.9 Propagation Losses	37

2.9.1	Geometrical Spreading Losses	37
2.9.2	Attenuation Losses	38
2.10	Acoustic Scattering.....	40
2.10.1	Echo from a target.....	41
2.10.2	Target Strength	41
2.10.3	Directivity Index (DI).....	42
2.10.4	Detection Threshold (DT).....	43
2.11	Sonar Equation.....	43
2.12	Basic Sonar Principles.....	44
2.12.1	Beamforming.....	46
2.12.2	Sonar resolution	47
3	Applications of Underwater Acoustics.....	48
3.1	Single-Beam Echo Sounder.....	48
3.1.1	Transducer Placement.....	49
3.1.2	Receiver	50
3.1.3	Echogram Interpretation	50
3.1.4	Typical Echoes	54
3.2	Multi-Beam Echo Sounder.....	54
3.3	Sonar	56
3.3.1	Detection Limits	57
3.4	Side-Scan Sonar.....	57
3.4.1	Reception Processing.....	59
3.4.2	Echo Construction	60
3.4.3	Side scan sonar resolution	60
3.5	Sub-Bottom Profiler	61
3.5.1	SBP Systems	62
3.5.2	Theory of Operation	63
3.6	Doppler Velocity Log & Acoustic Doppler Current Profiler	66
4	Underwater Navigation.....	69
4.1	Inertial/Dead Reckoning Techniques	70
4.1.1	State estimators – Observers.....	71
4.2	Short Baseline (SBL) Positioning	73
4.2.1	SBL with beacon/pinger	75
4.2.2	SBL with transponder/responder	76
4.2.3	Corrections to apparent positon	77
4.3	Ultra-Short Baseline (USBL)	77

TMR4120 Underwater Engineering

4.3.1	Propagated uncertainty estimation for USBL positioning	79
4.4	Long Baseline (LBL).....	80
4.4.1	Installation of LBL	82
4.5	Depth measurement	82
4.6	Other positioning components.....	83
4.6.1	Surface Positioning – GPS and dGPS	83
4.6.2	Heading measurement	84
4.6.3	Inertial measurement unit (IMU).....	84
5	Underwater Vehicle Design.....	85
5.1	Remotely Operated Vehicles (ROVs).....	85
5.2	Autonomous Underwater Vehicles (AUVs)	86
5.3	Typical Tasks for Underwater Vehicles.....	87
5.3.1	Site Survey.....	87
5.3.2	Drilling Assistance.....	87
5.3.3	Installation Assistance	88
5.3.4	Operation Assistance.....	88
5.3.5	Inspection	89
5.3.6	Maintenance and Repair.....	89
5.4	Operation of Underwater Vehicles	90
5.4.1	ROV Launch and Recovery Systems (LARS).....	90
5.4.2	Umbilical and TMS.....	90
5.4.3	Cable Handling	91
5.5	Components of underwater vehicles.....	91
5.5.1	Frame.....	91
5.5.2	Buoyancy.....	92
5.5.3	Electronics Cylinders.....	92
5.5.4	Connectors.....	92
5.5.5	Primary Subsystems	92
5.5.6	Hydraulics	93
5.6	Vehicle Buoyancy and Stability	93
5.6.1	Hydrostatic Equilibrium	94
5.6.2	Transverse Stability	95
5.6.3	Buoyancy.....	96
5.7	Power Systems.....	96
5.7.1	Electrical Systems.....	96
5.7.2	Hydraulic systems.....	99

5.8	Design theory.....	100
5.8.1	Traditional Design Process	100
5.8.2	Axiomatic Design.....	103
6	Hydrodynamics of underwater vehicles	106
6.1	Vehicle dynamics	106
6.1.1	Kinematics.....	106
6.1.2	Kinetics.....	108
6.1.3	Motion equation for a submarine	110
6.1.4	Hydro dynamics for AUV's	113
6.1.5	Hydro dynamics for ROV's	114
6.2	Drag Forces.....	116
6.2.1	Skin Friction Drag	117
6.2.2	Pressure Drag.....	118
6.3	Thrusters.....	119
6.3.1	ROV Thrusters	119
6.3.2	Cable Drag.....	122
6.4	AUV Thrusters.....	123
6.5	Experimental Testing of Hydrodynamics for ROV.....	125
6.5.1	Longitudinal C_d -coefficient.....	127
6.5.2	Polar Diagram of Drag Resistance and C_d -coefficient.....	128
6.5.3	Open Water Test of ROV Thruster	132
6.5.4	Summary of Hydrodynamic Experiments	134
7	Seabed Mapping Equipment.....	137
7.1	Multi-Beam Echo Sounder.....	137
7.1.1	Application	137
7.1.2	System	138
7.1.3	Calibration of Swath Sounders using the Patch Test.....	139
7.1.4	Practical Considerations	144
7.1.5	Data Processing	147
7.2	Side Scan Sonar	148
7.2.1	Installation	148
7.2.2	Data Processing	151
7.2.3	Applications.....	154
7.2.4	Installation	154
7.2.5	Signal Processing and Presentation.....	156
7.3	Error Sources and Budgets	162

TMR4120 Underwater Engineering

7.3.1	Horizontal Mapping Accuracy	162
7.3.2	Sounding Related Uncertainties.....	166
7.3.3	Other Error Sources	167
7.4	DTM Horizontal Error Budget	167
8	The Underwater Imaging Process.....	168
8.1	Image Modeling	170
8.1.1	Direct and Forward-Scattered Component	171
8.1.2	The Backscatter Component.....	173
8.2	Sensor Suite	174
8.2.1	Cameras	174
8.2.2	Light.....	175
8.2.3	Scaling Devices	177
8.2.4	Recorders.....	177
8.3	Processing.....	178
8.3.1	Processing and Interpretation.....	178
8.3.2	Online	178
8.3.3	Offline.....	178
8.3.4	Data Interpretation	179
8.3.5	Data Products.....	179
8.4	Photo Mosaic	179
8.4.1	Image Capture.....	180
8.4.2	Illumination.....	180
8.4.3	Photo Mosaic Construction.....	180
8.5	Photogrammetry.....	181
8.5.1	The Photogrammetry Process.....	182
8.6	Underwater Hyperspectral Imaging (UHI).....	183
8.6.1	Benefits and resolutions of UHI	184
8.6.2	Spatial Resolution.....	184
8.6.3	Spectral Resolution.....	184
8.6.4	Radiometric Resolution	185
8.6.5	Temporal Resolution	185
8.6.6	UHI on Different Underwater Platforms.....	185
1	Bibliography	189
1	Bibliography	190
1	Bibliography	191
1	Bibliography	191

TMR4120 Underwater Engineering

9 References.....	192
-------------------	-----

Preface

These lecture note are based on lecture notes for the course TMR4120 "Underwater Engineering, Basic Course" taught at the Department of Marine Technology at NTNU in Trondheim, Norway. The MSc-students Tharindu Dilshana Hewage, Kristine Klingan and Erik Bjørklund Holven have developed large parts of these lecture notes.

The presented text is a first edition and can be considered a draft. All feedback on content, organisation, grammatics and spelling is appreciated.

This lecture note has been prepared for the course TMR4120 "Underwater Engineering, Basic Course" taught at the Department of Marine Technology at NTNU in Trondheim, Norway.

This lecture note is based on existing literature. The following list presents the literature each of the sections in this lecture note is based on:

- Section 1:

Hovem, J. M. (2012). *Marine acoustics: the physics of sound in underwater environments*. Los Altos Hills, Calif.: Peninsula Publishing.

Kommentert [EH1]: Skal nye kilder listes her?

- Sections 1.4, 2, 4 – 7, 10.2 and 10.4.2:

Lurton, X. (2002). *An introduction to underwater acoustics: principles and applications*. London: Springer.

- Section 3:

Brechovskich, L. M., & Lysanov, J. (2003). *Fundamentals of ocean acoustics*. New York: AIP Press.

- Sections 8 and 9, 10.1 and 10.3:

Diner, N., Mr. . *Theory of Fish Detection*. Fishing Vessel Technology - 20th Graduate School Module 2 - Fishing Gear and Other Equipment. French Research Institute for Exploitation of the Sea.

- Section 10.4:

Mazel, C. (1985). *Side Scan Sonar: Record Interpretation ; Training Manual*: Klein Associates Inc.

- Section 10.5:

University of Southampton. (2011). Marine Seismic Reflection. Retrieved 01.07. 2015, from <http://www.soes.soton.ac.uk/research/groups/3dchirp/background.htm>

Introduction

This lecture note has been prepared for the course TMR4120 "Underwater Engineering, Basic Course" taught at the Department of Marine Technology at NTNU in Trondheim, Norway.

Learning objectives:

Understand the processes in the ocean and how they are important input to our engineering design work.

This lecture note is based on existing literature. The following list presents the literature each of the sections in this lecture note is based on:

- Section 1.1:

Allmendinger, E. E. (1990). Submersible vehicle systems design. Jersey City, N.J., Society of Naval Architects and Marine Engineers.

- Section 1.1.4.4:

Valiron, F. (2001). Descriptive Physical Oceanography, Taylor & Francis.

- Section 1.2:

Karlsen, L., et al. (2001). Fiskeriteknologi. [Oslo], Landbruksforl.

Positioning

This lecture note has been prepared for the course TMR4120 "Underwater Engineering, Basic Course" taught at the Department of Marine Technology at NTNU in Trondheim, Norway.

This lecture note is based on existing literature. The following list presents the literature each of the sections in this lecture note is based on:

- Section 2:

Paull, L., Saeedi, S., Seto, M., & Li, H. (2014). AUV Navigation and Localization: A Review. *Oceanic Engineering, IEEE Journal of*, 39(1), 131-149. doi: 10.1109/JOE.2013.2278891

- Sections 3 and 4:

Milne, P. H. (1983). Underwater acoustic positioning systems. London: Spon.

- Sections 4.1 and 4.2:

Ludvigsen, M. (2010). An ROV toolbox for optical and acoustical seabed investigations (Vol. 2010:74). Trondheim: Norges teknisk-naturvitenskapelige universitet.

- Section 5:

Lekkerkerk, H.-J., van der Velden, R., Haycock, T., & Jansen, P. (2006). Handbook of offshore surveying : Vol. 1 : Preparation & positioning. London: Clarkson Research Services Limited.

Martin Ludvigsen
August 2017

1 Hydrography

1.1 Physical Oceanography

The marine environment consists not only of the water column, but also the atmosphere above the water's surface and the seafloor and sub-seafloor (sediments and rocks). A comprehensive study of the marine environment is enormous in scope and thus is often subdivided into its disciplinary components – biological, chemical, geological and physical oceanography, metrology and geophysics. This chapter will focus on those features of the marine environment that are of particular interest to designers and operators of submersibles.

Every aspect of submersible design is influenced to varying degrees by one or more environmental factors. These factors comprise one of the several groups of so-called external design constraints – that is, constraints that are independent of or external to the mission on which the design is based. For example, temperature, salinity, pressure, and density gradients in the water column are encountered by all submersibles as they move through the water column irrespective of their individual missions. These external constraints may be subdivided into those that are fixed by mission requirements and those that are variable. An example of the former is the mission requirement of a maximum operating depth that fixes the pressure on which the design is based. But the same mission requirements for maximum operating depth and locations of operating areas do not fix specific values of temperature, salinity, and density of the seawater that will be encountered. In the latter example, the mission requirements indicate only ranges of these parameters that the submersible must be designed to accommodate.

It is convenient to view the marine environment from the perspective of its vertical profile, which is composed of three basic regimes: atmosphere, water column, and sub-seafloor. Of course, the characteristics of the water column are of primary interest in submersible design, but not to the exclusion of the other two environments and the interfaces between them. Figure 1 summarizes the various factors influencing submersible design and operations.

The following brief overview is intended to introduce the submersible designer to the elements of the marine environment that are most influential on submersible design. This overview starts at the top and works downward through the water column to the sub-seafloor.

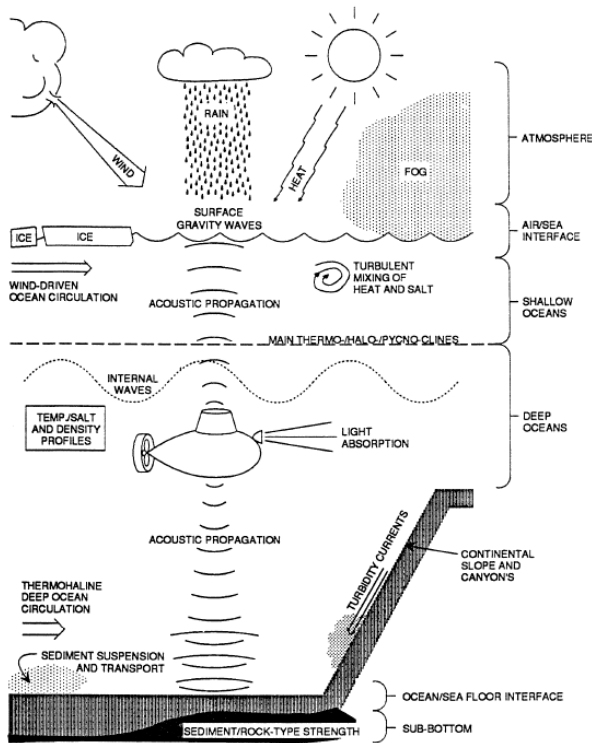


Figure 1: Important factors regarding submersible design and operations ()�.

1.1.1 The Atmosphere

The atmosphere, much like the water below it, is a fluid in constant motion. Many of the same dynamical principles control the ways in which both fluids move, despite the large density differences between the two. The interface between the atmosphere and ocean is characterized by a continual exchange of energy between the atmosphere and the upper portion of the water column. Of particular interest are the exchanges of thermal energy (heat) which influence sea and atmospheric temperature, and the kinetic energy associated with winds which are responsible for the generation of surface waves and currents.

Certain atmospheric factors such as wind, fog, rain, and icing at higher latitudes affect submersible operations on the sea surface. These factors influence design considerations related to retrieval and become more critical in abnormal conditions where considerable time may elapse between the time a submersible surfaces and the time it is picked up. Heeling moments due to wind place constraints on the design of the extent and distribution of the submersible's lateral area above the water line as well as provide adequate dynamic stability to limit heel angles. Fog and rain, or adverse weather in general, reduce or obliterate visual communications, stressing the need for other, highly reliable means of contacting the support ship. The possibility of icing and its effects on stability must concern the submersible designer.

1.1.2 The Air/Sea Interface

The interface between the atmosphere and ocean can be open water, partial ice cover, or solid ice cover. The air/open water interface is the interface of primary interest for underwater system design and is the one discussed here. Partial and solid ice cover interfaces will require very specific operational set ups to ensure safe navigation, launch and recovery.

Surface waves are one of the primary concerns in subsea design. The sea-state limitations imposed by surface waves play a major role in establishing the cost-effectiveness of the mission system, that is, the percentage of at-sea time a underwater vehicle can be used. Surface waves must be considered in connection with dynamic stability requirements to limit the angle of heel due to wave action and on freeboard requirements to protect the access hatch from waves and to facilitate retrieval procedures. Surface waves produce direct wave-slap forces on the submersible that need to be considered, and create splash-zone corrosion considerations if the vehicle is not hosed down between dives.

The magnitude of expected surface currents affects the manoeuvring requirements of a submersible design. The problem may not be severe if the support vessel is also being affected by the same uniform surface currents. In addition, currents can affect the submersible during the descent or ascent so it may not arrive precisely at the dive target or support ship and thus may have to spend valuable time positioning itself.

1.1.3 The Water Column

For the purpose of discussion, the water column is subdivided into zones or layers, and each of the following environmental factors is discussed in terms of its principal effect on submersible design.

1.1.3.1 *Surface Gravity Waves - Shallow and Deep Layers*

Although surface gravity waves are most apparent at the air/water interface, their effects can extend to great depths in the ocean. The amplitude of surface waves and their associated currents are attenuated so that their effects become negligible (less than 5 percent) by a depth $L/2$ where L is the wavelength. For typical wind waves (period of 20 s) in deep water this depth is about 300 m and almost never exceeds 1000 m. Consequently, the underwater vehicles experiences forces in the shallow-depth layer (several hundred meters) due to surface wave action. This motion may be severe enough to exert considerable influence on the design of the launch and recovery system, including that portion on the submersible, and put limits on the sea states in which safe operations can be considered.

Tides and tsunamis are other surface waves which have such long wavelengths (long periods) that their amplitudes are not attenuated appreciably with depth even in the deepest oceans. However, because their periods are so much longer (minutes to a day) than typical wind waves, the water velocities associated with them are generally small. An important exception to this case occurs in coastal regions where tidal currents can be significant.

1.1.3.2 *Internal Gravity Waves - Shallow and Deep Layers*

The vertical density gradients found in the ocean allow for another class of waves: internal gravity waves whose maximum velocities are found at the depths of the maximum density gradients. The

vertical excursions associated with these waves can be very large (10's of meters) with periods of minutes to an hour.

1.1.3.3 Wave Generation Drag - Surface and Deep Layers

The low air/water density ratio permits surface gravity waves to be generated at the interface by a underwater vehicle moving near the surface. Internal gravity waves are also generated by underwater vehicles moving along strong density gradients in the water column. The term "dead water" is used in association with such gradients found in or near fjords or estuaries.

The generation of any of these waves creates a wave-making resistance and increases the energy required to move the underwater vehicle. This resistance tends to be greatest where the density gradient is largest, but the amount of energy used in making waves is dependent on the geometry and design speed of the vehicle. For example, vehicles with missions requiring high speeds in the shallow ocean (where density gradients are large) should have geometries that minimize wave-making resistance. Conversely, vehicles with tasks requiring high speeds in the deep ocean (where density gradients are small and wave making is less significant) should have geometries which minimize frictional and form resistances. The vehicle geometries in these two cases are considerably different.

1.1.3.4 Temperature, Salinity, Pressure and Density (Specific Weight) of Seawater – Upper and Lower Layers

Seawater temperature, salinity, and density vary substantially in the upper layer of the water column, which extends down to about 1000 m. These variations, in general, are due to the influences of heat exchange and precipitation/evaporation across the air/sea interface at a particular latitude and season. In the lower layer, below 1000 m, these characteristics tend to be relatively constant. The upper layer may be subdivided further into regions of seasonal and main thermoclines (haloclines) - where temperature (salinity) gradients are largest-extending, respectively, from the surface to about 60 m and from this depth to about 1000 m.

Density or specific weight of seawater is a function of temperature, salinity, and pressure. Consequently, this property will vary nonlinearly in the upper layer of temperature and salinity variations down to about 1000 m. In the lower layer, it may be approximated as a linear or exponential function of depth.

Hydrostatic pressure in the water column is the integral of the density times gravity from the surface down to the depth of interest (that is, the weight of the water above). Therefore, the in situ pressure includes the effects of temperature, salinity, and seawater compressibility, and varies nearly linearly with depth. A unit volume of seawater moved from the surface to a depth of 9000 m is compressed by about 4 percent.

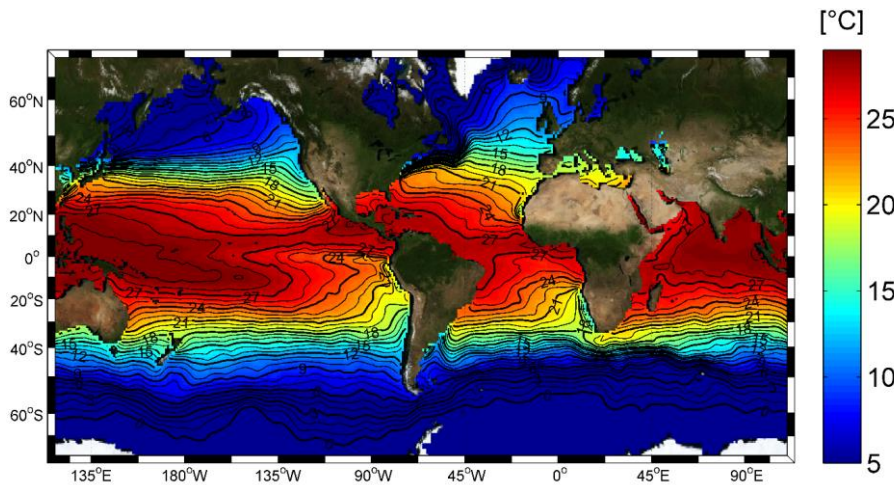


Figure 2: Annual mean of the sea surface temperature (World Ocean Atlas, 2005).

These environmental factors, individually and collectively, influence most aspects of underwater vehicle design and operation - including shell structure strength, corrosion considerations, acoustical systems, electric/mechanical systems exposed to sea water, and buoyancy control systems.

1.1.4 Physical Properties of Sea Water

Seawater can be characterized by its temperature, salinity (the dissolved solids), and pressure. From these three quantities and the equation of the state of seawater, the ocean scientist or engineer can calculate other desired quantities, such as the density, sound velocity, heat capacity, or electrical conductivity.

1.1.4.1 Temperature

The temperature, T , of a water parcel is expressed in degrees Celsius ($^{\circ}\text{C}$) and gives an indication of the energy or work that has been done on or associated with that water parcel. Temperature is now being easily and accurately measured by electronic thermometers employing thermistors or platinum resistance probes as the sensing elements. These sensors are capable of resolving micro degree temperature fluctuations, and are stable to mill degrees over a period of months.

Oceanographic temperature tends to vary systematically with depth and latitude. The surface water is warmer at low latitudes (maximums of 25 to 30°C). Where there is an excess of incoming solar radiation which heats the surface water. Surface water is cooler at the poles (minimums equal to the freezing point of saltwater-about -2°C), where energy is lost to the atmosphere by radiation. The distribution of temperature with latitude is not smooth, due to the general oceanographic circulation patterns, and will vary with seasons. Figure 2 shows typical summer sea surface temperatures.

Figure 3 shows typical vertical distributions of oceanic temperature. There is a relatively shallow region of uniform temperature (from 0 to 10's of meters thick) associated with the mixed layer at the surface (caused by surface wave mixing). Below this, the temperature decreases sharply in a seasonal thermocline (found largely at mid-latitudes), which varies in depth and intensity. It can disappear entirely during the winter, because its strength depends on the weather during the past year. The vertical gradients in the seasonal thermocline are about $0.05^{\circ}\text{C}/\text{m}$ below the seasonal thermocline (which is generally confined to the upper 100 m), there is the main (or permanent) thermocline which is found between 100 and 1000 m and is maintained by the general oceanographic circulation and mixing. The temperature gradient here ($0.02^{\circ}\text{C}/\text{m}$) is less than in the seasonal thermocline.

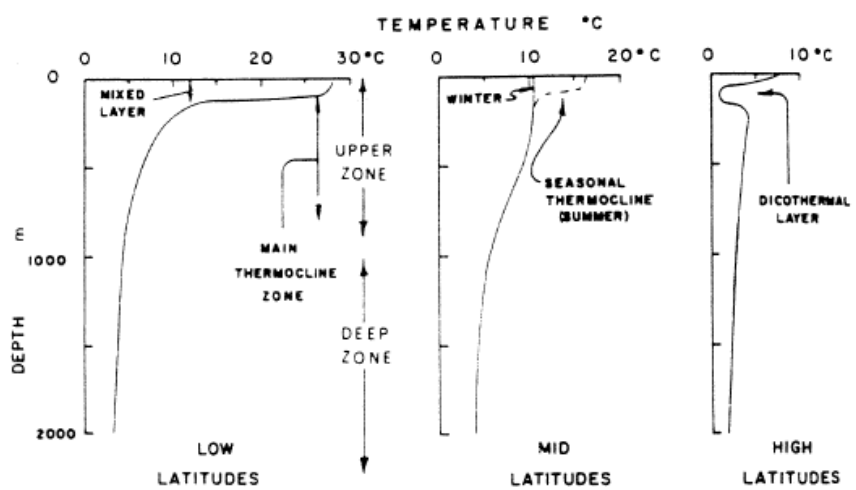


Figure 3: Typical vertical distribution of oceanic temperatures () .

Water is slightly compressible, so that the volume of a parcel of water moved from the surface to the ocean floor (5000 m depth), where the pressure is over 7000 psi (almost 500 times atmospheric pressure), will decrease by about 2 percent. If this compression is done adiabatically (without loss or gain of heat), the work done by the pressure moving the water molecules closer together will raise the temperature of the water parcel at a rate of about $1.4 \times 10^{-4} ^{\circ}\text{C}/\text{m}$. For example, if a parcel of seawater at $5.000^{\circ}\text{C}/\text{m}$ at a 4000 m depth were raised adiabatically to the surface, the temperature would decrease to 4.574°C . Conversely, if a parcel with temperature of 5.000°C at the surface were moved to a 4000 m depth, the temperature would increase to 5.438°C . In the North Pacific, the temperature below 3500 m increases with depth at a rate which is about the adiabatic gradient ($1.5 \times 10^{-4} ^{\circ}\text{C}/\text{m}$), indicating that the water is very well mixed, but the compressibility effects seemingly cause the temperature to increase with depth.

To compare the temperature of two parcels of water, the oceanographer refers to the potential temperature, or θ , which is the in situ temperature, T (the temperature of the parcel at its site in the ocean as measured by a thermometer), which has been corrected for these compressibility effects. Generally, temperatures are corrected to the surface or zero relative pressure, but to compare two parcels at great depth, it is sometimes more accurate to correct to a common or a standard non-zero

pressure surface. This is because our knowledge and estimation of the compressibility effects is not perfect, and the results are sometimes better if only small corrections were made to each observation, rather than comparing two numbers after subtracting large corrections. (Note that oceanographers refer to zero pressure as the pressure at the ocean surface, which is really one atmosphere absolute pressure, or about 1.00 ATA.)

1.1.4.2 Salinity

The salinity of seawater, S , is the total amount of dissolved material or "salt" in the water. It is the total weight of solid material (in grams) found in 1 kilogram of seawater when all the carbonate has been converted to oxide, the bromide and iodine replaced by chlorine, and all organic matter completely oxidized.

Table 1: Composition of seawater-concentration of constituents in seawater having chlorinity of 19% (Diner).

	g/kg	g/unit of chlorinity
Chloride, Cl^-	18.890	0.99894
Sodium, Na^+	10.560	0.5556
Magnesium, Mg^{++}	1.273	0.06695
Sulphate, $(\text{SO}_4)^{--}$	2.649	0.1394
Calcium, Ca^{++}	0.4104	0.02106
Potassium, K^+	0.380 mg/kg	0.02000
Carbon, as $(\text{HCO}_3)^-$ or $(\text{CO}_3)^{--}$	28	0.00735
Bromide, Br^-	65.9	0.00340
Strontium, Sr^{++}	8.1	0.00070
Boron, as H_3BO_3	4.6	0.00137
Silicon, as silicate	0.01–4.5	—
Fluoride, F^-	1.4	0.00007
Nitrogen, as $(\text{NO}_3)^-$	0.01–0.80	—
Aluminum, Al^{+3}	0.5	—
Rubidium, Rb^+	0.2	—
Lithium, Li^+	0.1	—
Phosphorus, as $(\text{PO}_4)^{-3}$	0.001–0.1	—

The salinity is usually expressed in grams of solids per kilogram of seawater or parts per thousand, which is abbreviated ‰ . The composition of the various constituents of sea water are summarized in Table 1.

(Note that sodium and chlorine make up more than 85 percent of the dissolved solids.) The concentrations of the dissolved elements are surprisingly constant, except in coastal regions where there is appreciable input of fresh water or in regions containing an odd mixture of elements, such as near hydrothermal vents in the seafloor. Therefore, there is an implicit assumption that the ionic composition of the ocean is fairly constant, as given by Table 1.

Historically, the salinity was determined by the chemical titration of a sample collected in a bottle lowered on a wire from the ship. This titration determined the chlorinity of sea water, which could be directly related to salinity by:

$$\text{salinity} = 1.80655 \times \text{chlorinity} \quad (1)$$

Presently, instead of directly measuring salinity, we use various sensors to measure the electrical conductivity of seawater and then calculate the salinity from the equation of state. The electrical conductivity of seawater is about 4 siemens/meter or S/m, where a siemen is inverse ohms or the S⁻¹ unit of conductivity. The equation of state of sea water used to calculate salinity lead to the adoption of the Practical Salinity Scale of 1978 (PSS-78). For details, see (Allmendinger, 1990).

< Insert relation between conductivity and salinity >

The surface distribution of salinity is less zonal and shows less variation than the temperature distribution. The amount of salt is largely controlled by evaporation and precipitation in open ocean regions, fresh river runoff in coastal zones, and ice formation and melting in polar regions (both sea ice and glaciers). The lowest salinities (0 to 30 ‰) are found in estuaries and polar regions. Coastal salinities are typically higher than estuaries (30 to 34 ‰), but less than open ocean salinities (33 to 37 ‰). The average oceanic salinity is 34.7 ‰. Semi-closed evaporation basins such as the Mediterranean and the Red Sea exhibit such high salinities as 39 and 41 ‰. The outflow of the salty Mediterranean waters into the North Atlantic makes the Atlantic slightly saltier than the Pacific. The highest open ocean salinities are found in the centre of the oceanic gyres (see the section on wind driven circulation), and there is a relative low salinity band along the equator due to excess rainfall. Figure 4 shows sea surface salinities for the northern hemisphere during the summer.

The salinities also vary vertically, as shown in Figure 5. As with temperature, there is a surface mixed layer with relatively low salinity gradients. Below this there is a strong halocline where the salinities decrease and have a destabilizing influence. The depth of the halocline roughly agrees with the depth of the thermocline. There tends to be a salinity minimum around 800 to 1000 m at mid latitudes. At low latitudes there tends to be a high surface salinity, and low surface salinities are found at high latitudes.

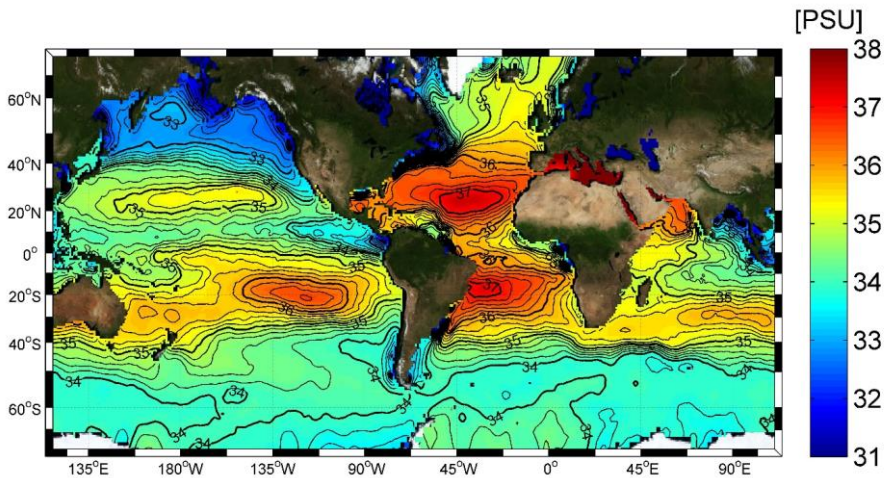


Figure 4: Annual mean of the sea surface salinity distribution (World Ocean Atlas, 2005).

1.1.4.3 Density

The most important dynamic property of sea water is its density, ρ . This is sometimes expressed as the specific volume (the inverse of density), $\alpha = 1/\rho$. Density is generally calculated from the equation of state of sea water, which is expressed as a function of temperature, T, salinity, S, and pressure, P. (Oceanographers often use the decibar as a pressure unit since 1 decibar is nearly equal to the pressure due to 1 m of sea water. Note 1 decibar = 10^4 pascals. SI unit of pressure.) Typical values of surface oceanic density vary from 1020 to 1030 kg/m³. Oceanographers tend to get tired of writing the 1000 every time, so have expressed density more conveniently in terms of the *in situ* density anomaly, σ_{STP} , which is defined as:

$$\sigma_{\text{STP}} = \rho - 1000 \quad (2)$$

The currently accepted reference for calculations of seawater properties is the 1980 equation of state of sea water (EOS-80) as given by (Allmendinger, 1990).

As with temperature, pressure effects on density are important since the volume of a parcel of water decreases as the depth or pressure increases. Hence a parcel with a density anomaly of 28.106 kg/m³ at the surface will have a density anomaly of 46.644 kg/m³ at 4000 m. As can be seen by this example, the pressure effect can be significant and especially in the deep ocean can obscure the effects of temperature and salinity variability. To compare the density of two water parcels, oceanographers have defined two further quantities. Sigma-t, σ_t , is defined as the density anomaly with the *in situ* salinity and temperature, but zero relative pressure. This removes the largest effect of the pressure on the volume, but does not consider the change in temperature. Sigma-θ, σ_θ , is the density anomaly with the *in situ* salinity, the potential temperature, and zero pressure. Thus we have a quantity which is defined in terms of the intrinsic properties of water properties at zero pressure or at the surface where the water probably acquired these characteristics. The external influence of

pressure on the volume and temperature of the water has been removed, and the density of two parcels of water can now be truly compared.

An important feature of the ocean is its vertical density gradient or stratification. Normally, density increases with depth because there is the tendency for heavier parcels to sink below lighter parcels. When a parcel is displaced from its equilibrium position, there is a restoring force (due to the density difference and gravity) that tends to return the parcel to its equilibrium position. The strength of this restoring force is related to the vertical potential density gradient, (Note that this restoring force gives rise to a class of oscillations called internal waves which are discussed further below.) Oceanographers express the strength of this restoring force as the Brunt-Vaisala frequency, or natural frequency of oscillation (units are rad/s):

$$N(z) = \sqrt{\frac{g}{\rho} \frac{\partial \sigma_0}{\partial z}} \quad (3)$$

It is the slope of the vertical density profile corrected for the effects of compressibility. If N is positive, heavier water is on the bottom and the water column is stable. If N is zero, the water is of neutral stability; it is an indication of well-mixed water. If N is imaginary, then there is heavier water sitting on top of lighter water, or the stratification is unstable, and one would expect vertical water motion. Therefore, one can express the vertical profile of density by either density as a function of the depth, or by the Brunt-Vaisala frequency, N, as a function of the depth.

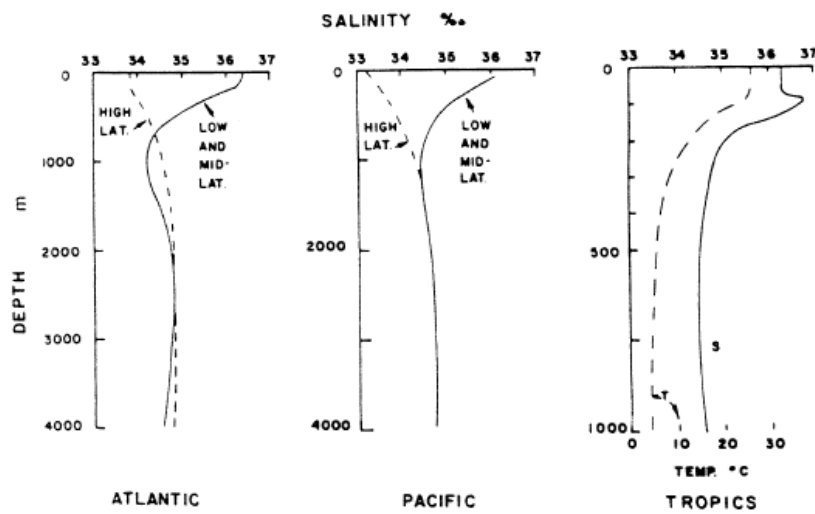


Figure 5: Vertical variation of oceanic salinities (Allmendinger, 1990).

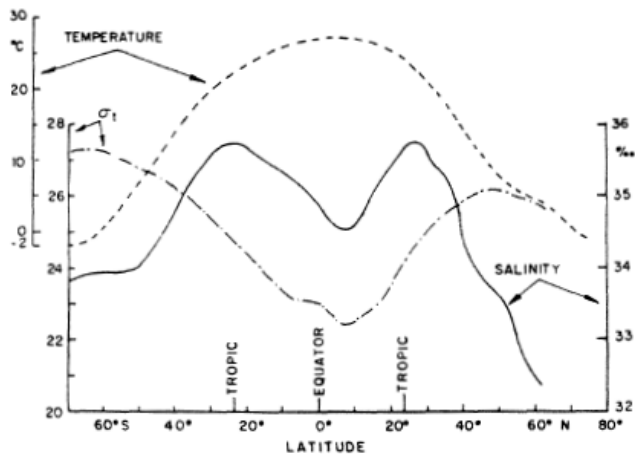


Figure 6: Latitudinal variation of oceanic temperatures, salinities and densities (Unesco, 1989).

Figure 6 shows the variation of temperature, salinity, and density (σ_1) with latitude. Density is largely controlled by temperature except in Polar Regions where salinity variations become significant. Representative vertical profiles of density are shown in Figure 7. The regions of high-density gradient (high N) are called pycnoclines and indicate regions of high stability. These regions strongly resist displacement, but can trap internal waves, which can in turn interact with a submersible operating in or passing through these regions.

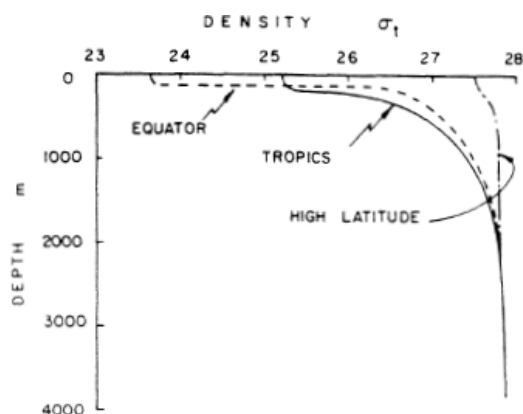
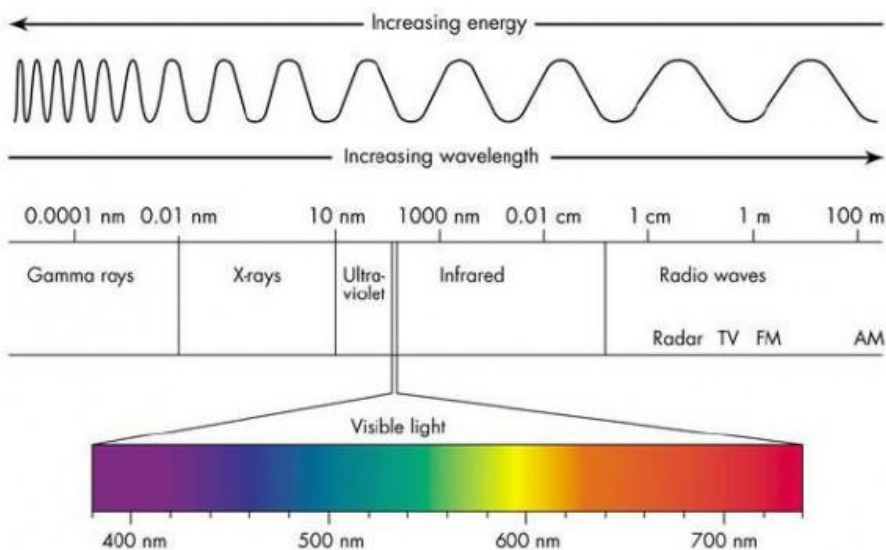


Figure 7: Vertical profiles of densities at various locations (Unesco, 1994).

1.1.4.4 Light Transmission in Sea Water

The transmission of light in the ocean is important in several ways. Light is a fundamental prerequisite for photosynthesis and hence for all life in the ocean. The sunlight penetrating from the surface through various layers of the ocean is important from the point of view of primary

production. By utilizing the light energy, the phytoplankton in the sea produce for themselves the carbohydrates by the process of photosynthesis. Due to light transmission in sea water, oceans contain abundant wealth of animal life. The importance of light to the behaviour of fish and their fish is well known. There are several aspects of fish behaviour, e.g., feeding, response to current, schooling, which are influenced by light. For man in the sea, light is essential for seeing and for the application of photography and television. Light is also means for quantitatively describing water based on particulate substances present in sea water. It thus provides a useful method for detecting and tracing the movement of ocean water mass.



Figur 1 <Insert caption describing this figure about EM emission>

Sun supplies most of the energy to the ocean. Among the different forms of electromagnetic energy radiated by the sun one form, the visible light, occupies a very narrow part of the electromagnetic spectrum, within wavelengths from 0.4 to 0.8 μm . Water is basically opaque to all forms of electromagnetic energy except the visible light part of the spectrum. Visible light can be subdivided by wavelength into violet, indigo, blue, green, yellow, orange and red. These wavelengths of light when combined produce white light. It should be recognized that part of the incoming solar radiation arrives as diffuse skylight. Solar light incident upon the ocean surface is partly selected and the rest is refracted, scattered or absorbed. The amount of visible light reflected varies with the angle of incidence. The amount of light that actually enters the sea depends in the angle of the sun, sea surface condition, sky condition and clarity of sea water. When light enters the sea, it is refracted downward, since the velocity of light is greater in air than in water. Absorption and scattering play an essential role in the propagation of light in sea water.

As light travels through sea water, it loses its intensity due to absorption and scattering. There are four causes for light to suffer a decrease in intensity on passing through sea water. These are: (1) absorption of light by sea water, (2) absorption of light by suspended particles, (3) scattering of light by sea water and (4) scattering of light by suspended particles.

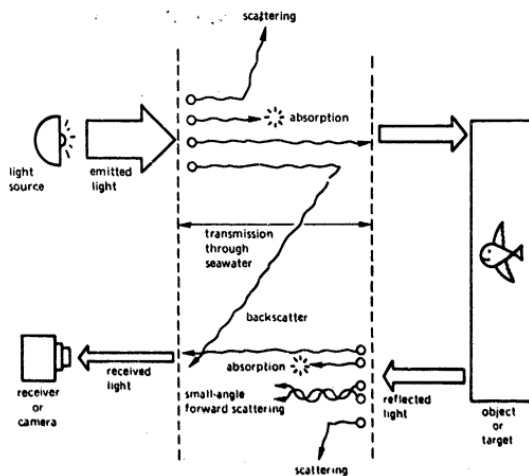


Figure 8: Basic imaging situations in sea water (Allmendinger, 1990).

Thus, absorption and scattering together decrease the direct penetration of light intensity into sea water. The term "attenuation" is a preferred term for representing the combined loss due to absorption and scattering.

Figure 8 shows some special cases of the causes for light intensity loss in sea water. These are:

1. Some source light is scattered out of the beam, and does not reach the target.
2. Some source light is absorbed or converted to a different form of energy, such as thermal kinetic energy or chemical potential energy, and does not reach the target.
3. Some source light, scattered backwards into the receiver's field-of-view, does not reach the target and tends to reduce the contrast at the receiver.
4. Some reflected light is absorbed, and does not contribute to the image.
5. Some reflected light is scattered out of the receiver's field-of-view, and does not contribute to the image.
6. Some reflected light undergoes small-angle forward scattering, introducing resolution losses.

In oceanography, much importance is given to the rate at which downward travelling light radiation decreases. The rate of decrease in light intensity, can be expressed by means of a coefficient called attenuation coefficient. This coefficient can be calculated from the following equation (Allmendinger, 1990):

$$X_\lambda = 2.30[\log I_{\lambda,Z} - \log I_{\lambda,(Z+1)}] \quad (4)$$

Where X_λ represents the attenuation coefficient, $I_{\lambda,Z}$ and $I_{\lambda,(Z+1)}$ represent the radiation intensities of wave length λ on horizontal surfaces at depths Z and $(Z+1)$ metres.

Ocean water is a complex physico-chemical and biological system. It contains dissolved substances, suspensions and several other living organisms. Due to the presence of minute suspended particles,

ocean water scatters light strongly. These suspended particles also absorb radiation. In addition, the dissolved "yellow substance" present in sea water is responsible for greater absorption of light radiation. As a result of all these, the attenuation coefficient in the sea water are greater than this in absolutely pure water.

In the higher latitude regions of the oceans, the waters are normally less transparent due to the abundance of plankton in them. Similarly, nearshore waters are less transparent because of suspended matter and more plankton in them. So, the attenuation coefficient values are more in these waters. In the open ocean also, large differences in attenuation coefficient values occur from one region to another region, depending on the ocean current pattern. Very clear waters (attenuation coefficient less) in the open ocean are usually observed in regions of converging surface currents, which are associated with sinking water. Such waters have low fertility. On the other hand, generally turbid waters (attenuation coefficient more) in the open ocean are found in regions of diverging surface currents, which are accompanied by upwelling of subsurface water. These waters have high fertility. A comparison of water attenuation coefficients values of pure water and different types of ocean water reveal that the attenuation coefficients in the clearest ocean water are two times more than those in pure water. For the more turbid waters of the open ocean, the attenuation coefficient may be ten times higher than those in pure water. The attenuation coefficients in coastal waters may be even 30-40 times more than those observed in pure water.

1.1.5 Temperature – Salinity Relationship

Water from different parts of the ocean tends to have different and distinctive temperature and salinity characteristics. Oceanographers have classified "water masses" by their T-S relationship. Figure 9 shows the principal water masses of the world defined and shown for comparison. Superimposed on the T-S plot are lines of equal density, sigma-t. Oceanographers use such relationships to study water motion and mixing, but they can also give underwater vehicle designers a summary of the temperatures and densities they will encounter in different parts of the world's oceans.

1.1.5.1 Specific Heat

The specific heat of seawater, C_p , is defined to be the heat in joules required at a constant pressure to raise the temperature of one kilogram of sea water one degree Centigrade. Thus the units are $J/(kg\text{ }^{\circ}\text{C})$. C_p is a function of temperature, T , salinity, S , and pressure, P . For seawater, the specific heat increases with temperature and decreases with salinity and pressure. Typical values are around 4000 $J/(kg\text{ }^{\circ}\text{C})$. The best empirical fit at zero pressure is given by Millero et al.. 1973, which extends to low temperatures. The pressure effect has not been directly measured, but has been estimated by Fofonoff and given in the UNESCO papers, 1983.

1.1.5.2 Sound Velocity

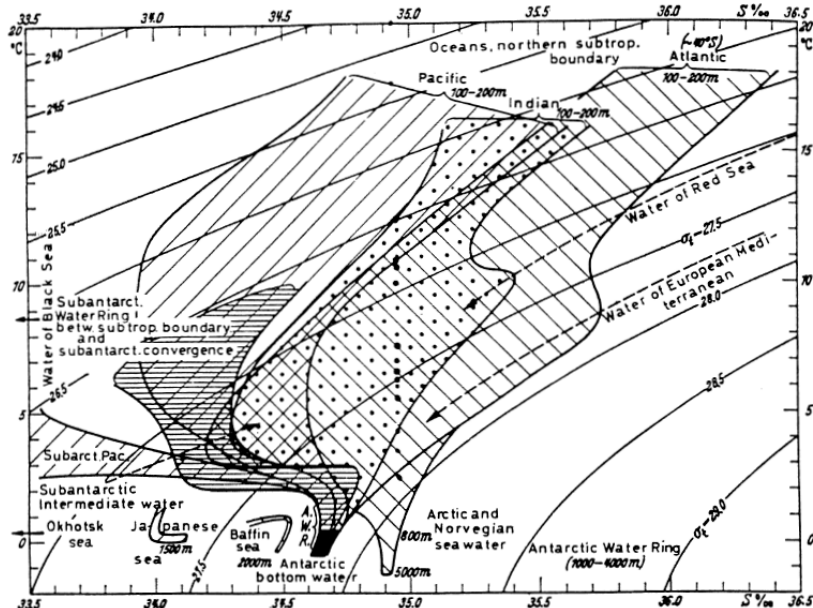


Figure 9: Relation between temperature and salinity below the distributed near-surface layer for the entire world ocean (Allmendinger, 1990).

Because seawater is compressible, it can support turbations or fluctuations in pressure about the mean. We call these pressure oscillations sound, and they travel in the ocean with a velocity of about 1500 m/s, which is about five times faster than in air. The ocean is relatively opaque to all forms of electromagnetic radiation (from long radio waves through short ultraviolet), but transmits these sound oscillations much better than the atmosphere. Here acoustics are a valuable tool for communication and getting a "view" through the ocean. The velocity of sound is a function of the temperature, salinity, and pressure, increasing with all three factors. The most recent work by Chen and Millers, 1977, used standard sea water and so is consistent with the PSS-78 and in good agreement with values computed from the EOS-80.

Temperature effects dominate the sound velocity profile in the upper ocean, causing a decrease in sound velocity with depth. Pressure effects dominate in the deep ocean, increasing sound velocity with depth. Therefore, the resulting profile has a minimum at about 1200 m depth. The variations in sound velocity with depth have little effect on vertical or near-vertical transmissions of sound, as in communications between a submersible and a mother ship directly above. However, the sound velocity profile and the minimum or "sound channel" has important implications for horizontal or near-horizontal transmission of sound.

Sound travelling from a point source will spread out spherically, so that the sound energy will decrease as the square of the distance from the source. The limit of sound transmission is reached when the energy density decreases until it is equal to the ambient noise level (see below). If the energy were confined between two vertical surfaces, then in cylindrical spreading the reduction in

energy would be proportional to the distance, so it will travel further before decreasing to ambient noise level. Sound travels along paths or “rays” which are governed by Snell’s law:

$$C_1 \sin \theta_2 = C_2 \sin \theta_1 \quad (5)$$

where C is the velocity of sound, θ is the angle of the ray from vertical, and the subscripts refer to the different layers. Hence it is obvious that the rays are bent toward lower velocity, and that a ray path from a source at the depth of the sound channel will be refracted toward the sound channel.

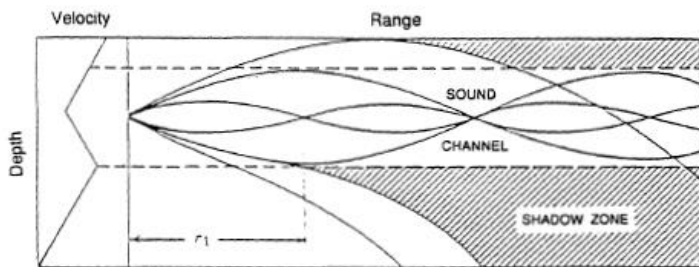


Figure 10: Acoustic ray trace showing sound channel and shadow zone (Funk, Bryant, Heckman, & Department, 1972).

Hence the rays are concentrated at that depth and consequently travel a large distance. The energy contained within a solid angle marked by four rays being emitted from the source is constant, so when the energy is concentrated in the sound channel, the spreading is closer to cylindrical than spherical. Hence, it is not surprising that large distances can be obtained by transmitting near the depth of the sound velocity minimum.

There are other source velocity profiles that are of greater concern to the submersible operator. Consider the case of a mixed layer where the sound velocity is controlled by pressure and increases with depth. Any sound transmitted into this region will be bent toward the surface. If this layer is above a layer with decreasing temperature that dominates over pressure, then rays penetrating into this layer will be refracted toward the bottom. This results in a shadow zone where acoustic communication or detection is impossible (Figure 10).

1.1.5.3 Hydrostatic Pressure

For most practical purposes, the vertical equation of motion reduces to:

$$\frac{\partial P}{\partial z} = \rho g \quad (6)$$

and integrating from the surface (where we take the pressure to be zero) to depth z gives:

$$P(z) = \bar{\rho} gz \quad (7)$$

where is the average or integrated density to depth z . This states that the pressure at a depth is due to the weight of water over it, and ignores any dynamic effects. P is sometimes called the hydrostatic pressure, because if all motion were to cease, the equations of motion would simply reduce to equation (7). This also gives a method to convert pressure (as measured by a pressure sensor) to depth. If one assumes the density of an average ocean profile, then equation (7) converts gage pressure to depth. For example, a pressure of 4062 dbars (5891 psi) converts to a depth of 4000 m.

1.1.6 Acoustic Ambient Noise

The limitation to acoustic transmission and detection in the ocean is the ambient noise level. This is due to a number of factors which add up to a background spectrum, as shown in fig. 10. The noise level decreases with increasing frequency. Chief sources of low frequency noise (1 to 100 Hz) are seismic activity and explosions. In mid-frequency ranges (10 to 1000 Hz), ship noise is predominant except during rainstorms, when the noise of the rain hitting the surface becomes significant. At high frequencies (100 to 10 000 Hz), wind-generated noise dominates and is a function of wind speed.

1.1.7 Freezing and Sea Ice

The freezing temperature of seawater is dependent on the salinity and pressure of the water. Millero and Leung, 1976 (or UNESCO, 1983), give an empirical form to laboratory measurements at low pressure. For example, seawater of 35 ‰ at the surface has a freezing temperature of -2.54°C. As seawater freezes, the salt settles out in brine channels, which, because it is thus concentrated salt, is denser and settles. Thus cold, salty water tends to form in areas where sea ice is being formed.

In regions where ice is melting, the salinity will be low, and a low salinity or freshwater layer is found at the surface. This reduces the density considerably and has implications for the buoyancy requirements of a submersible which is operating here.

1.1.8 Coefficient of Thermal Expansion

One of the unique properties of fresh water is the reversal in the sign of the coefficient of thermal expansion at 4°C. Thus, water starting to freeze at 0°C is less dense than water at 4°C. As the salinity increases, this temperature of maximum density decreases. At a salinity of 24.7 ‰, the freezing point and temperature of maximum density are equal at -1.33°C. For salinities greater than 24.7 ‰ the water continues to decrease in density with decreasing temperature until the freezing point is reached. A typical value of the coefficient of thermal expansion is 2×10^{-4} °C. This value increases with temperature and pressure.

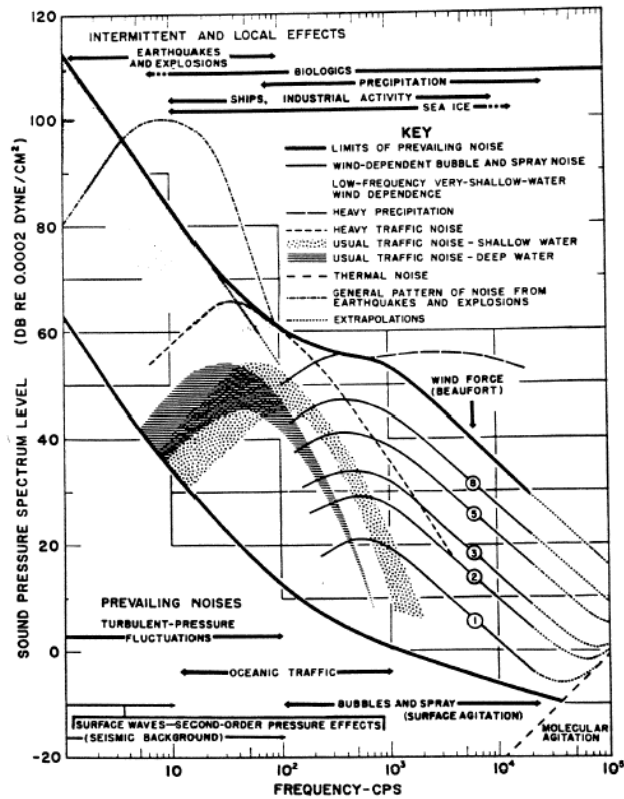


Figure 11: Background spectrum of ambient noise level in the ocean (Valiron, 2001).

1.1.9 Dynamical Processes, Surface Gravity Wind Waves

Waves are an efficient method of transporting energy from one point to another. The waves transport energy but, unlike ocean currents, do not transport the water itself. Figure 12 summarizes the energy density spectrum (proportional to wave amplitude squared) of surface waves according to wave frequency. The major energy in surface waves appears at the once- and twice-a-day tidal frequencies and in the 1- to 40s wind wave frequency band. Waves are like simple harmonic oscillators where the density discontinuity at the air/sea interface and the force of gravity form the restoring force analogous to the mass and spring used in introductory physics classes. In addition to gravity for the long-period waves such as tidal motion, the effects of the earth's rotation become apparent in the restoring force. To gain an understanding of the principles involved, we shall first examine a single frequency, small amplitude, simple sinusoidal wave at the ocean's surface and then expand our description of the ocean spectrum shown in Figure 12 as a sum of these simple waves.

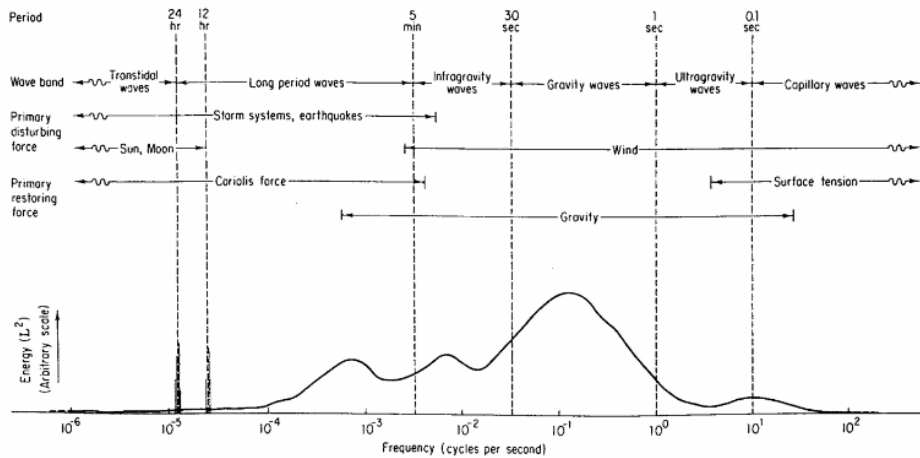


Figure 12: Estimated schematic representation of the energy contained in the surface waves of oceans (Allmendinger, 1990).

1.2 The Ocean

The ocean water is almost constantly in motion. This motion compromises of everything from large-scale oceanic circulation to small-scale turbulence. The forces behind these motions can be divided into two groups: the primary forces, which sets the water into motion, and the secondary forces, which are both a result of and a cause of the motions. The primary forces are horizontal pressure forces, atmospheric pressure forces, wind- and tidewater forces. The secondary forces are the Coriolis force and different friction forces. Horizontal pressure forces are caused by the fact that the density of water can differ according to location and the ocean surface is not entirely horizontal. The addition of fresh water has a double effect. First of all, the sea-level rises and secondly, the density is affected. Water from high-pressure areas will flow to areas of lower pressure in order to achieve equilibrium. The atmosphere pressure have a significant impact on the ocean. High atmospheric pressure will cause the sea surface to be pushed downwards, while low atmospheric pressure causes it to rise. The latter phenomena can be observed along the Norwegian coast during large low-pressure activities. Varying sea-levels between different areas will give rise to horizontal pressure forces in the water. The wind causes water current due to the friction forces between the surface and the air above it.

The tidal forces are a result of the gravitational pull exerted by the sun and moon. The moon's impact has a period of 12.5 hours, while the sun has a period of 12 hours. The largest difference between high and low tide occurs when the forces exerted by the sun and moon work together (spring tide). When the gravitational forces exerted by the sun and moon counteract each other the difference is smaller (neap tide). This occurrence have a period of 14 days. The tides are affected by water depth and water-land interactions. Different tidal waves affects each other as well.

After the water have been set into motion by the primary forces, the Coriolis force and friction forces act upon the water. The effect of these forces and from the bottom topography are significant for the ocean currents. The Coriolis force is caused by the Earth's rotation. This force bends all

motion to the right in the Northern Hemisphere. In the Southern Hemisphere all motion bends toward the left regardless of the original direction of the motion. The friction forces are caused by water bodies sliding against each other or the sea bed.

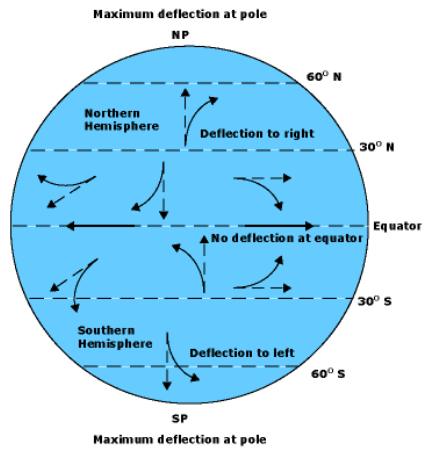


Figure 13: How wind is deflected in each hemisphere due to the Coriolis Effect (Allmendinger, 1990).

1.2.1 The Ekman Spiral

One would believe that wind driven current followed the wind direction. However, due to the Coriolis force the surface current will go 45° to the right of this direction. The surface water, which is driven by the wind, will drag the water beneath itself due to friction. This will in turn drag the water layer beneath itself. The current velocity decreases gradually with water depth. Due to the Coriolis force the current that arises will be increasingly bend toward the right the deeper one goes. At ca. 50 m water depth, the water current will move in opposite direction to the surface current. However, at this depth the current will only be 4 % of the current on the surface. Considering all the layers affected by the friction forces, the average water transport moves 90° to the right of the wind direction.

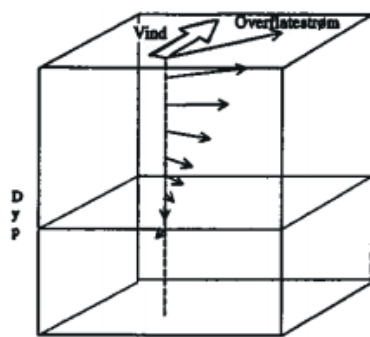


Figure 14: The Ekman Spiral (Allmendinger, 1990).

1.2.2 Seabed Effects

The effects of the bottom topography on the water motion are complicated and hard to describe accurately. Even in deep water, the bottom topography can affect the currents all the way at the surface. Generally, the current will follow the isobaths along inclined seabed. The current might have trouble following isobaths in areas of large peaks, depressions or abrupt deflections, which in turn can result in the water to swirl. The velocity of the water current changes as the water depth varies. When the same amount of water is to travel in both deep and shallow waters, the velocity have to increase over the shallow areas. As the velocity increases, the Coriolis forces have a larger effect such that the direction of the current also changes. This situation can also cause the formation of water swirls. In straits where a large amount of water travels through, the current velocities can be high.

1.2.3 Upwelling

Upwelling is an important phenomena that is caused by the hydrographical circulation patterns in the world's oceans. It has a large impact on the biological production in the ocean, and will therefore be discussed in this chapter.

The mechanisms behind upwelling is driven mainly by the Coriolis Effect in situations where water moves along the coast of a continent in a direction that causes the Coriolis force to bend the current away from the coast. In the Northern Hemisphere, this particular direction is southwards along the east side of the oceans and northwards along the west side. The opposite is the case in the Southern Hemisphere. When the surface water is driven away along the coast, water from deeper layers flows to the surface to replace it. This process is called upwelling.

Primary production of organic matter from inorganic matter through photosynthesis occurs in the upper water layers where the sunlight can penetrate. Due to this process, the upper layers will be devoid of inorganic matter. Further production requires supply of inorganic matter, which can be found in deeper layers. At higher latitudes, this is provided by winter cooling of the surface water with mixing of the different water layers as a result. In tropical and subtropical areas, upwelling is the single most important mechanism for this process. In these areas there is enough sunlight for the photosynthesis to take place the entire year, but the high temperatures causes a permanent separation of the water layers with the warm layers at the top and colder at increasingly deeper waters, separated by a significant thermocline. This prevents the supply of inorganic matter to the upper layers by mixing. Large areas of the world's oceans, that does not have upwelling, can therefore be considered as barren of biological matter. However, the areas where upwelling occurs are highly productive. The effect of upwelling is largest along the west coast of the continents.

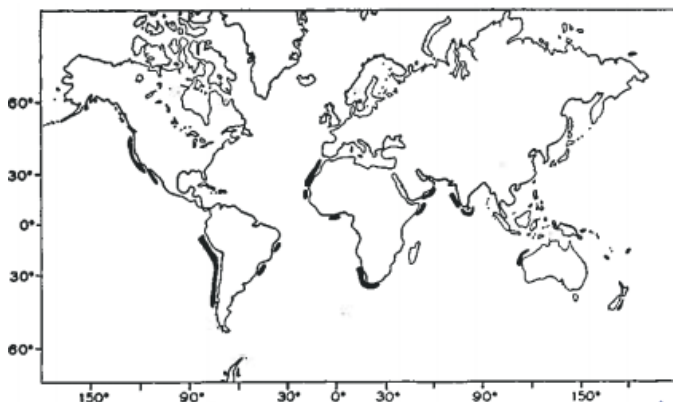


Figure 15: Main upwelling areas (Allmendinger, 1990).

The most important areas in the Pacific Ocean are along the coast of Peru in South America and along the California in North America. In the Atlantic Ocean, areas of high upwelling are outside the coast of Namibia in Southern Africa and along Morocco in the north. In the Indian Ocean there is seasonal upwelling outside the coast of India, the Arabian Peninsula and Somalia. In these areas, the phenomena is driven by the monsoon wind. The monsoon winds are seasonally dependent. Except along the southern pole continents, where the upwelling is permanent, upwelling at higher latitudes occur occasionally and have less significance for the biological production than in subtropical areas. Areas of upwelling can be readily recognised by lower temperatures at the water surface than one would expect. These areas have been mapped through studies of organic matter in the bottom sediments, and are known for large production. Important fisheries are often related to these areas.

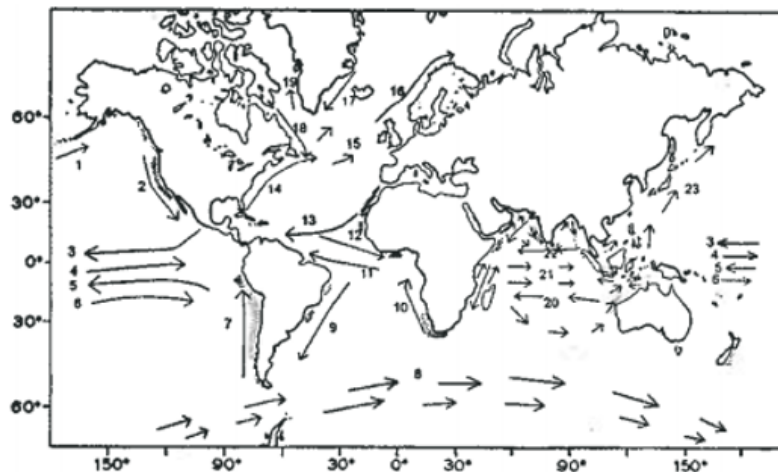
1.2.4 Typical Patterns of Ocean Circulation

The hydrography of the world's oceans are characterized by more or less permanent ocean currents. This is due to the atmospheric conditions, which constitute the main drivers for the current, also are relatively permanent. There are two subtropical anticyclones in the Atlantic Ocean, the Pacific Ocean and the Indian Ocean that rotates clockwise at northern and anti-clockwise at southern latitudes. In between them, there is a belt of easterly winds along the Equator and westerly winds at higher latitudes. These permanent wind fields result in large whirlpools in the upper water layers that circulate in the same way. In the Atlantic Ocean these permanent atmospheric conditions result in a westerly equatorial current both in the Northern and Southern Hemisphere. In between them, along the Equator, there is an easterly equatorial counter current. In the Northern Hemisphere, the equatorial current bends away along the northern coast of South America, flows through the Caribbean Sea and proceeds along the east coast of North America. This part of the current is named the Gulf Stream. Parts of the Gulf Stream will continue northeast as the North Atlantic Drift, while other parts will go east and southeast along the west coast of North Africa. The South Equatorial Current bend towards the south when it reaches the east coast of Brazil (the Brazil Current) before it continues across the southern part of the Atlantic Ocean and up the west coast of Africa (the Benguela Current) towards the Equator. The North Atlantic Drift continues into the Nordic Seas as the Norwegian Current and affects the hydrography up to Svalbard in the north. Along the east coast of Greenland, the cold East Greenland Current flows towards the south. Part of the East Greenland

Current turn to the west at the southernmost point of Greenland and continue north to the Baffin Bay as the West Greenland Current. The Labrador Current is flows along the west side of the Baffin Bay, around Newfoundland and along the Gulf Stream towards the south of the east coast of USA.

Equivalent patterns of circulation are found in the other oceans. The current flowing towards the north along South America in the Pacific Ocean is called the Humboldt Current. In the northerly Pacific Ocean, the Kuroshio Current flows towards the north on west side and the California Current towards the south on the east side. The current patterns are more complicated in the Indian Ocean since there are larger seasonal variations of the currents. When the Northeast Monsoon wind blows from November to March, the North Equatorial Current is well developed, and a northern current is established outside Arabia and East Africa north of the Equator. During the Southwest Monsoon from May to September, the North Equatorial Current is reversed, and the Southwest Monsoon Current flows north along Somalia (the Somali Current), through the Arabian Sea, around India and into the Bay of Bengal. The current pattern south of the Equator is more permanent. The Agulhas Current flows to the south along Africa, continuing in the West Wind Drift towards Australia before returning as the South Equatorial Current.

South of the continents there are permanent westerly winds that set up permanent currents from the west to the east around the South Pole continent. It is more complicated in the Northern Hemisphere since the continents prevents circulation as seen in the south.



1	The North Pacific Current	13	The Atlantic North Equatorial Current
2	The California Current	14	The Gulf Stream
3	The North Equatorial Current	15	The North Atlantic Drift
4	The North Equatorial Counter Current	16	The Norwegian Current
5	The South Equatorial Current	17	The East Greenland Current
6	The North Equatorial Counter Current	18	The Labrador Current
7	The Humboldt Current	19	The West Greenland Current
8	The Antarctic West Wind Drift	20	The Indian South Equatorial Current
9	The Brazil Current	21	The Indian Equatorial Counter Current
10	The Benguela Current	22	The Indian North Equatorial Current
11	The Atlantic South Equatorial Current	23	The Kuroshio Current
12	The Atlantic Equatorial Counter Current		

Figure 16: Main world ocean currents (National Snow & Ice Center, 2013).

1.2.4.1 Hydrography in the Norwegian sea areas

The coastal and sea areas outside Norway are characterized by relatively warm water from the Atlantic Ocean. Because of this the Norwegian climate is mild despite its location at higher latitudes. Without the contribution of warm water from the Atlantic Ocean, the climate would have been arctic and some of the sea areas frozen.

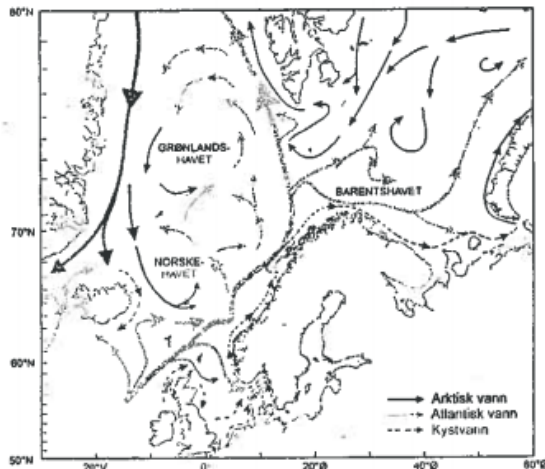


Figure 17: Current patterns in the North Sea, the Norwegian Sea and the Barents Sea. Black arrows: arctic water, grey arrows: Atlantic water, dashed arrows: coastal water (Karlsen, Hamre, & Gjøsæter, 2001).

Water from the Atlantic Ocean flows into the Nordic Seas north and west of the United Kingdom. This water transport has been calculated to be roughly between 5 and 10 Sv (1 million cubic meter per second is called a sverdrup with the symbol Sv). Informally, this current is called the Gulf Stream, however the branch of the Gulf Stream reaching the Norwegian sea areas is actually named the North Atlantic Drift. This current branches out into several areas. One part bends to the south and enters the North Sea, one continues northeast along the Norwegian coast while several branches bend to the west in to the Norwegian Sea. Nevertheless, most of the water from the North Atlantic Drift proceeds further to the north, where it branches out into two separate currents; one flowing along the coast of Svalbard and the other goes east into the Barents Sea.

2 Sound Theory

The theory of sound is very similar to that of light as both phenomena consist of waves which are propagated through a medium. Both are subject to scattering, reflection and absorption. In water, sound can be transmitted over a much longer distance than light but water is an imperfect acoustic medium. Energy is removed from the sound by suspended solids particles or also converted into heat by physical absorption.

Acoustic waves originate from the propagation of a mechanical perturbation. Local compressions and dilations are passed on from one point to the surrounding points, because of the medium's elastic properties. From one point to the next, this perturbation will propagate away from its source. The propagation rate of this perturbation of the medium will be called velocity. When an acoustic wave passes through a substance, it causes local changes in the density of the medium, as well as a local displacement of mass. This displacement leads to the formation of forces that create movement aimed at bringing the density back to the state of equilibrium.

The acoustic wave equation for fluids and gases is derived by the application of three simple principles.

- The continuity equation, or conservation of mass
- Newton's second law: force equals mass times acceleration
- The equation of state: the relationship between changes in pressure and volume

Application of these principles yields the linear acoustic wave equation:

$$\nabla^2 = \frac{1}{c^2} \frac{\partial^2 p}{\partial t^2} \quad (2.1)$$

Where ∇^2 is the Laplace operator, sound pressure p and sound velocity c .

We will often treat signals and waves with sine or cosine form, also called harmonic signals and waves. Formally, we move from the time domain to the frequency domain by using Fourier transformation. The angular frequency is:

$$\omega = 2\pi f \quad (2.2)$$

Where ω is in rad/s and frequency f in Hz. The acoustic wave number k and the wavelength λ are defined by:

$$\omega = \frac{\omega}{c} = \frac{2\pi}{\lambda} \quad (2.3)$$

2.1 Sound Velocity

The propagation velocity of an acoustic wave is imposed by the characteristics of the propagation medium: it depends on the density ρ and the elasticity modulus E :

$$c = \sqrt{\frac{E}{\rho}} \quad (2.4)$$

Thus the sound speed is given by the square root of the ratio between volume stiffness and density. In the sea, both depend on ambient conditions, in particular water temperature, salinity, and the surrounding pressure or depth of the water. If these parameters are measured and known, the following simplified formula can be used with sufficient accuracy for most purposes:

$$c = 1449.2 + 4.6T - 0.055T^2 + 0.00029T^3 + (1.34 - 0.01T)(S - 35) + 0.016z \quad (2.5)$$

Where temperature T is expressed in $^{\circ}\text{C}$, salinity S in parts per thousand (‰), depth z in metres, and sound velocity c in m/s. Equation (5) will ensure reasonable accuracy for applications with $z < 1000$ m. In general the sound velocity in sea water is around 1450 – 1500 m/s.

As observed from equation (5), sound velocity increases with temperature, salinity and depth. The increase of salinity by 1‰ at $T=10^{\circ}\text{C}$ and of depth by 100m lead to an increase of the sound velocity of 1.2 m/s and 1.6 m/s, respectively. The increment of the sound velocity due to a change in temperature of 1°C depends on the value of the temperature. When the temperature and the salinity are constant, the sound velocity increases with a rise in the hydrostatic pressure (hydrostatic gradient of the sound velocity). The vertical gradient of the sound velocity in most regions of the ocean is about a thousand times the horizontal one, except in areas of the convergence of cold and warm currents where the horizontal and vertical gradients are sometimes comparable. Thus, in a first approximation, the ocean may be considered as a plane-stratified medium, the characteristics of which vary only with depth and are constant in the horizontal plane. The influence of internal waves, large eddies, currents, and some other factors perturbing this picture must be considered separately.

2.2 Pulse Length

As we will see later, acoustics in underwater applications are often used as sound pulses. The pulse length, l_p , gives the length of the sound pulses sent through the water. It is a function of the number oscillations of the pulse, n, and the wavelength λ :

$$l_p = n\lambda = n \frac{c}{f} \quad (2.6)$$

The pulse length is related to the amount of sound energy of the signal, and therefore also the sound intensity. Longer pulse lengths are used for devices and instruments that will be used in long-range applications, rather than those for short-range applications.

2.3 Intensity and Power

The propagation of a sound wave is associated with an acoustic energy. This energy can be decomposed into a kinetic part (corresponding to particle movements) and a potential part (corresponding to the work done by elastic pressure forces). The acoustic intensity I is the mean

value of the energy flux by unit of surface and time (Watts/m²). One can show it equals the average of the product of acoustic pressure by particle velocity. For a plane wave of amplitude p_0 , this yields:

$$I = \frac{p_0^2}{2\rho c} \quad (2.7)$$

The acoustic power P received by a surface S is intensity, corrected for the surface considered. For the plane wave, this would be:

$$P = I \times S = \frac{p_0^2 S}{2\rho c} \quad (2.8)$$

Like acoustic pressure, intensity and power can vary enormously. A high-power sonar transmitter may deliver acoustic power of several tens of kilowatts, whereas a nuclear submarine in silent mode might radiate only a few milliwatts.

2.4 The Decibel and Absolute Reference Level

Because of their huge dynamics, acoustic values like pressure or energy are usually quantified on a logarithmic scale, and noted in decibels (dB). By definition, the decibel corresponds to ten times the base-10 logarithm of the ratio of two powers. For example, $10\log(P_1/P_2)$ quantifies the difference between two powers P_1 and P_2 , and a 10-dB difference means that P_1 is in fact 10 times higher than P_2 .

The decibel can be adapted to other physical values: for example, the acoustic pressure. As the power P_i is proportional to the square of pressure p_i^2 , the same ratio can be expressed as:

$$10 \log \left(\frac{P_1}{P_2} \right) = 10 \log \left(\frac{p_1^2}{p_2^2} \right) = 20 \log \left(\frac{p_1}{p_2} \right) \quad (2.9)$$

We shall therefore remember to use $10\log(X_1/X_2)$ for quantities akin to energies (e.g., power, intensity) and $20\log(x_1/x_2)$ for quantities akin to acoustic pressure. A difference of 3 dB between two signals will therefore correspond to an energy ratio of 2, and an amplitude ratio of $\sqrt{2}$, of their acoustic pressures. A 10-dB difference will correspond to an energy ratio of 10 and an amplitude ratio of $\sqrt{10} \approx 3.1$. A 1-dB difference (which one can consider as a practically achievable limit of the accuracy of current underwater acoustic measurements) corresponds to around 10% variation in acoustic pressure. One should also remember that the product of several variables translates into the sum of their values in dB, because of the properties of logarithmic operations. But the sum in dB of physical values does not equal the sum of the individual values in dB.

A reference level is necessary if one is to give absolute pressure or intensity levels in dB. In underwater acoustics, the pressure reference is usually the microPascal. The intensity reference, especially for sonar and echo sounder, is often the intensity 1 m from the instrument.

2.5 Multiple Paths

Because the propagation medium is limited by the sea surface and the seabed, the signals transmitted undergo successive reflections at the interfaces. Variations in sound velocity within the

medium may also deform the paths of sound waves. Due to these processes, a given signal can therefore propagate from a source to a receiver along several distinct paths, corresponding to distinct directions and durations. The main, "direct" signal arrives along with a series of echoes, of amplitudes decreasing with the number of reflections undergone. The time structure of the signal to be processed is of course somewhat affected, and the performance of a system can be highly degraded by these parasite signals, in particular for data transmission applications. The number of noteworthy multiple paths is highly variable, depending on the configuration; none in the best case, several tens or even hundreds in long-distance propagation cases (these multiple paths are then impossible to distinguish individually, and show up as a continuous signal trail).

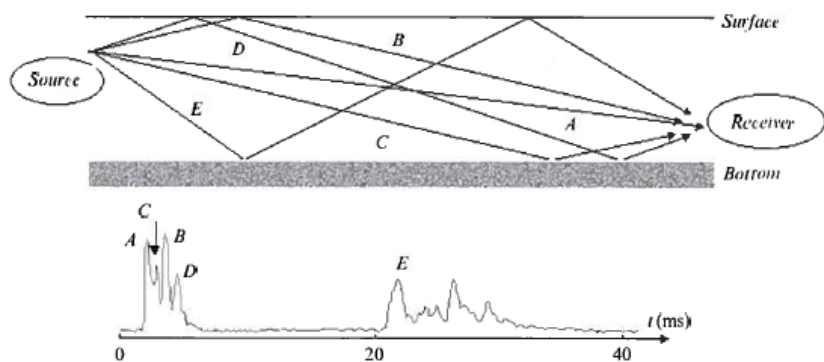


Figure 18: (Top) multiple paths: (A) direct path; (B) reflection on surface; (C) reflection on the bottom; (D) reflection on the surface and bottom; (E) reflection on the bottom and surface. (Bottom) multiple paths as visible in a time domain signal (Karlsen et al., 2001).

Multiple paths may be considered from two points of view, depending on the configuration. In high frequency, for short signals (shorter than the typical delay between path arrivals), their effect is observable in the time domain, with typical sequences of multiple echoes (Figure 18). Whereas, for low-frequency permanent signals at fixed frequencies, the contributions add together permanently; this creates a stable interference pattern, with strong variations in the field amplitude.

These multiple paths are typical of underwater acoustics, and can be very penalising. Their effects will be different from multiple paths encountered in electromagnetic propagation, even if they both correspond to similar physical processes. The multiple paths of radio or radar waves interfere and cause fading, but the delayed time echo is not always troublesome when decoding the received signal (because the speed of light induces very short delays). In underwater acoustics, on the contrary, the propagation velocity is low, and the time delays are much more important (Figure 18). They create distinguishable echo and reverberation effects. The physical anisotropy of the waveguide (velocity variations, influence of the interfaces) is also much more marked than in electromagnetic propagation.

2.6 Typical Vertical Profiles of Sound Velocity and Corresponding Conditions of Sound Propagation

The form (profile) of curve $c(z)$ and the distribution of the sound velocity gradient with depth, rather than an absolute value of the sound velocity, are most important for the propagation of sound in the

ocean. For one type of profile $c(z)$ the sound can propagate hundreds and thousands of kilometres, and for another type, sound of the same frequency propagates only as far as a few tens of kilometres or even less.

The $c(z)$ profiles are different in the various regions of the ocean and vary with time as well. The largest fluctuations are in the upper ocean, mainly due to seasonal and diurnal variations of temperature and salinity. At depths below 1 km vertical variations of temperature (as well as of salinity) are usually weak, and the increase of the sound velocity with depth is almost exclusively due to the increasing hydrostatic pressure. As a consequence, at great depths the sound velocity increases almost linearly with depth.

We will now consider the main forms of the profiles $c(z)$ and the corresponding types of sound propagation.

2.6.1 Underwater Sound Channel (USC)

The USC is often called the SOFAR channel. In the deep-water regions the typical profile $c(z)$ is that for which the sound velocity minimum is at a certain depth z_m (Figure 19(a)). This depth is an axis of the underwater sound channel. Above this axis the sound velocity increases mainly due to temperature increases; below it the increase in hydrostatic pressure is mainly responsible for increasing the sound velocity. If a sound source is on the axis of the USC or near it, some part of the sound energy is trapped in the USC and propagates within it, not reaching the bottom or surface, and, therefore, not undergoing scattering and absorption at these boundaries. The ray diagram in the USC is given in Figure 19(b). The rays leaving the source at a small or moderate grazing angle (angle with a horizontal plane) return to the channel axis repeatedly. This is a kind of waveguide propagation. The USC is one particular case of a natural waveguide. There is an analogous acoustic waveguide in the atmosphere, as well.

Waveguide propagation for the case shown in Figure 19 is observed in the interval of depths $0 < z < z_c$. The depths $z = 0$ and $z = z_c$ are the boundaries of the USC. The channel traps all sound rays which leave the source (located on the axis) at grazing angles $\chi < \chi_{\max}$, where

$$\chi_{\max} = [2(c_0 - c_m)/c_m]^{1/2} \quad (2.10)$$

and where c_m and c_0 are the sound velocities at the axis and boundaries of the channel, respectively. Hence, the greater the difference $c_0 - c_m$, the larger is the interval of angles in which the rays are trapped, i.e., the waveguide is more effective.

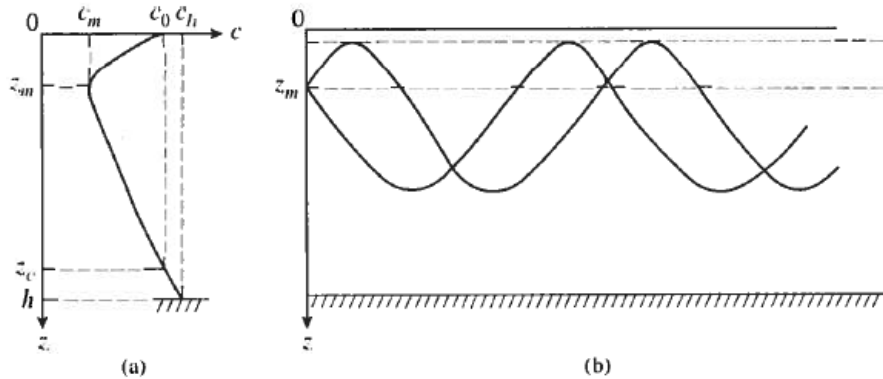


Figure 19: Underwater sound channel of the first kind ($c_0 < c_h$). (a) profile $c(z)$ (b) ray diagram (Karlsen et al., 2001).

The depth of the axis of the USC is usually 1000-1200 m. In the tropical zone it falls down to 2000 m, and rises up closer to the surface at high latitudes. At moderate latitudes (say from 60°S to 60°N) the sound velocity on the USC axis ranges from 1450 to 1485 m/s in the Pacific and from 1450 to 1500 m/s in the Atlantic Ocean.

If the sound velocity below the axis of a sound channel increases only due to the hydrostatic pressure, we say that such a sound channel is hydrostatical. However, in some cases in the ocean a USC arises as a result of the presence of warm waters with high salinity below the channel axis. This type of USC is called thermal. The typical thermal USC occurs, for example, in the Baltic and Black Seas.

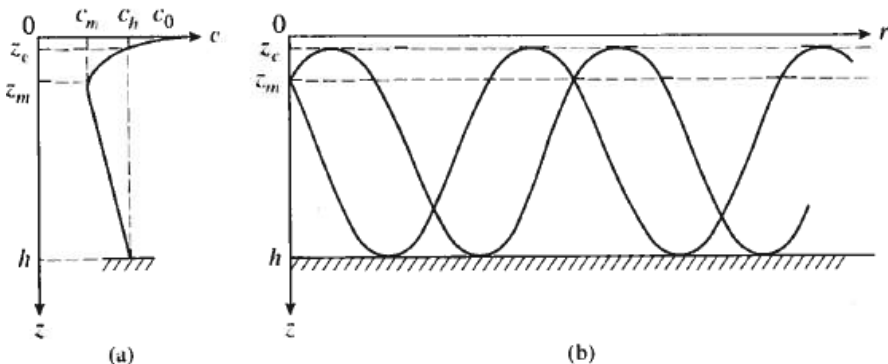


Figure 20: Underwater sound channel of the second kind ($c_0 > c_h$). (a) profile $c(z)$, (b) ray diagram () .

There are two types of USC depending on the ratio c_0/c_h . The case when $c_0 < c_h$ is shown in Figure 19(a). For regions of shallower water the opposite case $c_0 > c_h$ is true (Figure 20). Here the USC extends from the bottom up to the depth z_c where the sound velocity equals c_h . Two limiting rays are shown for this case. Trapped rays do not extend above the depth z_c . Only the rays reflected from the bottom reach this zone.

The maximum distance of sound propagation in the USC is limited mainly by absorption in sea water. Sound of sufficiently low frequency, for which absorption is fairly small, can propagate over distances of hundreds and thousands of kilometres. For example, sound signals generated by a 57-Hz source located at a site near the Heard Island (the Indian Ocean) at a depth of 157 m (the local sound channel axis) have been detected by several receiver sites in the Indian, Atlantic, and Pacific Oceans at distances of 18 000 km. Such sound propagation is called long-range sound propagation.

A number of interesting features arise for the case of a source near the ocean surface. A typical case for the USC "zonal structure" of the sound field - a sequence of insonified and *shadow zones* - is clearly seen in the ray diagram (Figure 21). Shadow zones are denoted by $A_1, A_2, \dots, B_1, B_2, \dots$. Trapped sound rays do not penetrate into them. As the source approaches the USC axis, the width of the shadow zones decreases and that of the insonified zones increases. If the depths of the source and the USC axis coincide, shadow zones disappear at this depth. Quite a number of rays arrive at the receiver in this case if the latter is not far from the USC axis. Such multipath propagation is one of the most characteristic features of the sound field in the USC.

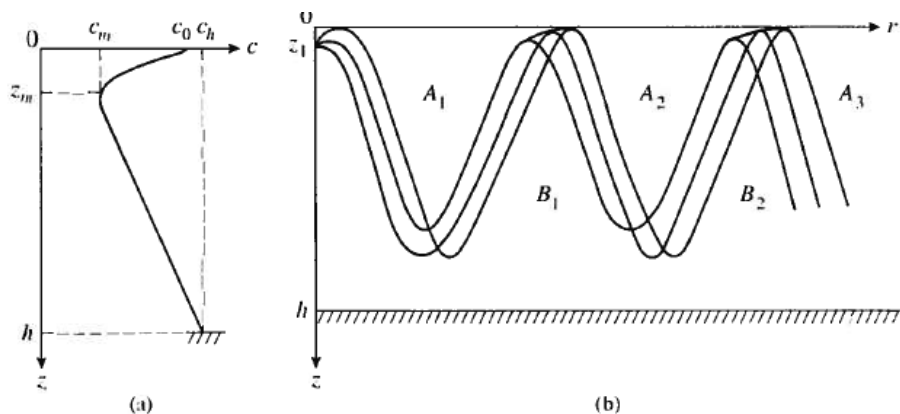


Figure 21: Typical zonal structure of a sound field in the USC. $A_1, A_2, \dots, B_1, B_2, \dots$ are shadow zones (Hovem, 2012).

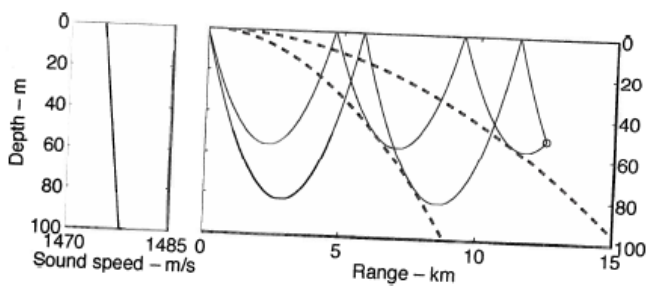


Figure 22: Raypath near a caustic. caustics are shown with dashed lines

The secondary emergence of sound rays at small depths after their refraction in deep layers is usually associated with their convergence and the formation of so-called caustics (dashed lines in Figure 22). As a result, these areas are called convergence zones. They are characterised by high sound intensity levels.

Distinct zonal structure is sometimes observed at great distances. In the tropical Atlantic between distances of 400 and 2300 km up to 37 convergence zones were observed (frequency: 13.89 Hz). At greater distances the zonal structure was smeared due to variations of the profile $c(z)$ along the path of sound propagation.

2.6.2 Surface Sound Channel

This channel is formed when the channel axis is at the surface. A typical profile $c(z)$ for this case is shown in Figure 23(a). The sound velocity increases down to the depth $z=h$ and then begins to decrease. The corresponding ray diagram is shown in Figure 23(b). Rays leaving the source at grazing angles $\chi < \chi_b$ (where χ_b is the grazing angle of the boundary ray tangent to the lower boundary of the channel) propagate with multiple reflections from the surface. If the ocean surface is smooth, these rays remain in the sound channel regardless of distance from the source and give rise to waveguide propagation. If the ocean surface is rough, part of the sound energy is scattered into angles $\chi > \chi_b$ at each contact with the surface and, therefore, leaves the sound channel. As a result in this case, the sound field decays in the sound channel, but in the area below the channel its level increases.

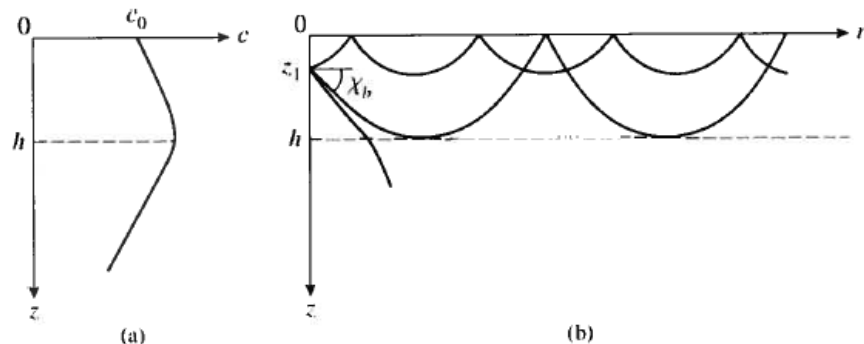


Figure 23: Surface sound channel. (a) profile $c(z)$, (b) ray diagram (Lurton, 2002).

The case shown in Figure 23 frequently occurs in the tropical and moderate zones of the ocean, when the temperature and salinity in the upper ocean layer are almost constant due to wind mixing. In this case the sound velocity increases with depth due to the hydrostatic pressure gradient.

An increase in the sound velocity can be observed from the surface to the very bottom in the Arctic and Antarctic regions, in Mediterranean seas in the tropical, and in shallow seas during autumn and winter. The typical profile $c(z)$ for the Arctic Ocean is schematically shown in Figure 24. The existence of a thin surface layer with very low sound velocity and a large sound velocity gradient is characteristic.

Kommentert [EH2]: Figuren viser vel ikke «caustics» med en tykk linje. Figuren viser bare «sound propagation path»? Jeg vet at det er noen gode figurer på caustics i Hovem 2012 i kapittel 6. For eksempel figur 6.17 eller 6.18 på side 143 i Hovem 2012.

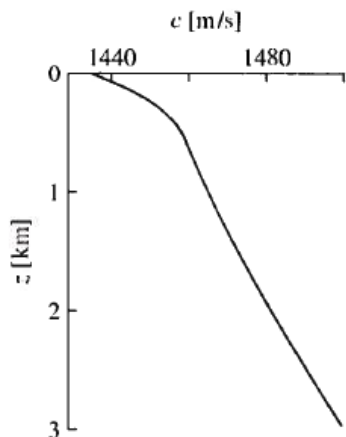


Figure 24: Typical sound velocity profile $c(z)$ for the Arctic Ocean (Brechovskich & Lysanov, 2003).

2.6.3 Antiwaveguide Propagation

The simplest kind of antiwaveguide propagation is observed when the sound velocity monotonically decreases with depth (Figure 25(a)). This is often the result of the intensive heating of the upper layers by solar radiation. The ray diagram is shown in Figure 25(b). All rays refract downwards. The ray tangent to the surface is the limiting one. The shaded area represents the geometrical shadow zone. For typical conditions in the ocean, the distance from the source to the shadow zone is only a few kilometres.

The geometrical shadow zone is not a region of zero sound intensity. In the ideal case shown in Fig. Figure 25 the sound energy does not penetrate into the shadow zone, but in the real case this will happen due to diffraction. In real cases sound waves reflected from the bottom and scattered by the random inhomogeneities of the medium also produce some insonification of this zone.

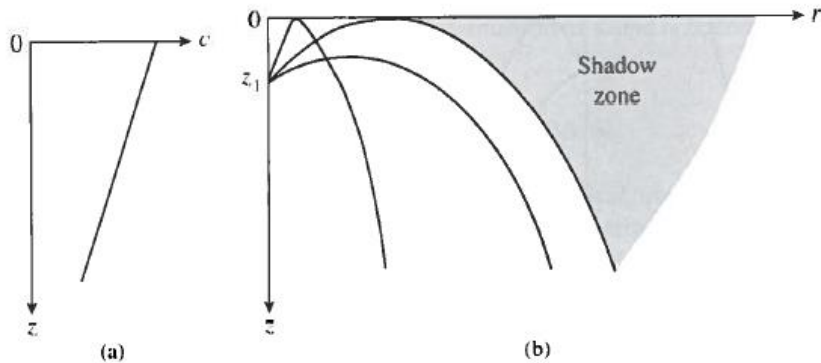


Figure 25: Formation of a geometrical shadow zone when the sound velocity monotonically decreases with depth (Brechovskich & Lysanov, 2003).

2.7 Deformation of underwater acoustic signals – Doppler Effect

The Doppler Effect corresponds to a shift of the apparent signal frequency after propagation, due to a change in the duration of the source receiver paths during transmission time, caused by the relative displacement of the source and the receiver, or the source and the target.

Let us consider a source transmitting Dirac-like pulses with a regular period T , towards a receiver at distance D . If D does not vary with time, the receiver gets each pulse after a time $t=D/c$. The period of the signal is therefore not modified, and the apparent frequency remains $f_0=1/T$.

Conversely, if D decreases (for example) with time as $D(t) = D - v_r t$, because of the relative speed v_r between the source and the receiver, the length of time between the pulses received will change too.

If the first pulse (transmitted at $t=0$) arrives at time $t_1=D(t_1)/c$, the second pulse (transmitted at $t=T$) arrives at time:

$$t_2 = T + \frac{D(t_2)}{c} = T + \frac{D(t_1) - v_r T}{c} \quad (2.11)$$

The time lag between the two successive receptions is then:

$$t_2 - t_1 = T - \frac{v_r T}{c} = T(1 - \frac{v_r}{c}) \quad (2.12)$$

instead of T . The apparent frequency of the signal is then modified:

$$f = \frac{1}{T(1 - \frac{v_r}{c})} = \frac{f_0}{\left(1 - \frac{v_r}{c}\right)} \approx f_0 \left(1 + \frac{v_r}{c}\right) \quad (2.13)$$

The frequency variation δf created by the Doppler Effect is thus:

$$\delta f = f_0 \frac{v_r}{c} \quad (2.14)$$

where v_r is positive when moving closer, negative when moving away. For an echo on the target, as the sound travels both ways, we get:

$$\delta f = 2f_0 \frac{v_r}{c} \quad (2.15)$$

The Doppler Effect complicates the processing of signals, particularly in communication and data transmission applications. But it can be put to good use for some applications. For example, its measurement can be used to determine the speed of a ship relative to the bottom or the water

column, or to measure the characteristics of a marine current. In Anti-Submarine Warfare (ASW), the Doppler shift is useful to track a target, and even identify it by measuring its speed.

2.8 Underwater Acoustic Noise

Noise is an important component of underwater acoustics, covering many different processes; all of which add to the expected signals and decrease the performance of underwater acoustic systems.

The causes of noise can be grouped in four categories (Figure 26):

- Ambient noise. This type of noise originates from outside the system, and stems from natural (e.g., wind, waves, rain, animals) or man-made (e.g., shipping, industrial activity) causes. It is independent of the sonar system or the conditions of its deployment.
- Self-noise. This is the noise suffered by an underwater acoustic system itself, when caused by the supporting platform (e.g., radiated noise, flow noise, electrical interference) or the system's own electronics (thermal noise).
- Reverberation. This type of noise affects only active sonar systems, as it is caused by parasite echoes (generated by the sonar's own signals). It can be so loud as to mask the detection of the expected target echoes.
- Acoustic interference. This type of noise is generated by other acoustic systems working in the vicinity, usually onboard the same ship or underwater platforms, sometimes from sources farther away.

From these definitions, we can see that the concept of “noise” is more related to its nature than to a specific acoustic content. Structurally, noise can correspond to very different waveforms: completely random in the case of ambient noise, diffuse echoes from the transmitted signal in the case of reverberation, or clearly recognisable signals for interference caused by other instruments.

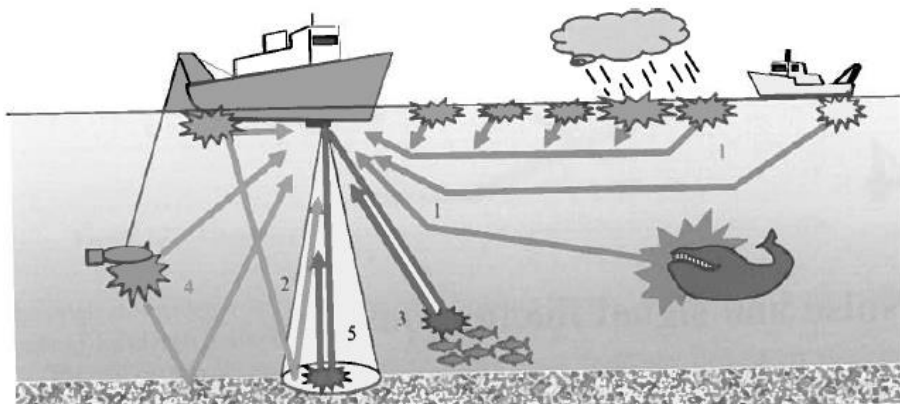


Figure 26: Types of acoustic noise affecting a hull-mounted sonar system: (1) ambient noise; (2) self-noise (from the ship); (3) reverberation; (4) acoustic interference (signals from other systems); (5) expected target echo (Brechovskich & Lysanov, 2003).

2.9 Propagation Losses

When acoustic waves propagate, the most visible process is their loss of intensity, because of geometric spreading (divergence effect) and absorption of acoustic energy by the propagation medium itself. This propagation loss (or transmission loss) is a key parameter for acoustic systems, as it will constrain the amplitude of the signal received, hence the receiver's performance, directly dependent on the signal-to-noise ratio.

2.9.1 Geometrical Spreading Losses

An acoustic wave propagating from a sound source will spread the transmitted acoustic energy on a larger and larger surface. As energy is conserved, the / intensity will decrease proportionally to the inverse of the surface. This process corresponds to the geometric spreading loss.

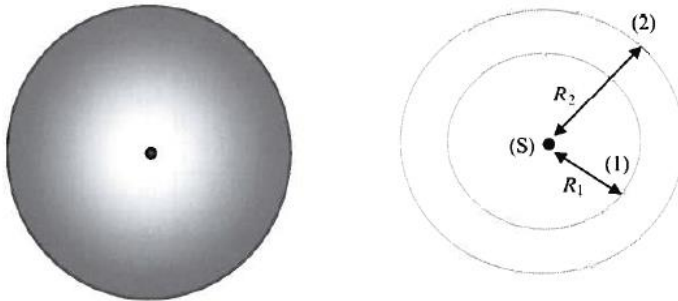


Figure 27: Spherical spreading: the acoustic intensity decreases with distance from the source, in inverse proportion to the sphere's surface ().

The simplest (and most useful) case is the homogeneous, infinite medium, with a small-dimension source radiating in all directions (point source). The energy transmitted is conserved, but will be spread over spheres of larger and larger radii (Figure 27).

The decrease in local acoustic intensity between points (1) and (2) (Figure 27) is inversely proportional to the ratio of the surfaces S_1 and S_2 , of the spheres:

$$\frac{I_2}{I_1} = \frac{S_1}{S_2} = \left(\frac{4\pi R_1}{4\pi R_2} \right)^2 = \left(\frac{R_1}{R_2} \right)^2 \quad (2.16)$$

where R_i is the radial distance from the source. Intensity decreases in $1/R^2$, and pressure decreases in $1/R$. The spreading transmission loss considered from the reference unit distance $R_{1m}=1m$ can be expressed in dB:

$$TL = 20 \log \left(\frac{R}{R_{1m}} \right) = 20 \log(R) \quad (2.17)$$

Equation (17) is the most common way of expressing the geometrical spreading transmission loss.

2.9.2 Attenuation Losses

Sea water is a dissipative propagation medium; it absorbs part of the energy of the transmitted wave, which is dissipated through viscosity or chemical reactions. The local amplitude decrease is proportional to the amplitude itself; the acoustic pressure then decreases exponentially with distance. This will add to spreading losses. Attenuation is quantified by an attenuation coefficient α , most often expressed in decibels per kilometre (dB/km).

Attenuation is often the most limiting factor in acoustic propagation. Its amount depends strongly on the propagation medium and the frequency. In sea water, attenuation comes from:

- the viscosity of pure water;
- the relaxation of magnesium sulphate ($MgSO_4$) molecules above 100 kHz;
- the relaxation of boric acid ($B(OH)_3$) molecules above 1 kHz.

Molecular relaxation consists in the dissociation of some ionic compounds in solution (e.g., $MgSO_4$ and $B(OH)_3$), due to local pressure variations created by the acoustic wave. This process is dominant for sound absorption in sea water. If the period of the local pressure variation is longer than the time necessary for the molecule to recompose itself (relaxation lime), the process is reproduced at every change and permanently dissipates energy. The attenuation due to this process appears at frequencies lower than the characteristic relaxation frequency of the relevant compound.

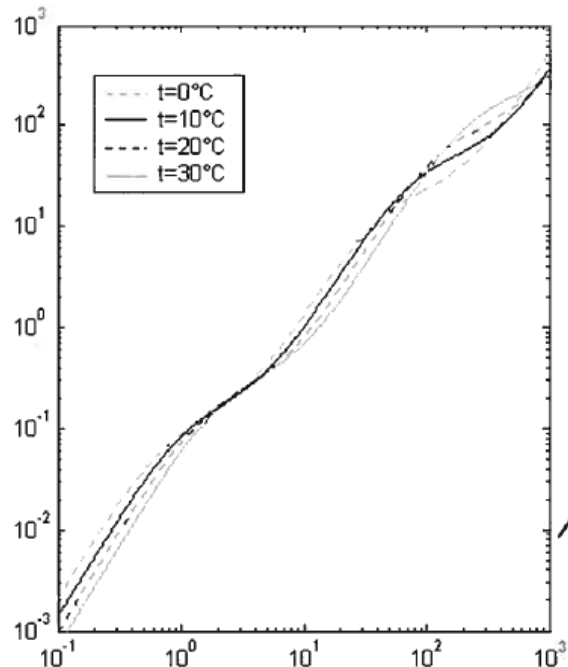


Figure 28: Sound absorption coefficient in sea water, as a function of frequency, for a salinity of 35 p.s.u., a depth of zero and different values of temperature (Brechovskich & Lysanov, 2003).

Ever since the beginnings of underwater acoustics, a high amount of attention has been brought to the modelling of absorption coefficients, and many models have been proposed. The model most used today was developed by Francois and Garrison. This model is shown in Figure 28; it explicitly uses temperature, salinity and hydrostatic pressure, as well as frequency. Based upon a large number of previous experimental results and theoretical studies, it is very complete and precise; its use is highly recommended. Figure 28 shows that attenuation increases very rapidly with frequency, and that the orders of magnitude are highly variable. For frequencies of 1 kHz and less, sound attenuation is of a few hundredths of dB per km, and is therefore not a limiting factor. At 10 kHz, a coefficient of around 1 dB/km forbids ranges of more than tens of kilometres. At 100 kHz, the attenuation coefficient reaches several tens of dB/km and the range cannot extend further than 1 km. Underwater systems using frequencies in the MHz range will be limited to ranges of less than 100 m, with an attenuation of several hundreds of dB/km.

2.9.2.1 Conventional Propagation Loss

Spherical spreading, corrected from attenuation, is systematically used as a first approximation when evaluating the propagation loss and the performance of under-water acoustic systems. In dB, the transmission loss reads:

$$TL = 20\log(R) + \alpha R \quad (2.18)$$

All systems using the echo from a target are undergoing propagation losses on the outgoing and returning paths; the total loss is therefore:

$$2TL = 40\log(R) + 2\alpha R \quad (2.19)$$

One must pay attention to the units used in Equations (18) and (19). R is expressed in metres, but α is most often expressed in dB/km. The units should be converted appropriately.

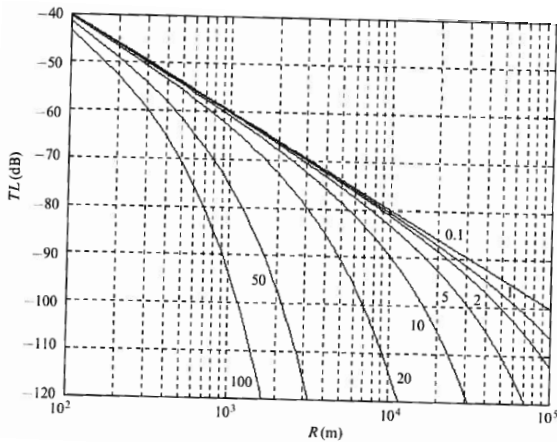


Figure 29: Conventional propagation loss $-TL = -20\log R - \alpha R$, as a function of range, for frequencies 0.1, 1, 2, 5, 10, 20, 50 and 100 kHz. The absorption coefficient α is calculated for ambient conditions: $T=10^\circ\text{C}$; $S=35$ p.s.u; $z=10$ (Brechovskich & Lysanov, 2003).

2.10 Acoustic Scattering

An acoustic wave propagating in the ocean will often "collide" with obstacles either in the water column itself (fish, plankton, bubbles, submarines) or at the limits of the medium (seabed and sea surface). These obstacles will send back to the sonar system some echoes of the signal transmitted, a portion of which will be perceived by the sonar system. These echoes will then be either desirable (if the obstacle is the target wanted) or undesirable (if they are jamming the useful signal). In all cases, understanding their properties is essential to the good functioning of the sonar system, either because the echoes need to be received in the best possible conditions, or because they need to be reduced or filtered out as much as possible.

Several distinct physical processes contribute to the formation of underwater acoustic echoes. The multiple paths studied in the previous chapter are associated with the well-known and rather intuitive reflection by plane interfaces (see Snell's law in previous lecture notes): the incident wave is reflected in a direction symmetrical to its direction of arrival (as with a mirror, hence the name of specular reflection), with a loss of amplitude. Reflection studies are therefore more particularly useful for underwater acoustic systems where the transmitter and receiver are distinct (data transmission or multi-static sonars), or for configurations where the propagation between the sonar and the target is prone to generate multiple echoes (when the propagation directions are close to the horizontal). Contrary to these reflections from the "average" bottom and surface, different types of echo are generated by local obstacles present in the water column or at the interfaces. Because of their shape, these irregularities scatter acoustic energy in all directions, and are therefore more likely to affect the signals received in any configuration. The scattering of acoustic energy back towards the sonar is called backscattering. Most sonar systems working in monostatic configuration (i.e., transmitter and receiver located at the same point) use backscattered echoes.

The convention of underwater acoustics is to call reverberation any return of energy towards the sonar system, coming from something other than the echo of the desired target. Surface and bottom reverberation (boundary effects due to backscattering of sound by the relief of interfaces) are traditionally distinguished from volume reverberation (volume effects due to backscattering from

fish, plankton, suspended particles or bubble clouds). The distinction between target echoes and reverberation is of course arbitrary and depends only on the type of system considered. For active detection military sonars, reverberation includes any echo that is not coming from a submarine; for example, echoes from the sea surface and the seabed. Conversely, mapping side-scan sonars will only use signals backscattered from bottom topography and obstacles; they will be perturbed by surface reverberation or volume reverberation from fish schools or plankton. And fisheries sonars will instead be designed specifically to target these.

2.10.1 Echo from a target

Most underwater acoustic systems are designed to receive echoes from targets. The latter are highly varied in nature and in structure: seabed insonified at normal or oblique angles of incidence, single fish or entire schools, submarines, objects laid on the bottom (mines, shipwrecks), buried objects (natural, like sedimentary layers, or artificial, like pipelines), etc. The incident acoustic wave will be scattered by the target in all directions of space, and a portion will be scattered back towards the transmitter. The target acts as a secondary source retransmitting the acoustic wave.

Two types of target will be envisaged. First are the targets with dimensions small enough to be completely insonified by the sonar beam and signal (Figure 30, A, B). They behave as "points": their strength is an intrinsic strength, independent of the distance to the sonar or its characteristics (beam width, signal duration). Conversely, other targets will be too large to be ensonified completely at once by the same beam (e.g., large fish schools, seabed or sea surface) (Figure 30, C, D, and E). The strengths of these targets will depend on their geometric intersection with the sound beam. The target strength is no longer a point value, but uses the insonified space (surface or volume), associated with a surface or volume backscatter coefficient. The latter is therefore an expression of the amount of energy scattered by a "unit scattering element". It is therefore expressed in dB re 1 m² or dB re 1 m³, respectively. The backscattering strength depends on the incidence angle and the frequency, and will be specific to the processes observed.

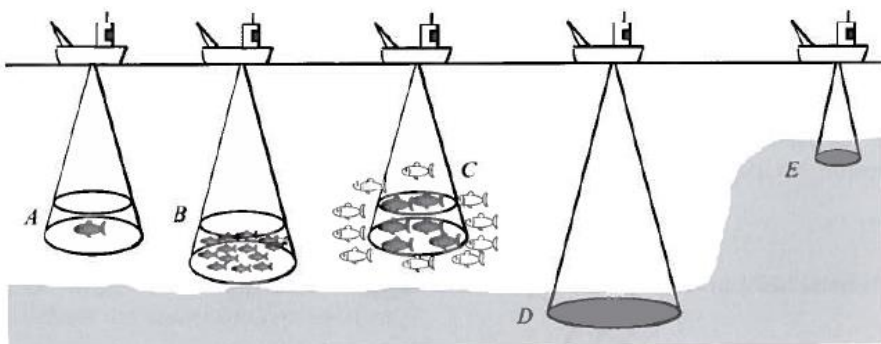


Figure 30: Examples of point targets (A, B) and extended targets (C, D, E) (Brechovskich & Lysanov, 2003).

2.10.2 Target Strength

The target strength TS is defined as the ratio (in dB) of the intensities of the back-scattered and incident waves:

$$TS = 10 \log \left(\frac{I_{bs}}{I_i} \right) \quad (2.20)$$

It is therefore the relative amount of energy sent back by the target towards the sonar. It depends on the physical nature of the target, its external (and possibly internal) structure, and the characteristics of the incident signal (angle and frequency).

2.10.3 Directivity Index (DI)

In order to increase accuracy and resolution sonars that are creating acoustic waves will concentrate the acoustic energy in one desired direction. This cause more of the acoustic power to be directed towards the target. When the acoustic signal is reflected from the target the intensity of the signal will be stronger, compared to an omnidirectional source, since more acoustic energy is directed towards the target, and the reflected signal will thus be easier to detect. The directivity index can be calculated by dividing the intensity of the beam at $I(\theta = 0)$, with the intensity of an omnidirectional source of equal total power. The directivity factor is defined according to the following equation (Lurton, 2002).

$$D = \frac{I(\theta = 0)}{I_{ref}} \quad (2.21)$$

In order to obtain the directivity index, the directivity factor is converted to decibel scale according to the following equation

$$DI = 10 * \log(D) = 10 * \log \left(\frac{I(\theta = 0)}{I_{ref}} \right) \quad (2.22)$$

The directivity index of some simple transducer types can be seen below

Transmission or reception (one-way configuration)	Linear, length $L > \lambda$	Disc, diameter $D > \lambda$	Rectangle, sides $a, b > \lambda$
Directivity pattern $D(\theta)$	$(\sin A/A)^2$ $A = (\pi L/\lambda) \sin \theta$	$(2J_1(A)/A)^2$ $A = (\pi D/\lambda) \sin \theta$	
Directivity index DI (dB)	$10 \log(2L/\lambda)$	$20 \log(\pi D/\lambda)$	$10 \log(4\pi ab/\lambda^2)$
Main lobe width $2\theta_3$ (°)	$50.8\lambda/L$	$58.9\lambda/D$	
First sidelobe level (dB)	-13.3	-17.7	
Equivalent aperture Φ (rad)	λ/L	$1.08\lambda/D$	
Equivalent solid angle Ψ (sr)	$2\pi\lambda/L$	$(4/\pi)(\lambda/D)^2$	$\lambda^2/(ab)$

Figure 31: Directivity characteristics for simple antenna types, for one-way transmission or reception (not both ways). The angle theta is relative to the normal of the antenna. Expressions are approximations valid for small angular apertures (Lurton 2002).

2.10.4 Detection Threshold (DT)

Sonar systems must be able to distinguish between the ambient noise and the signal it is "listening" for. For this to be possible, the signal level must be larger than the noise level, otherwise the signal will be indistinguishable from the ambient noise. For the sonar to detect the signal, the returning signal must be some level higher than the ambient noise. This is the detection threshold. We can therefore write the following requirement in order for the signal to be detected, according to (Lurton, 2002) :

$$EL \geq NL + DT \quad (2.23)$$

Where EL is the echo level, NL is the noise level and DT is the detection level. The value of the detection level can be determined on the basis of statistical requirement and can be found by use of ROC curves.

2.11 Sonar Equation

It appears interesting to regroup all the terms from the sections 2.9.2.1 and 2.10.2 in a single equation so as to be able to calculate the performance of a system. The sonar equation is adapted for this type of approach, and it expresses the intensity EL of the echo received by the sonar system after backscattering:

$$EL = SL - 2TL + TS = SL - 40\log(R) - 2\alpha R + TS \quad (2.24)$$

For a system that is noise limited the following equation must be satisfied for a successful detection

$$EL - DT \geq NL \quad (2.25)$$

Where DT is the detection threshold and NL is the noise level. We find the detection threshold that yield maximum range for our sonar as

$$DT = SL - 2TL + TS + NL \quad (2.26)$$

where SL is the level transmitted by the source (source level).

The limit of performance of a system is reached when the echo level of a target cannot be detected i.e. when this level is lower or similar to the level of the noise which is also recorded on the equipment: in that case the useful signal (echo) cannot be distinguished. The range limit is then reached for the considered target and the system used. With a noise level NL, it is generally considered that the limit range is obtained when:

$$EL = NL + 10 \text{ dB} \quad (2.27)$$

The lower the noise, the lower can be the EL and, with a determined target and equipment, it is possible to increase TL and thus R. For a given NL, the range will also increase according to the reflective qualities of the target or the performances of the system.

Kommentert [EH3]: Er denne formelen korrekt? Jeg får:
 1. $DT = SL - 2TL + TS - NL$ Eller 2. $DT = SL - 2TL + TS - RL$, Der $NL = NSL + 10\log B - DL$, slik at i 1. får vi $DT = SL - 2TL + TS - NSL - 10\log B + DL$, så enten må NL være med eller DL , og enten NL eller RL

Kommentert [EH4]: Er denne formelen korrekt? Jeg får:
 1. $DT = SL - 2TL + TS - NL$ Eller 2. $DT = SL - 2TL + TS - RL$, Der $NL = NSL + 10\log B - DL$, slik at i 1. får vi $DT = SL - 2TL + TS - NSL - 10\log B + DL$, så enten må NL være med eller DL , og enten NL eller RL

2.12 Basic Sonar Principles

Figure 32 shows the basic elements of any active sonar system, from a simple depth sounder to a sophisticated side scan sonar. It is in the detail of the design and implementation of the various components that systems differ. An active system is distinguished from a passive one in that it transmits sound and listens for the returning echoes from objects. A passive system does not produce any sound of its own, but simply listens to the sound which is present in the medium.

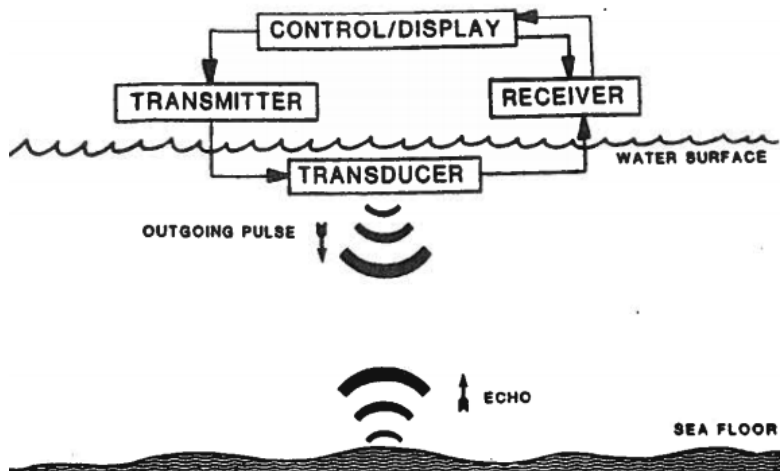


Figure 32: Basic sonar system elements (Lurton, 2002).

At the heart of any acoustic detection system is the transducer. The primary function of the transducer is to transform electrical energy into sound energy while emitting and inversely when receiving an echo. In a similar way to how loudspeakers and microphones are used in the air, they convert acoustic energy into electric energy, and vice versa. Most of the time in acoustic detection equipment, the same transducer is used to emit and receive the signals. Underwater acoustic sources are called projectors (equivalent to loudspeakers). The reception transducers are called hydrophones (by analogy with microphones). Extended transducers are named antennas, or arrays. The last name is usually reserved for structures made up of several elementary transducers. A transmitter is made up of a projector and its associated low-level electronics (preamplifiers and filters).

Underwater acoustic transducers can call on several physical processes to generate or receive sound waves. Most of them use the piezoelectric properties of some crystals, natural or artificial (ceramics). Natural piezoelectric crystals (such as quartz) were used in the early days of underwater acoustics. Such crystals are now replaced by synthetic ceramics. They are made by mixing components under high temperature and high pressure. The resulting material is then machined to the dimensions required and coated with metal. The ceramics produced is not spontaneously polarised; this is created artificially by applying a very intense electric field to induce a remanent polarisation. The piezoelectric crystal changes its physical shape when a voltage is applied across it.

It converts the oscillating electric field produced by the transmitter into a mechanical vibration. This vibration is transferred into the water as an oscillating pressure, the sound pulse. When receiving sound pulses, the piezoelectric material is stressed by the sound waves which in turn generate an electric potential between its sides.

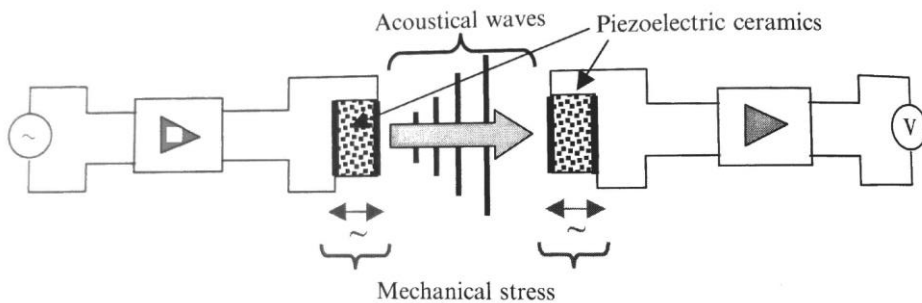


Figure 33: Piezoelectric effect: (left) transmission: applying an electric signal to a piece of piezoelectric material induces a mechanical deformation, generating an acoustic wave; (right) reception: the mechanical stress caused by the acoustic wave is transformed by the piezoelectric material into an electric voltage (Lurton, 2002).

When transmitting, underwater transducers generally work around their resonant frequency, to yield the best output level achievable. But it is often possible to look for a compromise with a bandwidth broad enough to pass several close frequencies, or a wide-spectrum modulated signal. The receiving transducers used in sonars generally work around their resonance regime. However, hydrophones that are used for laboratory measurement are wideband devices.

Finally, directional transducers are often preferred, as specific directions of transmission and/or reception can be achieved and controlled. The directivity pattern of an antenna can be obtained either from the transducer geometry or from signal processing with an array of elementary transducers. These characteristics are paramount to the correct operation of sonar system. They control both the signal-to-noise ratio of the measurement (via the directivity index) and the target angle estimation, essential in many sonar systems.

It is the transmitter which produces the oscillating electric field, which is turned into a mechanical vibration by the transducer. As the returning acoustic echo is converted into electrical energy by the transducer, the receiver detects and amplifies it. This has to be done since the electrical signal produced in the transducer is usually weak, and must be amplified several thousand times before being passed on to the recorder. The operator can select the receiver gain, so as to visualize the desired echo levels. There must also be some master unit which performs the control function, regulating the precise timing that is required for the various elements to synchronize their operations. The recorder is part of this control function and has three primary functions: convert time into depth, display the received data and give some memory by keeping the echoes displayed during some minutes.

2.12.1 Beamforming

Acoustic systems will always use many transducers together in a line array or plane of transducer. The acoustic signal produced from one transducer will propagate away from the transducer in a spherical way. When several transducers are used the transmitted or received signal from each individual transducer are coupled. We will see that this allows us to design the created sound field, where some area have large sound intensity, that we call the beam. By using sonars to create beams of sound intensity we are able to obtain higher performance, than what would otherwise been possible.

The acoustic field created by a number of sources (in our case transducers) can be calculated by summing up the contribution of all separate elements, by the use of the superposition principle. Since all individual transducer produce an oscillating sound field, the resulting sound field will consist of region with increased intensity and regions with reduced acoustic intensity. To illustrate this we will consider a typical line array. A line array is a line of transducers, with length L . The strength of the transducers along the line can be characterised by a source strength function $q(x)$ per length unit. It can be shown, (Lurton, 2002), that the beam pattern for such an array will be

$$B(\theta) = \int_{-L/2}^{L/2} q(x) * \exp(i\kappa x \sin(\theta)) dx \quad (2.28)$$

In the equation above $B(\theta)$ is the beam pattern, θ is the angle from the normal of the line array. x is a variable along the length of the array, while κ is the wave number. It is assumed that the integral of $q(x)$ over the length of the array equal to unity. From the equation above, it is apparent that the transmitted beam pattern $B(\theta)$ is dependent on the source strength distribution. If we consider the simplest possible source strength distribution, a constant distribution, it can be shown that the beam pattern will be

$$B(\theta) = \frac{\sin\left(\pi \frac{L}{\lambda} * \sin(\theta)\right)}{\pi \frac{L}{\lambda} * \sin(\theta)} \quad (2.29)$$

We can see that this uniform source strength yields a beam pattern on the form $\sin(x)/x$. We can observe that the beam pattern, that illustrate the intensity of the acoustic pressure, have a peak at $\theta = 0$, that is called the mainlobe. Several secondary maxima or sidelobes can also be observed. There are two parameters that are of value to consider. These are the width of the mainlobe $\Delta\theta$ and the intensity of the first sidelobe. In order to achieve good resolution for the sonar, we want the beam we emit to be as small as possible, and thus reducing the width of the mainlobe is desired. We also want to achieve low value of the sound level for the sidelobes, since these are usually unwanted, and cause noise that deteriorate the performance of the system. The beamwidth can be approximated, (Hovem, 2012), as

$$\Delta\theta \approx \frac{\lambda}{L} \quad (2.30)$$

when the uniform source strength distribution is used. From this we can see that we can obtain smaller beamwidth in two ways. Either by reducing the wavelength of the acoustic wave. As we saw in section 6.2, reducing wavelength strongly affect the attenuation coefficient, and thus reduce the

Kommentert [EH5]: Kansje legge in figur 9.4 på side 236 fra hovem 2012 for å ilustrere dette.

Kommentert [EH6]: Foreslår å legge in en figur som viser denne beam pattern eks figur 9.5 fra hovem, eventuelt har jeg jeg lage en tilsvarende i matlab

range of the sonar. We can therefore conclude that a sonar operating on a very high frequency will have short range but high resolution. The beamwidth can also be reduced by increasing the length of the sonar. There are however limitation to how large the transducer can be. The vessel carrying the sonar will be of limited size, and large transducer array will also increase the cost. The discussion of the line array can also be extended to cover two dimensional arrays, where similar results are obtained. The reader is referred to (Hovem, 2012) for such a discussion is covered.

It is also worth noting the relation between the beamwidth and the directivity index described in section 7.3. Recall that the directivity is defined as the ratio between intensity at $\theta = 0$ and a reference intensity. From this, we can see that a smaller beamwidth with higher intensity will give larger directivity index.

2.12.2 Sonar resolution

On the basis of the previous discussion we can now define two type of resolutions that are relevant for sonars. The angular resolution is according to (Mazel, 1985) defined as the sonar system's capability to distinguish between two equally strong targets at the same distance but with a small difference in bearing. In order to distinguish between two targets the distance between them must be equal to or larger than the beamwidth. Smaller beamwidth will therefore provide better angular resolution. The second relevant resolution is the range resolution. The range resolution is defined as the ability to distinguish between two equally strong targets at the same direction, but with a small difference in distance. For this to be possible the echo from the two targets must not overlap at the time of arrival at the receiver. A sonar with the pulse length ΔT , the range resolution Δr can be calculated as:

$$\Delta r = \frac{c * \Delta T}{2} \quad (2.31)$$

c is the speed of sound. From the equation above we can see that range resolution improves when the acoustic pulse gets shorter. Range resolution can also be improved by applying modulated pulses, like frequency modulated pulse (FM). If the modulated pulse have a bandwidth B , the range resolution will improve with increasing bandwidth.

3 Applications of Underwater Acoustics

Today, underwater acoustics are used in various applications such as navigation, military, fishery, mapping and geology, physical oceanography and underwater intervention. Some of these applications of underwater acoustics is presented in this chapter with emphasis on sonars and echo-sounders.

3.1 Single-Beam Echo Sounder

The vertical single-beam echo sounder is a widely used underwater acoustic system, often found in the fishery industry. The transducer of the echo sounder is installed on the ship hull and fixed. The acoustic beam is orientated downwards and only explore the water volume under the vessel (Figure 34). It is used to detect and locate fish schools, and even isolated individual targets. The single-beam echo sounder system consist of the basic acoustic system components presented in chapter 2.12.

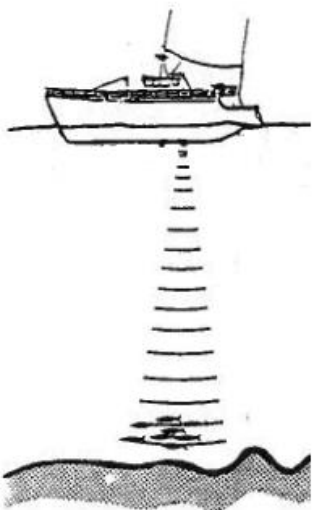


Figure 34: Active detection equipment on a vessel: single-beam echo sounder (Hovem).

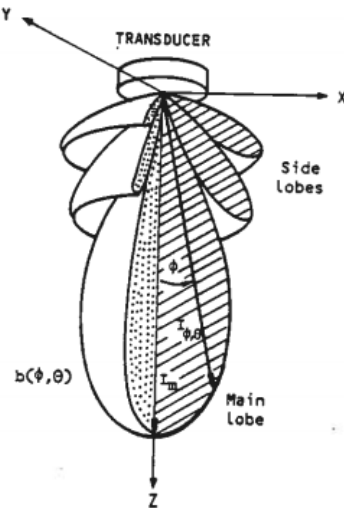


Figure 35: 3D view of the directivity pattern of a circular transducer (Hovem).

The echo sounder system do not actually measure depth or distance. What they are really measuring is the time it takes for the transmitted acoustic pulse to travel from the transducer to the target and return. The accuracy depends on the system's ability to measure this time precisely. We are not really interested in time, though, but in distance. The range is related to the travel time by the speed of sound in the water. One should keep in mind that it is the two-way travel which is measured, and this must be accounted for when determining the distance.

The transmitter generates an electrical pulse at the particular frequency for which the transducer is designed. The typical frequencies of the echo sounders used in fisheries applications range between 20 and 200 kHz. Each constructor have more or less his standard frequencies. The electrical power of the pulse produced by the transmitter is an important feature of any echo-sounder and it may vary

from a few watts up to several kilowatts. It is important to note that the indicated transmitted power is not always a proper measure of the sound energy transmitted into the water. It also depends on the efficiency and the directional pattern.

The pulse duration depends on the nominal frequency of the echo-sounder but for each equipment generally many durations can be chosen. For high frequencies, pulses as short as 0.1 ms can be used while for middle frequency it is necessary to increase these duration up to at least 0.5 ms. On vertical echo sounders, a maximum duration of 5 ms is generally proposed but it is better to use a short one: the longer the pulse is, the larger is the equipment resolution. However when long ranges are requested, it is necessary to increase the pulse duration so as the echo energy, coming back after a long distance covered, i.e. with a level deeply reduced by the propagation losses, remains high enough. On some equipment the duration is automatically switched according to the range in use.

The transmitter ping rate varies according to the range used: before emitting a new pulse, it is necessary to wait that all the multiple echoes are low enough. A rough adopted value is 3 times the necessary time for the sound to come back from the maximum range. It means a ping of 0.4 per second for 100 m range increasing to 0.8 for 200 m and to 2 for 500 m.

It has been mentioned previously that the transducer transforms electrical energy into sound energy, and vice versa. An additional function of the transducer is to concentrate the sound energy into a beam. The beam opening depends on the frequency and dimensions of the active transducer face. It is very variable and stands between 5° and about 30°. There are different shapes: a circular one which produces a conical beam width (Figure 35) and a rectangular one, the main advantage of which is to offer two different openings. The roll angle being greater than the pitch one, the beam is generally larger athwartship than alongship without decreasing too much the global beam directivity. The possibility of changing the beam width is also very common and done by exciting all the elements or only part of them. Such a transducer is called a dual beam one and is used for instance for adapting the beam opening to the vessel movements. With transducer stabilization, the beam angle can be reduced compared to cases without stabilization. Before, it was done mechanically, the transducer installed on a stabilized platform, but now the stabilization is electronically made. Each group of elements is connected to a separate transmitting and receiving channel excited in a controlled mode according to information related to the vessel movements. The result is a beam always perfectly vertical whatever roll and pitch. The possibility of angle reduction gives a better directivity. It is very profitable for deep sounding as it increases the equipment performances and also as, in this case, the vessel movements, during the few seconds necessary for the echo to come back from a distant target, may have changed the beam orientation pointing in a direction different from the emission.

The maximum power emitted by a transducer cannot be increased indefinitely: it is limited by the cavitation which appears, under normal conditions of temperature and near the surface, at about 2 W/cm². This value increases with the operating depth: 5 W/cm² at 200 m. Practically, for fisheries operations the electrical power reaching the transducer stands between 100 W and about 5 kW. The higher values are used with large low frequency transducers and on most equipment two power levels are offered.

3.1.1 Transducer Placement

The positioning and installation of the transducer are often decisive to ensure proper performances. Normally the transducer should be placed between one third and one half of the vessel length from

the bow and, on ordinary shaped hulls, approximately one meter away from the keel. The ideal position of the transducer is at the deepest, and at the same time most noise free point of the vessel. This point may be difficult to determine since the propeller noise and the noise produced by the flow of the water along the hull may vary with the trim and the speed of the vessel. As the propeller and the rudder are the most important sources of noise, the transducer must be placed away from them. Neither the transducer should be too close to the bow as the vertical movements in this place could interfere with the quality of the recordings, the transducer position being the zero reference. In bad weather, sound energy may also be totally refracted by the highly accelerated water thrown under the ship in this way and this is an additional reason for a position not too close to the bow.

The transducer is usually housed in a streamlined blister to reduce water noise and turbulence. The surface of the transducer should always be tilted about 2° forward in order to prevent turbulences on the transducer itself. It produces also an effect of shadowing from the propeller noise. In some cases, it is recommended to put a brim around the blister so as to prevent the bubbles, running in the water flow near the hull, from passing on the transducer active face. On the other hand, some constructors recommend, when the hull shape and profile have been specially studied so as to avoid bubbles in the fore part, to mount the transducers flush. In this case the turbulences are reduced compared with the blister solution but it is worst when the flow is aerated.

All this means that it is not easy to determine the ideal position and installation for a transducer on a vessel and a good practical experience is needed. In many cases the performances of the equipment depends of the success or not of the hull installation of the transducer. If great performances are expected from the equipment - very deep sounding for fish for example - test in specialized tanks must be done so as to determine the best hull shape for a quiet water flow and then choose the ideal position. In many cases, bulbs and bow thrusters (at least without closing doors) must be avoided as they generate bubbles.

3.1.2 Receiver

The electric signal must be amplified before being sent to the recorder. In most modern echo-sounders, an automatic sensitivity control is adjusted to compensate for the depth dependence of the echo level. The strength of an echo is thus independent of depth and dependant only from the target strength of the reflecting object. This type of depth adjusted amplification is called Time Varied Gain (TVG). As the propagation losses increase rapidly with the frequency and as the dynamic range of the receiver amplifier is limited, the TVG range is generally depending of frequency.

Most echo-sounder receivers are also equipped with a threshold device which function is to cut down weak echoes. The operator can thus, for example within the TVG range, choose to record only the strongest echoes corresponding to the desired targets, weak echoes produced by the noise or by organisms like plankton being removed.

3.1.3 Echogram Interpretation

The echo image, also called an echogram, will be displayed on a screen and provides visualization of the results from the echo-sounder for interpretation. The vertical extension on the screen corresponds more or less to the height of the target while the horizontal one is in relation with the time of recording, i.e. the length of the target if the vessel is moving.

The first problem encountered when observing an echogram is the great dissimilarity between the vertical and horizontal scales of representation. The vertical scale is a function of the screen width and the range used, which is generally well defined. For the horizontal case, the scale generally depends on ping rate and the vessel speed. In some configurations, there is a possibility of having a high ratio between the two scales, the result being a great distortion in the echo representation. This causes an increase in bottom slopes and the shapes of the fish schools appear quite always higher than wider, which is not the case in the reality (Figure 36).

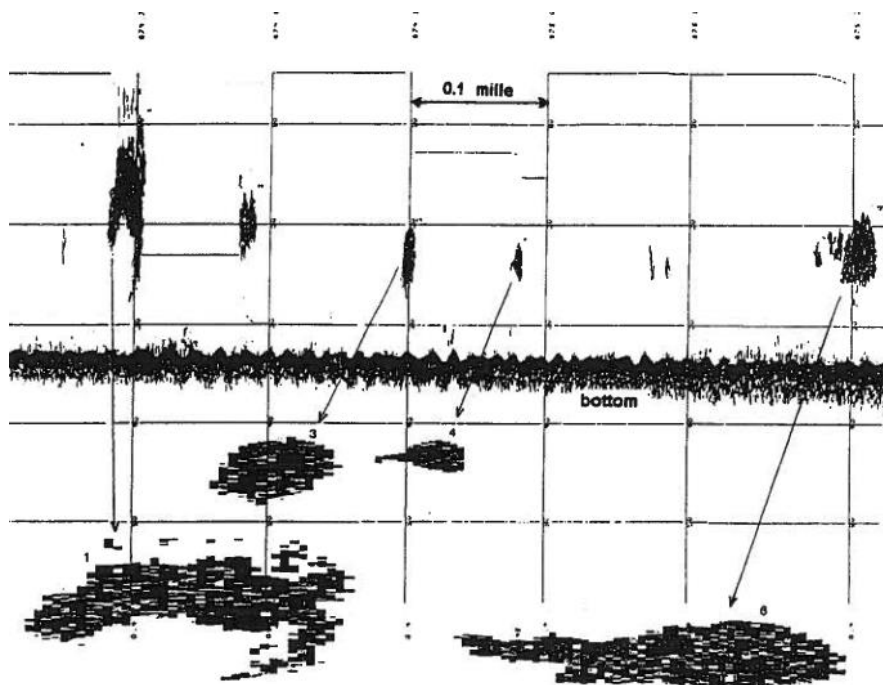


Figure 36: Echogram of some schools: -upper part: as really recorded on an echo-sounder, -lower part: corrected pictures with the same vertical and horizontal scales (Hovem).

Another important point is the vertical resolution is not constant but depending on the pulse duration. The representation of the same aggregation of targets can thus be quite different according to the pulse length (Figure 37).

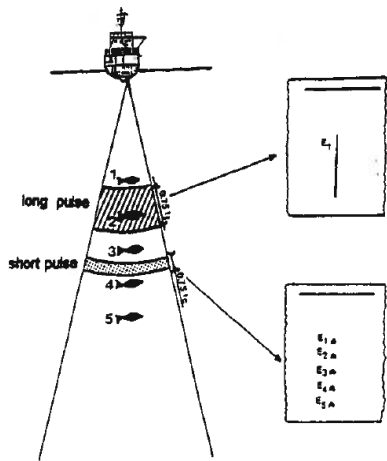


Figure 37: The vertical resolution is depending of pulse duration. A short pulse give as many echoes as target while a long pulse produces only one (Hovem).

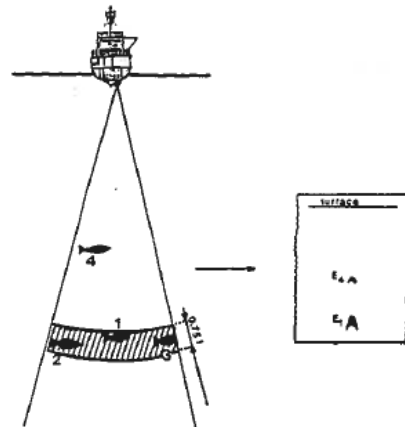


Figure 38: The width covered by the beam increases with depth. Targets 2 and 3 are detected even really under the vessel. Within one pulse length, 1,2 and 3 produce only one echo (multiple) while produces a single one (Hovem).

The horizontal resolution is depending of the beamwidth, the target position under the vessel being determined within the precision of the beam angle Θ . The width covered by the beam increasing with the depth, a target can be detected even if it is not exactly under the vessel (Figure 38). The result is a great position uncertainty increasing with depth and beam angle: at a depth of 200 m using 15° beam, this width is more than 50 m. This may also induce some uncertainties in bottom profile determination. If the beamwidth exceeds the dimensions of some bottom hole, they cannot be really detected (Figure 39 and Figure 40).

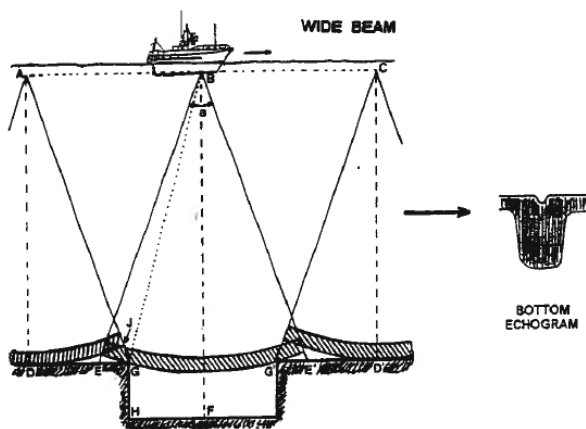


Figure 39: Using wide beam, some bottom holes cannot be really detected (wide beam) (Diner).

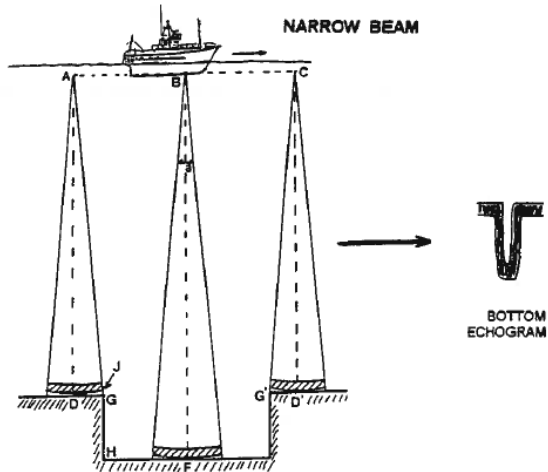


Figure 40: Using wide beam, some bottom holes cannot be really detected (narrow beam) (Diner).

Recording fishes or other targets close to the bottom is not easy first because of the bad distance resolution due to the pulse duration. Secondly on the sides of the beam, the fish echoes will also be obscured by the stronger bottom echo returning from the central part of the beam which is closer to the transducer. The field in which fish echoes are obscured is called the dead zone. When the bottom is uneven or sloping deeply the dead zone will increase (Figure 41).

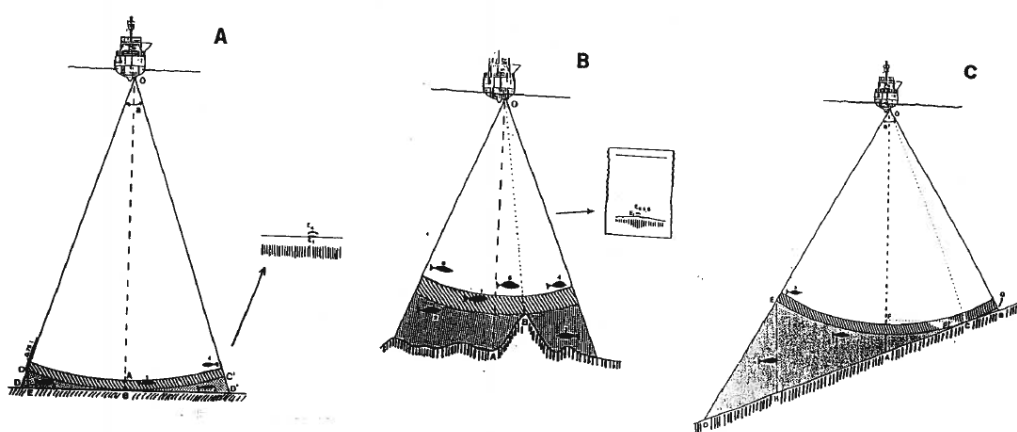


Figure 41: Principles of the dead zone (grey) which volume increases very much on rocky bottom (B) or in presence of a slope (C) () .

3.1.4 Typical Echoes

On a vertical echo-sounder, information on the bottom are first requested by the user. The bottom echo appears on the echogram as a continuous thick line. The bottom echo level is very high so it is represented on the screen by the more intensive colour (red ordinary). When the scale range of the recorder is large enough, it is possible to obtain another line, parallel to the bottom echo, which is the second bottom echo. It is caused by part of the sound having done a double trajectory between surface and bottom. Besides depth, which is easy to read on the recorder, the echo-sounder can give information on a number of characteristics of the sea bed itself. The most important of these characteristics are whether it is smooth or rough, soft or hard and how it slopes. This requires some practical experience and also a good setting of the equipment.

Between surface and bottom, there are many targets that can be detected by an echo-sounder. Firstly, the fishes produce quite typical traces. A single echo is obtained when there is only one fish constituting the target, i.e. only one fish in a volume - called sampling volume - constituted inside the beamwidth by a disk with thickness same as the acoustic pulse length. Generally they appear as dots or points, the wider the beam the longer will be the individual traces. Especially with wide beam or at great depth, these single echoes appear under the form of an inverted V. Single echoes are mainly obtained during nighttime when the fishes are very scattered.

When the fish density exceeds the limit of resolution of the echo-sounder, the records overlap to form a continuing trace which may appear as a layer or as a distinct solid blot. When the schools are very dense, the returned signal may be as high so as it blocks the receiver like the bottom echo and produces a white line. A typical feature of dense pelagic schools is their echo length or "comet tail" due to multiple reverberation inside the school. In this case it is obvious that the vertical extension of the echo recorded is bigger than the real school height. The different records obtained from different species of fishes are more or less in relation with their specific behaviour. This is why the eye of an experienced fisherman is able to differentiate between many species by observing the echo-sounder records: shape and volume of the school, density, relative vertical position.

In addition of the layer type fish traces caused by schools as described above, other types of diffuse layers traces are also commonly produced by dense concentrations of smaller organisms, for instance small fish species, larvae and plankton. They are often associated with a discontinuity layer (temperature, salinity) in water column and appear as finely grained clouds or layers which may cover large areas. Such layer traces are produced by organisms whose individual reflecting ability is close to or under the detectable limits of the echo-sounder. But when occurring at high densities, they give characteristic diffuse traces called scattering layers or deep scattering layers (DSL).

3.2 Multi-Beam Echo Sounder

The multi-beam echo sounder is in many ways an extension of the single-beam echo sounder. Instead of transmitting and receiving a single vertical beam, the multi-beam sounder transmits and receives a fan of beams with small individual widths across the axis of the ship. The immediate interest is the possibility of multiplying the number of simultaneous depth measurements (typically 100-200), sweeping a large corridor around the ship's path.

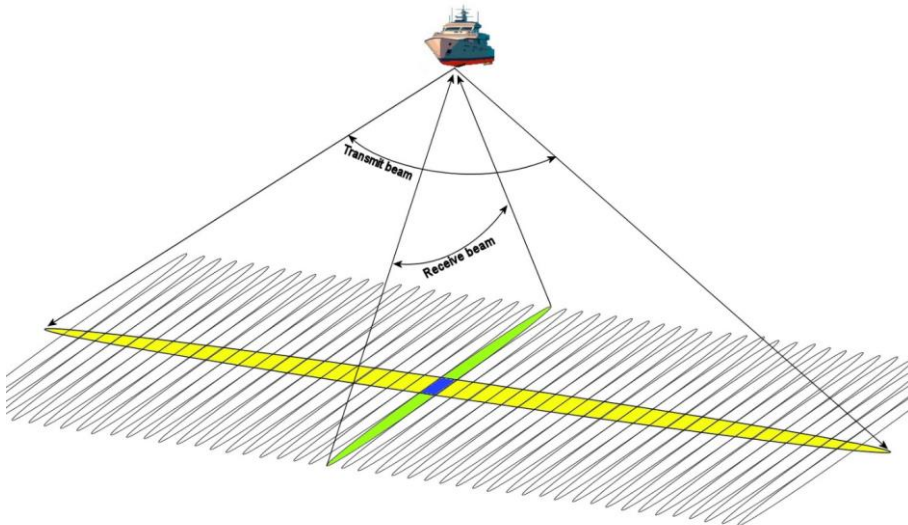


Figure 42: Multi-beam sonar footprint. The transmitted acoustic beam is narrow along track and wide across track. There are many received beams but each one is along track and narrow across track (Diner).

Multi-beam echo sounders have become very popular and are mainly used for sea floor mapping operations. Generally speaking, there are three main categories of multi-beam echo sounders:

- Deepwater systems (12-30 kHz): for regional mapping. Due to the large dimensions of the arrays used, this type of system is limited to larger vessels.
- Shallow-water systems (100-200 kHz): for mapping of continental shelves. Often used for hydrography.
- High-resolution systems (300-500 kHz): for local studies such as locating shipwrecks and inspection of underwater installations. The small dimensions of the system enables installation on AUVs and ROVs.

The multi-beam echo sounders are used to measure multiple depths from one transducer array. The depths are measured along with a swath fanning out from the transducer array. Multi-beam echo sounders are characterized by the following parameters:

- frequency, typically ranging from 12 to 500 kHz
- swath sensor/swath width, typically ranging from 90° to 180° (2 to 12 × water depth). Accuracy generally degrades with higher swath widths. For accurate measurements, swath widths are normally limited to 4 times the water depth (120°)
- beam width, typically ranging from 0.5° to 3°
- range resolution, depending on depth, best resolution 1-15 cm.

An acoustic signal is sent from the transducer to the bottom. Depending on the type of multi-beam, this signal will cover the entire swath, or just part of it. The signal reflects on the bottom and returns

back to the transducer. Three types of principles are used for determining the direction from which signals are returned. Sometimes a combination of principles is used to determine the direction:

- interferometric detection
- amplitude detection
- phase detection.

3.3 Sonar

Like the vertical echo-sounder presented section 3.1, the transducer in a sonar system is also on the hull. The difference is the possibility of orientating the acoustic beam. Sonar operates in much the same way as an echo-sounder and has the same four main components: transmitter, transducer, receiver and recorder (display). The functions and performances of each component is basically the same as described in section 3.1. However, the essential sonar particularity is to use an orientable beamwidth involving a special installation for the transducer. The transmission which deviates from the vertical, induces also some differences mainly on the types of received echoes.

Because the transmission is more or less horizontal, pitching and rolling the vessel is very important and a sufficiently wide beam is required. Practically beam angles less than 10 ° are not used and 12-15° are very common. The sonar beam must be able to move in azimuth and should also be tiltable usually from about + 5°, i.e. slightly towards the surface, to - 90°, i.e. down to the sea bed like an echo-sounder. Some years ago that was done mechanically, but now it is made electronically. The transducer overall shape is generally spherical and composed of several elements, up to 250 for sophisticated sonars. In order to avoid the turbulent layer and aerated water along the hull, and also not to be partially blinded by the keel, the transducer is lowered to about 1 m below the vessel bottom when in operation. A special raise/lower mechanism is used for that and when not in use, the transducer is raised in a special well in the hull. In the case of sonar, positioning the transducer on the hull is not a simple problem as very high performances are expected. That means low noise levels and few turbulences and bubbles. It is the reason for what some constructors propose streamlined domes composed of special material transparent to the sound energy. The turbulences around the sonar transducer are thus reduced and the equipment can be used at higher vessel speeds.

The controls of the transducer are usually mounted with the recorder in the wheelhouse console and the operator can command directly there and get information of all the beam orientation changes. More elaborate sonars have in addition automatic pre-set training programmes for the transducer, which may be by steps or continuous. Some functions offer also the possibility of an automatic pointing of the beam towards a preselected target. In a stepped training system, the beam is held in the transmitting position to allow reception of all the possible echoes from the range scale selected. The total time between 2 transmissions depends on the range and should be adjusted to suit the actual obtainable sonar range. For long range, it takes many several minutes at the exploration of for instance the whole 180° sector in front of the vessel, which is very long. In presence of very fast swimming fishes it is thus quite difficult to follow an echo and not to lose it when using a single beam equipment. So there exist now multibeam or omnidirectional sonars which, in one transmissions explore a great angular sector or the whole 360° around the vessel. This is a very appreciable improvement especially when the equipment picks also up the navigation parameters offering to the operator very complete information on the colour display. True motion representations can then be offered where school's course, speed and depth are also computed. The general consequence of omnidirectional transmission is a lower source level as all the energy is split

into a large volume and the maximum detectable range of a target decreases. For overcoming this, some sophisticated sonars can operate on many modes: single, multibeam or omnidirectional.

3.3.1 Detection Limits

A transmitted beam, operating more or less horizontally rather than vertically, introduces a number of differences compared to vertical echo-sounders. The first effect is the beam bending which results from change of temperature with depth. Sound travels faster in warm than in cold water, hence the result is a beam bending towards the cold water. This can be a limitation in the effective detection range of the system and in false indications of range and depth of a detected target. The best propagation conditions are generally encountered in winter when homothermic vertical profile is generally the rule. In summer, the upper layers are warm, getting colder with depth; sharp downwards bending of the beam limits in this period the sonar range and brings interferences from bottom echoes.

Reverberation is the back scattering of the transmitted pulse by particles and irregularities both in the water and on the surface or the bottom. When the sonar beam hits the sea bed or the surface, especially in bad weather with rough aerated interface, reverberation is produced. In some cases, the level of this phenomenon can be so high such to cover the useful echoes of fishes. On rough bottom, this may restrict the use of sonar for the detection of demersal fishes. The reverberation level can be lowered by reducing the beam width or using short pulse length.

More or less horizontal sounding also means that the secondary lobes of the beamwidth are orientated more perpendicular to the bottom than the main lobe. The result is, mainly in shallow water, a bottom echo coming through this secondary lobe and appearing on the display, for instance in omnidirectional mode, as a circle around the vessel, the radius being function of the depth and the beam tilt. The interpretation of sonar echoes is more difficult than in the case of echo-sounder where, within the limits of surface and bottom, all echoes are coming from the midwater. It is not the case for the sonar where a school can for example be detected at a distance greater than the bottom echo. Interpreting sonar echoes requires therefore a good practical experience.

3.4 Side-Scan Sonar

The side scan sonar is a type of sonar system, and is first and foremost considered as a visualisation tool providing acoustic images of the seabed. This type of sonar system is very sensitive and can, depending on the system, measure features smaller than 10 centimetres. Some typical uses of side-scan sonar include:

- Object detection (mines, sunken ships, pipelines, downed aircraft, lost cargo)
- Bottom classification (sediment type, rock outcrop, and ripples/waves)
- Inspection of underwater constructions (offshore constructions, wellheads, oil pipes, bridges, piles, harbor walls)

The side-scan sonar configuration is characterized by the following elements:

- Sideways look: transducers emit the sonar pulses laterally
- Two channels: acoustic beam is duplicated and sent out from both sides of vessel/tow fish
- Narrow beam: the wide beam angles which were useful for general coverage in other applications are not suitable for side scan work, where you are trying to achieve high

- resolution along a strip of the seafloor. For this reason side scan sonars use a sound pulse which is narrow in the horizontal plane
- Towed body (tow fish): The acoustic beams are emitted from a towed body, which is decoupled from the ship's motions.

They are usually installed on a fish towed near the bottom (Figure 43). With a side scan sonar the image is built up by laying down successive scans of the sonar on the display device to form a composite image. The narrow horizontal beam makes control of beam direction important. This is difficult to do on a ship which is often working in rough water, so towed bodies are used. There is increased danger of losing tow fish this way, at no little expense, but the risk is more than outweighed by the improvement in record quality gained by decoupling the sonar from the ship's motions. Since short-range sonars must be operated relatively close to the ocean bottom, the use of an appropriate tow cable permits working in any water depth. This configuration makes them work in good stability and noise conditions, and at grazing incidence. A sidescan sonar insonifies the bottom with two side antennas with a very narrow horizontal directivity (around a degree or less). The signal backscattered by the seabed, recorded along time, reproduces the structure of small irregularities on the seabed, which are better imaged at grazing angles of incidence.

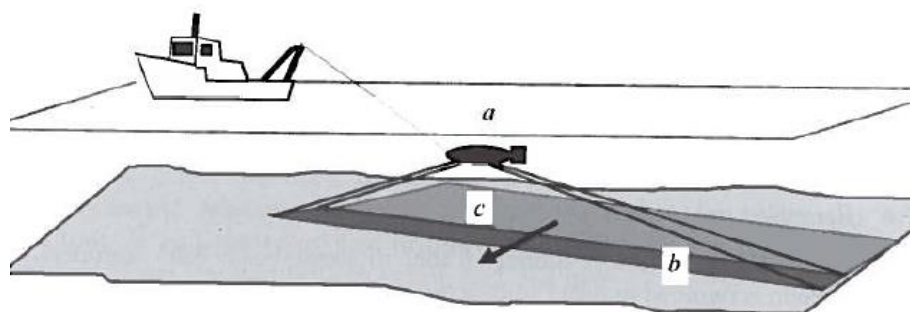


Figure 43: Side-scan sonar deployment: (a) tow fish; (b) instantaneously insonified area; (c) area covered by previous transmissions (Diner).

The working principle of the side-scan makes is simple: a narrow sound beam is transmitted at grazing incidence and will intercept the bottom along a thin strip spreading out with distance (Figure 8.12). Inside this strip, the very short signal transmitted will delimit the area insonified, of very small dimensions, sweeping over the entire area covered. The echo received along time will represent the bottom reflectivity along the swathe, and particularly the presence or irregularities or small obstacles. The signal is recorded laterally, hence the name "side-scan sonar". It is added to the signals recorded at previous positions of the tow fish and, line by line, it creates a genuine image of the seabed. In order to obtain the best possible results, most of the systems are dual frequency systems. High frequencies such as 500 kHz to 1 MHz give excellent resolutions, but the acoustic energy only travels a short distance.

When the pulse sent by the side scan sonar reaches the seafloor several things can happen to the sound pulse. Some of the sound may be absorbed by the seafloor. Some of the sound is almost always reflected. There are several different ways the sound can reflect. The sound can be reflected directly like light does on a mirror, or it can be scattered in many different directions, see Figure 25. Sound that is scattered back toward the sonar fish is called backscatter.

How much scattering, backscattering and absorption occur depends on the material properties. Hard materials, like rocks, will scatter more sound while soft materials, like mud, will absorb more sound. Different amounts of scattering produce different amounts of sound returning to the sonar fish and a different image of the bottom.

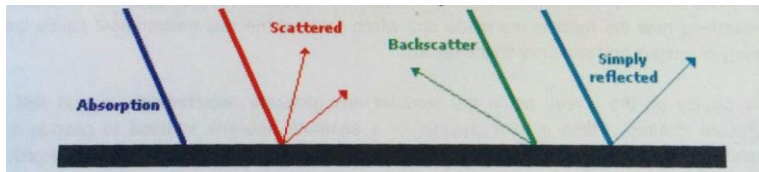


Figure 44 Diagram showing absorption, scattering and reflection of sound waves (Lekkerkerk, et al., 2006).

Side scan sonar data represent backscatter received by the side scan sonar fish from an insonified region of seafloor. Acoustic backscatter is thought to be a function of the followings:

- The angle of incidence of the acoustic wave front to the seafloor
- Surface roughness
- Impedance contrast across the solid-water interface (harder/firmer seabed sediment or objects produce higher backscatter and show up darker on the final record; rock and gravel are of better reflectors than mud or sand)
- Topography (up sloped facing the sonar fish are far better reflectors than down slopes due to difference in incidence angle.)

With side scan sonar imagery, high backscatter is represented by dark tones, low backscatter by light tones, zero backscatter is represented by white tones. In general, areas of high backscatter are associated with relatively coarser-grained sediments, hard substrata, steep slopes, and rough seabed; areas of low-backscatter with relatively finer-grained sediments, flat and smooth seabed. White tones are also known as shadows. They are the result of acoustic blanking, when an object or structure blocks sound pulse from the side scan sonar.

3.4.1 Reception Processing

The echoes are recorded and displayed as a function of time: for every ping, the backscattered intensity is drawn as a line of pixels perpendicular to the tow fish track. As a first approach, one simply displays a pile of successive echo lines, recorded along time. The raw image built this way permits us to control the. However, it is a poor physical representation, insufficient to get an accurate image of the seafloor. Geometrical problems arise when trying to reconstruct an undistorted image of the seabed, using these time records. As time and distance on the seabed are not proportional, equidistant time samples do not correspond to regular seabed samples. To replace the time samples in a spatially correct fashion, a geometric correction must be applied. When the seabed is not flat, geometrical correction requires simple a priori assumptions about the topography (e.g., regular slope) or additional recording of bathymetry (possibly obtained by the side-scan sonar itself, if it is equipped with an interferometer).

If the tow fish is equipped with a navigation and motion data unit, its movements may be compensated and the pixels relocated in a precise geographic frame, where several tracks of the

sonar may be added; the result is named a sonar image mosaic. Finally the image is interpolated between the various pixels.

3.4.2 Echo Construction

The spatio-temporal structure of the signals received by a side-scan sonar is shown in Figure 45. The signal transmitted will first propagate in water (Figure 45, Point A); the sonar will only receive background noise, and possibly echoes from mid-water targets (e.g., fish, bubbles). The actual seafloor echo will only start taking shape when the pulse strikes the nadir of the sonar (Figure 45, Point B). This reflection creates a first, very intense echo (as the backscatter strength is maximal and the transmission loss minimal). This cannot be used for the imaging itself, but is very useful to estimate the altitude of the sonar above the bottom. As it propagates with time, the signal will then explore the angular zone close to the vertical. This first part, with high reflectivity and poor horizontal spatial resolution, is generally of bad quality. Finally, the signal reaches oblique and grazing incidence, and then becomes really useful for imaging. Its average level will then depend on the local type of seafloor, with possible modulations by the array directivity patterns.

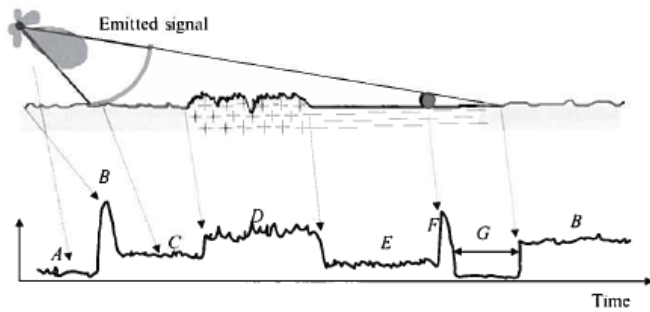


Figure 45: Echo generation for a side-scan sonar: (A) noise and reverberation in the water column; (B) first bottom echo; (C) sand area; (D) rock; (E) silt; (F) target echo; (G) shadow from the target (Diner).

An interesting effect is the formation of shadows on the seabed. A large enough obstacle will intercept part of the angular sector transmitted, and prevent back-scattering from the bottom at times normally associated with these angles. The echo received will thus be very low for a duration depending on the grazing angle and the height of the masking object. This will create on the sonar image the shadow commensurate with the object's shape. Its analysis will provide estimates of the size and shape of the object.

3.4.3 Side scan sonar resolution

The resolution along the direction of the movement of the side scan sonar is dependent on a narrow beamwidth θ_y , where y is the direction of the sonar movement / along-track direction. The cross-track resolution is dependent on the pulse length. We are also interested in the slant range, which is determined from the signal travel time τ , while the horizontal range x is determined by the sonar's height H above the sea floor , (Diner). From this we can define

$$r = c * \frac{\tau}{2} \quad (2.32)$$

$$x = \sqrt{r^2 - H^2} \quad (2.33)$$

We can now determine the resolution area on the sea floor, also called footprint, by the following equation

$$A = \left(\frac{cT}{2}\right) * r\theta_y \quad (2.34)$$

3.5 Sub-Bottom Profiler

Sub-bottom profilers (SBPs) are, as the name suggests, used for generating sonar imagery of the geology beneath the seabed. A typical SBS can generally reach several tens of meters down the sediment layers. The principal operational structure is the same as a single-beam sounder working at high level and low frequency.

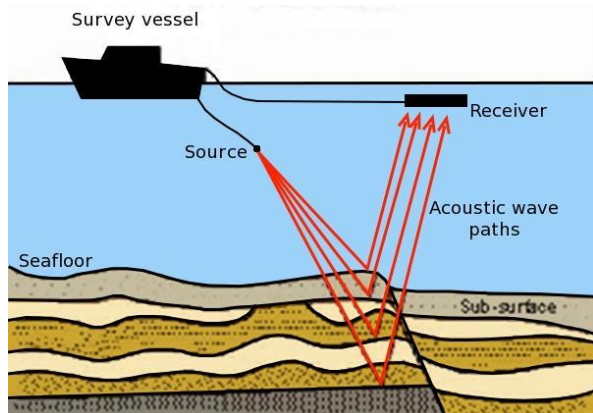


Figure 46: Basic overview of how a SBP works (AML Oceanographic, 2015; Diner).

Artificially generated acoustic waves propagate down through the water column into the subsurface and are reflected from structures and objects that show a contrast in acoustic impedance (Figure 46). These reflected waves are recorded using hydrophones and, after processing of the data, the subsurface can be visualised. These techniques allow structures such as sediment stratigraphy, faults, scours, gas fronts, fluid escape chimneys, and buried objects to be mapped.

The echo signal comes from the reflection and not the backscattering. The echoes gathered while the ship is moving are juxtaposed graphically, reconstituting a vertical cross-section of the sediment layer discontinuities. It is also possible to retrieve the reflection and absorption coefficients of the various sediment layers.

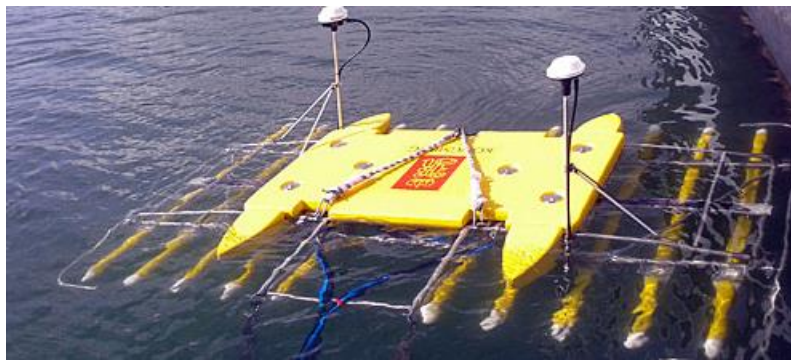


Figure 47: There are many types of SBPs. The picture shows an advanced 3D high resolution SBP delivered by Kongsberg ().

3.5.1 SBP Systems

There are a large variety of SBP systems. There is a rough classification in two types. The first type is the transducer array. These are instruments that in most cases combine the source and the receiver. In general the sound is generated by electrostriction. The second type has a separate source and receiver. The source can be electrical or mechanical and the receiver is a so called hydrophone, which in most cases is physically separated from the source.

3.5.1.1 Transducer Arrays

The transducer array consists of one or more transducers that can operate at different frequencies. They generally use electrostriction. This element is capable of transmission and reception of the signals. The advantage of this system is that there is no offset between the source and receiver, they generate a relatively narrow beam and that in most cases they are easy to operate. Most of these systems are small, relatively lightweight and easy to install. Transducer arrays are typically operated at frequencies of 3.5 kHz and higher. This limits the penetration capabilities to a maximum of 20 to 50 meters, depending strongly on the soil type.

3.5.1.2 Pinger

The easiest way to describe a pinger is as a low frequency echo sounder, where the transmitted pulse reflects off and penetrates through the bottom. The system is easy to operate and not too sensitive to damage. From a geophysical point of view the only disadvantage is the pulse signature, which consists of multiple wave lengths and hampers the interpolation of a pinger record.

The parametric echo sounder combines the parametric effect with high frequency echo sounding. The parametric effect is that two simultaneous transmitted waves with different frequencies (f_1 and f_2) result in two waves with a high and a low frequency (f_1+f_2 and f_1-f_2) wave. In general the very high frequency, f_1+f_2 will be disregarded, the middle frequencies, f_1 and f_2 will be used for detailed depth registration and the low frequency, f_1-f_2 will penetrate and can be used as a sub bottom profiler. See Figure 24.

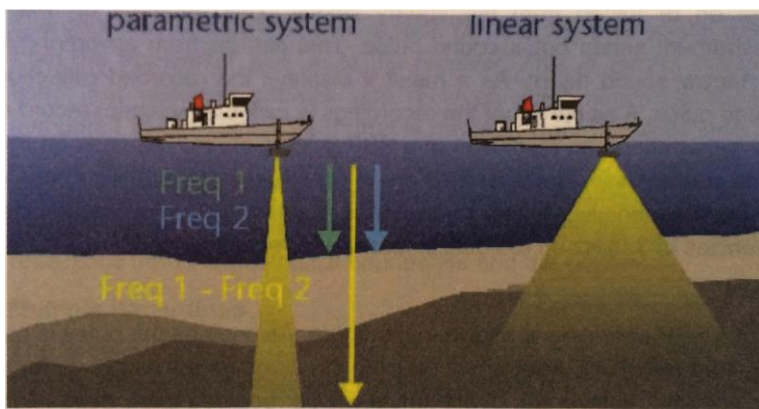


Figure 48 Schematic view of principle of parametric system compared to conventional "linear" systems (Lekkerkerk, et al., 2006).

One major advantage of the parametric echo sounder is that there is a very narrow beam angle for a relatively low frequency, which results in a better resolution at low frequencies compared to the pinger systems.

3.5.1.3 Chirp Profilers

Chirp profilers use digitally produced linear frequency modulated acoustic transmissions to produce high-resolution sub bottom data. The system is based on conventional pinger technology but designed to increase resolution without limiting the range. Chirp profilers became available once digital signal processing could be performed real time.

The sound pulse is swept through a wide frequency band imbedding high and low frequencies and therewith combining penetration and resolution. In a conventional single-frequency system, the limit of resolution is determined by the pulse length of the transmitted waveform whereas in a chirp system it is the bandwidth of the transmitted pulse that determines the system's resolution.

3.5.2 Theory of Operation

SBPs are mounted on or towed from the survey vessel. This depends on the type of equipment. The instrument sends out a sound pulse. This can be from an omni-directional sound pulse to a narrow sound beam. As a result it displays the recorded reflections from every separate sound pulse. A whole set of the recordings is called a (seismic) record or a sub bottom profile. The penetration and resolution of a SBP system mainly depends on the shape and frequency of the sound pulse. However they are in continuous conflict. High penetration is only possible with low frequencies. A high resolution is obtained with high frequencies. SBP systems use frequencies of 1 kHz up to 200 kHz.

3.5.2.1 Geometry of SBP

A schematic view of a SBP operation is shown in Figure 25. As soon as the pulse is emitted at $t=0$ the system can start recording. For transducers the direct arrival will be at $t=0$, for systems with a separate source and receiver the direct arrival will be recorded later, depending on the distance between the source and the receiver. The sound pulse will partly reflect on the bottom and travel back to the receiver. This is recorded as the first bottom return. The transmitted sound will reflect and transmit the boundaries between the various geological layers.

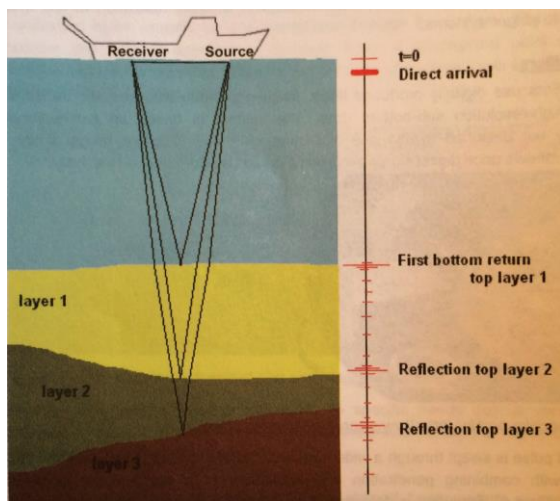


Figure 49: Schematic view of SBP operation

The reflections of a single pulse or shot are recorded as a time graph, where the recorded intensity is displayed as a function of the two-way-travel time (TWT time). A series of these time graphs from a record. The records are always on a time base, not on depth. Depths and thickness can be calculated by applying the speed of sound, which is different in water and in sediments. Some systems record the absolute value of the amplitude other system record the positive and negative amplitudes, corresponding with compressions and expansion.

The geometry of a SBP system is such that the recorded sound travels the path straight down from the transmitter and up to the receiver. This is always the case when transducers are used. For separate sources and receivers their horizontal distance should be negligible compared to the vertical path (that is travelled twice). In very shallow water this is not always negligible. Be aware of this fact during interpretation, because the thickness of a layer will be exaggerated. When the source and receiver are positioned close enough the SBP will record the reflections that have travelled vertically. Ideally the SBP system should only record the reflections from the geological boundaries and the bottom.

3.5.2.2 Multiple Recordings

The water surface is a good reflector. Depending on the depth and the penetration, the SBP records one or more multiples. The first is the recording of that part of the sound pulse that travelled the water column twice, as seen in Figure 26. In shallow water sometimes the second and third bottom multiple are recorded as well. Also the sound that has penetrated into the bottom can bounce up and down in the water column as well. There are various types of multiple recordings.

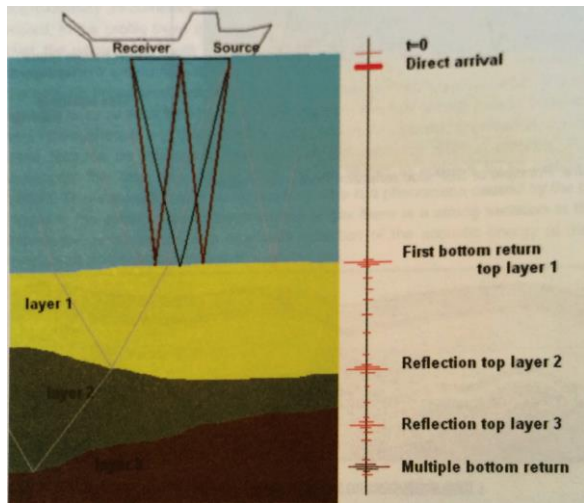


Figure 50: Schematic view of the travel path of the first multiple

They all have one thing in common, namely that one part of the path has been travelled up and down twice, mostly the water column. In general it is easy to recognize the multiple because the TWT time is multiplied. The TWT time of the first multiple is twice that of the first bottom return.

3.5.2.3 Side Reflections

Many SBP transmit sound omni directionally or in a broad beam. Only a small part of this acoustic energy will be recorded by the receiver, most of it will be dispersed in the water column or reflected and scattered on the bottom or on geological boundaries in all directions except for the receiver. Most of this scattered acoustic energy is not recorded. However, the SBP records strong reflections from hard contacts even when this contact is not exactly beneath the source/receiver, a so-called side reflection. For wider beams there will be more side reflections. Side reflections do occur in the vicinity of steep slopes and when there are hard objects that reflect much better than the surrounding soil. A pipeline will be displayed as a side reflection for several consecutive shots only with a different two way travel time. It is this effect that is used in order to position buried pipelines, as seen in Figure 27.

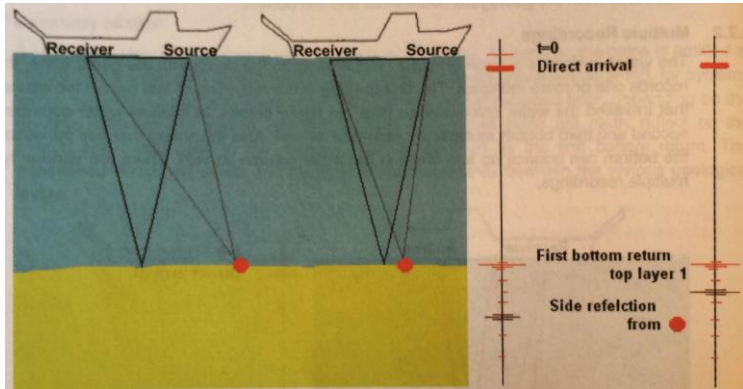


Figure 51: Principle of SBP side reflection from a hard object

3.6 Doppler Velocity Log & Acoustic Doppler Current Profiler

Doppler velocity logs (DVL) can be used to estimate the velocity of the structure they are attached to, or to estimate the current velocity of the water column. In the later setup the DVL is used as an acoustic Doppler current profiler (ADCP). They utilize the Doppler frequency shift (see section 2.7) of backscattered echoes, proportional to the speed of the sonar relative to the target. The medium off which the echoes rebound can for example be the seabed, if it is reached. This case is the most favourable, as it yields the most accurate results. If the seabed is too far away however, the signals will rebound off the water column, and current effects will then affect the measurements. This offset must as such be accounted for to achieve accurate navigation.

The DVL or ADCP will first transmit a signal with a fixed frequency. It will then listen to the echoes from scatters in water or from the sea bottom, as mentioned. The scatter in water come from small particles or plankton that reflect the sound back to the ADCP or DVL. When the refection come from the seabed, the velocity measurement will be relative to a fixed surface. However when the refection come from particles in the water column, these particles will on average move with the same velocity as the horizontal water velocity. When the acoustic wave hit the particles, most of the sound will move forward, unaffected by the particle. The small part that is scattered will be scattered in every direction, and some will return to the ADCP/DCL. If the particles scattering the sound is moving away from the ADCP, the returning signal will have a lower frequency than the transmitted signal. Conversely, if the particles have a velocity towards the ADCP the frequency will increase. From the equations presented in section 2.7, the relative velocity can then be calculated. The DVL or ADCP are only able to measure the relative velocity of motion parallel to the acoustic beam. For this reason will many devices consist of multiple beams. It is common for ADCP's to have four beams, where one pair of beam's are directed north and south, and the other pair is directed east and west. With this setup all three velocity component for three dimensional current flow can be determined. The first pair of beams obtain one horizontal component and the vertical velocity component. The second pair of beams produce a second, perpendicular horizontal component as well as a second vertical component. By doing this both horizontal velocity components are estimated, and two estimations of the vertical velocity is obtained.

For underwater vehicles like ROV's and AUV's DVL is used to provide a velocity estimate. Different kind of positioning systems are covered later, but on occasions where no external positioning is available, so called dead reckoning is used. This kind of positioning use the velocity estimate and compass or gyro heading to estimate the position. For this reason it is important to be aware of the error in the velocity estimate from the DVL, since this will affect the accuracy of the positioning system. In order to calculate a three dimensional velocity, three measurement is required. Systems that use four beams therefore have one more beam than what is necessary, something that both provide redundancy in case of failure and make it possible to evaluate the data quality.

Most ADCP's and DVL's are installed in a so called Janus configuration, named after the roman god who both faced forward and backward. ADCP's and DVL's will therefore both emit beams in the forward direction and backward direction, and in the starboard and port direction. This configuration is useful since it reduce error in the horizontal velocity estimate due to pitch and roll of the ADCP and DVL. This is because two opposing beams allow vertical velocity to cancel when computing horizontal velocity. The error due to pitch and roll on the velocity estimation is also reduced to be proportional to the square of the pitch and roll errors. The figure below show an ROV with a DVL where the beams are in a Janus configuration.

Doppler Velocity logs work at high frequencies, typically between 100 kHz and 1 MHz. Several beams are transmitted with distinct orientations in the horizontal plane, and the Doppler shift is measured in each of these various directions provides the spatial coordinates of the velocity vector. Common areas of application for these are on AUVs, ROVs and other submersibles to assist in navigation.

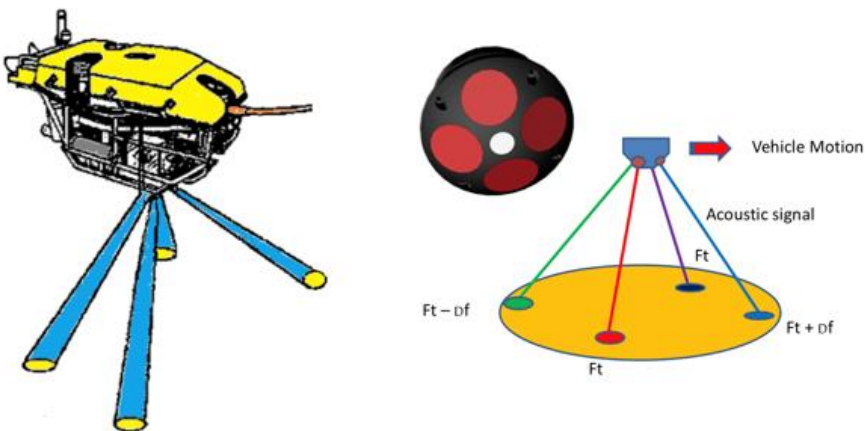


Figure 52: DVL on an AUV (right) and a simple illustration of the working principle (left).

Doppler velocity logs function in a manner similar to an INS (Inertial Navigation System), see chapter 3, as it uses sensor input to provide a dead-reckoning estimate of the relative displacement of the sensor. It can only give displacement outputs, and as such cannot give a geo-referenced output directly. To achieve this LBL and USBL systems can be utilized. If connected to an INS system, high accuracy positioning can be achieved.

TMR4120 Underwater Engineering

An Acoustic Doppler Current Profiler (ADCP) can be used to measure the velocity profile at a fixed point by mooring it in a support on the sea bed looking upwards (or under a buoy looking down) or along the path of a boat by attaching it to or towing it behind the ship.

In a fixed point system, the ADCP provides the water velocity directly by averaging the results from many pings, typically at one-second intervals over the course of several minutes. In this way, the precision of the estimated velocity can be significantly improved.

4 Underwater Navigation

Positioning is essential in all phases of underwater navigation, which in turn are used in such things as the offshore hydrocarbon industry, for military applications, marine geology and seafloor mapping and the fishery industry. The purpose of positioning, especially for ROVs and AUVs, is two-folded; the first is practical considerations, as it is necessary to know the location of the vehicle at all times for operational safety and to find the research targets. The second motivation is geo-referencing of collected data. As important as the data themselves is the knowledge of where the data are collected (Lurton, 2002).

Positioning is the term used for direct position measurement, as opposed to navigation which is a broader term. Above the surface of the ocean, most autonomous systems utilize radio or spread-spectrum communications in addition to global positioning systems for navigation. Underwater navigation unfortunately, brings with it a number of problems. Mainly the rapid attenuation of higher frequency signals in the subsurface environment. Such signals will only travel a short distance and render standard methods of navigation useless. As such, acoustic communications and sensors will yield better performance. During the last 10 years, research into underwater navigation has exploded, and older techniques are being re-evaluated and replaced. Underwater navigation, or AUV navigation systems more specifically, can be categorized into three main groups; inertial/dead reckoning, acoustic transponders and modems and geophysical techniques (Figure 53):

- Inertial/dead reckoning: Takes use of accelerometers and gyroscopes for increased accuracy in determining the present state. The downside of the methods is that the position error growth that is essentially limitless.
- Acoustic transponders and modems: These methods take use of the time of flight (TOF) of the acoustic signals from beacons or modems.
- Geophysical: Techniques that use external environmental information as references for navigation. This must be done with sensors and processing that are capable of detecting, identifying and classifying some environmental features.

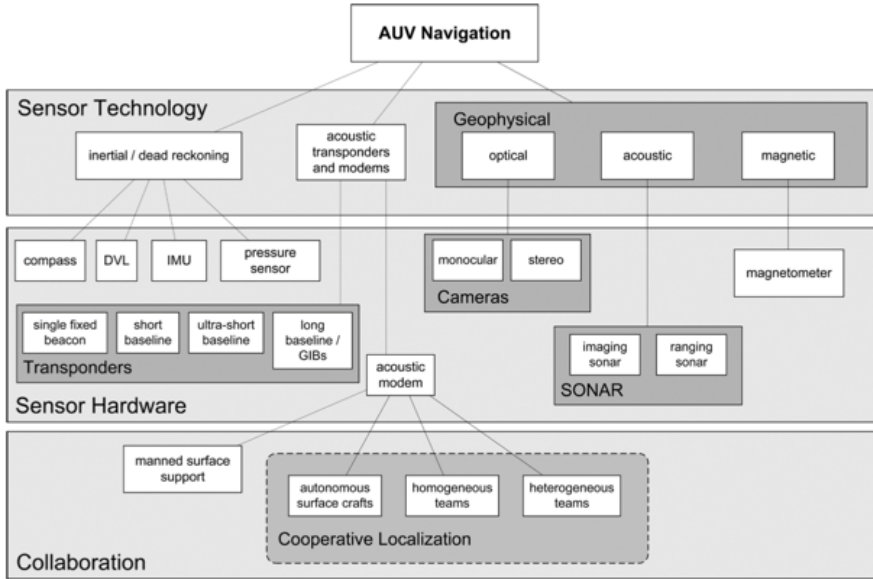


Figure 53: Outline of underwater navigation classifications. These methods are often combined in one system to provide increased performance () .

4.1 Inertial/Dead Reckoning Techniques

When the underwater vehicle positions itself autonomously, without any acoustic positioning support, it utilizes a technique known as dead reckoning (DR). As the vehicle advances its positions, it calculates its current position based on data from accelerometers and gyroscopes. With the knowledge of its previous orientation and its velocity or acceleration vector, its new position can be determined. This is not a primary means of navigation but is used in other more advanced navigation systems in underwater vehicles. One of the major disadvantages of dead reckoning is that all errors are cumulative. The further the vehicle travels, the higher the level of error in its position.

One simple method of DR pose estimation, for example, if heading is available from a compass and velocity is available from a Doppler velocity log (DVL), is achieved by using the following kinematic equations:

$$\dot{x} = v \cos \psi + w \sin \psi \quad (3.1)$$

$$\dot{y} = v \sin \psi + w \cos \psi \quad (3.2)$$

$$\dot{\psi} = 0 \quad (3.3)$$

Where (x, y, ψ) is the displacement and heading in the standard north–east–down coordinate system, and v and w are the body frame forward and starboard velocities. In this model, it is assumed that roll and pitch are zero and that depth is measured accurately with a depth sensor.

The basic kinematics model presented in equations 1, 2 and 3, is incomplete if the local water current is not accounted for. The current can be measured with an acoustic Doppler current profiler (ADCP). A Doppler velocity log (DVL) can also be used by measuring the velocity of the water relative to the vehicle and the velocity of the seabed relative to vehicle. By subtracting the former from the latter, the ocean current can be obtained.

Inertial systems aim to improve dead reckoning estimates by integrating measurements from the accelerometers and gyroscopes. Inertial proprioceptive sensors are utilized to provide a higher frequency of measurements and reduce the rate at which the error increases.

By using an inertial measurement unit (IMU) that

measure the acceleration the velocity and position is obtained by integration. The measurement of accelerometers and gyros will however be exposed to noise and have a tendency to drift over time due to sensor bias, misalignments and temperature variations. Since the measurement form the inertial sensors are the only measurement for inertial navigation systems, a drift in the measurement will cause a growing and unbounded error in the estimated position. To counter act this external positioning systems like GPS can be used to regularly obtain a position that is known, and thus limiting the drift of position. In extreme depths, where it is impractical to surface for GPS position updates, inertial systems are the predominant method of navigation. The key components of the IMU is the gyroscope and the accelerometers.

The best inertia navigation systems (INS) can achieve a drift of 0.1% of the distance travelled, however, more typical and modestly priced units can easily achieve a drift of 2%–5% of the distance travelled.

4.1.1 State estimators – Observers

The quality of raw measurement is usually limited, since any sensors will be subject to sensor noise, and all systems will be exposed to some kind of disturbances like waves or wind. In order to counteract this signal processing and state estimators are used. A state estimator is unit that is used to both remove noise from raw data, and to reconstruct unmeasured states. The state estimator removes noise by filtering it away. A state estimator is also called an observer, and works by using a mathematical model of the system, the control input (like thruster forces) and the noisy measurement to estimate more accurate states. By doing this the effect of noise on the system is greatly reduced. A state estimator can also be used to estimate position and velocity when no measurement is available, and correct the position when external measurement is available. This is especially applicable for AUVs, since GPS is not available and acoustic positioning can occasionally drop out. There are several ways of designing an observer. One of the most widely used observer design for marine applications it the Kalman filter.

The Kalman filter is a recursive filter that estimate the state of dynamic systems from a series of noisy measurement. When the measurement is lost, the filter behaves as a predictor that then is corrected when new measurement is available. This design require the system to satisfy certain conditions in order to guarantee that the output form the observer will converge to the true value.

formaterte: Engelsk (Storbritannia)

and the states of the systems x can be reconstructed through the measurements y . Since observers like this is implemented in a computer, a discreet time implementation is necessary. For the following system model on state space form the

$$\dot{x}(k+1) = \Phi x(k) + \Delta u(k) + \Gamma w(k) \quad (3.4)$$

$$y(k) = Hx(k) + v(k) \quad (3.5)$$

In the equations above x represent the state vector, while y is a vector containing the measured states. The vectors v and w is noise vector, and u is the input to the system. The matrices ϕ, Δ, Γ and H are describing the system properties. Figure 54 below illustrate a block diagram of a system that can be described by the equations above. The estimated states \hat{x} is the output from the observer based on the noise polluted measurements and the control input.

formaterte: Skrif: Ikke Fet
Feltkode endret

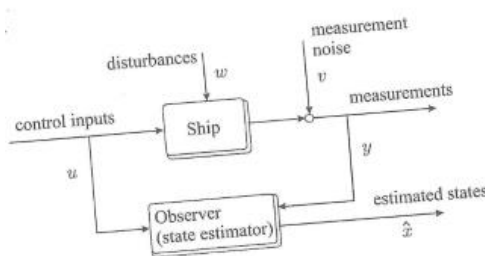


Figure 54: Block diagram of the system model and the observer.

For a system as the one presented above, the Kalman filter is described by the following set of equations, where \tilde{x} represent the error in the estimate, and the values $A(k)$ is the value of the A vector in this time step, where $A(k+1)$ is the predicted values of A in the next time step.

Initial conditions:

$$\tilde{x}(0) = x_0 \quad (3.6)$$

Formatert: Midtstilt, Hold sammen med neste

formaterte: Engelsk (Storbritannia)
formaterte: Skrif: Ikke Fet, Engelsk (USA)
Formatert: Bildetekst
Feltkode endret
formaterte: Engelsk (Storbritannia)

$$\tilde{P}(0) = E[(x(0) - \hat{x}(0))(x(0) - \hat{x}(0))^T] = P_0 \quad (3.7)$$

Kalman Gain matrix

$$K(k) = \tilde{P}(k)H^T(k)[H(k)\tilde{P}(k)H^T(k) + R(k)]^{-1} \quad (3.8)$$

State estimation update

$$\hat{x}(k) = \tilde{x}(k) + K(k)[y(k) - H(k)\tilde{x}(k)] \quad (3.9)$$

Error covariance update

$$\begin{aligned}\widehat{\mathbf{P}}(k) &= [\mathbf{I} - \mathbf{K}(k)\mathbf{H}(k)]\widetilde{\mathbf{P}}(k)[\mathbf{I} - \mathbf{K}(k)\mathbf{H}(k)]^T \\ &\quad + \mathbf{K}(k)\mathbf{R}(k)\mathbf{K}(k). \quad \widehat{\mathbf{P}}(k) = \widehat{\mathbf{P}}(k)^T > 0\end{aligned}\quad (3.10)$$

State estimate propagation

$$\tilde{\mathbf{x}}(k+1) = \Phi(k)\widehat{\mathbf{x}}(k) + \Delta(k)\mathbf{u}(k) \quad (3.11)$$

Error covariance propagation

$$\widetilde{\mathbf{P}}(k+1) = \Phi(k)\widehat{\mathbf{P}}(k)\Phi^T(k) + \Gamma(k)\mathbf{Q}(k)\Gamma^T(k) \quad (3.12)$$

In the equations above the matrices \mathbf{Q} and \mathbf{R} are design matrices. The matrices \mathbf{H} , Φ , Δ & Γ are given by the system model. The \mathbf{K} matrix is a gain matrix that is updated online. By implementing the Kalman filter described by the equation above one can obtain a set of estimated states $\widehat{\mathbf{x}}$ from the measurement y . The estimated state can contain more states than what we are able to measure, and the observer will thus reconstruct states that are unmeasured.

4.2

4.34.2 Short Baseline (SBL) Positioning

In a SBL system, there are minimum three (typically four) acoustic transducer in a triangular (or rectangular) pattern on the lower part of a vessel hull. The distances between these transducers, or “baselines”, can range from 5 -20 m. These transducers on the vessel hull are actually hydrophones that receive acoustic signals from a beacon/pinger/transponder/responder mounted on the seabed or alternatively on a submersible. The acoustic signal picked up by each of the hydrophones are then used to calculate the bearings and ranges to each of the transducers. In this way, a three-dimensional position fix is obtained.

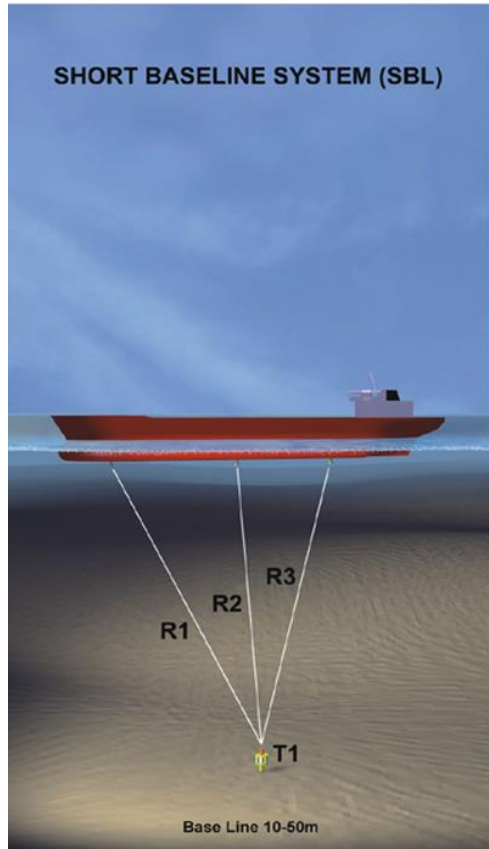


Figure 55: SBL acoustic navigation system. R_1 , R_2 and R_3 are the ranges from the seabed transducer, T_1 , to the hydrophones (Hovem, 2012; Lurton, 2002).

The term “short” is used as opposed to Long Baseline systems, where the transponders are placed at distances of several hundred meters (we will discuss this technique later). A typical SBL system requires a dedicated surface vessel with a hull-mounted array of hydrophones or transducers (or a combination of both). If a transponder (responder) or synchronized beacon (pinger) is mounted on the seabed, the time of arrival of the signals at the various elements of the array will give the slant ranges and bearings and hence lead to the calculation of the position of the surface vessel relative to the transponder or beacon.

Although in theory only three hydrophones are necessary, this does not allow the system to have any redundancy. Should one of the three hydrophones fail, the whole acoustic positioning system will fail. To avoid this, one can usually find more than three hydrophones installed on the vessel hull.

In general there are two fundamental ways a SBL system can operate. The difference is essentially in what instrument is installed on the seabed:

- Beacons/pingers
- Transponders/responders

In the following subsections, these two techniques will be discussed briefly.

4.3.14.2.1 SBL with beacon/pinger

In this type of configuration, the SBL system obtains the position fix by utilizing a bearing measurement method. This is done by measuring the difference in the arrival time of the acoustic signal at the hydrophones on the hull.

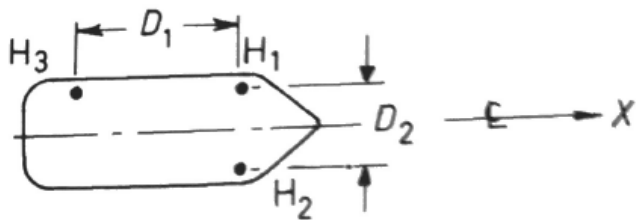


Figure 56: The placements of the hydrophones H_1 , H_2 and H_3 on a vessel seen from below (University of Southampton, 2011).

In the 2-D case (XZ-plane) seen in Figure 57, the differences in the ranges, dR , is given by:

$$dR = vdt \quad (3.134)$$

where v is the velocity of sound in the water. If the distance between hydrophones H_1 and H_3 with measured ranges of R_1 and R_3 , is D_1 , the bearing measurements will be:

$$\sin \theta_x = v(dt)_1/D_1 \quad (3.145)$$

where θ_x is the angle of inclination of vessel's hydrophone array above the beacon along the x -axis and $(dt)_1$ is the time difference between t_3 and t_1 , which is the measured time of arrival of acoustic signal at hydrophone H_3 and H_1 , respectively.

Furthermore, equation (3.156) gives the horizontal displacement of beacon along x -axis from centre of hydrophone array, x :

$$x = z \tan \theta_x \quad (3.156)$$

where z is the depth of beacon below hydrophone array (assumed in a horizontal plane).

As seen in Equation (3.15), in addition to measuring the arrival time differences between the hydrophones, the water depth of the beacon on the seabed also needs to be known to calculate the position in three-dimensional space.

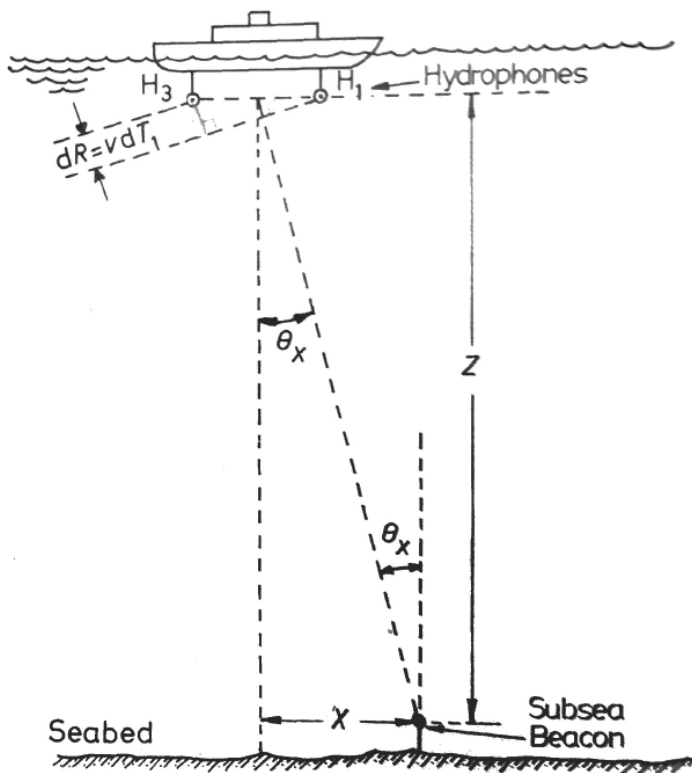


Figure 57: 2-D geometry in XZ plane for SBL beacon configuration (University of Southampton, 2011).

4.3.24.2.2 SBL with transponder/responder

As opposed to the SBL configuration with a beacon, the transponder configuration only transmit the acoustic signal when interrogated. Some of the benefits of a SBL configuration with transponder are:

- Since transponder only emits acoustic signal when interrogated, the battery life is extended.
- The access to absolute travel time provides a means to solve the geometry of the hydrophone/transponder 3-D relation without any simplifying assumptions. In the case of beacons in section 4.2.1, only time differences could be measured.
- The transponder interrogations can be programmed, and hence the rate of data collection adjusted to the navigation requirements. The interrogations can also be adjusted to avoid overlap of replies, if there are several transponders.

- Due to the interrogation requirement, it is possible to create time-interval for the reception of the replies of the hydrophones. By doing this, one can significantly reduce false data and multipath echoes since only acoustic signals received during the pre-set time interval is considered for position calculations.

4.3.34.2.3 Corrections to apparent positon

The position equations given in section 4.2.1 is based on a simplification of a motionless vessel with the hydrophone array in a horizontal plane. The corrections to the abovementioned assumption needs to be taken into account due to:

- Roll and pitch of vessel
- Hydrophone array centre offset from the vessel's reference point
- Array translation due to a combination of array offset and vessel roll and pitch

To ensure correct position readings, corrections must be computed for each of these errors.

Subsequently, these corrections must be implemented into the apparent position in order to obtain a corrected set of X and Y-coordinates of the subsea reference point relative to the vessel.

4.44.3 Ultra-Short Baseline (USBL)

Many SBL systems are being replaced by Ultra-Short Baseline (USBL) systems nowadays, which replaces the three separate hydrophones on the vessel hull with a single hydrophone/transducer unit with three sensors. This allows a much simpler installation without the need to measure all the individual transponder positions, which is the case with SBL systems. In addition, USBL can be installed on much smaller vessels (transducer/hydrophone diameter of around 230 mm) compared to SBL (baselines of around 5-20 m). The USBL system can also be deployed overboard. However, LBL is usually more accurate than USBL and the accuracy is not dependent on depth in the same way as for USBL since the transponders are situated on the seabed.

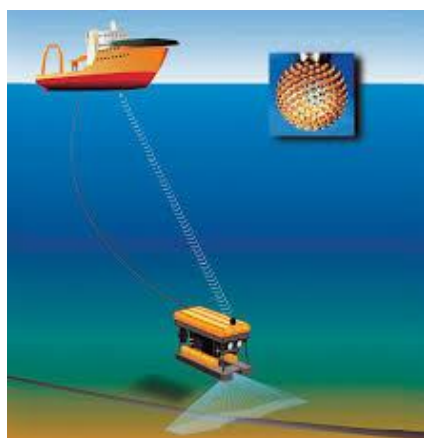


Figure 58: A USBL system used for ROV navigation. The USBL system only requires one hull-mounted transducer and one subsea transponder (Kongsberg, 2014).

The USBL system works by sending out an acoustic signal from the ship mounted transducer. This signal is then picked up by the subsea transponder. By using the time of flight of the acoustic signal, the range can be calculated (given the speed of sound in the water). The bearing angle is computed by phase difference of the acoustic signal, measured on the sensor elements at the ship mounted hydrophone.

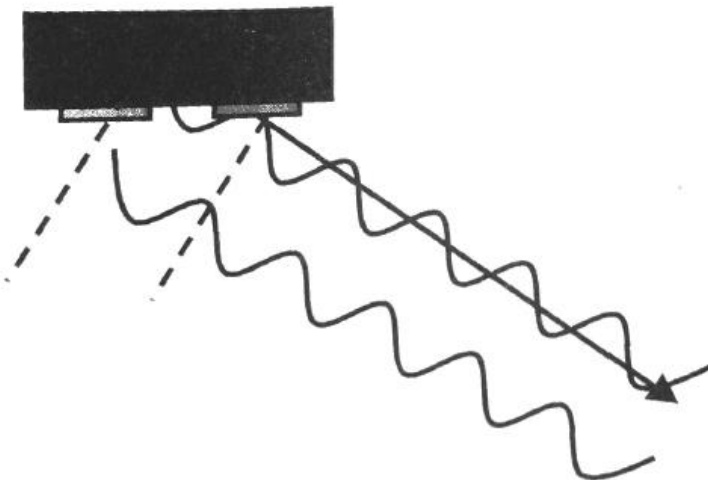


Figure 59: Phase difference measurement on two receive elements ()

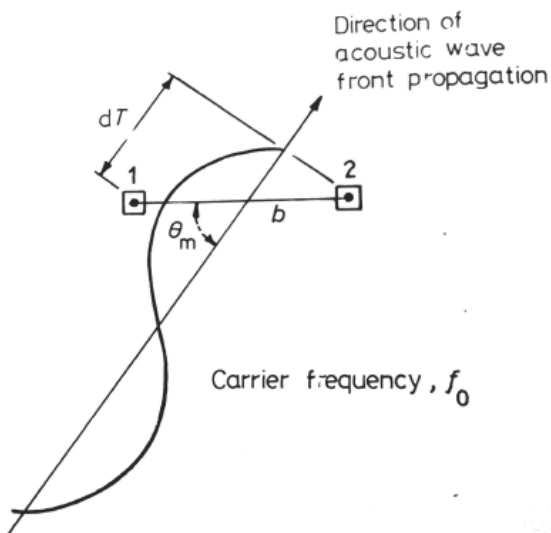


Figure 60: Phase delay of acoustic wave as a function of mechanical angle of incidence at the hydrophone ().

Figure 60 Figure 60 shows how the difference in the phase of an acoustic signal carrier frequency received by two sensors spaced, b , apart relates to the mechanical angle of incidence, Θ_m . This mechanical angle is in the plane formed by two sensors. By using Equation (3.16), the angle of incidence can be calculated:

$$\Theta_m = \cos^{-1}(dT / k) \quad (3.167)$$

where dT is electrical phase difference, $k=2\pi f_0 b/v$ and v is the underwater velocity of sound.

To finally compute the apparent position of the subsea beacon/transponder, the depth or the slant range will also have to be known, in addition to the incident angles. If both depth and slant range is known, there will be less uncertainty about the final computed position of the beacon/transponder.

In order to obtain a global position of a ROV using a USBL system, one also need a Differential GPS (dGPS). ~~The following subsection (section 4.1.5 section 7.1) aims to give a brief description of the dGPS.~~

4.5.1.1 Surface Positioning – GPS and dGPS

~~GPS positioning (Global Positioning System) is based on satellites in orbit around the Earth. On the surface of the Earth each GPS receiver calculates the ranges to a set of satellites by measuring the time of flight from the signal leaves the satellite till it arrives the receiver. The positions of the satellites are sent from the satellites to the receiver units. Using the satellite positions and ranges, the position of the GPS receiver unit on the ground can be calculated. Four satellites are necessary to solve a three dimensional position for the receiver unit. For conventional GPS navigation, 15 meters horizontal standard deviation is normal. The main error sources are: atmospheric distortions to the signal path, inaccuracies of the indication of the satellite orbits, satellite clock errors and numerical errors.~~

~~To increase the position accuracy on a given platform, ground based reference stations broadcast the system error. The error is determined by measuring the difference between known positions of the reference stations and positions estimated by GPS receiver units on the reference stations. The broadcasted difference between known position and the measured position is often differential correction. GPS system which offer differential correction are called dGPS. dGPS receivers typically offer position estimates with standard deviations varying from 5 m to 0.1 m depending on the quality of the differential correction service.~~

4.5.14.3.1 Propagated uncertainty estimation for USBL positioning

In a USBL setup (for example in a ROV application) the GPS, gyro and USBL system all contribute to the resulting global position accuracy. A basic approach to calculate the uncertainty of a complete navigation setup is to sum the statistical variances of the individual measurement as in:

$$\sigma_{total} = \sqrt{Var_{GPS} + Var_{Gyro_position} + Var_{USBL_position}} \quad (3.178)$$

Since the gyro measurement accuracy is specified as standard deviation of the heading angle, the gyro error contribution to the xyz position estimate depends on the geometry between the ROV and the support vessel. The situation is the same for the USBL xyz-position error contribution from the depression and bearing angles. The horizontal distance from the vessel to the ROV acts as an arm in the calculation of the error contributions from the bearing angle measurements and the gyro measurements. Ideally the vessel should be placed directly above the ROV to reduce the error components from vessel mounted gyro and USBL bearing angle measurements.

Equations (3.18) – (3.20) are set up to derive position standard deviation for the USBL position expressed in meters. v denotes depression angle for the USBL system, while ω is the bearing angle. R denotes the range from transducer to transponder and $R_{horizontal}$ denotes R projected to the horizontal plane.

$$\sigma_{USBL_position} = \sqrt{Var_R + Var_\omega + Var_v} \quad (3.189)$$

$$Var_{\omega_metric} = R_{horizontal}(\sin(Var(v)) + \cos(Var(v))) \quad (3.190)$$

$$Var_{v_metric} = R \cos(Var_v)(\cos(\omega) + \sin(\omega)) \quad (3.191)$$

4.6.4 Long Baseline (LBL)

The Long Baseline acoustic method of underwater positioning typically consist of an array of transponders installed on the seabed (see Figure 61). The baseline is in general several kilometres long (hence the name). In section 4.2 and 4.3, the SBL and USBL acoustic systems were discussed for finding the position of a seabed beacon or transponder relative to a central reference point on the vessel since the hydrophones or transducers were mounted on the vessel. Due to this, the position coordinates obtained with these acoustic systems are vessel oriented and also corrected for ship heading. On the other hand, the LBL system is not exposed to this disadvantage since the coordinates of a point are seabed-oriented. Thus, they can be related to a seabed or platform grid (absolute or relative terms).

In a LBL system configuration, the transponders reply on different frequencies. This enables their signals to be distinguished from each other. Aboard the ship or submersible, the time of transponder interrogation is recorded together with the time to reply. This round-trip travel time is then used to establish the range. This process is repeated for all transponders, and the position of the vessel relative to the array of transponders is then calculated or estimated.

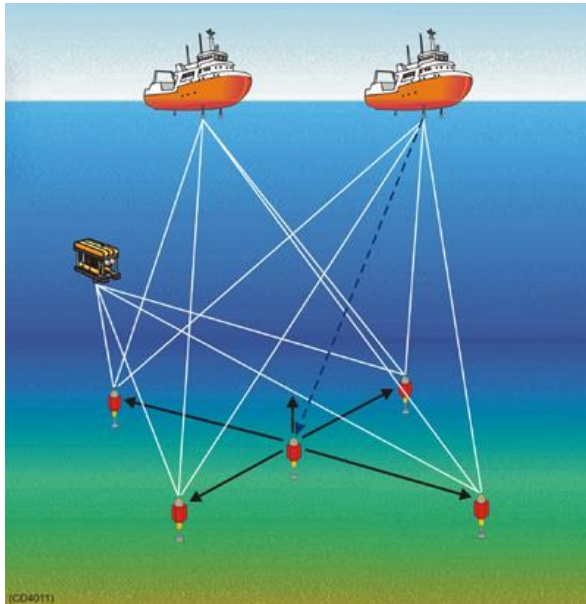


Figure 61: ROV and vessels performing LBL positioning ()�.

In principle, navigation can be achieved using just two seabed transponders. However, there is a possible ambiguity as to which side of the baseline the vessel may be on. Also, the depth or the height of the transducer have to be assumed. Three seabed transponders is the minimum required for unambiguous navigation in 3-D. Four is the minimum number required for redundancy.

Since the baselines are that much greater for LBL than for SBL or USBL, this type of acoustic system is generally more accurate. Another advantage with a LBL system is the repeatability characterized by the method. In addition, the accuracy is not dependent on depth in the same way as for USBL since the transponders are situated on the seabed.

The LBL system has two modes of operation. These two modes differ from each other in the way the interrogation process is conducted. The two modes are:

- Simultaneous interrogation
- Sequential interrogation

The Simultaneous mode is most commonly used where all transponders have a receiver tuned to a Common Interrogation Frequency (CIF), however, each individual transponder replies on its own Individual Reply Frequency (IRF). All transponders are interrogated by the transducer simultaneously but each transponder replies individually through their unique IRF.

In the Sequential mode all transponders are tuned to the CIF and their Individual Channel Frequency (ICF). The transponder replies on the Common Reply Frequency (CRF) to another transducer that interrogated it. A measurement is taken one at a time, and although this method of operation is more time consuming than in simultaneous mode, it is more accurate.

The accuracy of the LBL system can be chosen to fit specific project requirements. Typical operations where the LBL system can be used are:

- DP operations
- Acoustic spool piece metrology
- Positioning of pipeline during its initiation and lay down stage
- Positioning of seabed structures during the installation
- ROV positioning during surveys or construction support

4.6.14.4.1 Installation of LBL

Before any LBL backed positioning operation can begin, the installation of transponders on the seabed and positioning of the transponders are required.

During the installation work, special caution should be made to the mounting position of the transducer being used to interrogate the installed array. The transducer is required to be mounted so that when deployed, there is at least 1 m between it and the vessel keel or any protrusions extending vertically downwards from the hull, to eliminate acoustic reflections. Some considerations of a side mount are positions of the thrusters and main propellers and noise sources for example the engine room, as any air, turbulence and engine noise can obliterate or corrupt acoustic returns.

The geometry of the LBL array should be designed to provide the maximum coverage and accuracy required using the minimum practical distance between the target and the transponders. The topography of the seabed and any manmade seabed obstructions will have to be taken into account as this will cause blanking areas and will effect the design of the LBL array.

4.5 Depth measurement

In order to operate an underwater vehicle safely and efficiently it is important to have good estimation of the depth. This can be relevant with respect to seabed surveys, where it is interesting to know how deep the water depth is, or in manoeuvring and control of an underwater vehicle, where the user want to know where in the water column the vessel is. It is possible to determine the depth of the underwater vehicle from acoustic positioning systems mentioned earlier in this chapter, but it is common for ROV's and AUV's to be equipped with pressure sensors, to estimate the depth. The principle behind using a pressure sensor is that by measuring the hydrostatic pressure, one can calculate the depth, if the density and acceleration of gravity is known according to the following equation

$$P = \rho gh \leftrightarrow z = \frac{P}{\rho g} \quad (3.21)$$

The equation above is based upon some assumption that might not always be accurate. Firstly, it is important to be aware of the magnitude of the error from the pressure measurement device. This is important, since any error in this measurement will propagate to an error in the estimated depth. Secondly, the equation assumes that the density is constant with depth. As we have discussed earlier the density of the seawater will vary with depth, and this must be accounted for. Thirdly, it is also important to note that the acceleration of gravity will not be constant around the surface of the earth, but rather varies with the latitude. Based on this we can now rewrite the equation above accordingly for the depth of any unmanned underwater vehicle (UUV),.

$$z = \int_{p_{ATM}}^{p_{UV}} \frac{1}{\rho(S,t,p) \cdot g(L,p)} dp \quad (3.22)$$

In this equation, z is the depth, S is the salinity, t is the temperature, p is the pressure, L is the Latitude, $\rho(S, t, p)$ is the density as a function of pressure, temperature and salinity, and $g(L, p)$ is the acceleration of gravity as a function of Latitude and pressure. Furthermore, p_{UV} is the pressure at the UUV, and p_{ATM} is the atmospheric pressure. When analysing the error in the pressure estimate one must consider the error in all elements of the process of estimating the depth. Usually pressure sensors will have a known accuracy. The tide is also something that causes error in the depth measurement. The conventional way of measuring the tidal water is to place a pressure sensor at the seabed. The tide will cause the water surface to vary around the mean free water surface. This will then cause a corresponding increase or decrease in the estimated hydrostatic pressure. In the equation above, we can see that the density profile is important, and is integrated to find the depth. The relationship between the CTD measurement, conductivity, temperature and pressure, and the salinity are described by an international standard called Practical Salinity Scale 1978 PSS-78. Furthermore a common practice to compute the density profile from these data is to use the international Equation of State of Seawater, 1980 ESO-80.

The accuracy of this density profile can depend upon the following.,

- CTD temperature measurement accuracy
- CTD pressure measurement accuracy
- CTD conductivity measurement accuracy
- Absolute accuracy of PSS-78
- Absolute accuracy of ESO-80
- Density profile variation in time and space versus the CTD measurement frequency.

The effect of the acceleration of gravity on the depth calculation should not be forgotten. The error caused by inaccurate modelling of the acceleration of gravity can be modelled similar to the effect of error in estimated density. Lastly, it is also important to measure and evaluate the accuracy of the atmospheric pressure. From equation (3.22) it can be seen that the atmospheric pressure is one of the limit of the integration used to determine the depth. Thus, an error in the atmospheric pressure will propagate and cause an error in the estimated depth. When all the errors in all components have been determined, a full error budget can be established, and the accuracy of the depth measurement can be evaluated.

4.6 Other positioning components

4.6.1 Surface Positioning – GPS and dGPS GPS and dGPS

GPS-positioning (Global Positioning System) is based on satellites in orbit around the Earth. On the surface of the Earth each GPS receiver calculates the ranges to a set of satellites by measuring the time of flight from the signal leaves the satellite till it arrives the receiver. The positions of the satellites are sent from the satellites to the receiver units. Using the satellite positions and ranges, the position of the GPS receiver unit on the ground can be calculated. Four satellites are necessary to solve a three dimensional position for the receiver unit. For conventional GPS navigation, 15 meters horizontal standard deviation is normal. The main error sources are: atmospheric distortions to the signal path, inaccuracies of the indication of the satellite orbits, satellite clock errors and numerical errors.

Formatert: Punktmerket + Nivå: 1 + Justert ved: 0,63 cm + Innrykk ved: 1,27 cm

Formatert: Punktmerket + Nivå: 1 + Justert ved: 0,63 cm + Innrykk ved: 1,27 cm

Formatert: Overskrift 2

Formatert: Overskrift 3, Mellomrom Etter: 0 pkt.

To increase the position accuracy on a given platform, ground based reference stations broadcast the system error. The error is determined by measuring the difference between known positions of the reference stations and positions estimated by GPS receiver units on the reference stations. The broadcasted difference between known position and the measured position is often differential correction. GPS system which offer differential correction are called dGPS. dGPS receivers typically offer position estimates with standard deviations varying from 5 m to 0.1 m depending on the quality of the differential correction service.

There are today three commercially available Global Navigation Satellite Systems (GNSS) system including the GPS system. These are the Navstar GPS (USA), GLONASS (Russia) and GALILEO (European Union).

4.6.2 Heading measurement

There are two main instruments that is used to determine the heading. These are the gyroscope and compass. A compass have a small lightweight magnet, called the needle, that balance nearly frictionless on a pivot point. Since the magnetic field of the earth have a magnetic south end at the North Pole, and magnetic north end at the South Pole, the North end of the compass needle will point toward the North Pole. This is simple and cheap instrument, however since the magnetic field of the earth is not perfectly aligned with the rotational axis. This offset must be accounted for and is called the declination. If a gyroscope is used instead these problem will not be present.

A gyroscope is a device that use a rotating wheel set in a framework that allow it to tilt freely in any direction. Gyroscopes are used in instruments as compasses and automatic pilots on board ships (Fossen, 2011). With the invention of the gyroscopic a more reliable navigation system could be achieved. Unlike a magnetic compass the gyroscopes are not sensitive to magnetic disturbance, which can cause problems in steel hulls. The gyroscope was a key invention for automatic ship controls.

4.6.3 Inertial measurement unit (IMU)

An inertial measurement unit is a sensor that usually provide three-exes rate gyros, accelerometers and magnetometers. IMU's are core component of the previous mentioned INS system, where position is obtained by integrating acceleration twice and by integrating the gyro output once, the attitude is calculated. A problem with IMU's is that the measurement will drift due to bias, misalignment and temperature variations. By using an IMU in conjunction with a global positioning system, the bias can be removed.

5 Underwater Vehicle Design

Underwater vehicles come in a wide variety of types and sizes and are used for many different purposes. Figure 1 presents the different categories of underwater vehicles.

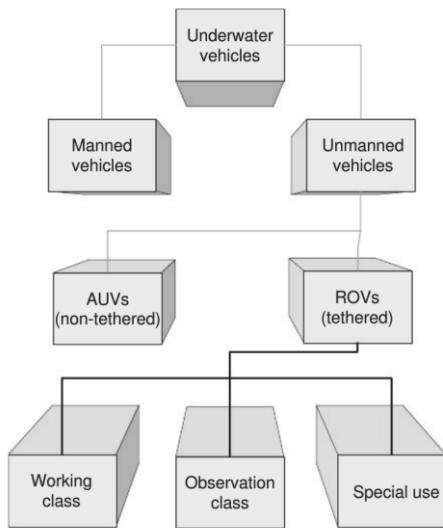


Figure 2: Underwater vehicles (Christ & Wernli Sr, 2007).

Some underwater vehicles carry human crew members or passengers and are known as manned vehicles. Examples include submarines and submersibles. Atmospheric diving suits are also included in this category, which essentially are one-person submersibles. However, manned underwater vehicles will not be covered in this course.

An increasingly popular alternative is the use of unmanned vehicles. These are partially or fully robotic machines. They are usually operated by remote control or are programmed to operate entirely on their own without guidance from a human pilot. The unmanned vehicles described in this course include remotely operated vehicles (ROVs), autonomous underwater vehicles (AUVs) (More, Bohm, & Jensen, 2010).

5.1 Remotely Operated Vehicles (ROVs)

The most common unmanned vehicles are remotely operated vehicles, or ROVs. These robot-like machines allow their operators to pilot them from a relatively safe, dry, and comfortable place, usually on a ship or platform located at the surface of the water above the ROV. The pilot directs the ROV to perform its underwater work, usually communicating with the vehicle by means of a cable (called tether or umbilical). This tether also transmits electrical power to the robot and allows data, including audio, video, still images, navigation information, and other sensor readings to be sent back to the pilot (More, Bohm, & Jensen, 2010).

The term ROV covers a wide range of equipment and no single vehicle can be described as 'typical'. Not only are there numerous ROV designs, but the same basic ROV can be modified to carry out different tasks (IMCA, 2009).

ROVs can be deployed either as free-swimming or via a tether management system (TMS). For a free-swimming ROV, the surface winch umbilical is directly connected to the vehicle. ROVs can also be deployed via a TMS where the surface winch umbilical is directly connected to the TMS. The TMS is a submersible winch with a tether connected to the ROV. The two main types commonly used are the side entry TMS (garage) or the ‘top hat’ TMS.

In the NORSO standard there is distinguished between three classes of ROV (NORSO , 2016). These are:

- Class I – Pure observation
- Class II – Observation with payload
- Class III – Work class vehicles

Pure observation class ROV’s are physically limited to video observation. They are generally small vehicles fitted with video camera, light and thrusters. They cannot undertake any other tasks without considerable modification, (NORSO , 2016).

The Observation class ROV’s can be divided in two subgroups. Class IIA observation with payload option and Class IIB observation with light intervention, survey and construction capabilities. ROV’s with class IIA should according to the NORSO u-102 standard be able to carry additional sensors such as “still colour camera, cathodic protection measurement systems, additional video cameras and sonar systems” (NORSO , 2016). Furthermore the standards state that an ROV with this class must be able to operate without loss of original function while carrying at least two additional sensors. The class IIB ROV’s are vehicles that are able to carry additional sensors, like class IIA, and must be able to operate without loss of original function while carrying at least two additional sensors. In addition to this class IIB vessels are able to carry light working manipulators and tool kits, and these vessel are capable of preforming light construction, intervention and survey tasks.

The last class of ROV’s covered by the NORSO standard is class III work class vehicles. The work class ROV’s are capable of carrying sensors, tooling and full size manipulators. The work class vessels can be divided in two, depending on their power. Class IIIA typically have power up to 100kW, and have typical through frame lifting capacity of up to 2000kg and a payload up to 200kg. Class IIIB have power more than 100kW, and have typical through frame lifting capacity of more than 2000kg and a payload more than 200kg (NORSO , 2016).

Some other definition of ROV classes do exist, where both trenching vessel, towed vessels and autonomous vessels are included.

5.2 Autonomous Underwater Vehicles (AUVs)

“Autonomous” describes the independent nature of these tetherless underwater robots – an AUV carries its own power supply and has no physical link to the surface. Also, no pilot directly controls this type of robot. Instead, preprogrammed computer or some sort of electronic circuit guides the vehicles on its mission. Onboard sensors connected to the computer bring in navigational information such as depth, speed, direction, and the location of potential obstacles. Additional systems may collect and store oceanographic data or other information for subsequent review by humans after the mission (More, Bohm, & Jensen, 2010).

AUVs may return to the surface periodically during a mission to establish radio communication with a ship, store facility, or satellites. Such a communication link can be used to retrieve data from the AUV, let the AUV update its position information, or provide the AUV with revised mission instructions. In some cases, AUVs can park themselves in underwater docking stations that have

cables to shore, thus enabling the AUV to recharge its batteries and exchange information with shore facilities through the cable (More, Bohm, & Jensen, 2010).

Since they are tetherless, AUVs are usually easier to launch and recover than tethered ROVs. Most do not require large support ships and many are able to work in virtually inaccessible places, such as under ice in polar regions. But these advantages are offset by some limitations, too. AUVs require very sophisticated systems for navigation and obstacle avoidance, so they tend to be expensive. They can store a limited amount of energy and are therefore restricted in the amount of work they can do before returning home to recharge batteries or otherwise replenish energy stores. Because of the physical properties of water that limit options for rapid, long-range data transmission, AUVs cannot transmit live video images nor easily receive complex commands while under water the way a tethered ROV can. And without such communication, they are entirely on their own in a very big ocean and can easily be lost without a trace if they become entangled, disabled, or simply fail to navigate accurately (More, Bohm, & Jensen, 2010).

In spite of these challenges, AUVs offer tantalizing possibilities. Certainly, AUV design is a very active area of research, with new ideas and new systems being tested every day. The sizable *Hugin* has already proven it can follow a pre-programmed track with high precision and efficiency, to create the detailed seabed maps necessary for deep water oil and gas explorations. And AUVs that actually perform heavy physical tasks are under development. Other remarkable AUV developments include underwater gliders and fleets of micro-AUVs that communicate with each other to accomplish complex tasks by working as a coordinated team (More, Bohm, & Jensen, 2010).

5.3 Typical Tasks for Underwater Vehicles

The typical tasks carried out by underwater vehicles can generally be grouped into the following categories:

- Site survey
- Drilling assistance
- Installation assistance
- Operation assistance
- Inspection
- Maintenance and repair (Bai & Bai, 2010).

5.3.1 Site Survey

A site survey has to be carried out before offshore activities such as drilling and installation to obtain the seabed's precise bathymetry and properties. This may be by visual observations from a ROV carrying video and still camera, or in increasingly by AUV. Detailed seabed mapping through precise bathymetry may be performed by a seamed reference system with differential pressure sensors and acoustic data transmission, which may be deployed and retrieved by an ROV. Seabed mapping can also be performed by use of a multibeam echo sounder or a side scan sonar mounted on an ROV or an AUV. A sub-bottom profiler for sub-bottom profiling may also be used to assess the quality of seabed properties for offshore installation foundation (Hallset, 2006).

5.3.2 Drilling Assistance

Drilling activities for production drilling and completion normally include:

- Deployment of acoustic units such as transponders or beacons by an ROV for surface or subsea positioning.
- Bottom survey by visual observation from a ROV with video and still cameras.

- Structure setting and testing of permanent guide base, temporary guide bare, Xmas tree, BOP, etc.
- As-built survey by ROV visual observation with supplemental equipment.

During the entire process, the observation tasks with video cameras, often with scanning sonar as supplemental “acoustic observation”, make up the majority of ROV drilling assistance. Tasks include conducting the bottom survey, monitoring the lowering of the structure and touching down, checking the structure’s orientation and level with a gyrocompass and bull’s-eye, respectively, and performing an as-built survey. Some necessary intervention work may have to be done with ROVs and remotely operated tools (ROTs) during structure setting and testing:

- Acoustic transponder or beacon deployment and recovery
- Debris positioning and removal from seabed and tree, including dropped objects
- Structure position assistance with ROV pull/push
- Guide wire deployment, recovery, and cutting during emergency conditions
- Rigging (e.g., shackle connection and disconnection)
- Cement cleaning on guide base with brush or water jet
- Valve operation with hydraulic torque toll or hydraulic stab-in
- ROV-operable guide posts, replacement, and pin pull release
- Control pod replacement if suitable for ROV (otherwise ROT)
- Anode installation by clamp and contact screw (Hallset, 2006).

5.3.3 Installation Assistance

Installation of subsea production equipment may be done in many ways, but the same basic activities are usually required. ROVs are normally used for observation and verification, and for engagement and release of guide wires and hooks. [1]

Subsea structures are widely positioned underwater using the long baseline method in which transducers used for position measuring, a gyro-compass for orientation measuring, a depth sensor for depth measuring may be mounted onto structure by packages that will be retrieved by the ROV. The orientation control may be assisted by the ROV, and the ROV has to verify via camera that the structure is aligned and level before the structure’s final set-down. ROVs may also be used to install chokes, multiphase meters, and subsea control modules. For seal pressure tests, ROVs can be used for hot stabbing.

ROVs can be used to assist in the installation of a dead anchor for pipeline/umbilical laying initiation. They can also be used to connect the pull-in line for J-tube or I-tube initiation. During normal installation and pipeline/umbilical laydown, the touchdown point is often monitored with ROVs in front and behind.

The connections between subsea production equipment and flowlines and subsea equipment and umbilicals may be completed through flying leads from the umbilical termination assembly to the tree/manifold, well jumper from the tree to the manifold, jumper from the manifold to the pipeline end terminations. The flying leads may be handled and pulled in by an ROV directly. Jumpers can be deployed from a vessel with spreader bars, and then positioned and connector actuated with the assistance of an ROV (Hallset, 2006).

5.3.4 Operation Assistance

Main production activities normally include:

- Flow control by chokes and valves operated by hydraulic actuators through control pods and umbilicals or externally by ROV or ROT intervention
- Monitoring of flow temperature and pressure by relevant measurement meters
- Chemical and inhibitor injection for corrosion, waxing, and hydrate formation resistance
- Flow separation of liquids, gases, and solids (filtering)
- Flow boosting by pumping
- Flow heating or cooling.

During the operation phase, ROVs are normally not required except for noncritical valve actuation and possibly intermittent status checks, taking samples, etc (Hallset, 2006).

5.3.5 Inspection

Inspection may be needed on a routine basis for the structures expected to deteriorate due to flowline vibration, internal erosion, corrosion, etc. Inspection includes:

- General visual inspection, including cathodic measurements and marine growth measurements
- Close visual inspection additionally requiring physical cleaning for close visual inspection, cathodic protection measurements, and crack detection by means of nondestructive testing
- Detailed inspection including close visual inspection, crack detection, wall thickness measurements, and flooded member detection
- Routine pipeline inspection including tracking and measurement of depth of cover for buried pipelines, which is also applicable for control umbilicals and power/control cables.

Cathodic protection potential measurements may be completed by cathodic protection probe, which is normally carried out by a work class ROV. Cleaning may be performed by an ROV with brushing tools or high-pressure wet jet grit entrainment. Crack detection may be performed by an ROV with magnetic particle inspection, eddy current, alternating current field measurement methods, etc (Hallset, 2006).

5.3.6 Maintenance and Repair

Maintenance activities include repair or replacement of modules subject to wear. Maintenance is normally performed by retrieving the module to the surface and subsequently replacing it with a new or other substitute module (Hallset, 2006).

Retrieval and replacement have to be anticipated during subsea equipment design. Some modules such as a multimeters, chokes, and control pods are subjected to removal and replacement. A completed replacement may have to be carried out due to the significant wear on to damage to non-retrievable parts of subsea equipment (Hallset, 2006).

Due to the difficulty and expense of maintenance and repair, the operation may be continued with regular monitoring if the damaged module is not readily replaced and does not prevent production (Hallset, 2006).

5.4 Operation of Underwater Vehicles

5.4.1 ROV Launch and Recovery Systems (LARS)

The LARS consists of a winch, winch power unit, crane/A-frame with fixed block, and ROV guiding system. The ROV system is presented in Figure 2.

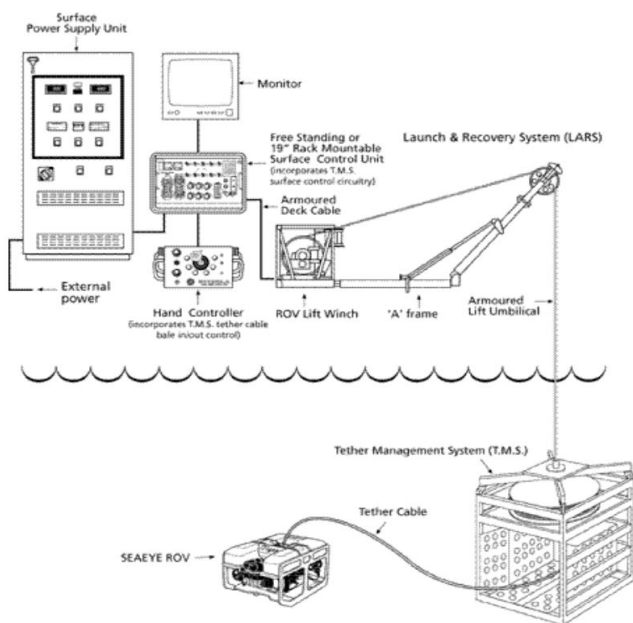


Figure 3: ROV system (denne figuren er tatt fra din power point – kilde ukjent).

Generally speaking, launch and recovery activities can be achieved by a simple rope with uplift force. However, to facilitate the deployment and recovery of the rope, a reel/drum is used, and a motor is usually used to rotate the reel and provide the uplift force. The motor may be either a hydraulic motor or an electromotor with/without a gear box used to reduce the rotary speed and increase the torque force. The system of motor, reel/drum, base frame, and other ancillary structures such as a brake and clutch is normally called a winch. A fixed block, sustained at the end of a crane boom/A-frame beam, is used to change the upward direction of the required winch force to a downward direction and position the winch on the lower structure, for example, the deck (Bai & Bai, 2010).

To restrain ROV motion while it is being lowered from the air to the water surface a LARS is used. This helps prevent, for example, damage to the umbilical by bilge keel if side deployment is being used. The LARS may be equipped with a docking head, cursor, or guide rails (Bai & Bai, 2010).

5.4.2 Umbilical and TMS

The ROV has an umbilical that runs between the support vessel and the ROV to transport hydraulic/electrical power from the vessel to the ROV and information gathered from the ROV to the surface. The diameter and weight of the umbilical should be minimized to reduce the drag force due to currents as well as lifting requirements during launch and recovery of the ROV from the water to

the surface. Normally the umbilical has a negative buoyancy, and the umbilical may be attached with buoyancy, for example every 100 m, to avoid entanglements between the umbilical and subsea equipment or the ROV itself during shallow water operation (Bai & Bai, 2010).

A tether management system (TMS) is used to deploy the ROV for deep water applications where the umbilical with negative buoyancy can launch and recover the TMS and ROV. The connection cable between the ROV and TMS can be an umbilical called tether that has a relatively small diameter and neutral buoyancy. The TMS is just like an underwater winch for managing the soft tether cable. A TMS has two significant advantages:

- ROVs can be moved more easily due to deleting the force implied by the umbilical, which may be the same as the flying resistance of the ROV itself in a water dept of 200 m and increase rapidly with increasing water depth.
- There is no need to use the ROV's own thrusters to get the ROV down to the working depth near the seabed. A powered TMS, i.e., installing some thrusters to TMS cages may be carried out to account for large drag force on TMS due to significant currents in some areas. The TMS is designed to manage the tether and can be either attached to a clump weight, mainly for the observations ROV, or to cage deployment system, mainly for work class ROVs (Bai & Bai, 2010).

5.4.3 Cable Handling

Nnnn nnn

5.5 Components of underwater vehicles

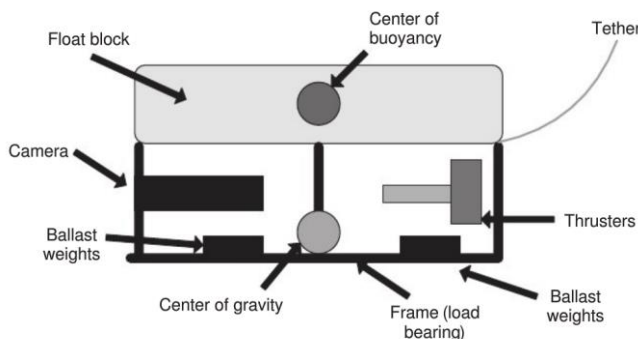


Figure 62 ROV components (Christ & Wernli Sr, 2007)

The major components of a typical ROV system, presented in Figure 3, is in this chapter described

5.5.1 Frame

The frame of the ROV provides a firm platform for mounting, or attaching, necessary mechanical, electrical, and propulsion components. This includes special instruments such as sonar, cameras, lighting, manipulator, scientific sensor and sampling equipment. In general, the material used for ROV frames are chosen to give maximum strength with minimum weight. Since weight has to be offset with buoyancy, this is critical (Christ & Wernli Sr, 2007).

The ROV frame must also comply with regulations concerning load and lift path strength. The frame can range in size from 6 in × 6 in to 20 ft × 20 ft. The size of the frame is dependent on upon the following criteria:

- Weight of the complete ROV unit in air
- Volume of the onboard equipment
- Volume of the sensors and tooling
- Volume of the buoyancy
- Load-bearing criteria of the frame (Christ & Wernli Sr, 2007).

5.5.2 Buoyancy

Archimedes' principle states: An object immersed in a fluid experiences a buoyant force that is equal in magnitude to the force of gravity of the displaced fluid. Thus, the objective of underwater vehicle flotation systems is to counteract the negative buoyancy effect of heavier than water materials on the submersible with lighter than water materials. A near neutrally buoyant state is the goal. The flotation foam should maintain its form and resistance to water pressure at the anticipated operating depth. The most common underwater vehicle floatation materials encompass two broad categories: rigid polyurethane foam and syntactic foam (Christ & Wernli Sr, 2007).

5.5.3 Electronics Cylinders

Mmm mmm

5.5.4 Connectors

Sensors propulsions and modules in an underwater vehicles must be connected. Unless the vessel is designed as one entirely closed hull, this connections must be done with cable connector. Such connection point is typical point of failure and can cause leakage into areas that should not be exposed to water.. An underwater connector can either be bought as connectors, made from cables or made with potting technique. The store bought connectors are expensive but have some advantages that is they can be more reliable and can avoid problem that cheaper solution can encounter. A cheaper solution to the store bought connectors is self made connectors. It can be tempting to use standard water proof cables, however this is not the same as true submersible cables. The main difference is that water proof cables will with a small cut in the wire will allow water to enter the cable and push through the wire. For this reason care should be taken when constructing underwater connectors. A technique called potting can also be used to create more reliable connectors. (Unmanned Vehicle Systems International (AUVSI) Foundation & US Navy Office of Naval Research (ONR) , 2014)

5.5.5 Primary Subsystems

The mission of the ROV is to sense the environment, either visually or through other means, and perform work at the desired location. The subsystems are necessary in order to accomplish this (Christ & Wernli Sr, 2007).

5.5.5.1 *Lightning*

The need for underwater lighting becomes apparent below a few feet from the surface. Ambient visible light is quickly attenuated by a combination of scattering and absorption, thus requiring artificial light to view items underwater with a degree of clarity. The main types or classes of artificial light sources used in underwater lighting are incandescent, fluorescent, high-intensity gas discharge and light-emitting diode (LED). All these types of light are meant to augment the natural light present in the environment (Christ & Wernli Sr, 2007).

5.5.5.2 Cameras

Currently, most small ROV systems use inexpensive charge-coupled device cameras as their main viewing device. These camera systems are mounted on small circuit boards and produce a video signal transmitted in a format sent up the tether to the video capture device on the surface (Christ & Wernli Sr, 2007).

5.5.5.3 Sensors

Most industrial ROV systems provide the capability to transmit data from the submersible to the surface. This allows the ROV system to deliver a suite of instruments to the work site, powered by the vehicle, with data transmitted through the tether to the surface. Any combination of sensor and instrument is available as payload to the modern ROV system, assuming proper data protocol transmission and power delivery are available (Christ & Wernli Sr, 2007).

5.5.6 Hydraulics

5.5.6.1 HPU

5.5.6.2 Valvepacks

5.5.6.3 Motors

5.5.6.4 Filters

5.5.6.5 Compensators

5.5.6.6 Piping

5.6 Vehicle Buoyancy and Stability

As presented in Figure 4, a vehicle has movement about six degrees of freedom; three translations (surge, heave and sway along the longitudinal, vertical and transverse axes respectively) and three rotation (roll, yaw and pitch about these same respective axes).

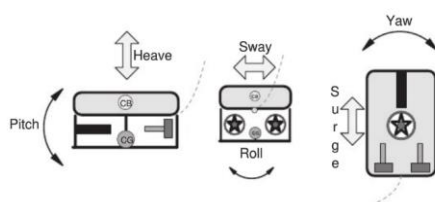


Figure 4: Vehicle degrees of freedom (Christ & Wernli Sr, 2007).

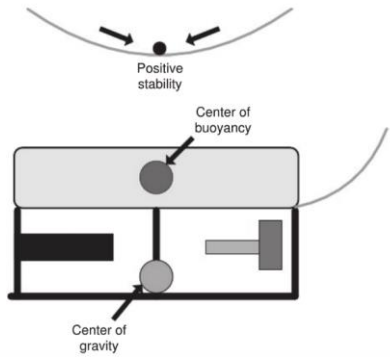


Figure 63 Positive ROV stability (Christ & Wernli Sr, 2007).

ROVs are not normally equipped to pitch and roll. The system is constructed with a high center of buoyancy (CB) and a low center of gravity (CG) to give the camera platform maximum stability about the longitudinal and lateral axes (Christ & Wernli Sr, 2007). Positive stability of the vehicle with location of CB and CG is presented in Figure 5.

5.6.1 Hydrostatic Equilibrium

Archimedes' principle states:

The magnitude of the buoyant force acting on an object is equal to the weight of the fluid displacement by the object.

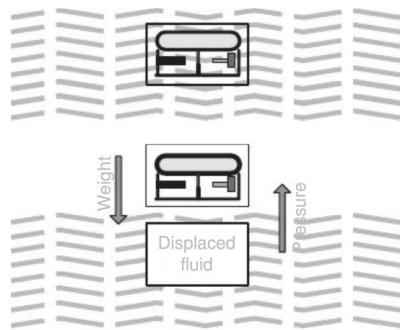


Figure 5: Hydrostatic equilibrium of ROV (Christ & Wernli Sr, 2007).

The hydrostatic equilibrium of the ROV is presented in Figure 6. The resultant of all of the weight forces on this displaced fluid is centered at a point within the body termed center of gravity (CG). This is the sum of all the gravitational forces acting upon the body by gravity given by

$$CG = \frac{1}{M} \sum_{n=1}^{i=1} cg_i \cdot m_i + \dots + cg_n \cdot m_n \quad (4.1)$$

where M is the total mass, and cg_i and m_i is the vertical location of the center of gravity and mass for component i , respectively. The resultant of the buoyant forces counteracting the gravitational pull acting upward through the CG of the displaced fluid is termed the center of buoyancy CB given by

$$CB = \frac{1}{B} \sum_n^{i=1} cb_i \cdot m_i + \dots + cb_n \cdot m_n \quad (4.2)$$

where cb_i and m_i is the vertical location of the center of buoyancy and mass for component i , respectively.

There is one variable in the stability equation that is valid for surface vessels with non-wetted area that is not considered for submerged vehicle. The point where the CB intersects the hull centerline is termed the metacenter and its distance from the CG is termed the metacentric height. For ROV considerations, all operations are with the vehicle submerged and ballasted very close to neutral buoyancy, making only the separation of the CB and the CG applicable reference metric for horizontal stability (Christ & Wernli Sr, 2007).

5.6.2 Transverse Stability

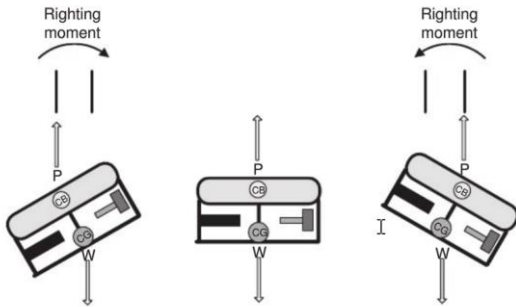


Figure 64 Righting force acting on an ROV (Christ & Wernli Sr, 2007)

The righting force acting on an ROV is presented in Figure 7.

Having located the position of the CG and the upright CB of the vehicle, the transverse stability can be investigated. This is done without regard to external forces, merely by considering the hull of the vehicle opposing forces of gravity and buoyancy. These moments are generated by horizontal displacements of the CB relative to the CG, as the vehicle inclines, such that these forces are no longer collinear, but are separated by the same distance d , which is a function of the angle of inclination, θ . The magnitude of both forces remains always the same, and equal to the vehicle's weight W , but their moment ($W \times d$) is similarly a function of θ . If the moment of the buoyancy force acts to rotate the vehicle about its same direction, it is called a heeling moment (Christ & Wernli Sr, 2007).

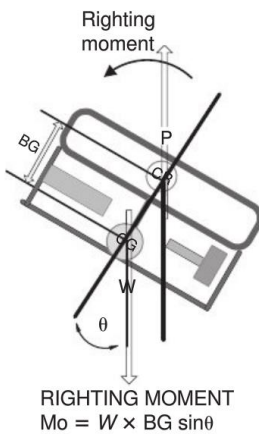


Figure 65 ROV righting moment (Christ & Wernli Sr, 2007)

As seen from Figure 8, as the BG becomes smaller, the righting moment decreases in a logarithmic fashion until static stability is lost (Christ & Wernli Sr, 2007).

5.6.3 Buoyancy

It is conventional operating procedure to have vehicles positively buoyant when operating to ensure they will return to the surface if a power failure occurs. This positive buoyancy would be in the range of about 450 grams for small vehicles and 5-7 kg for larger vehicles, and in some cases, work-class vehicles will be as much as 23 kg positive. Another reason for this is to allow near-bottom maneuvering without thrusting up, forcing water down, thus stirring up sediment. It also obviates the need for continual thrust reversal. Very large vehicles with variable ballast systems that allow for subsurface buoyancy adjustments are an exception. The vehicles operated by most observation-class operators will predominantly have fixed ballast (Christ & Wernli Sr, 2007).

5.7 Power Systems

Different power systems are applied depending on the type of vehicle and the tasks to be carried out. Most work class ROVs use a combination of electrical and hydraulic power while under water. The electricity is produced on the surface by a dedicated diesel or gasoline generator. High-voltage power from this generator is delivered by cable to a power distribution unit (PDU), which distributes this electrical power to the ROV, via a tether, and to related systems needed to operate the ROV, like the winch and the control consol. On the ROV, a portion of the electrical power is converted to hydraulic power, which is then available to operate thrusters, manipulator arms and tools (More, Bohm, & Jensen, 2010).

Although this is a typical power system for a work class ROV, some are all-electric. Smaller types of ROVs use a variety of power sources, from small generators, to standard wall outlets, to batteries (More, Bohm, & Jensen, 2010).

5.7.1 Electrical Systems

There are essentially two methods used to deliver electrical power to an underwater vehicle. One way is to draw the power from batteries placed directly on board the vehicle. Nearly all AUVs and a few ROV use this approach. The other is to deliver electrical power to the vehicle through wires bundled inside the tether. This is the most common method of supplying power to ROVs. The tether-

supplied power can come from any surface source of electrical power, including batteries, portable generators, or standard electrical outlets (More, Bohm, & Jensen, 2010).

The electrical power transmission techniques are an important factor in ROV system design due to their effect upon component weights, electrical noise propagation and safety considerations. The direct current (DC) method of power transmission predominates the observation-class ROV systems due to lack of need for shielding of components, weight considerations for portability, and the expense of power transmission devices. On larger ROV systems, alternating (AC) power is used for the umbilical due to its long power transmission distances, which is not seen by the smaller systems (Christ & Wernli Sr, 2007).

5.7.1.1 Batteries

The power source of an underwater vehicle is the main component that determines its range of travel and the tasks that it can perform. The on-board power is used for propulsion, vehicle equipment, mission or payload sensors, and on-board processing. To estimate the total power required for all these parameters needs to be taken into account. The following is a description of the energy to complete a mission for a survey of range, R , and speed, U :

$$E = \frac{(p_p + p_v + p_{ms} + p_{pc}) \times R}{3600 \times U} \text{ (kWh)} \quad (4.3)$$

such that

E = on-board energy (kWh)

p_p = propulsion power (W)

p_v = vehicle equipment power (W)

p_{ms} = mission sensor power (W)

p_{pc} = payload computer (W)

R = survey range (km)

U = velocity (m/s)

The propulsion power can be expressed as $p_p = F_D \times U$ such that drag force $F_D = \frac{1}{2} \rho U^2 S \times C_D$, C_D is the drag coefficient for the underwater vehicle form and S is the vehicle surface area (Seto, 2013).

On long missions, most of the energy consumed is for propulsion. The on-board space allotted for energy, in the form of batteries, is finite, so the objective is to carry batteries of the highest specific energy density possible. Given a constant energy density source, a larger vehicle will have more on-board energy than a smaller one. Generally, the size of the vehicle correlates directly with the speed and endurance possible. High-endurance and high-speed vehicles have to be larger (Seto, 2013).

Effort has gone into investigating energy sources for underwater vehicles, ranging from the common lead acid and lithium-based batteries to modern fuel cells. Fuel cells are an emerging technology that will affect how underwater vehicle power and energy requirements can be met with electrochemical or air-independent energy sources (fuel cells) (Seto, 2013).

Longer-range and more autonomous missions will require higher energy density batteries to be developed. This autonomy requirement is directly tied to higher energy density batteries. Autonomy could also consider mission plans that are more energetically favorable because the underwater vehicle is unexpectedly low in energy (Seto, 2013).

High energy density power sources could multiply the benefits of the underwater vehicles by conferring extended persistence and reach through superior endurance. Underwater vehicles would then be able to operate continuously over many days or weeks with powerful sensors and, at the same time, be just as capable with a smaller footprint. This would facilitate operations from vessels of opportunity. Thus on-board high energy density power sources are a critical enabler towards achieving autonomy on-board underwater vehicles (Seto, 2013).

5.7.1.2 Transmitting Electrical Power over a Tether

Most ROVs rely on surface-supplied electrical power delivered to the vehicle through the umbilical or tether.

Getting surface-supplied electrical power to an ROV at depth requires a minimum of two wires. For example, if a battery on the surface is supplying power to the submerged vehicle, there must be one wire to carry current from the battery's positive terminal down to the vehicle and another one to carry the returning current back to the battery's negative terminal in order to complete the power circuit (More, Bohm, & Jensen, 2010).

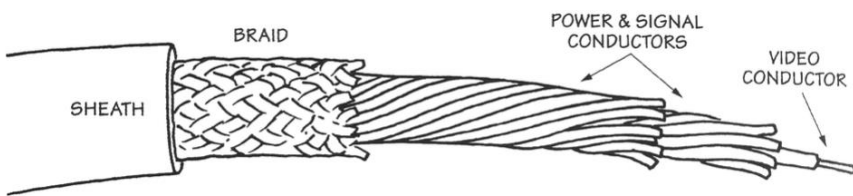


Figure 6: Complex tether cutaway view (More, Bohm, & Jensen, 2010).

Every wire, including the wire in an ROV tether, has some resistance in it. What this means is that some of the power you are trying to send down the tether to the ROV is being lost along the way, because it is heating the tether wire instead of powering the ROV. This power loss manifests itself in the form of a voltage drop, so the voltage available at the end of the tether is less than the voltage supplied at the top of the tether. This lost power reduces the overall efficiency of the vehicle's power system and undermines the performance of the vehicle. It is therefore desirable to minimize the amount of wasted power (More, Bohm, & Jensen, 2010).

Ohm's Law states that anytime current is flowing through the wires, some voltage will be lost as that current travels from one end of the wire to the other. This voltage drop, E , will be equal to the product of the current and the resistance:

$$E = I \times R \quad (4.4)$$

where I is the current and R is the resistance. Based on this, the rate at which the energy is lost from a wire due to resistive heating is found from:

$$P = I \times E = I \times (I \times R) = I^2 \times R \quad (4.5)$$

where P is the power delivered to the device. Note that the current, I, is squared in this equation. Hence, the current has a large effect on the amount of power wasted as heat. A good way to reduce the wasted power is therefore to reduce the current in the wire. The only way to reduce the current without also reducing the total power reaching the ROV is to increase the voltage to compensate. This is why long-distance power transmission is often done at very high voltages. It is simply more efficient (More, Bohm, & Jensen, 2010).

This is an attractive solution as the squared current in the equation means a modest increase in voltage results in a big payoff in terms of reduced power loss. AC power is typically used instead of DC power, because AC power is much easier and cheaper to convert from one voltage to another. This AC power is typically in the range of a few hundred to a few thousand volts. Unfortunately, high voltages can be deadly around water and require advanced techniques, materials and training to ensure adequate safety (More, Bohm, & Jensen, 2010).

Another approach to reducing the wasted power would be to reduce the resistance, R, in the wire. This could be done by making the wire shorter or by giving it greater cross-sectional area. However, if the tether is longer than a few tens of meters and/or more than three or four wires are in it, this option can get quite heavy, stiff and expensive. Moreover, in strong currents, a thicker tether will add to the drag experienced by the vehicle. It is possible to add more powerful thrusters to pull the fatter tether around, but that would require more power, leading right back to the initial problem (More, Bohm, & Jensen, 2010).

Distribution system

Ground faulting

5.7.2 Hydraulic systems

Many work class ROVs use hydraulic systems to power strong thrusters, manipulator arms, and a wide variety of saws, cutters, and other tools.

A hydraulic system is a means of distributing power from one place to another. This is done by using liquid pressure to transmit force and motion. The energy for the hydraulic system comes from electricity, and is transformed into kinetic energy by a prime mover. The prime mover is usually an electric motor connected by a drive shaft to a hydraulic pump. As the shaft rotates, the pump pressurizes and circulates the hydraulic fluid through pipes, hoses, or turbines – referred to collectively as hydraulic lines or lines. The pressurized liquid in the lines flows through one or more hydraulic actuators, such as rotary motors or linear rams, which is basically a piston in a cylinder. These actuators move whatever they are connected to when the fluid pressure presses on pistons, gears, or other mechanisms inside the actuator (More, Bohm, & Jensen, 2010).

Hydraulic force transfer, which is the basis for hydraulic power transfer, is based on Pascal's Law, which states that fluid confined in a container or any closed system of pipes or tubing can transmit force more or less instantaneously from one part of the system to every other part (More, Bohm, & Jensen, 2010).

- Basic hydraulics

- Power, flow, pressure

- Component and system knowledge

- Motor, pumps, valve blocks

Hydraulic power and efficiency ed

5.8 Design theory

5.8.1 Traditional Design Process

5.8.1.1 The Design and Associated Processes

Figure 10 shows the design and associated processes, which may be divided into

- Pre-design
- Design
- Post-design

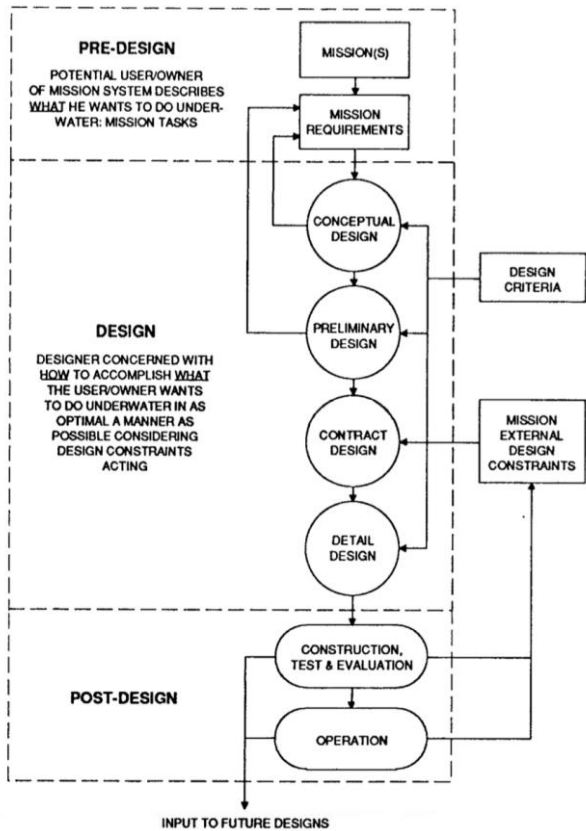


Figure 66 Design and associated processes (Allmendinger, 1990).

The pre-design process leads to the formulation of the basic input to the design process – the mission(s) statement(s) and associated mission requirements. The mission is a short concise statement of what the user/owner wants to accomplish. Mission system design may be based on single or multimission requirements, the latter including two or more categories of underwater

tasks. Mission requirements elaborate on the mission statement by specifying conditions under which the mission task(s) are to be carried out. They include information such as task-site locations and maximum depths, description of work objects and tasks to be performed, and such other information as the user may wish to stipulate (Allmendinger, 1990).

The design process is composed of three phases

- Basic design
- Contract design
- Detailed design

Basic design is the primary design phase concerned with how best to accomplish what the potential user of the mission system wants to do underwater as set forth by his mission requirements. Basic design can roughly be divided into two stages; conceptual design stage and preliminary design stage. The conceptual design is the first attempt to translate all the user mission requirements into performance requirements and characteristic of the systems composing the mission system. The preliminary design refines the characteristics and cost estimates of the system composing the optimum conceptual design. Contract design requires yet further refinement of design and additional detail. It provides contractual documents for the construction and alteration work. Detail design is the final phase of the design process and entails the development of detailed working planes from which the systems are constructed or altered (Allmendinger, 1990).

The post-design process is composed of three activities: construction/alteration, test and evaluation, and operation (Allmendinger, 1990).

5.8.1.2 Design Spiral

The iterative nature of the overall design process may be modeled by the design spiral. A design spiral is presented in Figure 11. The spiral consists of spokes and loops. The spokes represent design considerations including performance requirements, submersible characteristics, and cost estimates. The loops indicate design iterations with the design's refinement increasing for the loops spiral inward (Allmendinger, 1990).

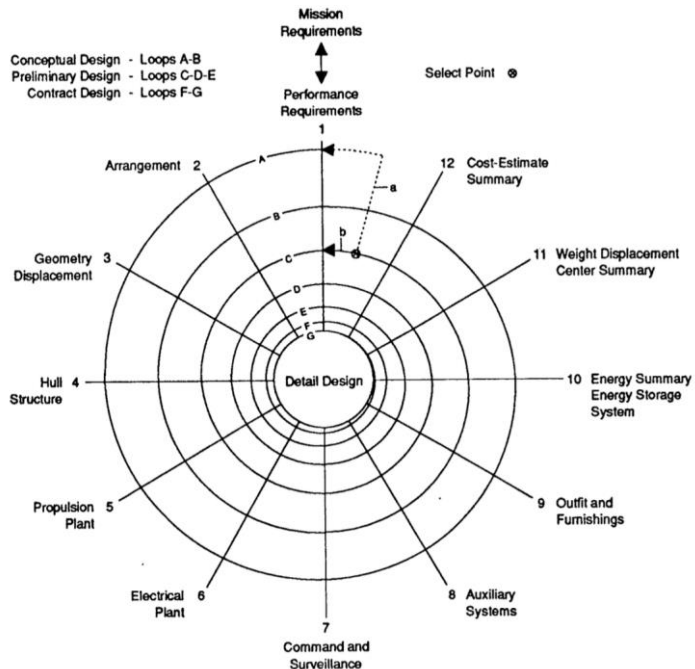


Figure 67 Design and associated processes (Allmendinger, 1990).

The intersection of loops and spokes form points which are identified alphanumerically. Thus, for example, 3B is a point in the spiral at which the geometric characteristics of the submersible are being considered in the second iteration in a more detailed manner than they were initially at point 3A. The design converges to a satisfactory solution to the design problem as the adjustments become progressively smaller with each succeeding loop through the conceptual, preliminary, and contract design. This fact is demonstrated on the spiral by the decreasing spacing between loops as they spiral inward. Convergence is illustrated by the innermost loop becoming a circle, indicating that all the design considerations are fully developed and require no further adjustments. At this point, the detailed design can begin (Allmendinger, 1990).

Conceptual design feasibility studies are somewhat arbitrarily confined to the A and B loops of the spiral. The “select point” may be thought of as a repository for completed alternatives – the point at which these alternatives are compared and the most cost-effective, viable one is selected. Paths (a) and (b) are shown issuing from this point. Path (a) leads back to 1A and the beginning of a new conceptual design alternative based on either changes in performance requirements, which call forth a new set of submersible characteristics and associated cost estimates which satisfy the same performance requirements. Path (b) leads to the beginning of the preliminary design and is followed by the conceptual design emerging from the “select point” as the optimum alternative from among those generated. Preliminary design is also arbitrarily limited to loops C, D and E (Allmendinger, 1990).

The A loop procedures are primarily concerned with the approximate sizing of the submersible and utilize empirical formulas and similar design data extensively. Sizing involves three steps: selecting the geometry and the major elements of the systems to be used for the particular conceptual design

alternative under the study; obtaining first estimates of sizing data for these systems; and the summarizing of these data to estimate the size parameters of total weight and displacement in the neutral buoyancy condition and the total cubic (Allmendinger, 1990).

The B loop procedures begin to develop the submersible and its systems in detail for the purpose of refining sizing data, obtaining cost estimates and obtaining assurance that the design condition criteria of neutral buoyancy, zero time, and adequate stability can be attained (Allmendinger, 1990).

The C, D and E loops involves preliminary design procedures of these loops progressively refine all aspects of the submersible's design, including those aspects not considered in the conceptual design phase. Only small adjustments, if any, are required at the spiral's point at the end of the E loop (Allmendinger, 1990).

5.8.2 Axiomatic Design

The design process presented in the previous section is an iterative process. In contrast, the axiomatic design process is linear. The process is presented in Figure 12. The first phase is to step into the situation of the problem-owner. In axiomatic design terminology this is termed the customer domain. The design proceeds as the designer proceeds from customer domain to the process domain (Ludvigsen, 2010).

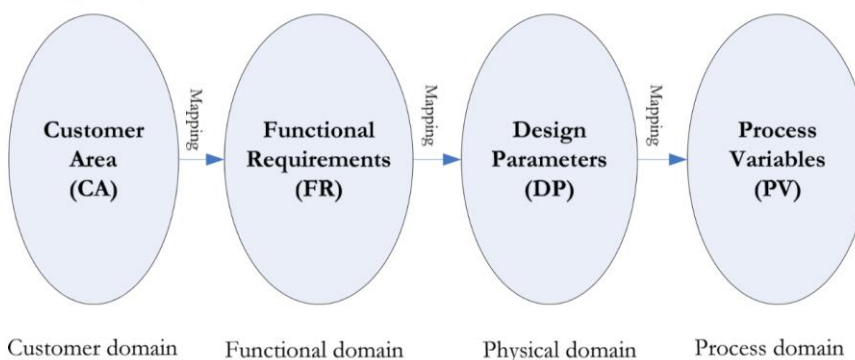


Figure 68 The stages of axiomatic design (Ludvigsen, 2010)

There are 7 central concepts in axiomatic design.

- *Axiom*: Self-evident truth or fundamental truth for which there are no counterexamples or exceptions. An axiom cannot be derived for other laws or principles of nature.
- *Colloray*: Interference derived form axioms or for propositions that follow from axioms or other propositions that haven been proven.
- *Theorem*: A proposition that is not self-evident but that can be proven from accepted premises or axioms and so is established as a law or principle.
- *Functional requirements*: A minimum set of independent requirements that completely characterize the functional needs of the product expressed in the functional domain. By definition each FR is independent of every other FR at the time the FR was formulated.
- *Constraints*: They are bounds for the acceptable solution. There are two kinds of constraints; input constraints and system constraints. Input constraints are imposed as a part of the design specification, while system constraints are imposed by the design choices made

underway during the design process. Constant parameters or parameters inaccessible for the designer are often categorized as constraints. When designing scientific marine surveys constraints can be cost, available vessels, vehicles and personnel.

- *Design parameter*: DP's are the key physical variables in the physical domain that characterize the design that satisfies the specified FR's. There should be one DP for each FR.
- *Process variable*: PV's are the key variables in the process domain that characterize the process that generate the specified DP's (Ludvigsen, 2010).

The colloraries and theorems of axiomatic design are intended as design guidelines. Axiomatic design is based on two axioms. From these axioms a number of theorems and colloraries are derived and from the basis for the axiomatic design.

1. Maintain the independence of functional requirements
2. Minimize information content

The first axiom prescribes to maintain independence of the functional requirements. It is common to arrange the FR and DR in a matrix, as presented in Table 1 (Ludvigsen, 2010).

When the system is configured with minimum dependence, each design parameter should address only one functional requirement, as in Table 1 A. This type of system is termed an uncoupled system. In a truly uncoupled system there are only correlations between the defined FR's and DP's along the diagonal as shown in the table. The advantage of an uncoupled system is that it is possible to change one FR without affecting other FR's in the system (Ludvigsen, 2010).

Table 1: Relation between FR's and DP's in an uncoupled system, a decoupled system and a coupled system (Ludvigsen, 2010).

	DP 1	DP 2	DP 3		DP 1	DP 2	DP 3		DP 1	DP 2	DP 3
FR 1	X			FR 1	X			FR 1	X	X	X
FR 2		X		FR 2	X	X		FR 2	X	X	X
FR 3			X	FR 3	X	X	X	FR 3	X	X	X
A				B				C			

In some situations it is difficult to find uncoupled FR's and a decoupled system can be defined. In a decoupled system there can only be correspondence along the diagonal and below the diagonal, as shown in Table 1 B. In the design process one will start with adapting "DP 1" to satisfy "FR 1", "FR 2" and "FR 3" for the general case in Table 1 B. The design for "DP 2" can then be chosen without interfering with the previous design choices. The design matrices shown in Table 1 can be established at multiple levels. The design for "DP 1" and "FR 1" can be detailed in a sublevel for design choices. The functional requirements in "FR 1" will then be broken down to new functional requirements FR 1.1, FR 1.2 and FR 1.3 with corresponding DP's. When the designer wants to proceed from the physical domain to the process domain, similar tables and matrices are constructed and the same preference for diagonal or triangular tables and matrices applies (Ludvigsen, 2010).

The second axiom prescribes to reduce the information content in the design. The information content I_i may mathematically be related to the probability P_i of satisfying FR_i through

$$I_i = \log_2 \frac{1}{P_i}$$

The second axiom is applied when several designs are equally acceptable from a functional point of view. The design with the lowest information content is the superior design. An uncoupled design has always lower information content than a decoupled system (Ludvigsen, 2010).

Even though axiomatic design is a linear design method, the design can collapse at any point before the design is complete. The design collapses when functional requirements cannot be kept independent or met by design parameters. Then the process has to start from the beginning and a different configuration of constraints, FR's and DR's must be attempted (Ludvigsen, 2010).

6 Hydrodynamics of underwater vehicles

6.1 Vehicle dynamics

The study of dynamics of a vessel can be divided in two, the kinematics and the kinetics. The kinematics is a term that describe the geometrical aspects of the motion. The kinetics involves the study of the forces that induce the motion. An introduction to kinematics of a vessel will be given by introducing the reader to reference frames. A description of vessel kinetics will also be presented.

6.1.1 Kinematics

For a marine craft moving in six degrees of freedom (DOFs), six independent coordinates are necessary to determine the position and orientation. The first coordinates, and their time derivatives, correspond to the position and translation motion along the x , y and z axis, while the last three coordinates and their time derivatives are used to describe orientation and rotational motion. For marine craft, the six different motion components are conveniently defined as surge, sway, heave, roll, pitch and yaw, as presented in Figure 1 (Fossen, 2011).

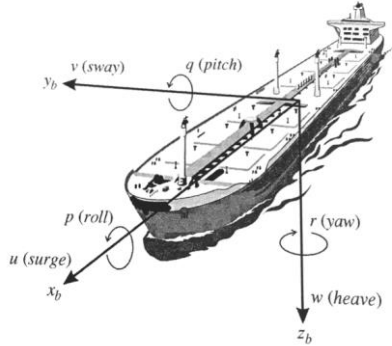


Figure 7: The 6 DOF velocities u , v , w , p , q and r in the body-fixed coordinate frame (Fossen, 2011).

Of these the first three and their derivative represent the position and translation along the x , y and z axis. The last three degrees of freedom represent orientation and rotational motion.

The degrees of freedom are combined in one vector, η , and the derivative in the $\dot{\eta}$ vector. We will also define the linear and angular velocities as v .

$$\eta = \begin{bmatrix} x \\ y \\ z \\ \phi \\ \theta \\ \psi \end{bmatrix}, \dot{\eta} = \begin{bmatrix} \dot{x} \\ \dot{y} \\ \dot{z} \\ \dot{\phi} \\ \dot{\theta} \\ \dot{\psi} \end{bmatrix}, v = \begin{bmatrix} u \\ v \\ w \\ p \\ q \\ r \end{bmatrix} \quad (5.1)$$

6.1.1.1 Reference frames

When analyzing the motion vessels it is useful to define some types of reference frames. A reference frame is a coordinate system where the axis can be fixed to a vessel or fixed to the earth. There are

several commonly used reference frames. Two commonly used earth centered reference frames are the earth-centered inertial (ECI) and the earth-centered earth fixed (ECEF). The ECI frame is an inertial reference frame, and is used for terrestrial navigation (Fossen, 2011). The origin of this reference frame is in the center of the earth, and the axis is presented in figure 2. The ECEF frame also has its origin in the center of the earth, however the axis of this reference frame rotate relative to the surface of the earth, with a rotation speed equal to the earth rotation speed. These two reference frames are called earth centered frames.

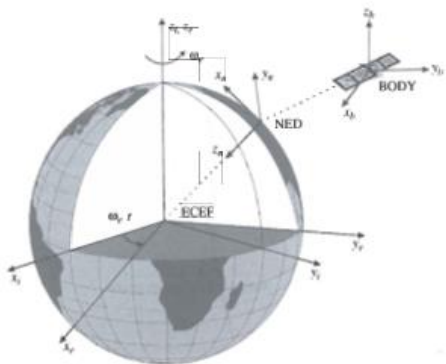


Figure 8: Reference frames (Fossen, 2011).

Two other reference frames that are more applied for analysis of vessel kinematics is the North-East-Down frame (NED) and the Body-fixed reference frame (BODY). The NED reference frame is the coordinate system we most commonly use in our life, and is a geographical reference frame (Fossen, 2011). This reference frame is defined as the tangent plane to the surface of the earth. Moving with the vessel. The x-axis is in this frame always in the direction of true north, y-axis is in the east direction, while z-axis is pointing down.

The second important reference frame is the BODY frame. This is frequently used when analyzing the movement of a vessel. The axis of this coordinate system is fixed to the body, and will rotate along with the body, unlike the NED frame. The x-axis is most commonly used as the longitudinal axis, which for a ship correspond to the fore to aft direction. The y axis is the transverse axis, and is directed to starboard. Finally the z-axis is directed from the top towards the bottom of the ship. Velocity measurement and acceleration is measured in the body frame.

When a vessel have a heading equal to true north, and no pitch or roll motion is present, the NED frame and the BODY frame will coincide. However for any other roll, pitch or yaw angle, the frames will not coincide, and convention of coordinate between the two reference frames involve trigonometric analysis. By applying a rotation angle between coordinate system, a set of equations can be developed. These equation that convert between reference frames can be presented on matrix form as bellow, (Fossen, 2011).

$$R_{x,\phi} = \begin{bmatrix} 1 & 0 & 0 \\ 0 & c\phi & -s\phi \\ 0 & s\phi & c\phi \end{bmatrix}, R_{y,\theta} = \begin{bmatrix} c\theta & 0 & s\theta \\ 0 & 1 & 0 \\ -s\theta & 0 & c\theta \end{bmatrix}, R_{z,\psi} = \begin{bmatrix} c\psi & -s\psi & 0 \\ s\psi & c\psi & 0 \\ 0 & 0 & 1 \end{bmatrix} \quad (5.2)$$

In the equation above, c is an abbreviation for cosine, and s is sine. These matrices are called rotation matrices, and transform a coordinate in one coordinate system, to a coordinate system where the axis is rotated an angle equal to ϕ , θ and ψ around the x, y and z axis, respectively.

Based on the discussion above we can now see that the relationship between the derivative of the position, $\dot{\eta}$, that related to the NED frame, and the velocities, v , related to the body frame, can be obtained by rotating the velocities. The complete rotation matrix can be written as

$$R(\phi, \theta, \psi) = R_{x,\phi}(\phi) * R_{y,\theta}(\theta) * R_{z,\psi}(\psi) \quad (5.3)$$

The relation between v , the velocity that are measured in the body frame, and $\dot{\eta}$, the derivative of the position in the NED frame, can now be written as

$$\dot{\eta} = R(\phi, \theta, \psi) * v \quad (5.4)$$

6.1.2 Kinetics

We will now consider the forces that cause the motions we have discussed. The equation of motion for the marine craft for the six DOFs, presented at the beginning of this chapter, may be represented by the equation below, which is developed based on Newton's laws of motion.

$$Mv + C(v)v + D(v)v + g(\eta) + g_0 = \tau + \tau_{wind} + \tau_{wave} \quad (5.5)$$

Where

$M = M_{RB} + M_A$	System inertia matrix (including added mass)
$C(v) = C_{RB}(v) + C_A(v)$	Coriolis-centripetal matrix (included added mass)
$D(v)$	Damping matrix
$g(\eta)$	Vector of gravitational/buoyancy forces and moments
g_0	Vector used for pretrimming (ballast control)
τ	Vector for control inputs
τ_{wind}	Vector for wind forces
τ_{wave}	Vector for wave-induced forces
η	Position vector
v	Velocity vector

Hydrodynamic potential theory programs can be used to compute the added mass and damping matrices by integrating the pressure of the fluid over the wetted surface of the hull. These programs assume that viscous effects are neglected. Consequently it is necessary to add viscous forces manually. The programs are based on the assumption that first- and second-order wave forces can

be linearly superimposed. The potential coefficients are usually represented as frequency-dependent matrices for 6 DOF motions. The matrices are

- $A(\omega)$ added mass
- $B(\omega)$ potential damping

where ω is the wave excitation frequency of a sinusoidal (regular) wave maker or the ocean.

In hydrodynamics it is common to assume that the hydrodynamic forces and moments on a rigid body can be linearly superimposed. This results in a hydrodynamic mass-damper-spring system that can be explained as:

Forces on the body when the body is forced to oscillate with the wave excitation frequency and there are no incident waves.

The contribution to the hydrodynamic mass-damper-spring forces is as follows:

- Hydrodynamic mass-damper:
 - Added mass M_A due to the inertia of the surrounding fluid. The corresponding Coriolis and centripetal matrix due to added mass is due to rotation of the body-related coordinate system with respect to coordinate system related to the Earth's ellipsoid and is denoted $C_A(v_r)$.
 - Radiation-induced potential damping D_P due to the energy carried away by the generated surface waves.
 - Viscous damping caused by skin friction, wave drift damping, vortex shedding and lift/drag

The resulting hydrodynamic force is written

$$\tau_{hyd} = -M_A \dot{v}_r - C_A(v_r)v_r - D_P v_r + \tau_{visc} \quad (5.6)$$

where $v_r = v - v_c$ with v_c as the relative velocity due to an irrotational constant ocean current. $M_A \dot{v}_r - C_A(v_r)v_r$ is the added mass and $D_P v_r$ is the potential damping. The viscous damping is given by

$$\tau_{visc} = -D_V v_r - D_n(v_r)v_r \quad (5.7)$$

with $D_V v_r$ representing the linear viscous friction and $D_n(v_r)v_r$ representing the nonlinear viscous friction.

- Hydrostatic spring stiffness
 - Restoring force due to Archimedes

$$\tau_{hs} = -g(\eta) - g_o \quad (5.8)$$

The potential coefficient matrices $A(\omega)$ and $B(\omega)$ can be computed using a hydrodynamic code with approximate expressions for M_A , D_P and $C_A(v_r)$. Fully coupled matrices M_A and D_P in 6 DOF can, however, be computed using model experiments or curve fitting experimental data. The total

hydrodynamic damping matrix $\mathbf{D}(\mathbf{v}_r)$ is the sum of the linear part \mathbf{D} and the nonlinear part $\mathbf{D}_n(\mathbf{v}_r)$ such that

$$\mathbf{D}(\mathbf{v}_r) := \mathbf{D} + \mathbf{D}_n(\mathbf{v}_r) \quad (5.9)$$

The nonlinear damping may be modeled using the ITTC resistance law and cross-flow drag formulations.

The hydrodynamic mass-damper-spring forces must be included in the equations of motion in order to integrate acceleration $\dot{\mathbf{v}}$ to velocity and position. Consider the rigid-body kinetics

$$\mathbf{M}_{RB}\dot{\mathbf{v}} + \mathbf{C}_{RB}(\mathbf{v})\mathbf{v} = \boldsymbol{\tau}_{RB} \quad (5.10)$$

Where

$$\boldsymbol{\tau}_{RB} = \boldsymbol{\tau}_{hyd} + \boldsymbol{\tau}_{hs} + \boldsymbol{\tau}_{wind} + \boldsymbol{\tau}_{wave} + \boldsymbol{\tau} \quad (5.11)$$

the vector $\boldsymbol{\tau}$ represents the propulsion forces and moments. Substituting Equation 2 and Equation 4 into Equation 7 gives

$$\begin{aligned} \mathbf{M}_{RB}\dot{\mathbf{v}} + \mathbf{C}_{RB}(\mathbf{v})\mathbf{v} + \mathbf{M}_A\dot{\mathbf{v}}_r + \mathbf{C}_A(\mathbf{v}_r)\mathbf{v}_r + \mathbf{D}(\mathbf{v}_r)\mathbf{v}_r + \mathbf{g}(\boldsymbol{\eta}) + \mathbf{g}_o \\ = \boldsymbol{\tau} + \boldsymbol{\tau}_{wind} + \boldsymbol{\tau}_{wave} \end{aligned} \quad (5.12)$$

where $\mathbf{M}_{RB}\dot{\mathbf{v}} + \mathbf{C}_{RB}(\mathbf{v})\mathbf{v}$ are rigid body forces, $\mathbf{M}_A\dot{\mathbf{v}}_r + \mathbf{C}_A(\mathbf{v}_r)\mathbf{v}_r + \mathbf{D}(\mathbf{v}_r)\mathbf{v}_r$ are hydrodynamic forces and $\mathbf{g}(\boldsymbol{\eta}) + \mathbf{g}_o$ are hydrostatic forces.

For an underwater vehicle operating below the wave-affected zone the six DOF nonlinear equation of motion can be written

$$\mathbf{M}\dot{\mathbf{v}} + \mathbf{C}(\mathbf{v})\mathbf{v} + \mathbf{D}(\mathbf{v})\mathbf{v} + \mathbf{g}(\boldsymbol{\eta}) = \boldsymbol{\tau} \quad (5.13)$$

with the hydrodynamic coefficients independent of the wave excitation frequency. Consequently,

$$\begin{aligned} \mathbf{M}_A &= \mathbf{A}(\omega) = \text{constant} \quad \forall \omega \\ \mathbf{B}(\omega) &= 0 \end{aligned} \quad (5.14)$$

This means that if a seakeeping code is used to compute the potential coefficients, only one frequency is needed to obtain an estimate of the added mass matrix. In addition, there will be no potential damping. However, viscous damping $\mathbf{B}_V(\omega)$ will be present.

6.1.3 Motion equation for a submarine

Similar to surface vessels, the equation of motion for a submarine can be developed from Newton's laws

$$\vec{F}_1 = \frac{d}{dt}(m\vec{U}) \quad (5.15)$$

Kommentert [EH9]: Bør det refereres til Berg 2014 oftere?

$$\vec{F}_2 = \frac{d}{dt} (I \vec{\Omega}) \quad (5.16)$$

In the equations above, \vec{U} is the linear velocities, while $\vec{\Omega}$ is the angular velocities. The result of the equation of motion for submarines are somewhat more complicated as the result consist of more than 100 coefficient. For the equation of motions for submarines the components can be classified as follow, (Berg, 2014):

- Internal force (the vessel and added mass/ added moment of inertia)
- Centrifugal forces due to the rotation of the submarine
- Damping forces
- Control forces from the rudder and planes
- Control forces from propellers and thrusters
- Gravity and buoyancy forces (static forces)

For many applications, the linear equation of motion can be used. The linear equations is very useful when studying small perturbations from a stable straight line motion for a submarine at constant depth, which is dynamically stable. When the linear motion equations are used, the following assumptions are common:

- Longitudinal motions do not generate any transverse motion
- First order transvers motion will not generate longitudinal motions
- The submarine makes small perturbations around the constant straight line motion
- Small angles control units (rudders, bow/stern planes)

These assumptions imply that motion in longitudinal direction and transverse direction is independent. With this, the submarine equation on of motion can be written by two sets of first order differential equation. One for heave and pitch, and one for sway, roll and yaw.

The linear heave and pitch motion can now be written as below, according to (Berg, 2014).

$$(Z_{\dot{w}} - m)\dot{w} + Z_w w + Z_{\dot{q}}\dot{q} + (mU + Z_q)q + z_\delta \delta = 0 \quad (5.17)$$

$$M_{\dot{w}}\ddot{w} + M_w w + (M_{\dot{q}} - I_y)\ddot{q} + M_q q - mg\overline{BG}\theta + M_\delta \delta = 0$$

It is useful to evaluate the equation non dimensional while calculating maneuverability. By dividing the equations by $\frac{1}{2}\rho U^2 L^2$ and $\frac{1}{2}\rho U^2 L^3$ respectively, we get:

$$(Z_{\dot{w}}' - m')\dot{w}' + Z'_w w' + Z'_{\dot{q}}\dot{q}' + (m' + Z'_q)q' + z'_\delta \delta = 0 \quad (5.18)$$

$$M'_{\dot{w}}\ddot{w}' + M'_w w' + (M'_{\dot{q}} - I'_y)\ddot{q}' + M'_q q' - m'\gamma\theta + M'_\delta \delta = 0$$

The restoring term $-m'\gamma\theta$ will be decisive significance at low speed. The prime is used to denote dimensionless quantities.

We can formulate the characteristic equation, by removing the heave dependency, the tow differential equations can be reformulated into one equation.

$$(AD^3 + BD^2 + CD + E)\theta = 0 \quad (5.19)$$

In this equation we have used $D = \frac{d}{dt}$.

$$\begin{aligned} A &= (M'_q - I'_y)(Z'_w - m') - Z'_q M'_w \\ B &= M'_q(Z'_w - m') + (M'_q - I'_y)Z'_w - (m' + Z'_q)M'_w - M'_w Z'_q \\ C &= M'_q Z'_w - (m' + Z'_q)M'_w - m'\gamma(Z'_w - m') \\ E &= -m'\gamma Z'_w \end{aligned} \quad (5.20)$$

Fixed-stick stability is achieved when the roots of the characteristic equation have a negative real part is negative.

The horizontal motion of a submarine consist of coupled motion in sway, yaw and roll. The linearized equation of horizontal motion can be developed and is presented below

$$\begin{aligned} (Y_v - m)\dot{v} + Y_r\dot{r} + Y_v v + (Y_r - mU)r + T_\delta \delta_R &= 0 \\ K_v v + K_r r + (K_p - I_x)\dot{p} + K_p p + K_\delta \delta_R - mg\bar{B}\bar{G}\phi &= 0 \\ N_v\dot{v} + (N_r - I_z)\dot{r} + N_v v + N_r r + N_\delta \delta_R &= 0 \end{aligned} \quad (5.21)$$

By again transforming to non-dimensional we rewrite the equation above.

$$\begin{aligned} (Y'_v - m')\dot{v}' + Y'_r\dot{r}' + Y'_v v' + (Y'_r - m')r' + T'_\delta \delta_R &= 0 \\ K'_v v' + K'_r r' + (K'_p - I'_x)\dot{p}' + K'_p p' + K'_\delta \delta_R - m'\gamma\phi &= 0 \\ N'_v\dot{v}' + (N'_r - I'_z)\dot{r}' + N'_v v' + N'_r r' + N'_\delta \delta_R &= 0 \end{aligned} \quad (5.22)$$

The stick-fixed stability in the horizontal plane, $\delta_R = 0$ is assumed. The yaw and sway dependency is then removed, and the equation of motion is written as

Kommentert [EH10]: Bør inkludere en ordentlig definisjon av begrepet med kilde

$$(A_1 D^2 + B_1 D + C_1)(E_1 D^2 + F_1 D + G_1)\phi = 0 \quad (5.23)$$

Similar to the vertical plane, we write $D = \frac{d}{dt}$, and the coefficient is defined as

$$\begin{aligned} A_1 &= K'_p - I'_x \\ B_1 &= K'_p \\ C_1 &= -m'\gamma \\ E_1 &= (Y'_v - m')(N'_r - I'_z) - Y'_r N'_v \end{aligned} \quad (5.24)$$

$$F_1 = (Y'_v - m')N'_r + (N'_r - I'_z)Y'_v - Y'_v N'_r - (Y'_r - m')N'_v$$

$$G_1 = Y'_v N'_r - (Y'_r - m')N'_v$$

By using the coefficients above and the condition for fixed stick stability, the vessels stability can be determined from tow second order algebraic equations.

Many of the coefficients that must be determined can be challenging to obtain. For this purpose, wind tunnel and water tank testing have been used to determine hydrodynamic coefficients like damping and added mass matrix. Potential flow theory have also been frequently used to calculate these coefficients as well. When determining the coefficients it is normal practice to ignore a large number of possible non-linear coupling terms. The reason for this is that many of them can not be measured or estimated well, and thus there is little or no data to determine these coefficient from. Alternatively model test can be preformed, but these tests and models are often complex.

6.1.4 Hydro dynamics for AUV's

AUV's are designed in order to minimize resistance. The AUV is self powered, and low resistance will therefore give longer mission duration. Initially AUV's were designed with a torpedo shape, but later the focus have shifted to developing hulls with little drag. When designing an AUV or UUV it is worth noting that the dimension of these are of such that most of these will be operating in a Reynolds number where the flow is changing from laminar to turbulent. Use of laminar flow design bodies will therefore not always be successful (Berg, 2014). In order to reduce resistance on the AUV, a suitable forebody geometry must be selected. From fluid dynamics it is known that the lowest drag coefficient is obtained with a streamlined body. The afterbody design will also influence the resistance of the AUV, especially the coming angle is an important parameter.

The most efficient form of propulsion for AUV is the single screw layout, however twin screw propulsion have some advantages over the single screw with respect to maneuverability. High propulsion efficiency is often difficult to obtain, but some general rules of thumb can be noted, with respect to efficiency. Open propellers are better than ducted ones, large diameter and high pitch with low blade area and few rotation per minute have are more energy efficient. These advantages come however at a cost, and some disadvantages is noted by (Dand, 1991).

In order to analyses the maneuvering characteristics of an AUV, a 6 degree of freedom model is used. We consider only small perturbations from a constant straight line motion. As we did earlier, we separate the equation of motion in one for the horizontal plane, and one for the vertical plane. This can be done since the two set of linear motion equation. When the wet weight of the vessel is W , the equations can be written as below.

Horizontal plane:

$$(Y_v - M)\dot{v} + Y_v v + Y_r \dot{r} + (Y_r - Mu)r + Y_\delta \delta = 0 \quad (5.25)$$

$$N_v \dot{v} + N_v v + (N_r - I_z) \dot{r} + N_r r + N_\delta \delta = 0$$

$$(Z_w - M)\dot{w} + Z_w w + Z_q \dot{q} + (Z_q - Mu)q + Z_\delta \delta = 0 \quad (5.26)$$

$$M_{\dot{w}}\dot{w} + M_w w + (M_q - I_y) + M_q q + \bar{B}\bar{G}W\theta + M_\delta \delta = 0$$

A simplified non linear equation is also used for the surge motion

$$(X_{\dot{u}} - M)\dot{u} + X_u u + X_{u|u}|u|u| + T_{n|n}|n|n| + T_{un}un = 0 \quad (5.27)$$

These equation is valid for streamlined bodies. Non-streamlined bodies the non-linear equation of motion should be used. In general is can be stated (Berg, 2014) that the directional stability and the turning characteristics, to a large extent are governed by the ratio of body length to diameter. A long slender body will have good directional stability and reduced turning capabilities, compared to a short and thicker one. In order to successfully design an AUV it must have some form of control actuator or controlled thrusters. Most commonly this is on the form of; lifting surfaces, like foils, main driver propulsors, mass / buoyancy effects and additional thrusters to control either yaw, sway or heave.

As mentioned earlier the challenge of determining the coefficients in the equation of motion could be solved in one of three basic methods. These are:

- Theoretical calculations
- Model test with fixed models
- Model test /full scale test with free-swimming vehicles.

In the calculation of the added mass, an initial estimation can be made with simplified two-dimensional calculations for the diagonal terms in the added mass matrix.

The damping forces associated with an AUV that is streamlined is comprised of three terms

- Inviscid fluid forces
- Viscous lift forces
- Lift forces in control planes

The inviscid fluid force can be calculated using a low aspect ratio wing theory. The Viscous forces is in some models identified as a cross flow drag on the aft of the vessel, where ass the final term is often calculated using an analogy of wings on a central body.

6.1.5 Hydro dynamics for ROV's

In order to design an ROV, it is important to design the vessel so that it is hydrostatically stable. In order to achieve this the hydrodynamic mass, or added mass, must be determined. It is necessary that all underwater vehicles have metacentric stability when they are submerged. With metacentric stability the vehicle will be able to retain an equilibrium after an external disturbance (Berg, 2014). The metacentric height is the vertical distance from the center of gravity to the center of buoyancy. Metacentric stability is assured when the metacentric height is positive, which implies that the center of gravity must be below the center of buoyancy. An increased metacentric height will cause increased metacentric stability and smaller pitch and roll angles for any given excitation. The frequency of the roll and pitch motion will also increase when the metacentric height increase.

The added mass is an extra inertia on the system due to the acceleration of water around the vessel. For a vessel that multiple degrees of freedom that is coupled, added mass will be a mass for the translation motion and mass moment for rotational motion. If there is coupling between the degrees of freedom, which there usually is, there will be off diagonal cross terms in the mass matrix. The added mass can for complex shapes and geometries be difficult to calculate. Furthermore it is important to be aware that the added mass can be different for oscillatory motion compared to one

directional motion. The oscillatory added mass may in some instances be more than twice as large as those for accelerated in on direction (Berg, 2014). It is also important to be aware that the hydrodynamic mass can be different for positive and negative have acceleration due to the form of most ROV's.

The added mass of the ROV is an important parameter, and it is important that this value is accurately determined. There exist several methods to estimate the added mass. These methods can be based on theoretical analysis, empirical data, model test or full-scale test. For the theoretical methods the vessel can be modelled as a rigid body with main dimensions of the ROV. The sources – sink method can then be applied in order to estimate the added mass. Methods can also be based on known hydrodynamic mass for some 2-dimentional shapes, together with 3-dimentional correction factors. In the mass matrix containing mass, mass moment and added mass, and the damping matrix, some of the diagonal terms can be determined from motion decay test. In these tests, a model of the vessel is released from an non equilibrium state. From the motion of the vessel when and the corresponding forces some added mass and damping terms can be determined.

Despite the fact that streamline bodies will have less resistance does most ROV's have a blunt shape. Only for some small observation ROV's have streamlining been considered. For medium and large work ROV's have design to minimize resistance been of little importance. The reason for this is twofold. One large ROV's receive power form a surface vessel through an umbilical. This means that the there is no big need to minimize the power consumption of the ROV, since much power is easily accessible. The second reason is that investigation on the subject have shown that streamlining an ROV to minimize the resistance in the surge direction will the depend on the length-diameter (L/D) ratio, and the optimal value is found to be $\frac{L}{D} = 2.7$ (Berg, 2014). With this L/D ratio it is easy to see that the lateral are will be large, and thus the resistance in heave motion will be large. Streamlining the body of an ROV in surge direction can therefore reduce the ability to operate in the lateral direction, and the ability to move in sway. The Reynolds number for most ROV's will be less than $5 * 10^6$. The resistance for ROV's will therefor depend on flow separation on parts of the vehicle, and rounding edges will thus influence the resistance of the vessel significantly. The damping of ROV's have been observed to be strongly dependent on the Keulegan-Carpenter number or KC number. If a streamlined shape is used for an ROV it is important to whether or not lift force can be generated by the shape. Some work type ROV's have design of the buoyancy block have introduced some areas where lift is generated, however these are often very small and can in general be neglected.

For ROV's the control units usually consist of the thrusters, rudders, rudder flaps, or removable ballast. Generally, thrusters are better at low speed, and rudders can be used for high speed. The thrusters on an ROV is usually placed within the volume of the ROV, but some disadvantages with can be relevant. Firstly the flow on the thruster will be disturbed, and therefor the efficiency will be reduced. Interaction effects between thruster might also occur, which is undesired and cause reduced efficiency. In the positioning of the thrusters the following must be taken into account

- Centre of gravity
- Centre of resistance forces
- Centre of lift forces
- Umbilical connection point

It should also be mentioned that thrusters may introduce a significant momentum drag when thruster jet are bent due to the ROV speed and the jet race follows the streamlined surface of buoyancy elements.

The umbilical of the ROV is there in order to communicate with the ROV, receive images and provide power to the ROV. The umbilical cord will introduce drag, and can be modeled as flow over a circular cylinder. For deep water the drag force from the umbilical cord will be significant. In order to reduce the force from the umbilical many operators will use a theater management system, where the ROV and the umbilical is lowered subsea, and the umbilical will therefore induce less force on the ROV.

Typical work class ROV's are equipped with robotic arms. The geometry of these are usually time and space specific. The rigid body inertia forces and hydrodynamic forces and moments will therefore depend on the movement of the robotic arm, and must be accounted for. In order for an ROV to be able to perform interventions subsea both positioning, orientation and speed, are used by the ROV's control systems. An ROV will typically have a control unit to calculate the power allocation for the different thrusters. Some modern ROV's are also equipped with control systems such as dynamic positioning systems that allow the ROV to keep its position in the water despite effect of waves, current or other forces acting on the vessel.

6.2 Drag Forces

When an object moves through water, two types of drag act on the object; skin friction drag and pressure drag. The relative importance of viscous and pressure drag depends on several factors:

- the size and shape of the object
- the density and viscosity of the fluid
- the relative speed of the object and the fluid (Moore, Bohm, & Jensen, 2010).

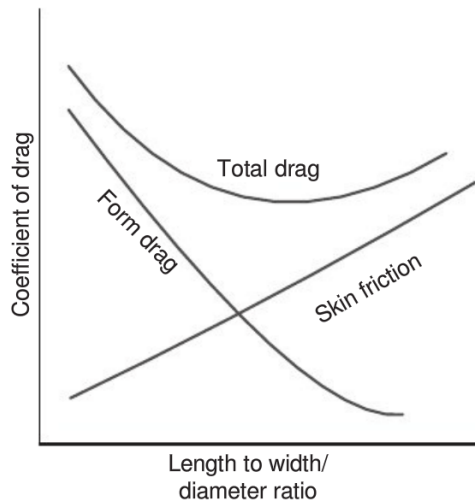


Figure 9: Vehicle drag curves (Christ & Wernli Sr, 2007).

As shown in Figure 2, there is an optimum aspect ratio whereby the total drag formed from both pressure drag, or form drag, and skin friction is minimized. Assuming a smoothly shaped contour forming a cylindrical hull, that aspect ratio is somewhere in the range of a 6:1 aspect ratio (length-to-diameter ratio) (Christ & Wernli Sr, 2007).

6.2.1 Skin Friction Drag

Viscosity is a molecular “resistance” which fluid particles exhibit against displacement in relation to each other and with respect to the surface of solid obstacles. Most directly, this type of resistance presents itself in the form of frictional drag. This means that in a manner roughly comparable to that of solid surfaces sliding along each other, a tangential force originates where air or any other fluid moves past the surface of a body. This force is the skin friction drag (Hoerner, 1965).

The skin friction drag on a submerged vehicle is shown in Figure 3.

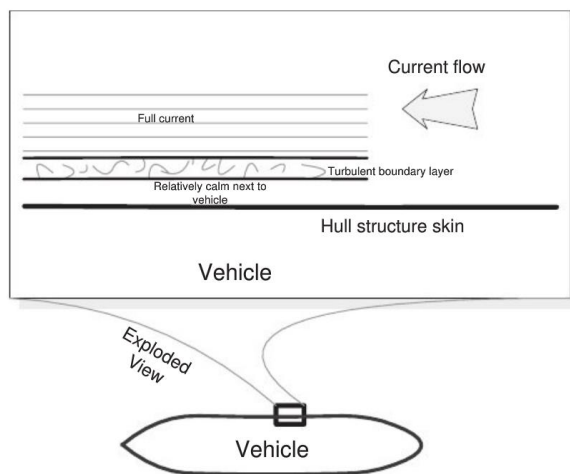


Figure 10: Skin friction drag (Christ & Wernli Sr, 2007).

The skin friction is a function of the viscosity of the water. Its effects are exhibited in the adjacent, thin layer of fluid in contact with the vehicle’s surface, i.e. the boundary layer. The boundary layer begins at the surface of the submersible where the water is at zero velocity relative to the surface. The outer edge of the boundary layer is at water stream velocity. Consequently, within this layer is the velocity gradient and shear stresses produced between the thin layer adjacent to each other. The skin friction is the result of stresses produced within this boundary layer. Initial flow within this boundary layer is laminar and abruptly terminates into a transition region where the flow is turbulent and the layer increases in thickness. To maintain high vehicle speed, the design must be towards retaining laminar flow as long as possible, for the drag in the laminar layer is much less than that within turbulent layer (Christ & Wernli Sr, 2007).

An important factor determining the condition of flow about a body and the relative effect of fluid viscosity is the Reynolds number, R_n , given by

$$R_n = \frac{uD}{\nu} \quad (5.28)$$

where

D = characteristic length of the body

ν = kinematic viscosity

u = velocity of vehicle

The Reynolds number expresses in non-dimensional form a ratio between inertia forces and viscous forces on a particle, and the transition from the laminar to the turbulent area occurs at a certain critical Reynolds number value. This critical Reynolds number value is lowered by the effects of surface imperfections and regions of increased pressure (Christ & Wernli Sr, 2007).

Essentially the skin friction drag is related to the exposed surface area and the velocities over the skin. Hence, for a given volume of vehicle hull, it is desirable to reduce the surface area as much as possible. However, it is also important to retain a smooth surface, to avoid roughness and sharp discontinuities, and to have a slowly varying form so that no adverse pressure gradients are built up, which cause increased drag through separation of the flow from the vehicle's hull (Christ & Wernli Sr, 2007).

6.2.2 Pressure Drag

A second effect of the viscous action of the vehicle's hull is to reduce the pressure recovery associated with non-viscous flow over a body in motion. Pressure drag is created as the water is moved outward to make room for the body and is a function of cross sectional area and shape. In an ideal non-viscous flow there is no resistance since, although there are pressure differences between the bow and stern of the vehicle, the net result is a zero force in the direction of motion. Due to the action of viscosity there is reduction in the momentum of the flow and, whilst there is a pressure built up over the bow of the submersible, the corresponding pressure recovery at the stern is reduced, resulting in a net resistance in the direction of motion. This pressure drag can be minimized by slowly varying the sections over a large body, i.e. tending towards a needle shaped body even though it would have a high surface-to-volume ratio (Christ & Wernli Sr, 2007).

The pressure drag, F_D , produced by the submersible is estimated by

$$F_D = \frac{1}{2} \rho C_d A U^2 \quad (5.29)$$

where

ρ = density of sea water

A = projected cross-sectional area under water

C_d = non-dimensional drag coefficient based on cross-sectional area of the vehicle

U = velocity of the vehicle

This expression is recognized as one of the terms in the Morison's equation (Fossen, 2011).

6.3 Thrusters

In general, a set of operational requirements in terms of endurance, range, speed, or operational time is specified for the underwater vehicle. These parameters are crucial in the design of the vehicle, and have a large impact on the resistance and energy analysis

$$Energy \text{ for propulsion} = \frac{Energy}{Hours} \times \frac{Hours}{\eta} \quad (5.30)$$

$$Range = Speed \times Hour \quad (5.31)$$

The Energy/Hours term represents the effective vehicle power required and varies with speed. η represents the total propulsion system efficiency, including the propulsive coefficient, losses in the motor and power lines, and losses in battery or fuel cell. Determining the maximum propulsion energy depends therefore on a trade-off between speed, drag at each speed, range, efficiency and operational hours (Allmendinger, 1990).

The propulsion system significantly impacts the vehicle design. The type of thrusters, their configuration, and the power source to drive them usually take priority over many of the other components (Christ & Wernli Sr, 2007).

6.3.1 ROV Thrusters

ROV propulsion systems come in three different types; electrical, hydraulic, and ducted jet propulsion. These different types have been developed to suit the size of vehicle and anticipated type of work. In some cases, the actual location of the work task has dictated the type of propulsion used. For example, if the vehicle is operated in the vicinity of loosely consolidated debris, which could be pulled into rotating thrusters, ducted jet systems could be used. If the vehicle requires heavy duty tooling for intervention, the vehicle could be operated with hydraulics (including thruster power). Hydraulic pump system are driven by an electrical motor on the vehicle, requiring a change in energy from electrical to mechanical to hydraulic – a process that is quite energy inefficient. A definite need for high mechanical force is required to justify such an energy loss and corresponding costs (Christ & Wernli Sr, 2007).

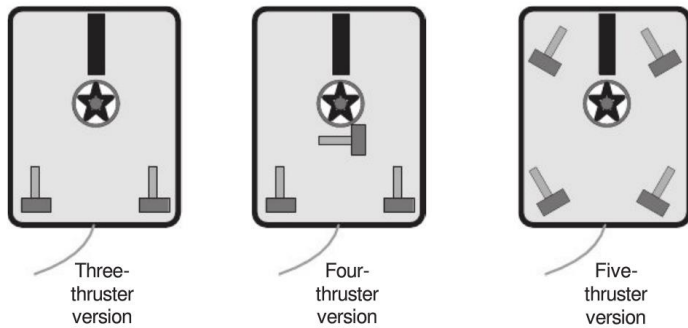
The main goal for the design of ROV propulsion systems is to have high thrust-to-physical size/drag and power-input ratios. The driving force in the area of propulsion systems is the desire of ROV operators to extend the equipment's operating envelope. The more powerful the propulsion of the ROV, the stronger the sea current in which the vehicle can operate. Consequently, this extends the system's performance envelope (Christ & Wernli Sr, 2007).

The propulsion system has to be a trade-off between what the ROV requires for the performance of a work task and the practical dimensions of the ROV. Typically, the more thruster power required, the heavier the equipment on the ROV. All parts of the ROV system will grow exponentially larger with the power requirement continuing to increase (Christ & Wernli Sr, 2007).

The ROV's propulsion system is made up of two or more thrusters that propel the vehicle in a manner that allows navigation to the work site. Thrusters must be positioned on the vehicle so that the

Figure 11: Thruster arrangements (Christ & Wernli Sr, 2007).

moment arm of their thrust force, relative to the central mass of the vehicle, allows a proper amount of maneuverability and controllability. Thrust vectoring is the only means of locomotion for an ROV. There are numerous placement options for thrusters to allow varying degrees of



maneuverability. Maneuvering is achieved through asymmetrical thrusting based upon thruster placement as well as varying thruster output (Christ & Wernli Sr, 2007).

The three-thruster arrangement, presented in Figure 4, allows only fore/aft/yaw, while the fourth thruster also allows lateral translation. The five-thruster variation allows all four horizontal thrusters to thrust in any horizontal direction simultaneously. Also, placing the thruster off the longitudinal axis of the vehicle, as shown in Figure 5, will allow better turning moment, while still providing the vehicle with strong longitudinal stability (Christ & Wernli Sr, 2007).

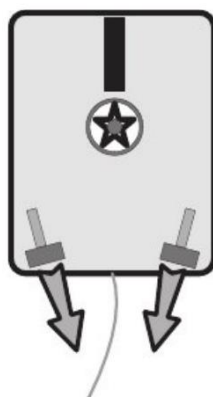


Figure 65: Thruster aligned off the longitudinal axis (Christ & Wernli Sr, 2007).

ROV electrical thrusters are composed of the following major components:

- Power source
- Electric motor
- Motor controller (this may be part of the thruster or may be part of a separate driver board)
- Thruster housing and attachment to vehicle frame
- Gearing mechanism (if thruster is geared)
- Drive shafts, seals, and couplings
- Propeller
- Kort nozzle and stators (Christ & Wernli Sr, 2007)

On a surface-powered ROV system, power arrives to the vehicle from a surface power source. The power can be in any form from basic shore power to a DC battery source. The purpose of this power source is the delivery of sufficient power to drive the thruster through its work task (Christ & Wernli Sr, 2007).

Electric motors convert electrical energy into rotational energy, which is used to drive the propeller on an electric thruster. Electric motors come in many shapes, sizes, and technologies, each designed for different functions. In a typical motor, the outside part is stationary and attached to something solid, like the vehicle frame. This part is called the stator. The inside part of the motor rotates and is called a rotor. The motor shaft, which transmits rotational energy from the motor to other machinery, forms the core of the rotor. Motors may be classified based on the nature of the electrical power to run them. There are two main categories: AC motors and DC motors. AC motors depend on the fluctuating nature of AC current to produce the fluctuating magnetic fields needed to run the motor. DC motors run on direct current. These motors must produce their own form of oscillating electric current to generate the fluctuating magnetic fields needed to make the motor turn. DC motors are common in battery-driven devices (Moore, Bohm, & Jensen, 2010). By far the most common thruster motor on observation class ROV systems is the DC motor, due to its power, availability, variety, reliability, and ease of interface (Christ & Wernli Sr, 2007).

DC motors can run from 8000 to 20 000 RPM and higher. This is far too fast for ROV applications if vehicle control is to be maintained. In order to match the operational speed of the motor with the efficient speed of the thruster's propeller, the motor will require gearing. Gearing allows two distinctive benefits – the power delivered to the propeller is both slower and more powerful. Further, with the proper selection of a gearbox with a proper reduction ratio, the maximum efficiency speed of the motor can match the maximum efficiency of the thruster's propeller/kort nozzle combination (Christ & Wernli Sr, 2007).

The shafts, seals, and couplings for an ROV thruster are much like those for a motorboat. The shaft is designed to provide torque to the propeller while the seal maintains a watertight barrier that prevents water ingress into the motor mechanism. Drive shafts and couplings vary with the type of propeller driving mechanism. Direct drive shafts, magnetic couplings, and mechanical (i.e. geared) couplings are all used to drive the propeller. There are various methods for sealing underwater thrusters. Fluid-filled thruster housings may be used to lower the difference in pressure between the seawater and the internal thruster housing pressure by simply matching the two pressures (internal and external). Another way is to use a lubricant bath between the air-filled spaces and the outside water. A common and highly reliable technique is the use of a magnetically coupled shaft, which allows the air-filled housing to remain sealed (Christ & Wernli Sr, 2007).

The propeller should convert the power delivered by the propulsion motor into thrust as efficiently as possible. The purpose of all propellers is to accelerate the water as it enters. This acceleration produces a change in the water momentum per unit time – thrust. Momentum is defined as the mass flow times the change in velocity. So to increase the change in momentum, the propeller can either increase the acceleration or increase the mass flow. In general, it is more efficient to the mass flow rather than increase the acceleration. Thus, the larger the propeller diameter, the greater mass flow and the greater efficiency (Allmendinger, 1990). Many thruster propellers are designed so their efficiency is much higher in one direction (most often in the forward and the down directions) than in the other. Propellers have a normal speed of maximum efficiency, which is hopefully near the vehicle's normal operating speed. Some propellers are designed for speed and others are designed for power (Christ & Wernli Sr, 2007).

A kort nozzle is common on most underwater thruster models. The efficiency of a kort nozzle is the mechanism's help in reducing the amount of propeller vortices generated as the propeller turns at high speeds. The nozzle, which surrounds the propeller blades, also helps with reducing the incidence of foreign object ingestion into the thruster propeller. Also, stators help reduce the tendency of rotating propellers' swirling discharge, which tends to lower propeller efficiency and cause unwanted thruster torque acting upon the entire vehicle (Christ & Wernli Sr, 2007).

6.3.2 Cable Drag

The function of the ROV submersible is to push its hull and pull its cable to the work site in order to deliver whatever payload may be required at the work site. The only significant metric that matters in the motive performance of an ROV is the net thrust to net drag ratio. If that ratio is positive, net thrust exceeds net drag, the vehicle will make headway to the work site. If that ratio is negative, the vehicle becomes very high-tech and very expensive boat anchor (Christ & Wernli Sr, 2007).

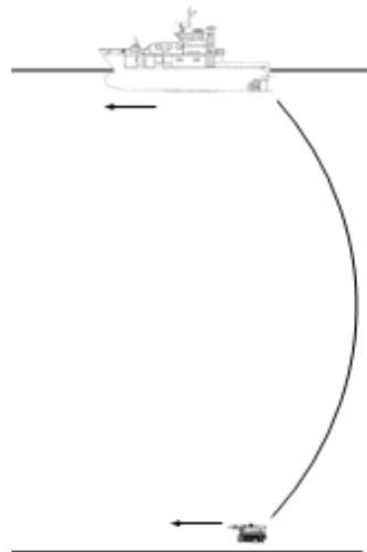


Figure 67: ROV with cable (Ludvigsen, An ROV toolbox for optical and acoustical seabed investigation, 2010)

ROV thrusters must produce enough thrust to overcome the drag produced by the cable and the vehicle. The total drag of the system is equal to the vehicle drag plus the cable drag. In the case of cables, the characteristic area, A , depends on the cable diameter (Christ & Wernli Sr, 2007).

The total drag of the system is defined as

$$F_{D,\text{total}} = \frac{1}{2} \rho C_{d,\text{vehicle}} A_{\text{vehicle}} U^2 + \frac{1}{2} \rho C_{d,\text{cable}} A_{\text{cable}} U^2 \quad (5.32)$$

For a circular cable in turbulent flow, C_d may be assumed to 1.2.

6.4 AUV Thrusters

Almost all AUVs use screw-type propellers because they are in general the most efficient propulsion devices at the operating speed of AUVs. These propellers are often hub driven, as shown in Figure 7.

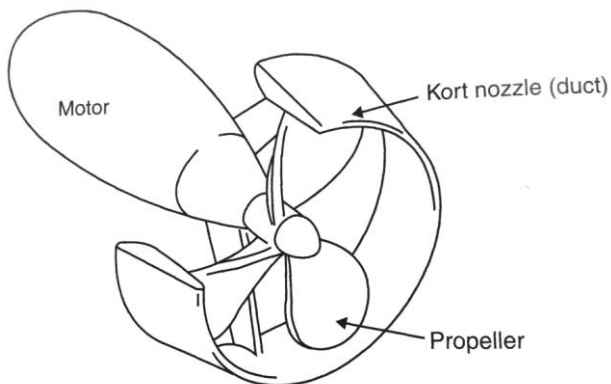


Figure 78: A hub driven ducted propeller (Griffiths, 2003).

The propeller hub is fitted onto the shaft of an electric motor, or alternatively, the motor might have an outer rotor on which the blades can be fitted, and thus the motor forms the hub of the propeller (Griffiths, 2003).

In general, for a particular pitch, diameter and thrust output, the power and torque requirements are not significantly affected by other parameters such as number of blades, blade thickness, hub size, rake etc., for well designed propellers. However, the shape of the duct wall cross-section can have large effect on power and torque, especially in the astern direction.

The size of an electric motor can be shown to be proportional to propeller torque, while the size of the power supply power is proportional to propeller power. The fluid friction loss in a motor with a radial gap is proportional to the cube of the speed and the fourth power of the diameter. Ohmic loss in the motor increases roughly as the square of motor torque for fixed motor dimensions (Griffiths, 2003).

As shown in Figure 8, for constant thrust and pitch, as the propeller diameter increases, torque and motor size increase while power and power supply size reduce. Hence, an optimum diameter can be selected to minimize the overall size or cost of the thruster system. In case of a hub driven propeller

the optimum choice of diameter may be biased towards reducing the torque and hence motor diameter (Griffiths, 2003).

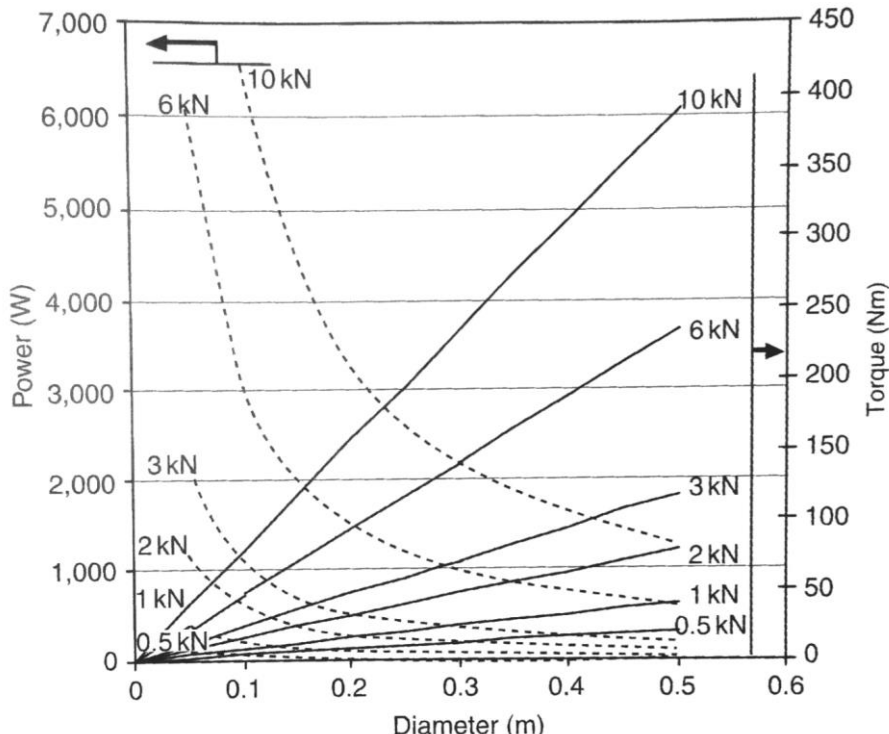


Figure 9: Effect of diameter of power and torque requirements of a Ka4-70 propeller with pitch ratio of 1.0 in 37-A duct (Griffiths, 2003).

The required speed of the thruster is inversely proportional to the square of its diameter, and hence by increasing diameter the fluid friction loss decreases. But this increase torque, and so for fixed motor dimensions ohmic loss increases. Again an optimum propeller diameter can be selected to maximize the overall efficiency (Griffiths, 2003).

On the other hand, power and hence power supply size is not significantly affected by pitch ratio, as illustrated in Figure 9. However, torque and hence motor size increase with increasing pitch ratio. In general, a small pitch ratio would therefore be preferred to reduce the size of the overall system, and reduce motor ohmic loss. But speed increases by increasing pitch, hence increasing fluid friction loss on the motor which can be large for motors of large diameters (Griffiths, 2003).

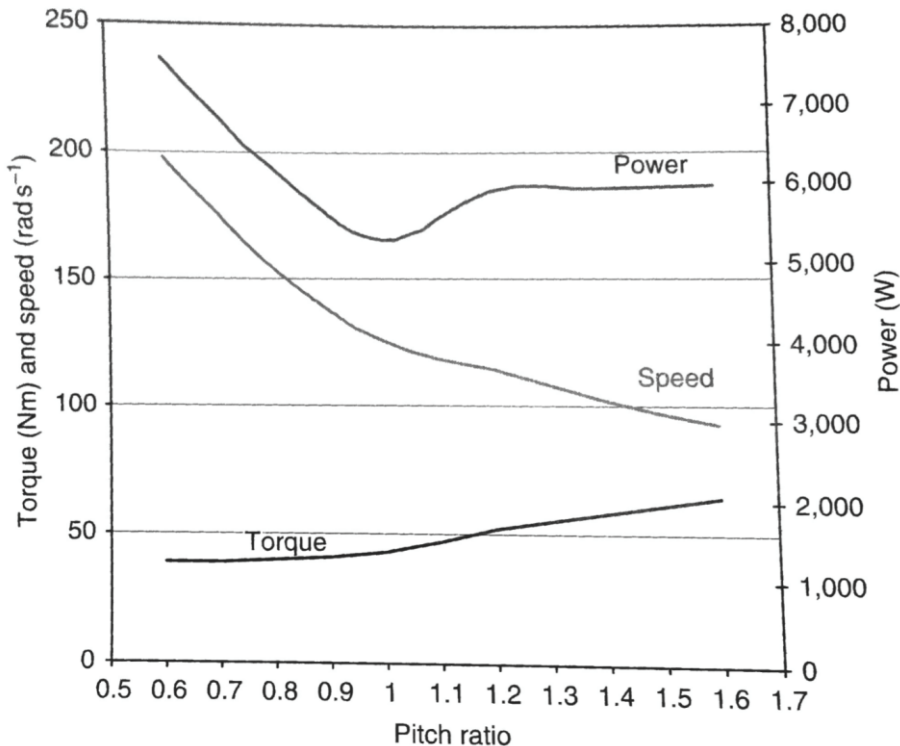


Figure 10: Effect of pitch ratio on power, torque and speed of a 300 mm diameter Ka4-70 propeller in 19-A duct producing 1800 N of thrust (Griffiths, 2003).

To summarize, the size and efficiency of the drive are determined by the design of the propeller. In general, attempting to improve overall efficiency results in increasing the size of the motor and vice versa (Griffiths, 2003).

Depending on type of drive, the optimization objective may either be to minimize the size or cost of the system, or to maximize the efficiency. This of course should be subjected to constraints on acceptable size of motor, power supply and propeller, and acceptable efficiency of the system (Griffiths, 2003).

6.5 Experimental Testing of Hydrodynamics for ROV

The following section gives a brief description of experimental testing of hydrodynamics for an ROV. The description is based on experiments performed with the ROV Minerva. For determining the drag force and drag coefficient a 1:5 scale model of Minerva is used. Figure 10 shows both full scale and model ROV.

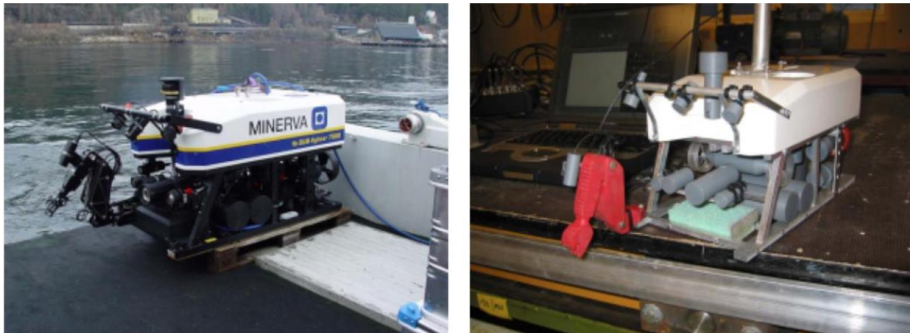


Figure 11: ROV Minerva full scale to the left and model to the right (Andresen, Ludvigsen, & Ødegaard, 2003).

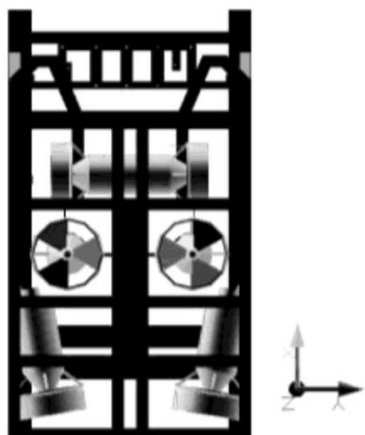


Figure 69 Thruster arrangement of Minerva with coordinate system (Ludvigsen & Ødegaard, Sammenfatning av hydrodynamiske forsøk med ROVen Minerva, 2006).

Minerva is equipped with five thrusters, with arrangement as shown in Figure 11.

Four of the thrusters are identical, while the fifth thruster has a through shaft with a propeller and nozzle at each end. The thrusters are shown in Figure 12.



Figure 70 Lateral thruster to the left and universal thruster to the right (Ludvigsen & Ødegaard, Sammenfatning av hydrodynamiske forsøk med ROVen Minerva, 2006).

Two thrusters are mounted vertically, while two other thrusters are pointing in the main speed direction with an angle of ten degrees (Ludvigsen & Ødegaard, Sammenfatning av hydrodynamiske forsøk med ROVen Minerva, 2006).

6.5.1 Longitudinal C_d -coefficient

The quadratic drag coefficient, C_d , in Equation 11 can be established by experiments. For the longitudinal motion this may be performed by connecting the model ROV to a torque dependent force sensor, detecting the drag in the longitudinal direction. The experiment is performed in the small towing tank and the setup is shown in Figure 13.

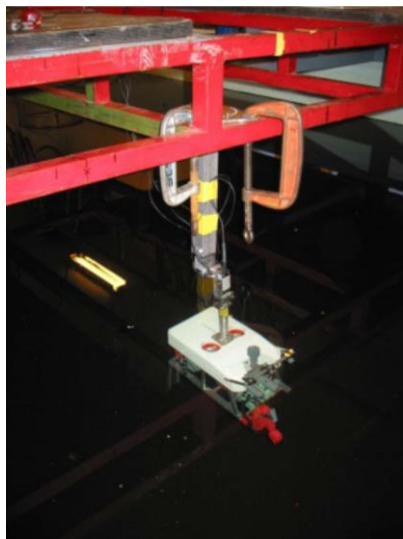


Figure 71 Setup of model (Andresen, Ludvigsen, & Ødegaard, 2003).

The model is then towed at different speeds. In order to obtain the correct drag for the model, the mounting arrangement with force sensor is towed without the model ROV. Drag force on the force sensor and the mounting rod is then established and removed from the total estimated force in order to find the drag force on the ROV-model itself.

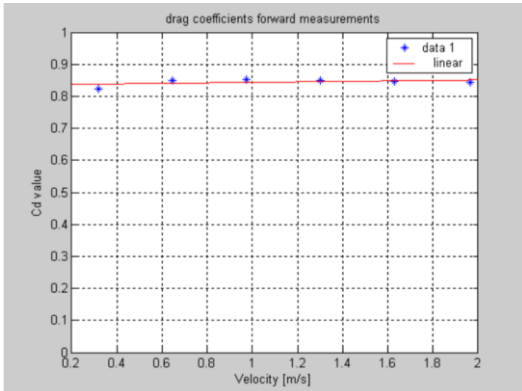


Figure 72 Cd versus velocity (Andresen, Ludvigsen, & Ødegaard, 2003).

The drag coefficient may then be plotted versus velocity as shown in Figure 14.

6.5.2 Polar Diagram of Drag Resistance and Cd-coefficient

In order to obtain polar diagram of drag resistance and Cd-coefficient for the ROV, the model may be attached to a rod with a power meter in x-direction and in y-direction. A torque meter may also be included in order to measure moment about z-axis. The model is then towed at different positions with degrees in the range of 0° to 180°, both forward and backward for all positions. Results for all angles from 0° to 360° is then obtained. The setup is presented in Figure 15.

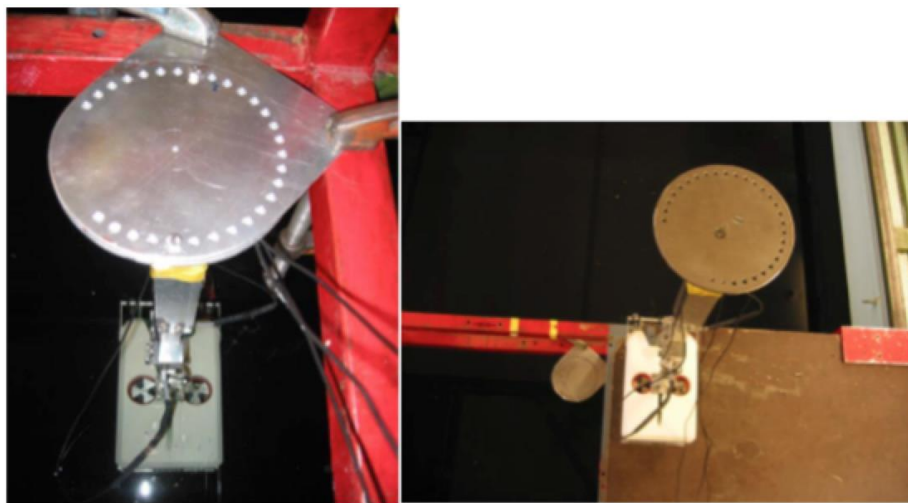


Figure 112: Setup of ROV. Angle adjustment for each ten degrees (Ludvigsen & Ødegaard, Slepeforsøk modell Cd-koeffisient i alle vinkler, 2003).

The forces are measured in the ROV-related coordinate system, as presented in Figure 16. The positive x-axis is defined forward along the ROV normal direction of speed, and the positive y-axis is defined starboard on the ROV-model.

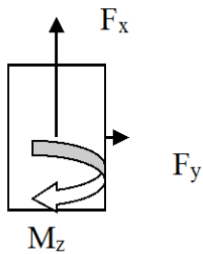


Figure 113: Forces in ROV-related coordinate system (Ludvigsen & Ødegaard, Slepeforsøk modell Cd-koeffisient i alle vinkler, 2003).

The total drag force may then be calculated by

$$F = \sqrt{F_x^2 + F_y^2} \quad (5.33)$$

Where F is given by Equation 11.

The drag force from the attachment and force meter is measured and removed from the total drag force.

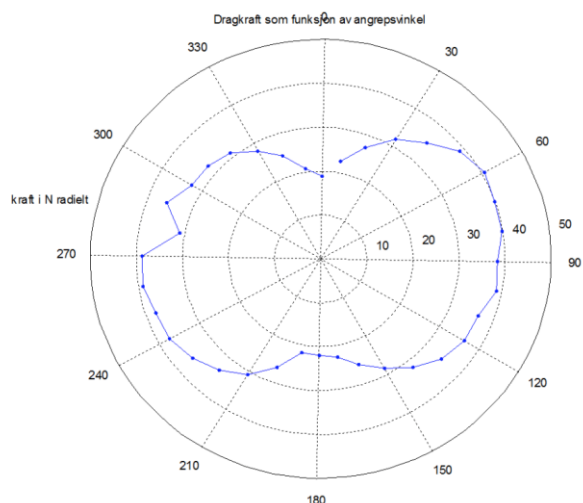


Figure 73 Polar plot of drag coefficient as function of angle of attack (Ludvigsen & Ødegaard, Slepeforsøk modell Cd-koeffisient i alle vinkler, 2003).

The drag force as a function of angle of attack may then be plotted as presented in Figure 17.

The drag coefficient is then calculated by use of Equation 11. The area A varies along with the angle of attack, ψ , in accordance with

$$A = A_x \cdot \cos(\psi) + A_y \cdot \sin(\psi) \quad (5.34)$$

A polar plot of the drag coefficient is shown in Figure 18.

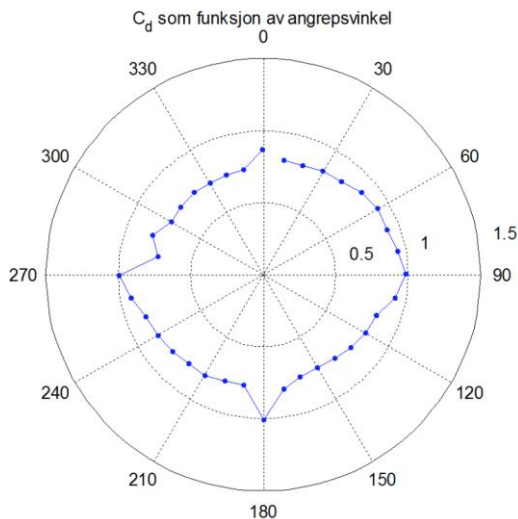


Figure 74 Drag force on vehicle as function of angle of attack. X- and Y-force added (Ludvigsen & Ødegaard, Slepeforsøk modell Cd-koeffisient i alle vinkler, 2003).

6.5.2.1 Full Scale Thrust Test

Four different tests are carried out in order to determine the thrust force forwards, backwards, downwards and sideways. The tests are performed in the MARINTEK's large towing tank.

In order to determine the forward thruster force the model is attached to the carriage by a steel wire. This wire is attached to Minerva at two points, in a manner to make the vector sum of the longitudinal drag and thrust coincident with the wire pull direction. The two wire pieces attached to the model are tightened together at a point just behind the stern passing through a thin metal tube, and continues to an annular force sensor. From the sensor further through a shackle in the lower end of a vertical pipe secured to the carriage, and from there upward to an attachment point at the carriage. The purpose of the rod is to keep the system approximately in the middle of the tank, at the desired depth. Figure 19 shows a drawing of the setup.

The correspondence between longitudinal ROV speed and thruster force is measured by allowing the ROV to pull in the tank's longitudinal direction while the carriage is located behind and controls the speed. Bollard pull is measured in the same configuration, by keeping the carriage stationary.

The model is run at full thrust in all measurements. It is attempted to pull in the tank longitudinal direction with minimum compensation for lateral thrusters. The speed of the carriage is stepwise

Kommentert [EH11]: Jeg la in "to" in" og "s" Uten dette ga ikke setningen noen mening. Var dette en riktig forståelse av hva du ville frem til.

increased from zero to approximately equal to the speed of the model. Bollard pull is therefore measured at the beginning, and the maximum speed at the end. The auto depth function of the ROV is activated all the time, except when measuring the maximum speed. Each speed is held until the situation appears stable for a number of seconds, i.e. oscillations in rod-wire system seems to have subsided, and the ROV is stable in the front of the carriage.

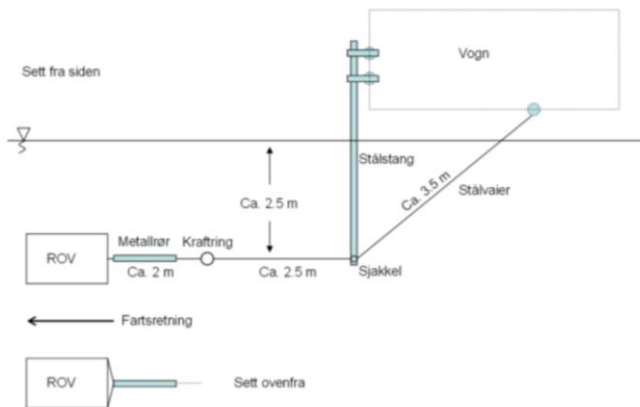


Figure 75 Setup (Ludvigsen & Ødegaard, Fullskala thrust-test av Minerva, 2004).

The sideways and backwards thruster force is determined by rotating the model 90° and 180° in the horizontal plane, respectively. Downward thruster force is determined by hanging the power sensor between a wire piece attached to the carriage and the models launch/recovery sling. Hence, the model is hanging underneath the carriage, and the maximum thrust downwards may be measured.

Thrust may then be plotted versus speed, as shown in Figure 20.

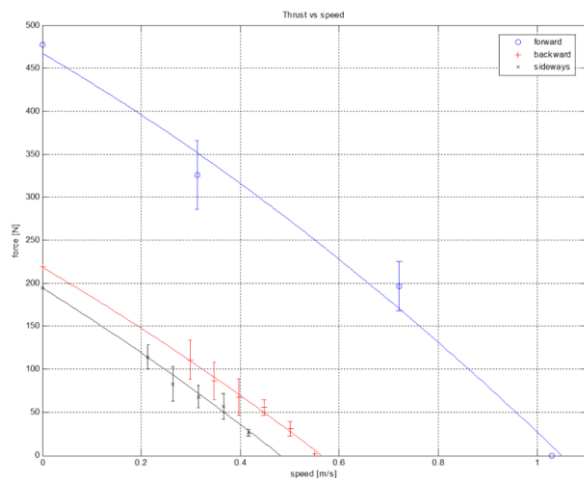


Figure 76 Thrust versus speed for motion forwards, backwards and sideways (Ludvigsen & Ødegaard, Fullskala thrust-test av Minerva, 2004).

The graph expresses the amount of force the ROV has to pull the cable as a function of speed forward, backward and sideways.

6.5.3 Open Water Test of ROV Thruster

The open water test is carried out in MARINTEK's cavitation tunnel. The focus of the test is to compare two different propeller/nozzle configurations with respect to thrust force.

The first configuration is a three bladed propeller with a diameter of 220 mm mounted in a simple, cylindrical nozzle. The nozzle has a diameter of 224 mm. This is the configuration Minerva uses today. The second configuration is a three bladed propeller of the same type, but with a diameter of 240 mm. The nozzle is designed by MARINTEK, and has a NACAD profile. The two configurations are shown in Figure 21.



Figure 77 NACAD nozzle to the left and Sperre nozzle to the right (Ludvigsen & Ødegaard, Friprøveforsøk med ROV-thruster, 2005).

The thruster propeller is powered by a four pole three phase motor. The three phase motor has a synchronous rotational speed determined by the electrical current frequency and the number of poles of the motor.

$$\omega_s = \frac{\omega}{P/2} \quad (5.35)$$

where ω is the angular velocity given in rad/s and P is the number of poles in the motor.

The synchronous rotational speed is not the same as the mechanical rotational speed. The slip, s , is given by

$$s = \frac{\omega_s - \omega_m}{\omega_s} \quad (5.36)$$

where ω_m is mechanical rotational speed. While the synchronous rotational speed is kept constant, the mechanical rotational speed may be reduced due to increased slip as the resistance increases.

The thruster, consisting of motor bottle, nozzle and propeller, is suspended from the ceiling in the cavitation tunnel as shown in Figure 22. The engine bottle is clamped with lined steel strip into a cylindrical steel bowl. This is again bolted to the end of a solid vertical aluminum rod, which via a shear force sensor and a solid steel rod is attached to a gap in the tunnel ceiling.

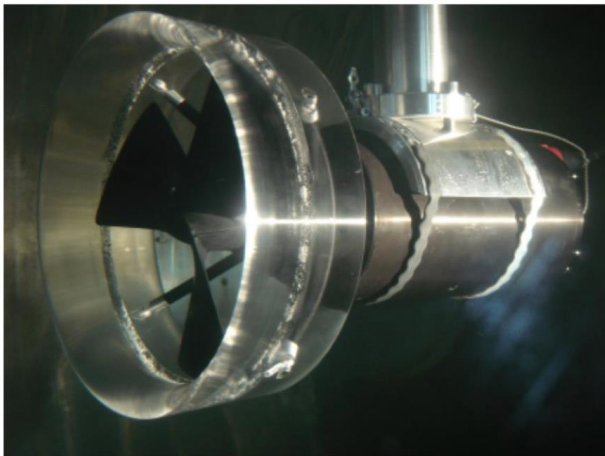


Figure 78 Thruster with large propeller and nozzle mounted in tunnel (Ludvigsen & Ødegaard, Friprøveforsøk med ROV-thruster, 2005).

The motor management system is a frequency regulator; one phase in and three phase out. The frequency is varied in order to control the rotational speed of the engine.

Applied voltage is read manually from a handheld multimeter connected to the output of the frequency regulator. Applied current is read from the regulator display. The frequency regulator calculates the motor rotational speed, which can be read from the display. This is the synchronous rotational speed.

The rotational speed of the propeller is measured by two strobe lights synchronously driven with a square pulse from a standard signal generator, through their respective amplifiers. The frequency of the pulse is adjusted manually so that the propeller seems to stand still.

Force on the thruster in the tunnel length direction is measured by a torsionally, torque independent shear force sensor.

Water velocity in the tunnel is measured with a pitot tube located near the bottom of the tunnel, upstream of the center of the vertical mounting rod.

The test is carried out by performing several runs with the propeller/nozzle configuration. The runs are divided into series covering all four quadrants of the K_T -plot:

1. Positive water velocity and positive propeller rotational speed
2. Negative water velocity and positive rotational speed
3. Negative water velocity and negative rotational speed
4. Positive water velocity and negative rotational speed

All series are run on two different rotational speeds.

Non-dimensional terms expressing the general performance characteristics may be found. The advance coefficient, J , is calculated by

$$J = \frac{V_A}{n \cdot D} \quad (5.37)$$

where V_A is the propeller real velocity forward through the water in m/s, n is rotational speed given as rotations per minute and D is the diameter.

The thrust coefficient, K_T , is calculated by

$$K_T = \frac{T}{\rho \cdot n^2 \cdot D^4} \quad (5.38)$$

where T is thrust force and ρ is water density.

A K_T/J -plot of all four quadrants may then be created, as shown in Figure 23.

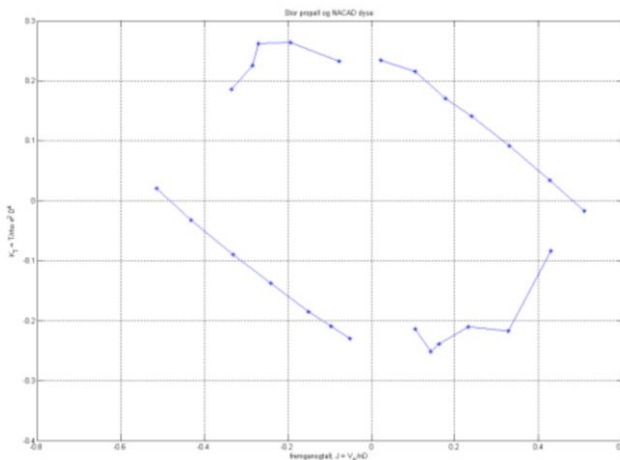


Figure 79 Thrust coefficient versus advance coefficient for large propeller and NACAD nozzle (Ludvigsen & Ødegaard, Fripørforsøk med ROV-thruster, 2005).

6.5.4 Summary of Hydrodynamic Experiments

The results obtained from the experiments described in section 3.1-3.4 may be compared in order to verify the experiments and obtain even more information about the hydrodynamic properties of Minerva.

The aim of this comparison is to provide capability plots for speed and force. A comparison of the C_d from the model test, measured maximum speed, measured bollard pull, thrust and rotational speed should also be compared. An evaluation of the most efficient propeller and nozzle configuration shall also be performed.

The C_d value from the model tests is used together with the K_T/J -plot that was established after the experiment in the cavitation tunnel. This data is used to calculate the maximum speed and bollard pull in all directions for Minerva.

Estimated maximum speed and bollard pull is compared to the full scale thruster test of Minerva in section 3.3.

Based on the thruster characteristics found in the cavitation tunnel, section 3.4, and the full scale thruster test, section 3.3, a capability plot for bollard pull and speed is established. Both calculated without cable. The bollard pull and speed is calculated using

$$T = K_T \rho n^2 D^4 \quad (5.39)$$

$$U = \sqrt{\frac{F}{\frac{1}{2} \rho C_d A}} \quad (5.40)$$

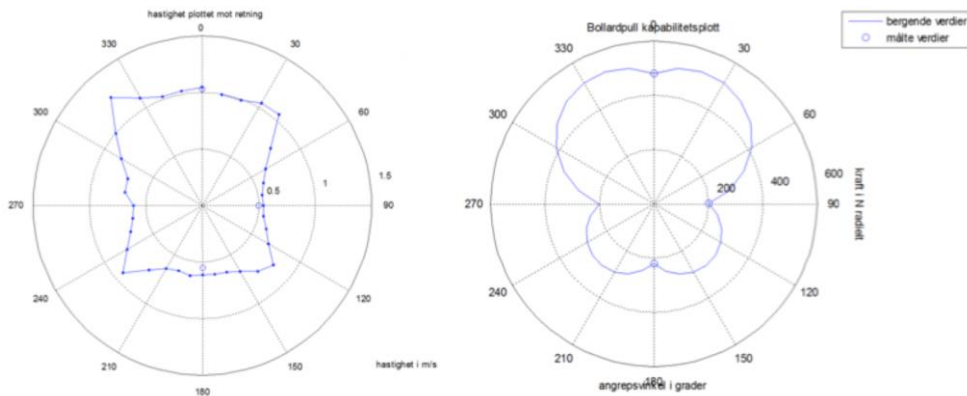


Figure 80 Capability plot of velocity to the left and bollard pull to the right (Ludvigsen & Ødegaard, Sammenfatning av hydrodynamiske forsøk med ROV-en Minerva, 2006).

Examples of capability plots are presented in Figure 24.

Minerva has significantly better bollard pull forward than backward. In an oblique angle of attack the bollard pull increases compared with movement straight ahead. This is because the oblique angle of attack makes it possible to utilize multiple thrusters

$$T_{x^\circ} = T_{forwards} \cdot \cos(x^\circ) + T_{sideways} \cdot \sin(x^\circ) \quad (5.41)$$

The maximum speed is calculated by

$$\frac{1}{2} \rho C_d A U^2 = K_T \rho n^2 D^4 \quad (5.42)$$

by solving for U . This is an iterative process as K_T depends on U .

These calculations are then compared to the results from the full scale thruster test, section 3.3.

Based on the data from the model test and the open water test, changes to Minerva's thrusters may

TMR4120 Underwater Engineering

be purposed and the impact of the changes may be quantified. Changes in rotational speed and propeller diameter are of interest.

7 Seabed Mapping Equipment

The most common combinations of system sensors for engineering applications are (Chakrabarti, 2005):

- Echo sounder – for measuring the water depth directly beneath the vessel. This also acts as a calibration device to the multi-beam sounder.
- Swath bathymetry – for measuring a wide swathe of seabed soundings either side of the survey vessel. 
- Side scan sonar – for generating a scaled image of the seabed morphology and features. 
- Sub-bottom profiler – for determining the stratification of soils to a depth of, perhaps, 50 m beneath the seabed, depending on frequencies and energy levels. 

A brief described of seabed mapping equipment was given in Chapter 2 “Acoustics”. However, the multi-beam echo sounder, side scan sonar and sub bottom profiler is in this chapter described with respect to system knowledge and data processing.

7.1 Multi-Beam Echo Sounder



Figure 81 Multi-beam echo sounder working model (Bai & Bai, 2012).

The multi-beam echo sounder, or swath echo sounder, is a high-precision method for conducting bathymetric surveys obtained at water depths and seabed gradients over the corridor along the proposed pipeline routes, as shown in Figure 1 (Bai & Bai, 2012). 

The multi-beam echo sounder is presented in chapter 2 regarding acoustics. In this section we will consider the application of this sonar system.

Kommentert [EH12]: Flyttet til kapitel 2

7.1.1 Application

Multi-beam echo sounders are used in almost every branch of hydrographic surveying, with each branch using the multi-beam echo sounder for a different purpose:

- Dredging: used for control on construction projects and projects where a high resolution combined with a 100% coverage is needed.

- Offshore: used for inspection of pipelines, fall pipe projects, inspections of structures with ROVs. If used for fall pipeline projects, two multi-beam echo-sounders are needed, one in front of the fall pipe to determine the condition of the pipeline and its location, and one on the back of the fall pipe to check the work done.
- Pre-design surveys associated with pipeline and cable routes: Typically a feasible route is defined based on a surface multi-beam. However, in deeper water, surface multi-beam has a reduced resolution and the surface survey is generally followed up by either an AUV or ROV based low fly swath survey, in those areas where detailed bathymetry is essential to complete the design.
- Charting: used in areas where a 100% coverage of the bottom is needed. This is may be required for harbors, shipping channels and shallow areas with a high traffic density. A large number of government charting organizations perform offshore charting projects using multi-beam technology.
- Government: inspections of dams, dikes and harbors. If used for inspection works, the multi-beam is often used in surface-looking mode, which means that the outermost angle of one side of the multi-beam is directed at the water level, creating at least a 90° coverage of the object inspected (Lekkerkerk, et al., 2006).

7.1.2 System

With the above environmental criteria considered in the design phase, a multi-beam system is manufactured consisting of the following parts:

- acoustic data processor
- control display
- multi-beam transducer array
- sound velocity probe (depending on type of multi-beam)

The acoustic data processor is the heart of the multi-beam system. Depending on the type of multi-beam this processor can be housed in a standard 19" rack unit or is a 19" rack by itself. The processor has to process a huge amount of data.

The control display is used to change the settings of the multi-beam. On this display the readings from the multi-beam will be displayed as well as the status of the multi-beam.

Multi-beam transducer arrays can be subdivided using a number of parameters such as frequency, number of beams, beam angle and maximum depth rating. All these parameters influence the size of the transducer. Apart from size, the multi-beam transducers can be divided into flat arrays and round arrays.

The main advantage of the round arrays is that there is a direct relationship between the position of the receive element of the transducer and the beam number. When using flat arrays, phase detection is used to electronically detect the beam number based on the return signal. This process is also called focusing of the array. Because the wavelength of the signal depends on the frequency and speed of sound, a sound velocity probe is used to correct for differences in sound velocity at the receive head.

Depending on the type of multi-beam, the transmit and receive array can either be separate or combined.

In order to operate a multi-beam system a minimum number of other survey systems are required as listed below:

- motion sensor for measuring heave, roll and pitch
- gyro compass for measuring yaw angles

- positioning system
- acquisition software
- sound velocity probe for measuring the speed of sound at different depths (sound velocity profile) (Lekkerkerk, et al., 2006).

7.1.3 Calibration of Swath Sounders using the Patch Test

The patch test is a method of using a specific patch of bottom for determining the alignment of the swath sounder. This technique is commonly used with multi-beam software.

The following parameters can be determined using the patch test:

- latency between positioning system and swath sounder
- roll offset of sounder
- pitch offset of sounder
- yaw offset of sounder

In order to execute a patch test, an area with a slope and a reasonably flat area should be used. The slope should be between 1:2 and 1:5, the flat area should be as deep as possible. In order to determine all four parameters, a minimum of four lines should be sailed over the slope/flat bottom combination as shown in Figure 2.

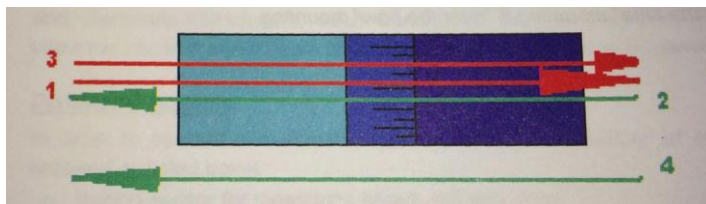


Figure 82 Line pattern for patch test (arrow size indicates velocity) (Lekkerkerk, et al., 2006).

The following combinations of lines are used to determine the parameters:

- 1+2: Pitch determination on the slope; Roll determination on the flat parts. An error in the pitch test offset will display a shift of the measured slope between the two sailed lines. An error in the roll offset will show as an angle between the two measured bottoms.
- 1+3: Latency determination on the slope. Latency will show as a shift in the measures profile between the slope and the fast line.
- 2+4: Yaw determination on the slope. An error in the yaw offset will show as an angle in the top view of the measured slopes (Lekkerkerk, et al., 2006).

7.1.3.1 Latency (place and depth) using the Patch Test

The latency between positioning system and multi-beam echo sounder is an important parameter. Commonly latency values between 0.2 and 1 second, causing positioning errors which, depending on the survey speed, can be anywhere between 0.3 and 5 meters. The latency correction is necessary because most positioning systems need time to calculate a position from the raw data measurements in contradiction to the echo sounder, which measures almost instantaneously. Latency error versus positioning error is shown for different survey speeds in Figure 3.

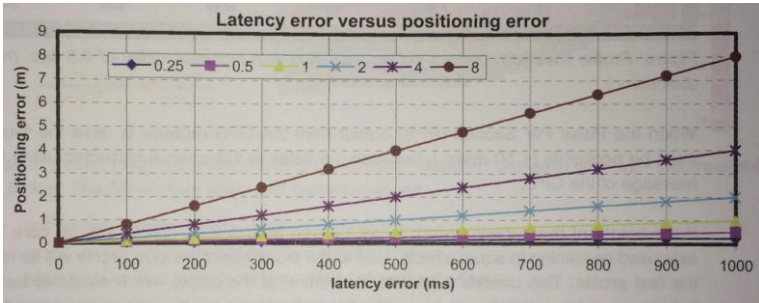


Figure 83 Latency error versus positioning error at different survey speeds (Lekkerkerk, et al., 2006).

In order to determine the latency, a select a slope with an angle in-between 1:2 and 1:5. Sail a line perpendicular to this slope at different speeds, one with survey speed and the other with either maximum speed or the speed at which the vessel is just maneuverable. These lines should be sailed in the same direction. A difference in the profiles of these slopes indicates a delay between positioning system and multi-beam.

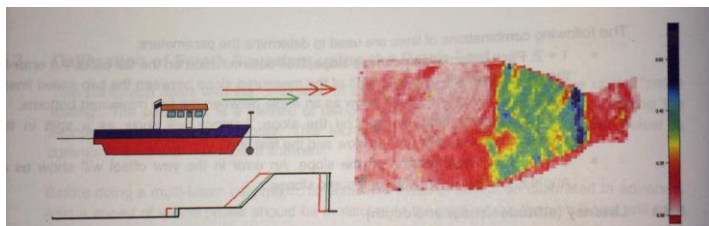


Figure 84 Delay determination using an artificial slope, standard deviation plot slope with wrong delay (0.5 s) (Lekkerkerk, et al., 2006).

In Figure 4:

- red profile: delayed position at fast speed/survey speed
- green profile: delayed position at survey speed/slow speed
- black profile: true position of the object without delay (Lekkerkerk, et al., 2006).

7.1.3.2 Roll Calibration using the Patch Test

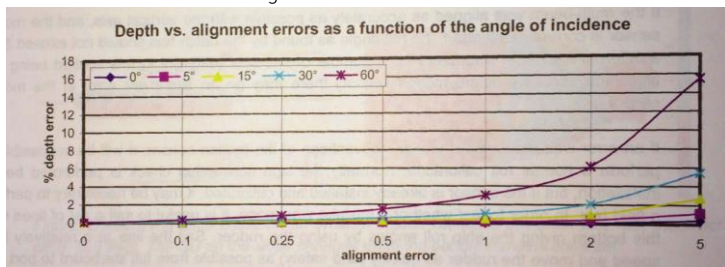


Figure 85 Roll alignment error vs. depth error at different angles of incidence (Lekkerkerk, et al., 2006).

Roll is a very important parameter when using swath sounders because most swath sounders will sweep perpendicular to the direction of movement of the measurement platform. Even a small

alignment error in the roll angle of the multi-beam will result in considerable errors. The error will be neglectable for the center beam and reach its maximum for the outer beam. Roll alignment error vs. depth error at different angles of incidence is presented in Figure 5.

In order to determine the roll offset, select an area that is as flat as possible. In general the deeper the seafloor, the more accurate the determination of the roll error will be. Sail a line in opposite directions over this flat surface. When no accurate height is available, make sure that the speed of the vessel through the water is the same in order to avoid squat errors. Plot a cross line profile of both sailed lines. This may give a profile like presented in Figure 6.

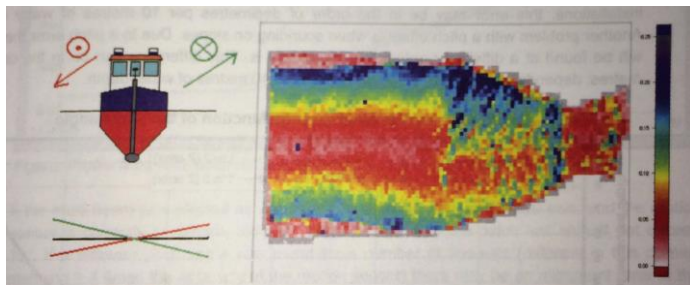


Figure 86: Determining roll offset using a flat bottom. Standard deviation plot with incorrect roll (0.5 deg) (Lekkerkerk, et al., 2006)

With:

- red profile: profile with roll offset of coming line
- green profile: profile with roll offset of going line
- black profile: true position of the bottom without roll offsets

If the multi-beam was aligned as accurately as possible with the vertical axis, and the motion sensor is correctly calibrated, the roll angle as found by the patch test should not exceed 5° (Lekkerkerk, et al., 2006).

7.1.3.3 Pitch Calibration using the Patch Test

Pitch is a very important parameter when sounding in deep water or when sounding on slopes. When surveying a flat bottom, a pitch offset will create a bottom that is either deeper or shallower than the real bottom, depending on the direction of the offset. For normal installations, this error may be in the order of decimeters per 10 meters of water depth. Another problem with a pitch offset is when sounding on slopes. Due to a pitch error the slope will be found at a different position than it actually is. This difference can be in the order of meters, depending on the slope and pitch offset, at 10 meters of water depth. Positioning error on slope due to pitch alignment errors are presented in Figure 7.

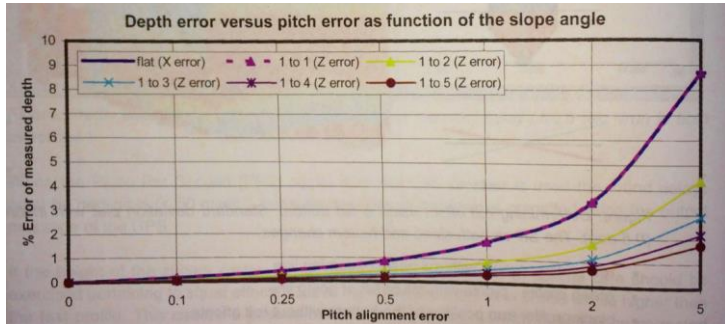


Figure 87 Positioning error on slope due to pitch alignment errors (Lekkerkerk, et al., 2006)

In order to determine the pitch offset, select an area that has a slope between 1:3 and 1:5. If possible, select a slope that is surrounded by a reasonably flat bottom. In general the steeper the slope, the more accurate the determination of the pitch error will be. Sail a line in opposite directions over this line. When no accurate height is available, make sure that the speed of the vessel through water is the same in order to avoid squat errors. Plot a cross line profile of both sailed lines. This may give a profile as presented in Figure 8.

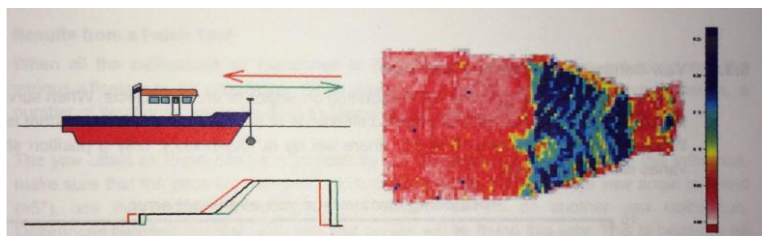


Figure 88 Determining pitch offset on an artificial object. Standard deviation plot with incorrect pitch (0.5 deg) (Lekkerkerk, et al., 2006)

Where:

- red profile: profile with the pitch offset of coming line
- green profile: profile with pitch offset of going line
- black profile: true position of the bottom without pitch offsets.

If the multi-beam was aligned as accurately as possible with the vertical axis, and the motion sensor is correctly calibrated, the pitch angle as found by the patch test should not exceed 10° (Lekkerkerk, et al., 2006).

7.1.3.4 Yaw Calibration using the Patch Test

Yaw is an important parameter when sounding on slopes or around objects. When surveying a flat bottom, a yaw offset will not create a difference at the depth at which the bottom is found. When surveying an area with slopes, there will be no depth error, only a position shift that varies with the distance. Figure 9 presents positioning error resulting from yaw alignment error.

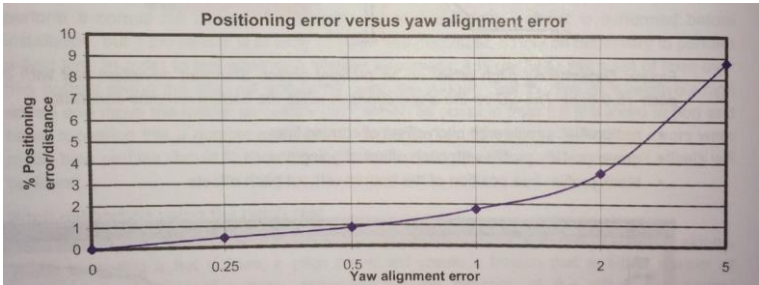


Figure 89 Positioning error resulting from yaw alignment error (Lekkerkerk, et al., 2006).

In order to determine the yaw offset, select an area that has either a slope between 1:3 and 1:5 or a distinct object on the bottom. If possible, select a slope or object that is surrounded by a reasonably flat bottom. In general the steeper the slope, the more accurate the determination of the yaw error will be. Sail two lines in the same direction next to the object. The distance between the two lines should be just enough to create an overlap in the middle of the tracks. Make sure the lines are sailed as straight as possible. Plot a cross line profile of both sailed lines. This may give a profile as presented in Figure 10.

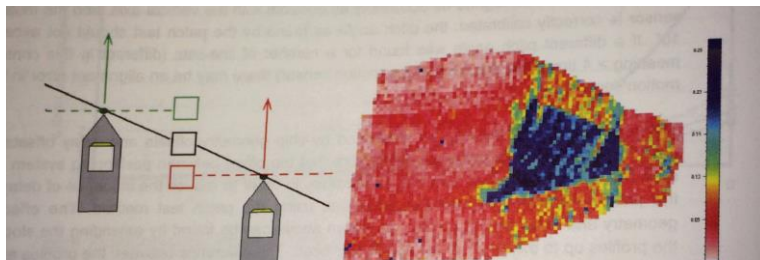


Figure 14: Determining yaw offset on an artificial object. Standard deviation plot with wrong yaw (0.5 deg) (Lekkerkerk, et al., 2006).

Where:

- red profile: position with yaw offset of sailed line
- green profile: position with yaw offset line
- black profile: true position of object without yaw offsets

When calibrating the yaw on a slope instead of an object, the slopes found will run parallel to each other, but at an offset. Contours not corrected for yaw will show a remarkable Z-shape in between the swaths surveyed (Lekkerkerk, et al., 2006).

7.1.3.5 Results from a Patch Test

When all calibrations as mentioned in have been carried out, the various offsets can be calculated. The yaw offset as found can be influenced by a pitch offset. In order to reduce this influence, make sure that the pitch is calibrated before the yaw angle. When a large yaw angle is found ($>5^\circ$), use this angle and recalibrate the pitch. After this do another yaw calibration. Differences between the first pitch and the yaw angle will be found this way. This is because no line can be sailed absolutely over

the same projected track, so position offsets and yaw angles will occur on the sailed lines generating mixed yaw and pitch offsets in the profiles (Lekkerkerk, et al., 2006).

7.1.3.6 Check on Survey Systems Absolute Z-value

It is good survey practice to perform a check after calibration on the survey systems absolute Z-value using a patch test. This can be done using a so-called "drempel". The principle is demonstrated in Figure 11.

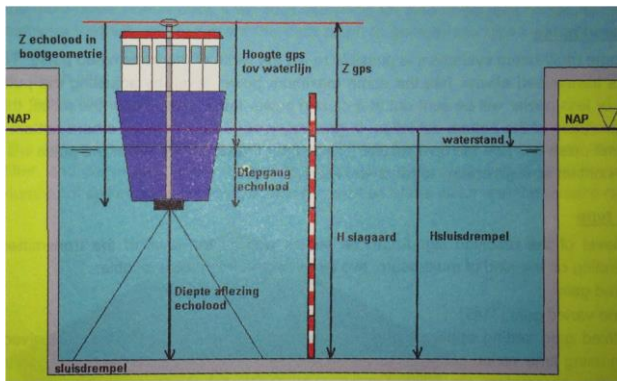


Figure 15: Equalizing the height of a known object (log) with a multi-beam measurement (Lekkerkerk, et al., 2006).

The following procedure can be followed:

- Check the reading of the echo sounder + draught with the reading on the lead line or sounding pole
- Check the height from the software with the (measured) height of the object, or determine this least one according to water level and sounding pole (Lekkerkerk, et al., 2006).

7.1.4 Practical Considerations

7.1.4.1 Coverage

A general bathymetric map of a large area may require only 1 depth per 25 m^2 whereas a construction survey requires 10 depths per 1 m^2 . In order to achieve this coverage, the required survey speed and line distances need to be established.

The achieved coverage when using a swathe sounder depends on the used sensor. The following sensor parameters influence the achieved coverage:

- Swath sector
- Beam angle
- Maximum update rate

Swath sector

The larger the swath sector, the wider the area covered with one sailed line.

Beam angle

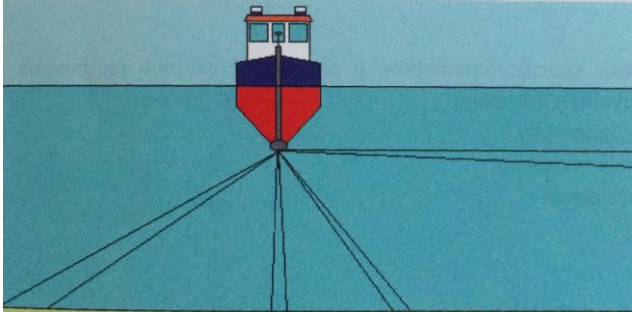


Figure 90 Footprint for different incident angles sectors (30° , 90° , 60° , 5°) (Lekkerkerk, et al., 2006).

For multi-beam echo sounders not only the swath sector defines the maximum coverage, but also the beam angle. The number of points per square meter is directly proportional to the incident angle (angle at which a certain beam hits the bottom) and the beam angle via the beam footprint, as shown in Figure 12. The incident angle is directly proportional to the beam number when surveying on a flat bottom.

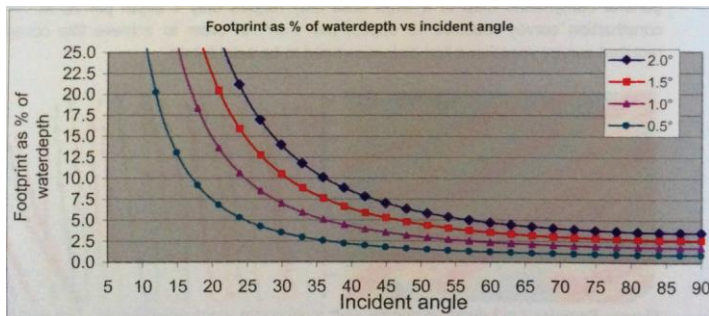


Figure 91 Relation between the size of the footprint as a function of angle of incidence (relative to the waterline) (Lekkerkerk, et al., 2006).

Figure 13 shows the relation between the size of the footprint as a function of angle of incidence (relative to the waterline). The footprint is presented as a percentage of the water depth. The real footprint is obtained by the formula: footprint [%]/100% * water depth. Footprints larger than 25% of the water depth are omitted in the figure because they will not occur in practice.

Determining the footprint the next rule of thumb may be used:

- Doubling the water depth will double the footprint
- Halving the beam angle will half the footprint.

Bottom coverage

Apart from these sensor specific parameters, a number of external parameters will also influence the bottom coverage achieved:

- Changes in bottom topography
- Line keeping of the survey vessel
- Alignment of the multi-beam
- Motion of the vessel

The effect of these parameters is shown in Figure 14.

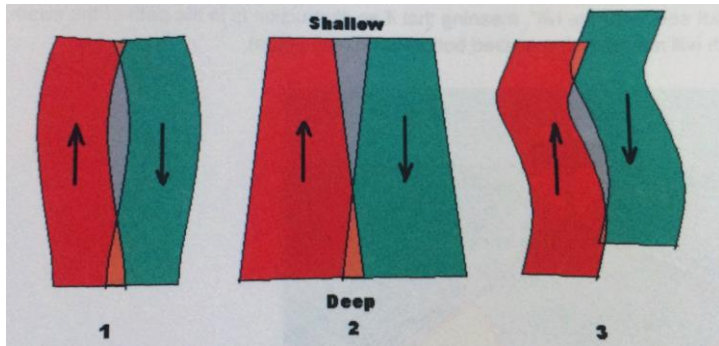


Figure 92 Coverage of multi-beam: 1 line keeping, 2 changes in bottom topography, and 3 roll motion of the vessel (Lekkerkerk, et al., 2006).

As a rule of thumb, lines are at an overlap between 20 and 200 % to keep the coverage of the bottom at the required level. For a reasonably flat bottom, with a good skipper and little waves an overlap of 20% may be sufficient. When surveying a bottom with a rough topography, overlaps of 100 to 200% may be required. Lines next to each other are generally sailed in opposite directions to check data integrity in the areas of overlap (Lekkerkerk, et al., 2006).

Kommentert [EH13]: Er dette riktig?!

7.1.4.2 Shading

Another problem with multi-beam surveying is the shading of the multi-beam signal. Multi-beam cannot see "over the hull", meaning that if an obstruction is in the path of the swath, part of the swath will not return the desired bottom echo, as shown in Figure 15.

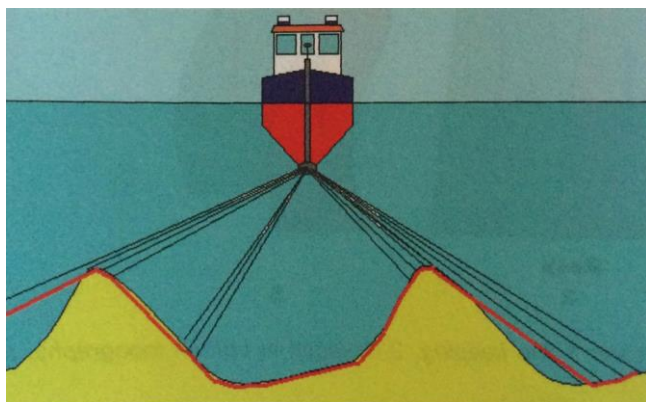


Figure 93 Over the hill" shading of multi-beam (Lekkerkerk, et al., 2006)

This problem arises mainly when surveying in shallow water or when surveying around areas with sand dunes. A solution to this problem is to space the lines such that they are always sailed at both sides of the (predicted) obstruction (Lekkerkerk, et al., 2006).

7.1.5 Data Processing

All data is stored and provided with an accurate time stamp. This time stamp allows the data to be merged and compared, which is very important in processing.

Data processing sheets are a crucial means of organizing data and keeping track of the data processing progress. It is important that datasets are processed in a similar fashion safeguarding a consistent approach.

Each type of data has its own validation and quality control routines. These data types have been broken down as follows:

- Position
- Depth (non-MBE)
- Video
- Depth (MBE)
- Geophysical

The whole operational system of the multi-beam echo sounder is quite complex, as there are many sensors that work together, which provide an integrated data solution. The processing is as a result complex and each individual sensor should be validated first prior to integrating into one data solution.

Consequently processing is very much data validation, which is ideally performed by validating the output of each sensor prior to data integration. Unfortunately not all software packages allow these QC tasks to be performed and the use filter settings instead. If the latter is the case it is important to ensure that the effect of the filter settings are unambiguous. In general the following processing sequence is performed:

- Removal of Spurious Data from the sensors
- Tidal/water level reduction if not applied RKT GPS applications
- Integrate data sets providing XYZ data
- Remove spurious data from the XYZ result
- Define sensible DTM
- Import XYZ
- Check result against original data set
- Generate contours and perform model smoothing to enhance chart readability
- Verify smoothing parameters by comparing raw spot map versus smoothed contour chart or compare raw and smoothed DTM
- Plot contour charts and visualize complicated areas in 3D.

Validation of raw data is carried out in order to remove spurious data. Integration of position and depth is then performed, so the first impression of the survey becomes available.

Viewing of data is then carried out in order to locate and repair possible errors that were created during the integration process.

Filters may then be used on the data smooth out irregular positioning. There are a number of available filters:

- Mean filter. A group of data is replaced by the average of the values.
- Median filter. A group of data is replaced by the middle value of that group. This implies the use of an odd number of measurements.
- Statistical filters. Statistical methods are used to smooth the data, taking into account the general direction of the data.

The last step is manual editing of all the data. The quickest way to check whether any manual editing is necessary is by comparing the current DTM with the original DTM. No further processing is needed this comparison looks fine. However, if irregularities are found then the data must be edited manually, or maybe even restored to the original (Lekkerkerk, et al., 2006).

7.2 Side Scan Sonar

Instead of measuring the depth to the ocean bottom, a side scan sonar reveals information about sea floor composition by taking advantage of the different sound absorbing and reflecting characteristics of different materials (SeaBeam Instruments , 2000). Graphic records that show two-dimensional (map) views of seafloor topography and of objects on the seafloor are provided (Lekkerkerk, et al., 2006). The theory on this sonar was presented in chapter 2, and in the following we will consider the application of this type of sonar system.

Kommentert [EH14]: Dekket i kapittel 2

7.2.1 Installation

Installation of side scan sonar systems can be done in several different ways, depending on the scope of the survey and the geographical conditions in the survey area. The sonar is most commonly towed from the stern. It is a very convenient and low cost method for survey in deep waters. In shallow waters and inland waterways the sonar is often mounted on the hull/in front of the vessel in order to reduce the noise level caused by the bow and stern waver from the survey vessel.

Furthermore several other methods for sonar surveys in deep and shallow water shall be discussed briefly?

In operating and processing side scan sonar data there are two very important issues:

- The sonar image has to be as good as possible.
- The positioning has to be correct.

A good quality sonar image must be obtained during operation and processing. The positioning of the sonar image will largely depend on good installation and calibration of the system.

Although it is possible to use a side scan sonar system as a stand-alone system this is not common. In general the complete setup consist of:

- A side scan sonar system, including a computer, plotter, tow fish and tow cable.
- A positioning system, including GPS receiver, computer for processing and displaying the navigation data.
- A data link between these two systems is required, in order to record processed navigation data on the sonar data (Lekkerkerk, et al., 2006).

7.2.1.1 Towed from Stern

This is the most common way in operating the side scan sonar system. It is simple, cheap and reliable. It can be performed from almost any vessel without making extensive modifications to the vessel. It is used in water depths from several meters up to thousands of meters. The tow cable acts as a buffer between the vessel and the sonar fish, so the movements of the tow fish are less strong than the movements of the vessel.

The limitation is in shallow water (<20 m), when the tow fish is too close to the water surface it will be extremely vulnerable for surface and ship's noise. Secondly, there is little control of the towed

fish path, especially when the tow cable is long or when there is a strong current. Normally the tow fish will be at a safe depth under the surface. Sometimes the tow fish will not be submerged enough. This problem can be solved by using a depressor. This device will help the tow fish to submerge and it will keep constant tension on the tow cable.

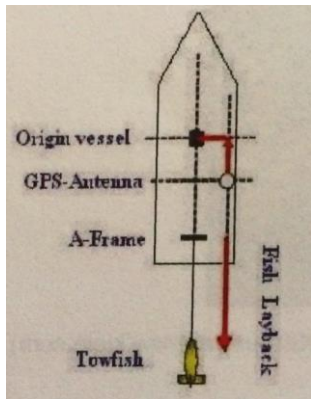


Figure 94 Layout survey vessel with towed side scan sonar (Lekkerkerk, et al., 2006).

A sketch of the situation is given in Figure 18. The sonar fish is towed from the stern. The tow cable is a power/data cable, the so-called umbilical, which can be several thousands of meters long. Usually the tow cables are stored on a winch, which makes it easy to deploy and change the length of cable (layback) during operation. Smaller cables, up to 50 m are often deployed by hand. The fish layback should be recorded and checked during operation. During installation an electronic (a winch cable-counter) or manual (marks on the tow cable) system has to be set up.

In order to be able to obtain the position of the fish one have to calculate the fish layback

$$\text{Layback} = \sqrt{(\text{cable deployed})^2 - (\text{towfish depth})^2}$$

This is no problem when the tow cable is in a straight line behind the vessel and when the cable forms a straight line. In practice this will not always be the case. The following can occur:

- Due to side-currents the tow fish and cable are drifted away. The sonar fish is not towed in a straight line form the vessel.
- Unless a depressor is used, the tow cable normally represents an arc, rather than a straight line between the tow fish and the tow point, as seen in Figure 19.

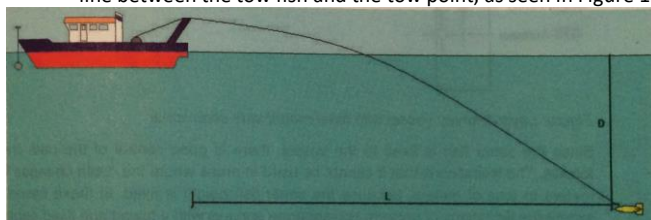


Figure 95 Incorrect fish position due to catenary in the tow cable (Lekkerkerk, et al., 2006).

There are several solutions to obtaining a better tow fish position:

- A mathematical solution: By measuring the angle between the vessel's heading and the tow cable a correction can be made for the drift. An arc-to-cord correction can be applied if the tow cable is not straight. The so obtained position remains a best estimate.
- Underwater acoustics: By using USBL, which consist of a transponder and a receiver. One connected to the tow fish, the other on the vessel's hull. The device measures the distance and angle, relatively to the vessels orientation, hence the "exact" position of the tow fish. The USBL is sensitive to surface reflections, and therefore works better when the tow fish is more than 20 meters under the surface.

Eventually the accuracy of the tow fish position varies from $\pm 1 \text{ m} + 1\%$ of the layback, if USBL is used to 1-10% of the layback, depending on how the layback is calculated.

The offsets from the instruments relative to the origin of the survey vessel have to be measured. The layout of the vessel and all the different offsets can be entered in the navigation-computer. Together with the tow fish position and the GPS- positions the navigation-computer can calculate the coordinates of the tow fish. These coordinates and other navigation data such as sonar fish heading, speed, fix-marks, kp-'s, should be sent to the side scan sonar computer. The sonar software will calculate the coordinates for every point on the sonar record (Lekkerkerk, et al., 2006).

7.2.1.2 Fixed Mounting

This method is used in very shallow waters such as inland waterways. Towing the sonar fish in these shallow waters will create surface and ship noise on the record. Furthermore there is always a risk of running the fish aground. Prior to use, the survey vessel should be modified with a construction that can be lowered in and out of the water easily. On this construction the sonar fish should be mounted. Make sure it is aligned with the vessel, so they both have the same heading. In general the sonar fish will be mounted in front of the vessel, approximately 50 to 100 cm under the surface, but in order to avoid damage to the sonar fish, never deeper than the hull.

Since the sonar fish is fixed to the vessel, there is good control of the path the sonar fish follows. The limitation is that it cannot be used in areas where depth changes from several meters to tens of meters, because the sonar fish height is fixed. In these cases one should except the limitations or perform two separate surveys with a towed and fixed sonar fish.

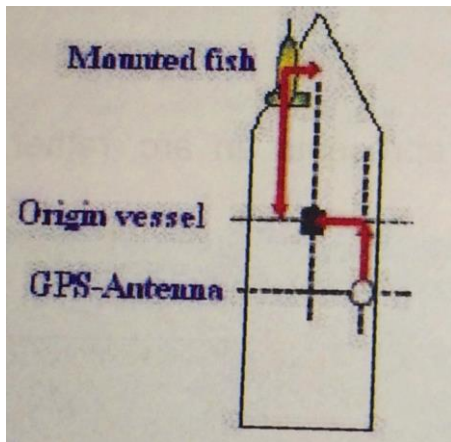


Figure 96 Layout survey vessel with fixed mount side scan sonar (Lekkerkerk, et al., 2006).

A sketch of the situation is given in Figure 20. The sonar fish is fixed on the bow. The offset position of the mounting construction in lowered position has to be measured. This is the position of the fish relative to the ship.

The layout of the vessel and all the different offsets must be entered in the navigation-computer. Together with the GPS-position the navigation-computer can calculate the coordinates of the sonar fish. These coordinates and other navigation data such as sonar fish heading, speed, fix-marks, kp's, should be sent to the side scan computer. The sonar software will calculate the coordinates for every point on the sonar record. The accuracy of this method is much better and in general will be better than 1 meter (Lekkerkerk, et al., 2006).

7.2.1.3 Other Methods for Deploying Side Scan Sonar

Mounted on ROV:

For inspection of offshore constructions, side scan sonar together with video recordings are performed and high maneuverability is required. Often these inspections take place in deep water. In these cases the first two scenarios do not apply. A solution is the use of a ROV. On the ROV several instruments can be attached, such as video, side scan sonar, vibrocore, bottom sampler. Operating side scan sonar systems mounted on a ROV is no different than operating any other side scan sonar system, as long as the position of the survey vessel, the ROV and the measured offsets are reliable.

Mounted under a floating device:

For surveys in shallow waters, where small boats are used it is not possible to mount a side scan sonar on the bow, because these boats are in general not stable enough. In these cases the side scan sonar is towed. In order to avoid surface noise the sonar fish is fixed with a frame under a floating device, such as a surfboard. The sonar fish acts as a keel for the surfboard and the whole construction moves steadily through the water thus reducing the surface noise. Due to the high resistance of the construction it can only be used at low speeds. Otherwise the turbulence around the construction will create noise. An exact value for the speed depends on the type of construction and weather conditions (Lekkerkerk, et al., 2006).

7.2.2 Data Processing

After understanding the information provided by the sonar image the data has to be processed. This means that the position, size and height of sonar contacts have to be determined. The location of areas with rock-dump, soft surface sediments etc. have to be obtained. Nowadays side scan sonar processing software contains tools that will obtain the position and calculate dimensions. However in the following includes the basic information to do it manually from the paper record.

It also includes that the data is modified, filtered and amplified in order to make a better representation (Lekkerkerk, et al., 2006).

7.2.2.1 Dimensions

The dimensions of a sonar contact are length, width and height. When the sonar record is corrected for speed and slant-range, it represents an evenly scaled 2D image of the bottom. The length and width can be measured from the record it self. Normally it is sufficient to estimate the length and width, scale lines on the record paper is good tools. To obtain good values for the length and width on a non-corrected paper record is a hideous task that includes so many uncertainties that an estimated guess is a better alternative. Assuming a rectangular contact, the position of the four corners points has to be calculated in order to calculate the size. To calculate one position, the sonar

position and sonar heading at that time is required and the measure angle to the contact; already uncertainties for one position.

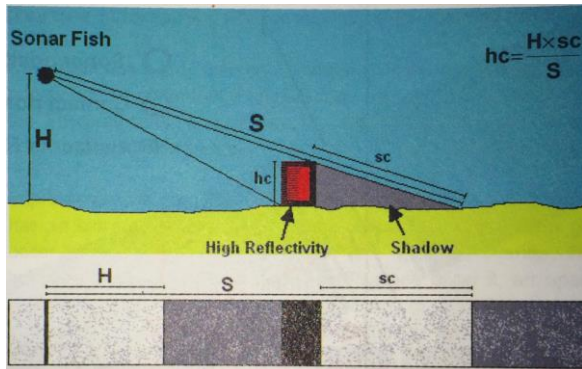


Figure 97 A schematic view of the underwater situation (top) and the resulting theoretical sonar image (bottom) (Lekkerkerk, et al., 2006)

The height of a sonar contact can easily be obtained from a sonar record. The length of the shadow in combination with the range and height of the fish are used to determine of the sonar contact, as seen in Figure 21. The same principle is used to calculate the height of a free span for pipelines and cables. The height of the contact shadow should be replaced with the distance between the high reflectivity and the shadow (Lekkerkerk, et al., 2006).

7.2.2.2 Position

The position of the contact can be determined from the sonar record, as seen in Figure 22. To be able to do this one should know:

- The heading of the sonar fish
- The position of the sonar fish
- The horizontal range to the contact, or the slant range and sonar fish height.

If the record is corrected for slant range, the horizontal range has to be measured from the record. If the record is uncorrected the horizontal range has to be calculated by using the Pythagorean Theorem. With this information the offset between the sonar fish position and the contact position can be calculated.

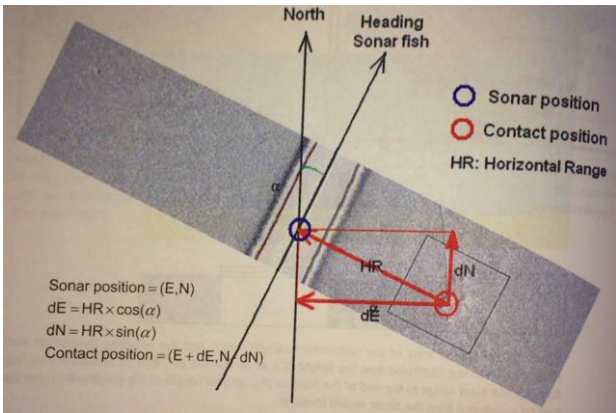


Figure 98 : A sketch illustrating how the position of a sonar contact can be calculated (Lekkerkerk, et al., 2006).

The described procedure calculates the position of a contact on one record. If the survey is performed with 100% track overlap or more, the same contact should be seen on other records. From these records the contact position can be calculated as well. Verify this position in order to make sure that the calculations have been performed correctly. The type of installation and the amount of layback will give an indication of how accurate the positioning is, and what the maximum difference between the both calculations should be (Lekkerkerk, et al., 2006).

7.2.2.3 Mosaic

A side scan sonar mosaic is an image of the seafloor line an aerial photograph, an evenly scaled 2D image. Most software programs have mosaicing tools that calculate a position to every recorded pixel. And the pixel is given a grey tone corresponding with the intensity of the returned echo.

Every pixel has a gray tone and a position. All the pixels of all the side scan sonar records in a survey can be plotted on a (digital) map. This map is a perfect tool for the processor to make the interpretations, to calculate the dimensions and positions of the contacts, to create contours for surface sediments variation, to locate hazardous objects, free spans etc. An example of a side scan sonar mosaic is presented in Figure 23 (Lekkerkerk, et al., 2006).

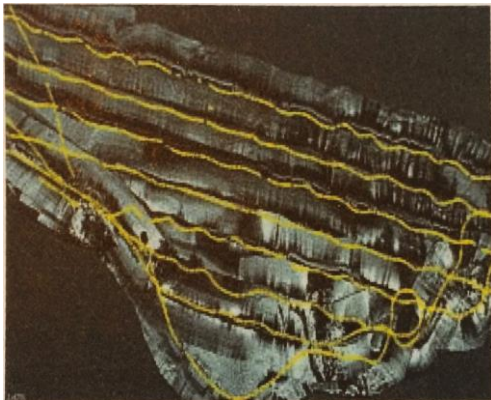


Figure 99 Example of side scan sonar mosaic (Lekkerkerk, et al., 2006).

Sub Bottom Profiler

Sub-bottom profilers, sometimes also referred to as single channel systems, are used throughout the industry for the shallowest seabed profiling (Chakrabarti, 2005). This section build upon the theory regarding the sub bottom profiler presented in chapter 2.

7.2.3 Applications

Sub bottom profiling (SBP) covers a wide range of systems and technologies in order to investigate the sub bottom conditions at sea, lakes and waterways. There are generally two major applications for sub bottom profilers in the survey industry:

- Mapping of geological structures below the bottom
- Detection of sunken or buried objects (Lekkerkerk, et al., 2006).

Kommentert [EH15]: Flyttet til kapittel 2

7.2.4 Installation

SBP systems can be installed in various different ways. This depends on the type of equipment and the technical possibilities and the construction of the survey vessel. Each method has its own (dis)advantages (Lekkerkerk, et al., 2006).

7.2.4.1 Fixed Construction

A fixed construction is mostly used for SBP systems that combine a source and receiver in one instrument. In general these systems are quite small, smaller than most towed SBP systems. The sound pulse that is generated by the transducer of the SBP systems is focused into a beam, with typical beam angle up to 20°. With a "narrow" beam it is easier to avoid side and surface reflections.

The advantages of a fixed construction are:

1. The SBP systems can be placed at a depth below the water surface, in order to reduce the surface noise and to avoid unwanted side reflections that travel just behind the emitted pulse.
2. The position of the SBP system can be calculated very accurately, which ideally corresponds with the position of the recorded reflections.
3. Surface swell on the SBP record can be filtered out easily with heave compensator. For a fixed construction the heave compensator aides in calculating the exact heave at the location of the SBP system.

The SBP system may be hull mounted, which is a permanent solution, or a side construction, which is more temporary solution (Lekkerkerk, et al., 2006).

7.2.4.2 Towed from the Stern

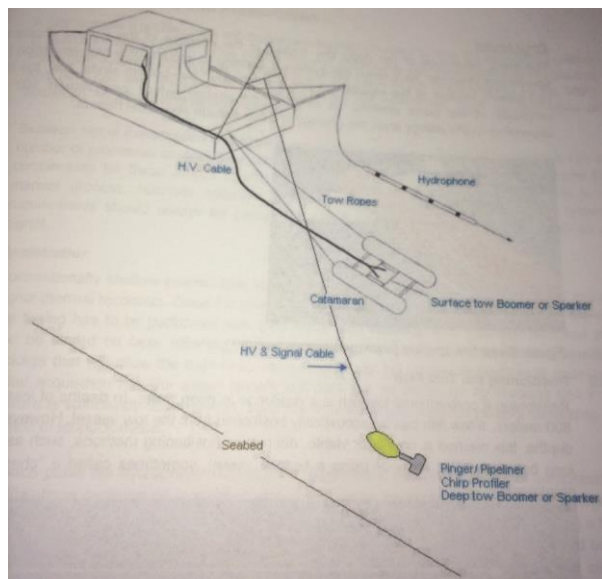


Figure 100 Schematic view of a survey vessel towing a surface and deep tow SBP system

A towed SBP system, as shown in Figure 28, is mostly used for separate sources and receivers. The hydrophone array is a sensitive piece of equipment that should be free in the water and it has to be relatively close to the seismic source. This is not possible for a fixed construction, because the vessel would be a major noise generator for the hydrophones; either by touching the vessel or by the wake created by the vessel. Therefore the best solution is a towed SBP system. Another advantage is safety, especially for sparkers. It would be far too dangerous to use this kind of high voltage equipment whilst it is in contact with the survey vessel.

A disadvantage is the accuracy of the positioning of the SBP system. Unless the SBP system is equipped with a beacon or antenna, the position has to be estimated. Which results in less accuracy for the position of the SBP system and the position of the recorded reflections (Lekkerkerk, et al., 2006).

7.2.4.3 Positioning the Tow Fish

Positioning a conventional tow fish is a challenge in deep water. In depths of less than about 800 meters, a tow fish can be acoustically positioned from the tow vessel. However, in greater depths, this method is no longer viable. Alternative positioning methods, such as deploying a long baseline (LBL) array or using a second vessel, sometimes called a "chase boat", are employed.

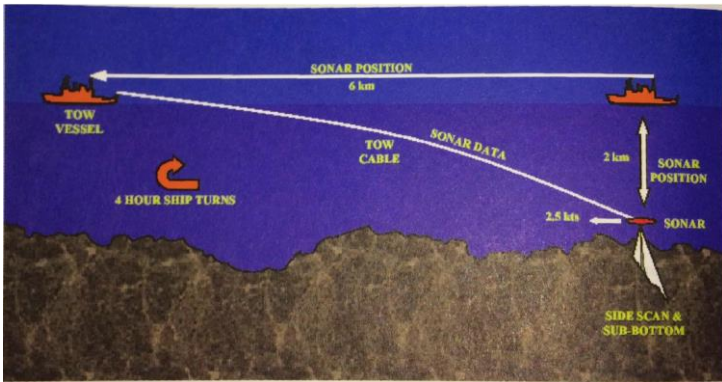


Figure 101 Use of a chase boat in deep waters (Lekkerkerk, et al., 2006).

Figure 29 depicts a typical deep tow survey scenario. In this example, a tow vessel with a deep towed sonar is followed by a chase boat, which positions the tow fish. Because a ratio of about three-to-one (cable length to water depth) is required, and the water depth is 2000 m, about 6000 m of cable is deployed. Tow fish positions are radioed to the towboat by the "chase boat" as the towboat attempts to steer the tow fish along a prescribed survey line (Lekkerkerk, et al., 2006).

7.2.5 Signal Processing and Presentation

Between signal transmission and signal reception, the signal is attenuated and distorted by a number of processes as described earlier or in the underwater acoustics syllabus. In order to compensate for these effects filtering and amplification is performed. Generally this is a manual process, however software controlled systems are also available (Lekkerkerk, et al., 2006).

7.2.5.1 Registration

Conventionally shallow seismic data is recorded on graphic recorders that at present are all digital thermal recorders. Once the data has been acquired it cannot be altered hence the online tuning has to be performed with care not to lose valuable data. The data acquired can also be stored on tape, allowing replay on paper, or acquired using seismic acquisition package that will allow the data to be reprocessed until the display of features is optimized. Digital acquisition has the added benefit that the data can be enhanced by stacking and if the software is sufficiently sophisticated, supports semi-automatic reflector picking, facilitating the creation of isopach maps.

For each pulse the hydrophone will record a wiggle trace showing a series of compressions and dilatations centered on a mean of zero. To enhance the presentation positive or negative amplifiers are filled, which is referred to as Variable Area Recording (VAR). By adding a trace at the time, a seismic time section is recorded of which a graphical example is provided below. Applications in shallow reflection profiling have a much larger trace density and a slightly different use of VAR. As a consequence the displays differ in their appearance whilst adopting the same principles. A pinger (pipeliner) section is presented in Figure 30.

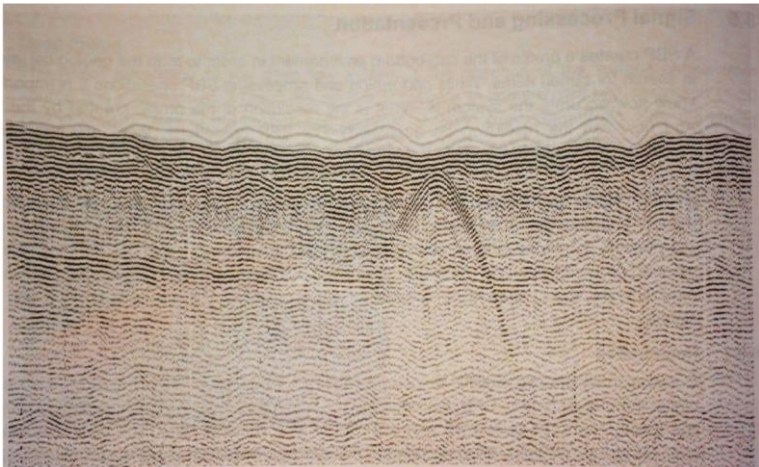


Figure 102 Example of a pipeline record (Lekkerkerk, et al., 2006).

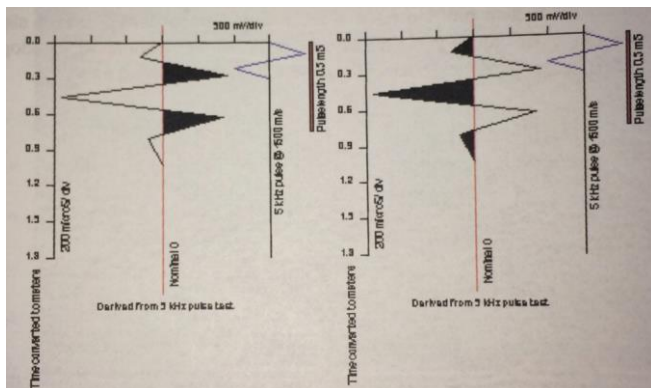


Figure 103 Positive and negative polarity respectively (Lekkerkerk, et al., 2006).

VAR in deep seismic provides amongst others, a tools to detect phase reversals in shallow refection seismic; the use is limited but available on conventional recorders as a polarity switch. As shown in Figure 31 a positive polarity would produce two moderately strong reflection, whereas opting for a negative polarity would provide a strong reflection flanked by two weak ones.

As indicated in Figure 32, the pulse signature has an effect on how features are displayed. Since piezo electric sources such as pingers have a multi-wave length pulse, this signature is very obvious on the record. The difference in polarities is shown in Figure 32. Note that for the extension of relevant depth measurements the polarity is relevant (Lekkerkerk, et al., 2006).

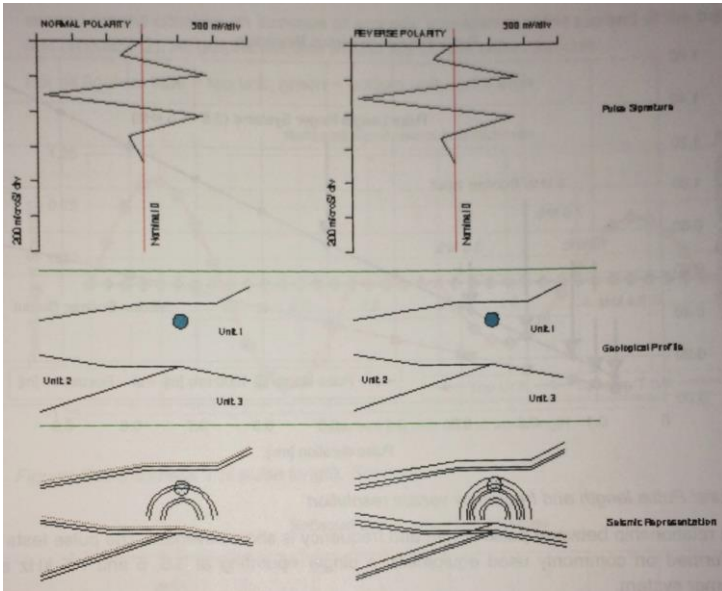


Figure 104 Effect of signature and polarity on display. Top: pulse signature (polarity), middle: geographical profile; bottom: seismic representation (Lekkerkerk, et al., 2006).

7.2.5.2 Time Depth Conversions

With all the techniques above, a time section has been generated which still needs conversion to a depth section. As the principle of velocity scan is not available to shallow single channel seismic, the time section is generally converted to a depth section using an assumed speed of sound for the sediments. Typical values are between 1600 and 1700 m/s. For most engineering purposes, the error made by assuming a wrong speed of sound can be ignored (Lekkerkerk, et al., 2006).

7.2.5.3 Vertical Resolution

Considering the sensor only, vertical resolution is predominantly determined by pulse length. Pulse length differs from signal frequency as shown on the graph in Figure 33. Whereas the system's frequency would provide a higher resolution, the pulse length is the determining factor due to penetrating capabilities and the associated convolution. The return frequency is significantly lower, in the order of 1 kHz, when compared to the transmission frequency of 5 kHz. The same effect is applicable to pinger systems but as these penetrate less, the effect is hardly noticeable.

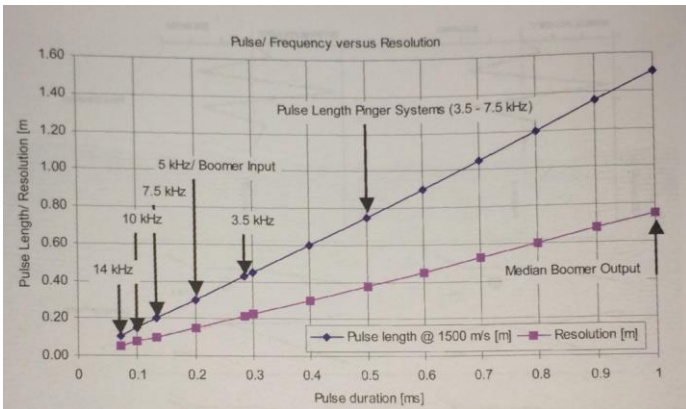


Figure 105 Pulse length and frequency versus resolution (Lekkerkerk, et al., 2006)

The relationship between pulse length and frequency is shown in Figure 34. The pulse tests were performed on commonly used equipment, a pinger operating at 3.5, 5 and 7.5 kHz and a Boomer system.

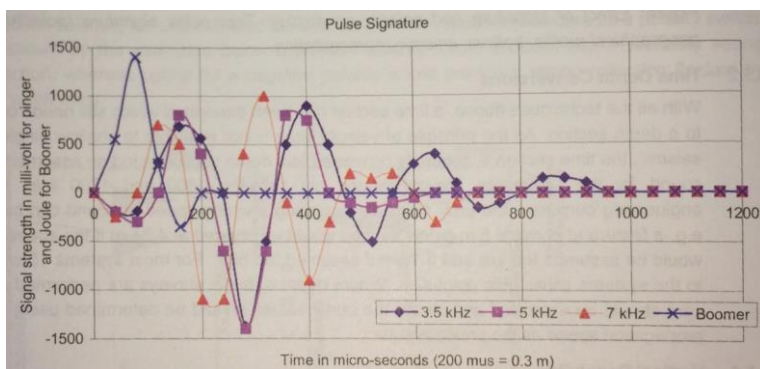


Figure 106 Pulse Signatures: note that all pinger frequencies have a 500 μ s pulse length (Lekkerkerk, et al., 2006)

It is quite obvious, that the quoted pulse duration of the pinger system (500 μ s) is an approximation of the frequency. As the seabed response is to the whole wave train, the resolution is related to the pulse length rather than the frequency (Lekkerkerk, et al., 2006).

7.2.5.4 Horizontal Resolution

The horizontal resolution is predominantly a function of the beam angle and the radius of the first Fresnel zone. Fresnel zones are also referred to as phase zones defining the areas contributing positively to the signal and which zones contribute negatively.

The general formula to calculate the radius of the first Fresnel zone is $r = \sqrt{\frac{\lambda \cdot h}{2}}$ with h being the distance to the reflective surface. In case of sub bottom profilers this Fresnel zones will be smaller than the actual footprint as graphically shown in Figure 35. The horizontal resolution will be in the

same order of magnitude as the radius first Fresnel zone. Small scale changes in structures will not be observable (Lekkerkerk, et al., 2006).

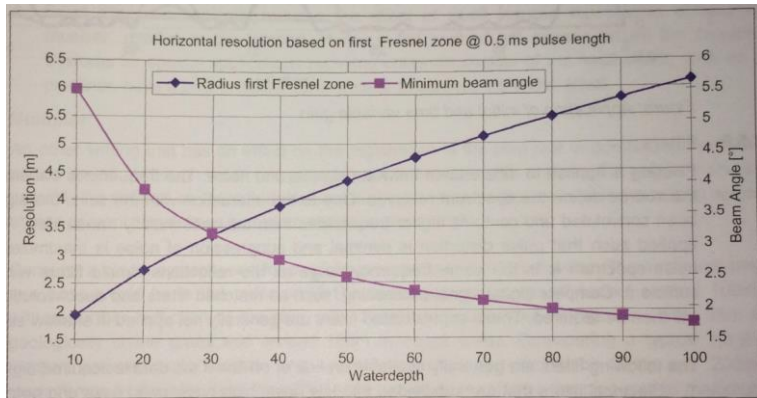


Figure 107 Horizontal resolution based on radius first Fresnel zone (Lekkerkerk, et al., 2006)

7.2.5.5 Amplifiers

Although one can differentiate between automatic and manual systems, in essence these systems are identical. Main components are overall gain and time variable gain (TVG). The gain settings enable definition of the balance between signal and ambient noise, whereas the TVG compensates for the attenuation of the signal as a result of natural processes. The majority of the current equipment or acquisition packages allow the application of different TVG types. Application would generally be based on overall image quality. Should an oscilloscope or oscilloscope function be available, raw signal and applied TVG could be visualized to aid the system's tuning. As a rule of thumb, a dense seabed requires a steep TVG slope, whereas a soft seabed does require a gentler slope. A schematic overview is presented in Figure 36.

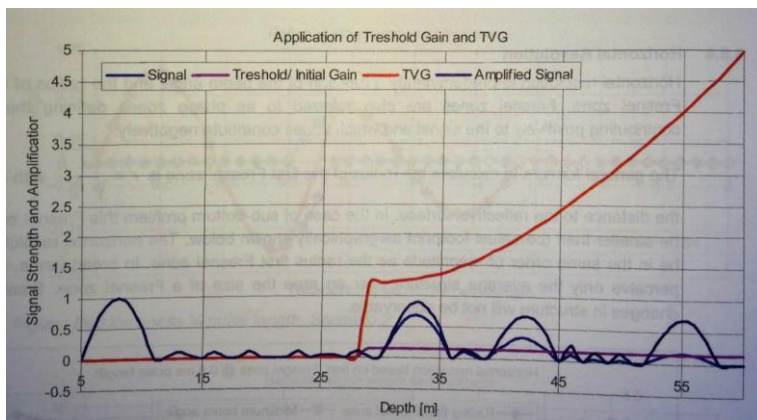


Figure 108 Application of initial and time variable gain (Lekkerkerk, et al., 2006).

7.2.5.6 Filters

Filtering is applied to differentiate between signals and noise. The frequencies transmitted by the source define the spectrum received. Due to the interaction with the soils, the signal has been convoluted and contains higher frequencies than the ones initially transmitted. A filter is applied such that pulse distortion is minimal and suppression of noise is maximized. If the noise spectrum is in the same frequency range as the reflections simple filters will not be sufficient. Complex digital signal processing, such as matched filters and deconvolution filters will then be required. These sophisticated filters are generally not applied in shallow seismic.

The following filters are generally available on-line and off-line if the data is acquired digitally.

1. Electrical filters that are subdivided into low pass, high pass, band pass and notch filters.
High pass filters, as indicated by the name allow high frequencies to pass freely, whereas low pass filters allow low frequencies to pass freely. If high and low pass filters are applied simultaneously they have the same effect as a band pass filter. Notch filters are used to suppress a narrow frequency band causing interference. See Figure 37.

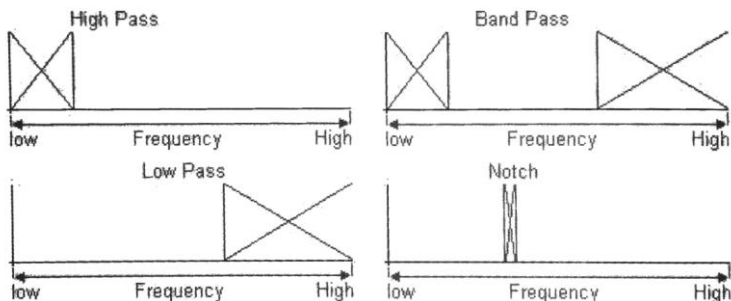


Figure 109 Different types of electrical filters (Lekkerkerk, et al., 2006).

2. The use of multiple hydrophones per channel, which eliminate random noise. A similar effect can be created by stacking the individual traces of a pinger system. In the latter case the data has to be acquired digitally.
3. Deconvolution filter. The main aim of this filter is to restore the original short signal, which has been convoluted and lengthened by the natural earth filter.
4. Swell filter, electronically reduces the effect of swell induced movements of source/receiver, relative to the seabed. Hence a flat seabed will appear flat on the records (Lekkerkerk, et al., 2006).

7.2.5.7 Multiples

In shallow waters multiples can be a major problem and in case of a flat seabed might appear almost as a true reflection. The position of a multiple is predictable as the first would occur at one times the water depth below the seabed and the second at two times. Other easy tests are (Lekkerkerk, et al., 2006):

1. The multiple of a gently sloping seabed will slope in the same direction but at a steeper angle and the second multiple at an even steeper one.
2. In case the seabed is gently undulating, the multiple will show the same undulations but with twice the amplitude.
3. If not evident and if possible, the altitude of the source can be altered, which results in the multiple moving in the same direction as the seabed but twice as much.

4. Ping rates in excess of the propagation velocity divided by twice the water depth should be avoided at all times, as this will cause the first multiple of the earlier ping to interfere with the current (Lekkerkerk, et al., 2006).

7.3 Error Sources and Budgets

Knowing the accuracy or reliability of the final chart of digital terrain model (DTM) is imperative for the end-user or institution. Accuracy denotes the degree of conformity (offset) of a measured or estimated quantity to its true value. Precision is the degree to which repeated samples or measurements under unchanged conditions show the same results (variability). For some applications such as making nautical charts it is crucial that the accuracy is high. This is particularly the case in shallow water. Precision is on the other hand indicative of the ability to build fine resolution images, and may therefore be necessary for other applications, e.g. archeology or military operations.

For a DTM the quantities of interest are co-registered depth and position data. A key observation is that the survey end product has no better accuracy than the least accurate component in the measurement chain, from surface navigation all the way down to the acoustic seabed footprint. The accuracy of each component or of the final DTM (total accuracy) may be stated by an uncertainty and some associate confidence level.

The following section discuss and analyze the achievable horizontal mapping accuracy in integrated hydrographic AUV systems (Hegrenæs, Sæbø, Hagen, & Jalving, 2010).

7.3.1 Horizontal Mapping Accuracy

The total horizontal uncertainty (THU) of a DTM is to be understood as the uncertainty of the combined AUV positions and sounding footprint positions (Hegrenæs, Sæbø, Hagen, & Jalving, 2010).

7.3.1.1 AUV Related Uncertainties

The following gives a discussion on uncertainties related to the horizontal positioning of the AUV (Hegrenæs, Sæbø, Hagen, & Jalving, 2010).

7.3.1.2 GPS Accuracy

Several GPS services applicable for AUV survey systems are available:

- GPS standard positioning service (SPS)
- GPS precise positioning service (PPS)
- Differential GPS (DGPS)
- Real-time kinematic GPS (RTKGPS)
- GPS precise point positioning (PPP)

SPS and PPS are both available worldwide, but PPS is only for authorized users and primarily intended for military purposes. Stand-alone single-frequency (L1) SPS solutions exist which have a horizontal accuracy on the order of 2m (1σ). Dual frequency (L1/L2) yields slightly better performance. Further accuracy improvement is achieved by incorporating correction data broadcasted from stationary reference stations. This is the case for both DGPS and RTKGPS. The systems differ in the use of code-phase and carrier-phase techniques, where the latter yields the best performance. DGPS typically provides a horizontal accuracy on the order of 0.5 m (1σ) while RTKGPS has an accuracy ranging from about 0.2m (1σ) down to a few centimeters or less. A post-

processing alternative to DGPS and RTKGPS which does no rely on a reference station infrastructure is GPS PPP. By fusing raw carrier-phase data from a single GPS SPS receiver (typically dual-frequency) with precise ephemerides and satellite clock corrections (freely available from the Internet), PPP yields an accuracy close to RTKGPS. [11] [SEP]

All the above mentioned GPS techniques and accuracy numbers are feasible for a surface ship, and hence for being used in the fusion with USBL acoustic position measurements. For the GPS mounted on an AUV the situation is more [11] [SEP] challenging due to the requirement of a pressure tolerant antenna. While a pressure tolerant molding satisfies part of this requirement it also leads to challenges related to damping and frequency shifts (Hegrenæs, Sæbø, Hagen, & Jalving, 2010).

7.3.1.3 Acoustic Positioning

While acoustic time of flight navigation has been around for decades, it is still today the most reliable position aiding tool while (deeply) submerged. Several approaches are available, where LBL and USBL are the most common within AUV navigation. USBL will be discussed here.

As for USBL, a typical approach is to measure the range and bearing (azimuth and elevation) of a transponder on the underwater vehicle relative to a transducer mounted on a surface vessel. A global position measurement, which may be transmitted to the submersible using an acoustic link can be obtained by combining surface ship GPS and USBL measurements, as covered in Chapter 3 “Underwater Positioning”. The following sources affect the combined GPS-USBL position estimate:

- GPS accuracy
- USBL measurement accuracy [11] [SEP]
- System installation accuracy [11] [SEP]
- Surface ship attitude accuracy [11] [SEP]
- Sound velocity profile (SVP) accuracy [11] [11] [SEP]

A general expression for the north-east-down (NED) position of the AUV relative to the ship is given as [11] [SEP]

$$\mathbf{p}^n = \mathbf{R}_b^n(\phi, \theta, \psi) \mathbf{R}_t^b(\phi', \theta', \psi') \mathbf{p}^t(\Gamma, \alpha, \gamma) \quad (6.1)$$

where $\mathbf{p}^t \in \mathbb{R}^3$ is the position of the AUV measured relative to the USBL transducer, represented in the transducer reference frame $\{t\}$. The position vector \mathbf{p}^t may be represented using spherical coordinates where Γ is the measured slant range, and α and γ are measured azimuth and elevation, respectively. Furthermore $\mathbf{R}_t^b \in SO(3)$ is a coordinate transformation matrix from $\{t\}$ to the ship reference frame $\{b\}$ (or alternatively, the rotation matrix from $\{b\}$ to $\{t\}$). The last matrix $\mathbf{R}_b^n \in SO(3)$ is the coordinate transformation matrix from $\{b\}$ to the NED frame $\{n\}$. The transformation matrices may be represented in many ways, but it is common to apply the zyx-convention using Euler angles. The measured surface ship roll, pitch and heading are given by ϕ, θ, ψ , respectively, while ϕ', θ', ψ' describe the transducer alignment offset in roll, pitch and heading. Note that the latter angles are not geographical angles, but generic roll, pitch and heading Euler angles. Typically the transducer is mounted such that the latter angles are small. Note that the expression in Equation 1 could have included an additional additive term $\mathbf{R}_b^n(\phi, \theta, \psi) \mathbf{p}_o^b$ where \mathbf{p}_o^b is the offset (lever-arm) between $\{b\}$ and $\{t\}$. With the purpose of doing error analysis the term is however disregarded since linear offsets between $\{b\}$ and $\{t\}$ can be measured within millimeters (the same is also the case for

the ship GPS antenna). The uncertainty introduced through \mathbf{R}_b^n when doing lever-arm compensation is also negligible compared to the other error sources when $\|\mathbf{p}_o^b\| \ll \|\mathbf{p}^t\|$. For brevity it is assumed that $\{b\}$, $\{t\}$ and $\{n\}$ share the same origin.

A common approach in error analysis is to look at each isolated error source and to *propagate the uncertainties*. As for Equation 1 a natural start is to look at the uncertainty in the horizontal position due to uncertainty in \mathbf{p}^t , i.e. USBL measurement uncertainty. If for the moment it is assumed that \mathbf{R}_t^b and \mathbf{R}_b^n are exact and equal to the identity matrix (all the angles are zero) we get that

$$\mathbf{p}^n = \mathbf{p}^t(\Gamma, \alpha, \gamma) \quad (6.2)$$

which means that an error in \mathbf{p}^t directly translates to a (geographical) horizontal and vertical position error. With the assumption of small errors (first order approximation), the error in \mathbf{p}^n may be approximated by

$$\Delta \mathbf{p}^n = \frac{\partial \mathbf{p}^t}{\partial \Gamma} \Delta \Gamma + \frac{\partial \mathbf{p}^t}{\partial \alpha} \Delta \alpha + \frac{\partial \mathbf{p}^t}{\partial \gamma} \Delta \gamma \quad (6.3)$$

If $\mathbf{f} := \mathbf{p}^t, \mathbf{x} := [\Gamma, \alpha, \gamma]^T$ and $\Delta \mathbf{x} := [\Delta \Gamma, \Delta \alpha, \Delta \gamma]^T$, the same expression may be written in component form as

$$\Delta p_i^n = \sum_{j=1}^3 \frac{\partial f_i}{\partial x_j} \Delta x_j, \quad i = 1, \dots, 3 \quad (6.4)$$

If the measurement error entries in $\Delta \mathbf{x}$ are independent, the position uncertainty along each axis may be stated in terms of the individual uncertainties, that is,

$$\sigma(\Delta p_i^n) = \sqrt{\sum_{j=1}^3 \left(\frac{\partial f_i}{\partial x_j} \right)^2 \sigma(\Delta x_j)^2}, \quad i = 1, \dots, 3 \quad (6.5)$$

Disregarding the directional component (i.e. the covariance), the final horizontal position error may be approximated by the root-sum-square (RSS) of the horizontal components, that is

$$\sigma(\Delta p_i^n) = \sqrt{\sigma(\Delta p_1^n)^2 + \sigma(\Delta p_2^n)^2} \quad (6.6)$$

A prerequisite for accurate USBL positioning is that alignment of the USBL transducer is well known. It is also eminent that the ship attitude accuracy is good. Any inaccuracies lead to a pointing error and hence a position error, as is evident from Equation 1. If \mathbf{p}^t and \mathbf{R}_t^b are exact, and \mathbf{R}_t^b equals the identity matrix, it follows that the horizontal position uncertainty due to uncertainty in the measured ship attitude can be calculated by applying Equation 4-6, with $\mathbf{x} := [\Gamma, \alpha, \gamma]^T$, $\Delta\mathbf{x} := [\Delta\Gamma, \Delta\alpha, \Delta\gamma]^T$, and with $\mathbf{f} := \mathbf{R}_b^n(\phi, \theta, \psi)\mathbf{p}^t$. The uncertainty in the alignment angles is typically slightly higher than for the attitude sensor.

For a non-constant SVP the true acoustic sound path is in general not a straight line from the ship to the AUV. While the SVP only has a minor influence on the acoustic positioning near the transducer vertical (nadir), the sound profile must be measured and compensated for when the AUV operates far from the vertical (i.e. large elevation angles). The effect of errors in the SVP, and consequently the uncertainty associated with the ray-tracing, may be analyzed in different ways. Another approach is to do Monte Carlo (MC) simulations. In the simulations performed herein, additive noise is added to a presumed known SVP. When investigating the effect on the USBL positioning the ray-tracing is carried out repeatedly for a fixed arrival angle and propagation time. The fixed (deterministic) values are chosen such that ray-tracing with the known nominal SVP yields a desired vertical and horizontal end-point position.

It should be pointed out that commercially available sound velocity sensors have an accuracy in the sub-centimeter per second range. The uncertainty in the ray-tracing resulting from SVP errors is consequently only due to variations with time and space, where the latter typically is the most challenging. A rule of thumb is therefore to keep the horizontal offset between the AUV and the surface ship as low as possible throughout in order to minimize the sensitivity to SVP errors (Hegrenæs, Sæbø, Hagen, & Jalving, 2010).

7.3.1.4 Aided Inertial Navigation System (AINS) Performance

Most AUV navigation systems are today based on an inertial navigation system (INS), which takes measured angular rates and specific forces from an inertial measurement unit (IMU) as inputs. The INS then calculates the position, orientation and velocity of the vehicle relative to the inertial space. Due to inherent errors in the IMU however, a pure INS solution will drift of rapidly with time. The aiding may be done using a wide range of sensors, including a depth sensor, acoustic positioning, GPS while at the surface, and some form of velocity aiding. Once a suitable aiding framework has been established, a Kalman filter (KF) is typically applied for carrying out the fusion of the disparate sensor data and the INS data.

The KF is only capable of estimating zero-mean time-varying errors with faster dynamics than the AINS error drift. The system is consequently well suited for removing errors attributed to e.g. white noise. Colored survey vessel attitude errors (assuming slower error dynamics than the AUV AINS error drift), SVP errors and survey vessel system installation errors are in general not observable while the AUV travels along a straight line. Some of these errors can become observable by maneuvering (Hegrenæs, Sæbø, Hagen, & Jalving, 2010).

7.3.2 Sounding Related Uncertainties

The uncertainties which are related to the bathymetric sensor and that contribute to the horizontal position uncertainty of the sounding footprint relative to the AUV is here presented.

7.3.2.1 Measurement Uncertainty

As when discussing USBL, a natural starting point is to look at the fundamental measurement accuracy of the sensor. In light of Equation 1 this relates to the uncertainty in the relative pointing vector, \mathbf{p}^t , from the sounding equipment to the sounding footprint. When discussing sounding related uncertainties, $\{b\}$ in the same expression now denotes the reference frame of the AUV navigation system. If for the moment it is assumed that \mathbf{R}_t^b and \mathbf{R}_b^n are exact, and \mathbf{R}_b^n equals the identity matrix we get

$$\mathbf{p}^n = \mathbf{R}_t^b(\phi', \theta', \psi') \mathbf{p}^t(\Gamma, \alpha, \Phi) \quad (6.7)$$

where a depression angle Φ has been used instead of elevation. As can be seen from the expression an across-track sounding error in $\{b\}$ corresponds to an error in the (geographical) east direction, and similarly, along-track is in the north direction. Note that since a bathymetric sensor typically is a side-looking sensor, the nominal azimuth angle α in \mathbf{p}^t is presumed zero.

The resulting horizontal position uncertainty due to uncertainty in slant-range and depression angle can be found by evaluating Equation 4-6 with $\mathbf{x} := [\Gamma, \Phi]^T$, $\Delta\mathbf{x} := [\Delta\Gamma, \Delta\Phi]^T$ and with $\mathbf{f} := \mathbf{R}_t^b \mathbf{p}^t(\Gamma, \alpha, \Phi)$. The uncertainty in the depression angle is complicated to determine since it depends on several factors, including SNR. The depression angle can be calculated from

$$\Phi = \sin^{-1}\left(\frac{c\tau}{l}\right) \quad (6.8)$$

where c is the sound velocity at the sonar head, τ the difference in travel time, and l the baseline between the receiver banks. The uncertainty related to c can be found by evaluating Equation 4-6?? with $\mathbf{x} := [\tau, c, l]^T$, $\Delta\mathbf{x} := [\Delta\tau, \Delta c, \Delta l]^T$ and with $\mathbf{f} := \sin^{-1}(c\tau/l)$. It is possible to obtain a measurement for c in two ways; computation from CTD data or direct measurement. For a good quality CTD the first case yields an uncertainty for c on the order of 0.3m/s (1σ), while commercially available sound velocity sensors have an accuracy in the sub-centimeter per second range (1σ). As for the baseline l it can be determined to within 0.2 mm (1σ). The estimated time-delay τ is obtained from the sonar images using the SNR (Hegrenæs, Sæbø, Hagen, & Jalving, 2010).

7.3.2.2 Sensor Alignment Error

Similar to carrying out USBL positioning, a prerequisite for determining an accurate horizontal position of the sounding footprint is that the alignment of the sounding equipment is known with sufficient accuracy.

The uncertainty associated with the alignment between the AUV INS and the sounding equipment may be analyzed analogously to the alignment of the USBL transducer relative to ship reference

frame. If $\{b\}$ in Equation 1 now denotes the AUV INS coordinate system, \mathbf{p}^t and \mathbf{R}_b^n are exact, and \mathbf{R}_b^n equals the identity matrix, the expressions in Equation 4-6?? can be evaluated with $\mathbf{x} := [\phi', \theta', \psi']^T$, $\Delta\mathbf{x} := [\Delta\phi', \Delta\theta', \Delta\psi']^T$ and with $\mathbf{f} := \mathbf{R}_t^b(\phi', \theta', \psi')\mathbf{p}^t$. Note that ϕ', θ', ψ' are not geographical angles, but generic roll, pitch and heading Euler angles (Hegrenæs, Sæbø, Hagen, & Jalving, 2010).

7.3.2.3 AUV Attitude Error

Similar to the alignment it is eminent that the AUV attitude accuracy is good. Any inaccuracy leads to a pointing error and hence a position error. If $\{b\}$ in Equation 1 now denotes the AUV INS coordinate system, \mathbf{p}^t and \mathbf{R}_t^b are exact, and \mathbf{R}_t^b equals the identity matrix, it follows that the horizontal position uncertainty due to uncertainty in the measured AUV attitude can be calculated by applying Equation 4-6, with $\mathbf{x} := [\phi, \theta, \psi]^T$, $\Delta\mathbf{x} := [\Delta\phi, \Delta\theta, \Delta\psi]^T$ and with $\mathbf{f} := \mathbf{R}_b^n(\phi, \theta, \psi)\mathbf{p}^t$. The AUV attitude it is estimated by the AINS, either in-situ or in post-processing.

7.3.2.4 Sound Velocity Profile

The sounding footprint position uncertainty due to errors in the SVP may be analyzed similar to the USBL positioning by performing MC simulations. There are however two important differences. While the entire SVP above the AUV is of significance in the USBL case, only the SVP below the AUV is of importance for the horizontal sounding position. The second difference is the magnitude of the arrival angles. Typical beam elevation angles relative to nadir are between 45° to 85° , hence SVP errors are of greater importance than in typical USBL operations. As mentioned, the SVP error usually becomes smaller with depth, and consequently also the SVP error of importance to the sounding equipment (Hegrenæs, Sæbø, Hagen, & Jalving, 2010).

7.3.3 Other Error Sources

While the list of error sources discussed above is fairly extensive, it is by no means complete. The need for accurate timing has not been discussed, but it is clearly a prerequisite – both for synchronization of payload and AUV navigation data, but also for synchronization of the AUV against the topside clock connected to the USBL positioning (Hegrenæs, Sæbø, Hagen, & Jalving, 2010).

7.4 DTM Horizontal Error Budget

Based on the analyses and discussion on the different errors sources, it is possible to derive an error budget for the total horizontal mapping accuracy using AUVs. Under the assumption of statistically independent errors, the total DTM position uncertainty can be calculated by taking the RSS of the different error contributions (Hegrenæs, Sæbø, Hagen, & Jalving, 2010).

8 The Underwater Imaging Process

In the underwater imaging process artificial lighting is projected on the target at the seabed and the reflections are recorded by the camera. Photons are transmitted and attenuated through the water column before the reflected photons are registered by the camera, see illustration in Figure 1. The image is made from the registration of photons reflected from the seabed back to an image sensor. When photons travel through seawater the water itself attenuates some portion of the light. The spectral attenuation, illustrated by arrow *B* and *D* in Figure 1, of visible light (400 to 700 nm) is dependent of the coloured dissolved matter, suspended matter and plankton in the water. In addition to the components in the seawater, the water itself heavily attenuates the red part of the light spectrum (600 – 700 nm). There are usually high concentrations of dissolved and particulate matter in seawater and when a given photon hits a particle the direction of the photon is changed either back towards the camera or out of the camera field of view, illustrated by arrow *A*, *C* and *F* in Figure 1. This light-scattering reduces the amount of light that is forming the imagery. The backward scattered light reduces the quality of the image (blurring), by lowering the contrast in the image. When the photons reach the seabed they are scattered and absorbed by the seabed constituents. A fraction of the photons from the seabed are reflected back to the camera they are again subject to scattering and absorption by seawater and it constituents. Some reflected photons are scattered at small angle (small-angle forward scattering). These photons reach the camera and become recorded in the image, but since their trajectory from the seabed to the camera is not straight, they blur the image and reduce the resolution of the image (Ludvigsen, 2010).

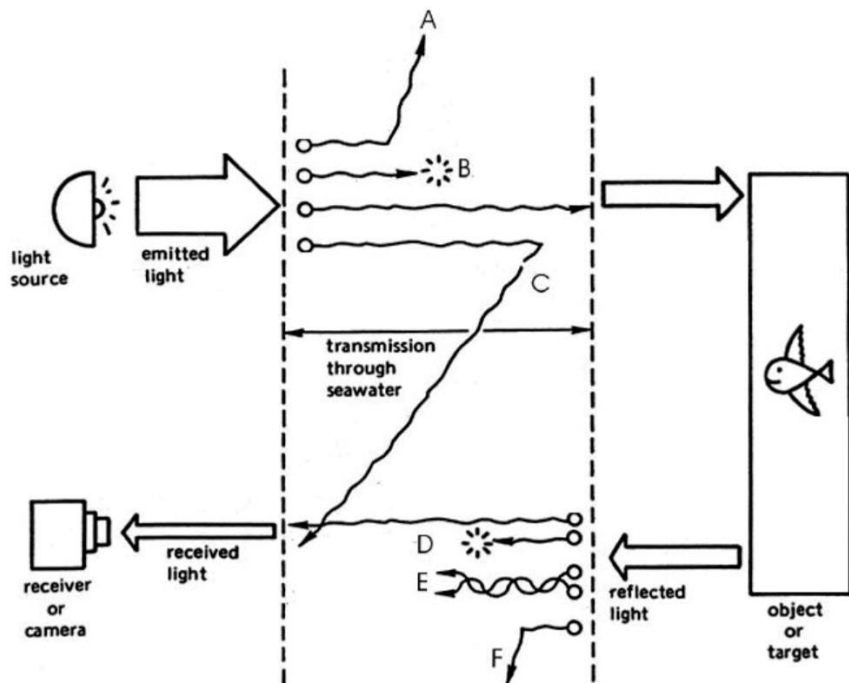


Figure 16: The underwater imaging process illustrating the losses of light to an image in an underwater imaging system (Ludvigsen, 2010).

Figure 1 illustrates the mechanisms causing loss of light intensity underwater:

- projected light outward scattered
- projected light attenuated
- projected light backscattered
- reflected light attenuated
- reflected light small angle forward scattered
- reflected light outward scattered

These six problems are special cases of the three more general problems; attenuation, backscatter and small-angle forward scattering.

The first of these problems is the attenuation of image forming radiation due to absorption and scattering. Water selectively attenuates light as a function of wavelength or color (Funk, Bryant, & Heckman, 1972). In pure water, blues and greens are transmitted quite well. However, even in pure water reds are attenuated quite strongly, as seen from Figure 2. This has several implications. First, the perceived color of an object will depend strongly on the range of the camera from the target. Secondly, reds are very difficult to detect at significant range (US Navy Office of Naval Research (ONR), 2014).

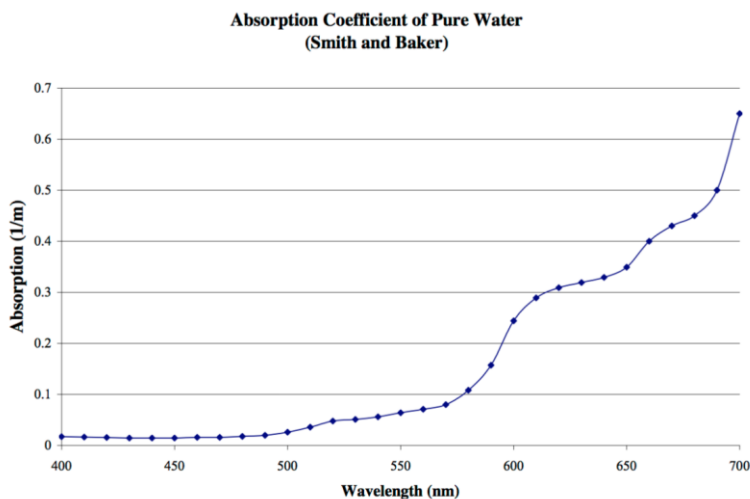


Figure 17: Absorption coefficient of pure water (US Navy Office of Naval Research (ONR), 2014).

This peak transmission normally shifts to longer wavelengths as the amount of dissolved organic material in the water is increased. However, even at peak transmission the ability to transmit light over long distances is severely limited. In clear ocean water, the maximum viewing ranges for advanced imaging systems are a few hundred feet. In turbid water, imaging is often limited to a few feet. Increasing these distances is difficult because the light is exponentially attenuated as a function of range (Funk, Bryant, & Heckman, 1972).

The second imaging problem is backscatter. Backscatter is that portion of source illumination reflected into the receiver's field-of-view by particles and inhomogeneities in the water (exclusive of light reflected by the target). When source light is scattered into the receiver's field-of-view by particles in water, image contrast is degraded. As more light is backscattered, a visibility condition arises which is similar to that encountered when automobile headlights are used in fog. Finally, the image contrast becomes so low that the image is no longer detectable or recognizable. A variety of techniques and systems have been devised to combat this phenomenon (Funk, Bryant, & Heckman, 1972).

The remaining problem, small-angle forward scattering, can introduce serious resolution losses. Scattering is the process by which the direction of individual photons is changed without any other alteration. Because most scattering of light in seawater is the result of the different sizes of particles, scattering is nearly independent of wavelength. The significance of these losses depends on the nature of the water, the imaging system and its geometry, and resolution requirements (Funk, Bryant, & Heckman, 1972).

8.1 Image Modeling

As shown in Figure 1 and discussed above, several pathways exist by which the light can travel to the image plane of the camera. These pathways may or may not include light which has been reflected by an object. Therefore the light which has entered the camera may or may not include light which

has been reflected by an object. Hence, considering the light reflected by the object, one can distinguish two components that are incident upon the camera plane: 1) Light which has not been scattered in the intervening water, called the direct component; and 2) light which has been small angle scattered, the forward scattered component. The irradiance being incident up on the pixel sensor is considered to be a linear superposition of three components: a) backscatter; b) forward scattering; and c) a direct component. Mathematically this can be written (Jaffe, 1990):

$$E_T(\text{total}) = E_d(\text{direct}) + E_{fs}(\text{forward scatter}) + E_{bs}(\text{backscatter}) \quad (7.1)$$

8.1.1 Direct and Forward-Scattered Component

In order to calculate the light reflected from the map, the irradiance pattern incident upon the reflectance map must first be calculated. The origin of this irradiance is the light source, considered here to be a point-source characterized by a beam pattern $BP(\theta_s, \varphi_s)$, a function of polar angles θ_s and φ_s . The units of $BP(\theta_s, \varphi_s)$ are in W/m^2 , where $BP(\theta_s, \varphi_s)$ is the irradiance on a hemispherical shell at a distance of 1 m from the light source. In order to calculate the irradiance incident upon the map, this beam pattern is attenuated and spherically spread. The irradiance incident upon the reflectance map can then be calculated as (Jaffe, 1990)

$$E'_I(x', y', \theta_s, \varphi_s) = BP(\theta_s, \varphi_s) \cos \gamma \frac{e^{-cR_s}}{R_s^2} \quad (7.2)$$

Here x', y' refer to the fixed coordinate system with respect to the planar reflectance map located at $z' = 0$; $R_s(x'_s, y'_s, z'_s, x', y', 0)$ is the distance 1 m from the source to a point on the reflectance map; γ is the angle between a perpendicular to the reflectance map at a given x', y' location and a line between the x', y' location and the source; and the constant c is the total attenuation coefficient. The geometry is illustrated in Figure 3. Note that the primed coordinate system is associated with the reflectance map, and the unprimed coordinate system is associated with the camera plane. A more accurate representation of the incident irradiance E_I takes into account the spreading of illumination due to the small-angle forward-scattered component as well as adding back in a contribution due to small-angle forward scattering. An approximate value can be found by a convolution with a point-spread function g . In this case (Jaffe, 1990),

$$E_I(x', y', 0) = E'_I(x', y', 0) * g(x', y' | R_s, G, c, B) + E'_I(x', y', 0) \quad (7.3)$$

Where

$$\begin{aligned} g(x', y' | R_s, G, c, B) &= \{ \exp(-GR_s) \\ &\quad - \exp(-cR_s) \} F^{-1} \exp(-BR_s f) \end{aligned} \quad (7.4)$$

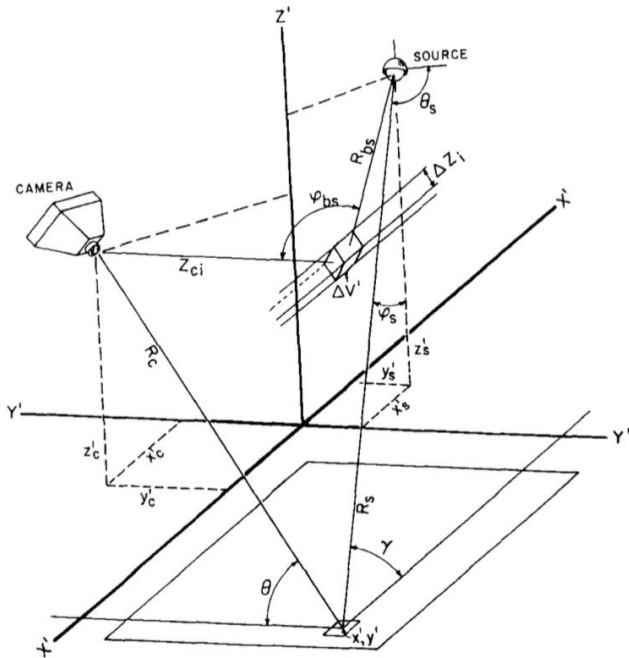


Figure 110 The coordinate system used for the image modeling (Jaffe, 1990).

And G is an empirical constant ($|G| \leq c$). The operator F^I indicates that an inverse Fourier transform is taken of a function of B , which is an empirical damping factor, and f , which is a radial frequency in cycles/rd. Note that the “*” operator denotes convolution (Jaffe, 1990).

In order to predict the irradiance incident upon the image plane of the camera, it is necessary to consider the geometric optics of the camera, the attenuation of the medium between the reflectance map and the camera, and the spherical spreading of the reflected wave. Taking these factors into consideration, the irradiance incident upon the image plane of the camera can be represented as (Jaffe, 1990)

$$E_d(x, y) = E_l(x', y', 0) \exp(-cR_c) \frac{M(x', y')}{4f_n} \cdot \cos^4 \theta T_l \left[\frac{R_c - F_l}{R_c} \right]^2 \quad (7.5)$$

where R_c is the distance from an x', y' position on the reflectance map to the camera, f_n is the f number of the camera of focal length F_l , and T_l is the transmittance of the lens. Typical values for objects of oceanographic interest are $0.02 \leq M(x', y') \leq 0.1$. The forward-scattered component can then be calculated from the direct component via the convolution relationship (Jaffe, 1990),

$$E_{fs}(x, y) = E_d(x, y, 0) * g(x, y | R_c, G, c, B) \quad (7.6)$$

Where g is represented by Equation 4.

8.1.2 The Backscatter Component

The backscatter component is by slicing the three-dimensional space into planes of thickness Δz_i that are parallel to the image plane of the camera. The irradiance incident upon each of these planes is then calculated, as above, by computing the direct component and then adding an additional amount of irradiance due to the light that is small angle scattered (Jaffe, 1990).

The next step in computing the backscatter component is to determine the resulting image due to each of these illuminated slabs. The irradiance incident upon the aperture of the camera is a superposition of these illuminated volume elements weighted by the value of the volume-scattering function. By representing the irradiance in three-dimensional space propagating away from the light source as $E_s(x', y', z')$ and following the above arguments, the irradiance incident on the volume elements can be viewed as a superposition of a direct and forward-scattered component (Jaffe, 1990):

$$E_s(x', y', z') = E_{s,d}(x', y', z') + E_{s,fs}(x', y', z') \quad (7.7)$$

$$E_{s,d}(x', y', z') = BP(\theta, \varphi) \frac{\exp(-cR_{bs})}{R_{bs}^2} \quad (7.8)$$

$$E_{s,fs}(x', y', z') = E_{s,d}(x', y', z') * g(x', y', z' | R_{bs}, G, c, B) \quad (7.9)$$

Now taking a weighted superposition of the intensities from a given slice, one can compute the radiant intensity which is scattered toward the camera element x, y due to volume $\Delta V'$ (Jaffe, 1990):

$$H_{bs}(\varphi, x, y) = \beta(\varphi_{bs}) E_s(x', y', z') \Delta V' \quad (7.10)$$

where $\beta(\varphi)$ represents the volume-scattering function; $\Delta V'$ is an incremental volume in three-dimensional space; and the angle φ_{bs} is the angle between a line from the volume under consideration to the light source and a line from the volume to the camera. Next, the image of this volume of water must be calculated. In this case, following arguments similar to those above, the direct component of this backscattered irradiance $E_{bs,d}(x, y)$ can be represented as (Jaffe, 1990)

$$E_{bs,d}(x, y) = \sum_{i=1}^N \exp(-cZ_{ci}) \beta(\varphi_{bs}) E_s(x', y', z') \cdot \frac{\pi \Delta Z_i}{4f_n^2} \cos^3 \theta T_l \left[\frac{Z_{ci} - f_l}{Z_{ci}} \right]^2 \quad (7.11)$$

Here ΔZ_i is the thickness of the backscattering volume $\Delta V'$; and ΔZ_{ic} is the distance from a point in the camera to the center of the backscatter slab. The value N extends from $i = 1$ for the first backscatter plane, to N for the plane adjacent to the target. As was noted previously, the total irradiance due to the backscattered image $E_{bs}(x, y)$ can then be calculated by adding an additional forward-scattered component (Jaffe, 1990):

$$E_{bs}(x, y) = E_{bs,a}(x, y) + E_{bs,d}(x, y) * g(x, y|R_c, G, c, B) \quad (7.12)$$

8.2 Sensor Suite

The most important components of the sensor suite for ROV-based video surveys are cameras and light sources. The system should provide clear images of both details and overview of the scene. The products generated from the sensors should match the scope of the survey and the best result is achieved when the illumination is optimized for sea conditions and the image sensor utilized. For biological surveys it is often necessary to have some possibility to measure scale in the image (Ludvigsen, 2010).

8.2.1 Cameras

The choice of camera will be a compromise since the perfect all-round camera does not exist. The camera characteristics determining the quality of the video imagery are: focus, contrast, light sensitivity, field of view and resolution. Most high resolution cameras with high colour rendition have low light sensitivity. Thus it is beneficial to have cameras suitable for different applications mounted on the ROV. The most basic needs are covered by two cameras, one low-light wide-angle camera for search, navigation and overview imagery and one low noise, high quality zoom camera to identify details (Ludvigsen, 2010).

The focus capability of a camera is controlled by the quality of optical objectives, image processing hardware and software. The depth of field is determined by the camera aperture opening. Larger aperture means that the camera is catching more light, but the depth of field is reduced, narrowing the focus area. ROV cameras come with manual focus, auto-focus or fixed focus modes. Manual focus is used on advanced cameras and requires an operator to control the camera during filming, and have the best potential for sharp images. Using auto-focus the operator is unnecessary, but there is a risk that the camera is unable to find focus or focuses on the wrong targets. For plain wide-angle over view and navigation cameras fixed focus is sufficient (Ludvigsen, 2010).

The camera image contrast is controlled by the MTF (Modular Transfer Function). MTF expresses the contrast measured in two nearby pixels. A camera with low MTF will have low contrast and often blurred images. The contrast level is not only dependent of the camera, but also the previously discussed backscatter resulting from optical properties of seawater and its optically active components (Ludvigsen, 2010).

In ROV applications, high light sensitivity is beneficial since it will give better viewing range. The light sensitivity of a camera is generally determined by the size of the image sensor and the image signal amplification. The image sensor is either a CCD-chip or in more recent systems a CMOS (Complimentary Metal-Oxide Semiconductor) sensor. A large image sensor usually results in better light sensitivity. High signal amplification results in better light sensitivity. In low light situations, the signal from the image sensor experience low signal, resulting in low signal to noise ration and noisy images. The demand for light sensitivity depends on the application of the video. For ROV navigation a camera with high light sensitivity is inherent reduced image quality can often be accepted. However for e.g. taxonomy applications the image quality cannot be compromised and one usually has to settle for a lower light sensitivity (e.g. 5 lux) (Ludvigsen, 2010).

The field of view for an ROV camera can be divided into three levels; wide, medium and narrow. The field of view does not relate to the distance from camera to target, but the viewing angle controlled by the camera zoom. The wide angle is used to get an overview of the scene, while narrow field-of-view and closed up images are produced by zoom cameras and are used to observe details (Ludvigsen, 2010).

8.2.2 Light

For artificial light sources in an ROV scene there are three important variables: light intensity, spectral distribution, and light patterns produced by the reflector and lenses. Three main groups of light sources available: incandescent (e.g. halogen), HID (High Intensity Discharge), and LED (Light Emitting Diode) lamps. The most common light source is the incandescent light bulb in which electric current is lead through a tungsten filament. The filament heats up and emits light when the electric current is applied. In halogen lights the light bulb is filled with an inert gas and a small amount of halogen. Incandescent light sources are usually robust and reliable. A 250 W halogen lamp is specified to put 4500 lumens in the water. In HID light an arc between tungsten electrodes is ignited inside a gas filled bulb. When the arc is lit it produces heat which vaporizes a mixture of salts forming plasma inside the bulb. The vaporized salts contribute significantly to the efficiency in the process. HID lights require a control system to ignite and maintain the arc during operation; this system is often called the ballast. A typical HID light source of 150 W is capable of

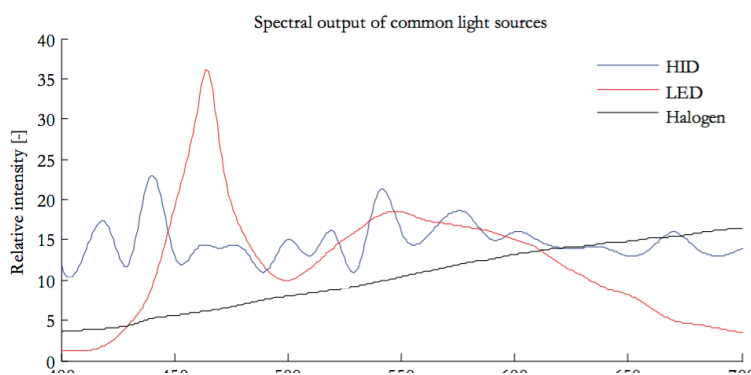


Figure 18: Comparison of light spectra for LED, HID and halogen light (Ludvigsen, 2010).

producing 12000 Lumens of light. Lately LED lights have entered underwater lighting. LED can only be produced in small units. To come around this limitation, LED lights for ROV have arrays of multiple diodes. LED has high efficiency, and a commercially available unit emits 2400 Lumens from only 44 W of electrical power (Ludvigsen, 2010).

The spectral distribution of a light source is important due to the spectrally dependency of the light absorption properties of seawater, Figure 5. HID light sources are usually beneficial in underwater applications since they output more light in a spectral band where seawater normally have low absorption, Figure 4. Incandescent light sources like halogen emit more power in the red part of the spectrum where the seawater light attenuation is higher. Incandescent light sources have an unfortunate spectral distribution in seawater and are less efficient than HID and LED (Ludvigsen, 2010).

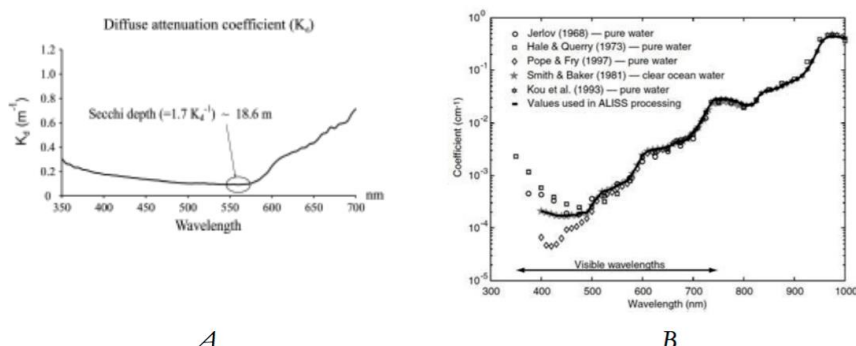


Figure 19: A) Diffuse spectral attenuation coefficient for Spitsbergen coastal seawater ($400\text{-}700 \text{ nm m}^{-1}$) Ny-Ålesund, Svalbard in May 2004. B) Spectral attenuation coefficient of pure water (Ludvigsen, 2010).

The light patterns in video imagery are directly dependent of the seabed altitude, positions of light sources and cameras, the seawater turbidity and light reflector and glasses. High seabed altitude enlarges the visible area but increases the potential for light attenuation and scattering and then reduces image quality. The contrast of the imagery will be reduced by high levels of backscattered light. In general the light reflectors should be wide enough to illuminate the field of view for the camera. But wide light cones increases the common volume of the light sources and the camera and thus the backscattered light. An effective way to reduce the common volume of the light sources and the camera is to increase the separation between light and camera, see Figure 6. This separation can however be overdone. If the visibility is good the video images are less sensitive to camera and light geometry and common volumes of camera field of view and light cones. In high turbidity conditions minimization of the common volume is more essential, but one can use the backscatter effect to an advantage. Directing two narrow light beams just out the field of view light will be scattered out of the light cones and this scattered light will illuminate the scene (Ludvigsen, 2010).

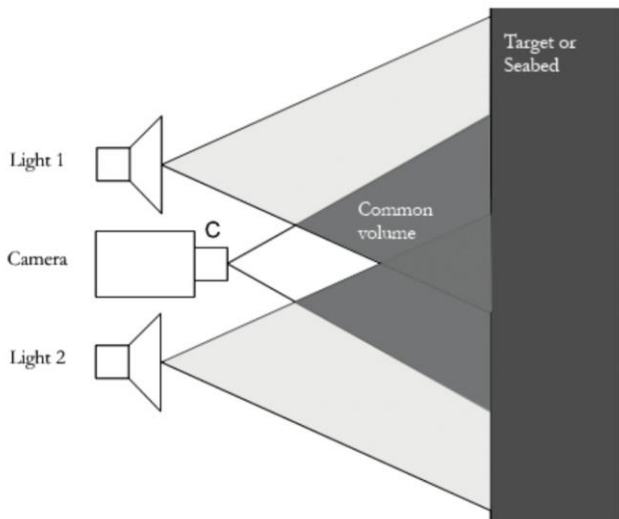


Figure 20: Illustration of common volumes for camera and lights sources (Ludvigsen, 2010).

8.2.3 Scaling Devices

To estimate the dimension of the objects seen on the video it is necessary to have some sort of size/distance measuring tool on the ROV since the video does not provide any depth vision. The simple variant is a meter scale placed in the picture close to the seabed or object of interest. A more convenient way to solve this issue is put two or more parallel lasers on the ROV making two dots with a known distance on the images. For orthogonally mounted cameras, the area covered can be calculated from field of view and measurements of the seabed altitude (Ludvigsen, 2010).

8.2.4 Recorders

The video signal is usually fed to a computer capture card, where it is digitized and stored on a hard disk. There is wide variety of formats available for digital video; the most common being avi and mpeg. It is important that the video is stored on a format which can be played with generic video software and that the codecs (Coder/DECoder) applied are free and openly available. The resolution of the video should not be lower than that of the source signal, i.e. SD (Standard Definition) video should be recorded on 720 by 576 pixels. The data compression should be sufficient for efficient storage, but should not reduce quality and produce image artefacts. When choosing image resolution and compression parameters one should bear in mind that video clips can always be downgraded later for storage, but the opposite is impossible. A normal bit-stream for video with sufficient quality is 1 – 3 Mbps, which results in 450 - 1350 MB per hour. The recording system should also contain a system to associate metadata like time, position, ROV heading, and ROV depth with the video. The data can be edited and the overlay view can be switched on and off depending on the usage of the video (Ludvigsen, 2010).

8.3 Processing

8.3.1 Processing and Interpretation

The design of the data processing pipeline depends on the instrument suite and the data acquisition plan and can only be completed subsequently to these. Cameras, lights sources, geo-referencing and video recorders form the instrument suite for video surveys. The processing pipeline contains online processing procedures, offline processing procedures, guidelines for data products, guidelines for data interpretation, strategy on data management, and a plan for reporting and quality control. The processing pipeline is presented in Figure 7 (Ludvigsen, 2010).

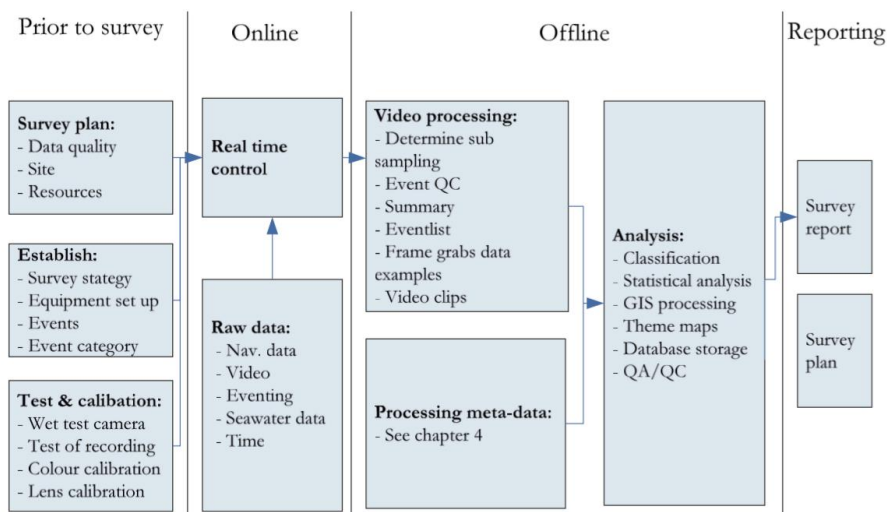


Figure 21: Video survey processing workflow from planning of an operation to the reporting of the findings (Ludvigsen, 2010).

8.3.2 Online

Online processing of the video is normally done by event marking of every interesting observation with time, position, observation category and comments. Continuous control of data recorders and image quality is an obvious part on the online operations (Ludvigsen, 2010).

8.3.3 Offline

The time required to analyze the information from a video survey depends inherently of the goals for the survey, but a useful rule of thumb is that two or three times the duration of the raw video recording is necessary to process the video. For some projects the amount of video becomes too large and processing too time consuming. Then the video has to be sub sampled by choosing video sections either randomly or of particularly interesting areas or objects of interest. Some attempts of automated processing have emerged, but taxonomy is

complicated and automated video processing and biological classification will only be applicable to special surveys also for the foreseeable future. One variant of automated processing is the creation of video mosaics. Video mosaics have many of the same advantages as photo-mosaics discussed later in this chapter (Ludvigsen, 2010).

8.3.4 Data Interpretation

Events will be created according to an event scheme. One can use an existing set of events and event categories and register observations accordingly (top-bottom approach), or one can create the event list and event categories from the observations (bottom-top). The former is best suited when surveys should be compared, but requires specific characteristic species and key physical parameters. When an area is classified to a known classification scheme like the EUNIS-system (European Nature Information System) a top-down approach analysing the events are necessary. When maximum information yield from a video survey is required the latter approach is best suited. With the bottom-top approach it is not necessary to ignore observations falling outside the event categories. To obtain quantitative information from a survey analysed by the bottom-up approach a large sample and statistical analysis is necessary (Ludvigsen, 2010).

8.3.5 Data Products

Geo-referenced digital video is also easy to include in a GIS (Geographic Information System) database. For GIS analysis both video and events can be used to produce theme maps including data from previous surveys from the same area. A database of geo-reference video increases the usability of the video since the data can be effectively compared to other data of the area (Ludvigsen, 2010).

8.4 Photo Mosaic

Serious attenuation and backscatter issues in seawater limit the field of view to a few square meters. To depict larger areas series of overlapping images can be compiled to a composite image with extended coverage. Photo mosaic is a tool for detailed documentation of a confined area, but the seabed coverage is modest. The desired information from photo mosaics is shape, colour, structure and texture of the seabed and the targets present. In the imaging process the 3D seabed is projected onto a 2D representation. The projection induces inaccuracies to the resulting photo mosaic (Ludvigsen, 2010).

The creation of seabed photo mosaics starts by collecting images in a structured way to depict the entire area of interest. These images are digitally corrected for light features and camera distortions before they are processed to one seamless image covering the whole area of interest. The process presented is based on still images and feature extraction (Ludvigsen, 2010).

8.4.1 Image Capture

The image capture for photo mosaics shares the main concepts with the imaging described for “The underwater imaging process”. The light reflected from the seabed is passing through an optic objective to a digital image sensor. The sensor is usually a CCD or CMOS chip and has millions of sensors in a matrix. When an image is shot the sensor is active for a preset period of time, typically 1/200 – 1/20 seconds. Each sensor outputs a signal for the light intensity sensed for one image pixel. This is put together to an image by a micro controller and later sent to storage. The image resolution is dependent of the number of elements in the image sensor, the MTF of the image sensor, and the precision of the lenses. The MTF-values of the image sensor should be high to produce sharp imagery. To generate sufficiently lit images from the deep water, the signal to noise ratio of the image sensor should be high. For colour imagery the colour definition is important in underwater applications since high colour definition allows for enhanced opportunities for image adjustments. For scenes with varying brightness, high colour definition enhances the ability to catch details in dark areas without overexposing bright areas of the image (Ludvigsen, 2010).

Objectives consist of several lenses and are characterised by their aperture size, focal length and magnification or angular opening. The camera and objective’s ability to find focus is essential to create sharp images. A small optical aperture increases the chances of finding focus, but reduce the amount of light passed on to the image sensor. The optical aperture is quantified by an f-number. The mechanical precision of the lenses and the position of the lenses determine the distortions of the images taken using the optic objective (Ludvigsen, 2010).

8.4.2 Illumination

The light sources can be constant sources like LED, HID, and incandescent, or they can be strobe lights. Light pattern, intensity and colour temperature (spectral irradiance) are important parameters of an underwater light source. See the section “Sensor suite” on light sources for video survey for a discussion in light setup and continuous light sources. However, in most cases strobe lights produces more light for still image capturing than its continuous counterparts (Ludvigsen, 2010).

Uniformly lit images are attractive for photo mosaic production since light intensity variations will make the mosaic look patchy. However the light intensity will in practice vary across the image frame to some level. During post processing the illumination component and reflectance component of the light captured by the image sensor is separated in the frequency domain. Illumination has low frequency while the reflectance is of higher frequency. Illumination is normalized and merged back with the reflectance to create a uniformly lit image (Ludvigsen, 2010).

8.4.3 Photo Mosaic Construction

There are two basic steps in photo mosaic construction; topology estimation and image blending. The term topology is used to describe the images’ internal position, rotation and

scale. After topology estimation the images are moved, rotated, and scaled before they are connected. This process is called image registration. To remove the edges between the images and create a seamless image a method called image blending is applied. An example of a photo mosaic construction is presented in Figure 8 (Ludvigsen, 2010).

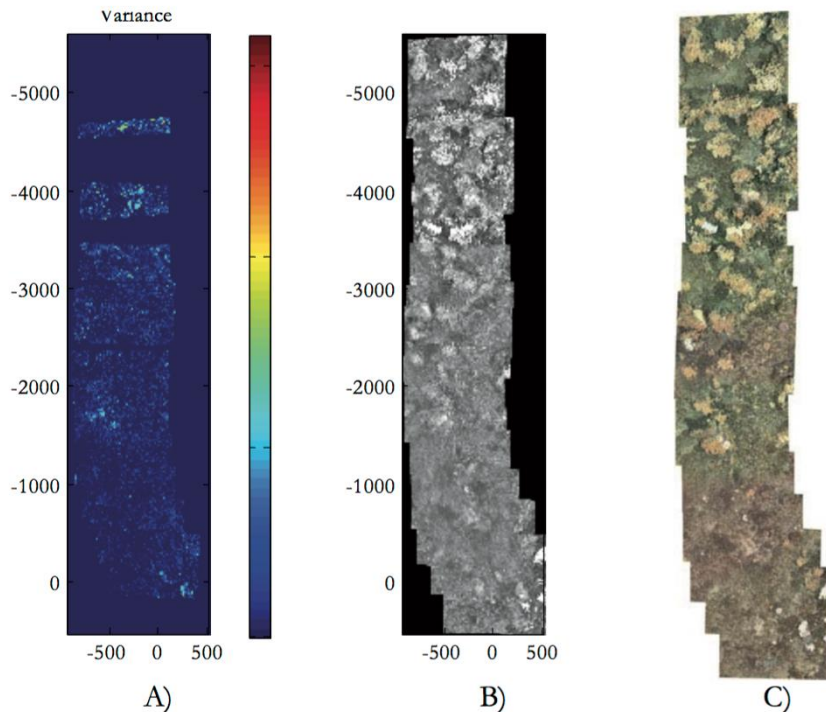


Figure 22: The axis in the figures are pixels. A) Variance of image intensity of overlapping pixels. B) Image registration prior to image blending. C) Resulting photo mosaic (Ludvigsen, 2010).

8.5 Photogrammetry

Photogrammetry is used to create detailed 3D models of small sceneries. From overlapping imagery the xyz position of common image points are calculated. The laws of physics governing photogrammetry allow higher resolution results than the acoustic processes determining the resolution for sonar data. For maritime archaeological sites and marine biological observation stations the position, dimensions, colour, texture and shapes of objects are important records (Ludvigsen, 2010).

Underwater photogrammetry is exposed to specific challenges not found in terrestrial photogrammetry due to the attenuation of light in seawater. Hence the distance from the camera to the seabed is limited and usually below 5 meters. The vertical extent of the object is often large relative to the distance to the object. The vehicle carrying the camera must also hold the light source and this causes the illumination of the given objects to shift from

image to image. Only small areas of the seabed can be covered in a single image and a photogrammetry model covering a site must be compiled from several two-view models. Photogrammetry relies on knowledge of the cameras position and orientation (pose) for each image. The navigation accuracy required for photogrammetric application is challenging to achieve with present underwater navigation systems. On the other hand, photogrammetry solutions can be used to reduce navigation uncertainties (Ludvigsen, 2010).

8.5.1 The Photogrammetry Process

The photogrammetry process is here presented based on survey conducted in the Trondheim Harbour in August 2014 using an ROV equipped with a stereo camera rig. The processing pipeline is presented in Figure 9.

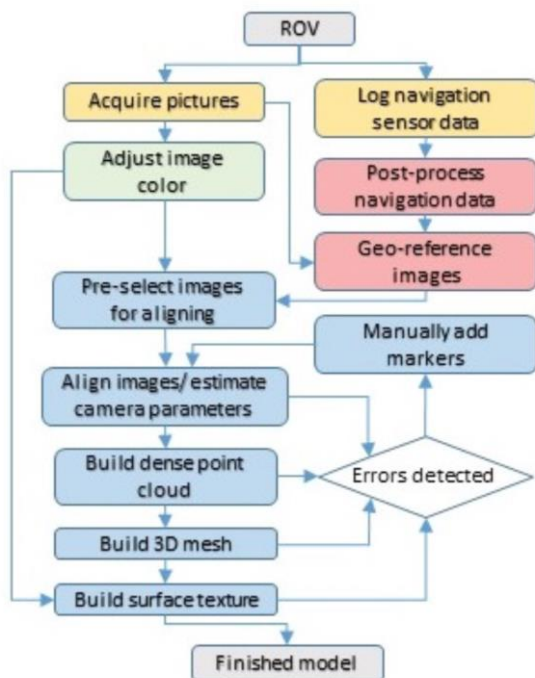


Figure 23: Photogrammetry processing pipeline (Nornes, Ludvigsen, Ødegård, & Sørensen, 2015).

In order to compensate for underexposed and overexposed images, the images are colour corrected. This is carried out by adjusting the colours of the image by stretching the red green and blue channels separately. This is performed by a command in a image manipulator program. The process is fast and can be run on the entire image set. With a dataset of several thousand images, efficient processing is obviously essential (Nornes, Ludvigsen, Ødegård, & Sørensen, 2015).

The 3D-model is then constructed from the regular 2D-images using a photogrammetry software. The aligning process produces a sparse point cloud Figure 10 A, and further processing yields a dense point cloud Figure 10 B and a 3D-mesh Figure 10 C. Finally, a mosaic of the original images are projected onto the 3D mesh, creating the final model seen in Figure 10 D (Nornes, Ludvigsen, Ødegård, & Sørensen, 2015).

Poor image quality and lack of discernable features can lead to images being improperly aligned, or not aligned at all. Large, obvious errors in camera orientation or position can be reset directly. More subtle errors can also give a large impact if they accumulate over sequential images, but may remain hidden until later in the processing. To counteract these, markers can be added manually to multiple images indicating a shared feature. The complete model is then realigned with the added information of the marker(s) (Nornes, Ludvigsen, Ødegård, & Sørensen, 2015).

Using the timestamps of the recorded images and the navigation data, the camera positions can be calculated using MATLAB. The navigation data provides geolocalization and scaling of the model. The navigation data also speeds up the aligning process, since the photogrammetry software can skip comparing images that are too far from each other to cover the same scene (Nornes, Ludvigsen, Ødegård, & Sørensen, 2015).

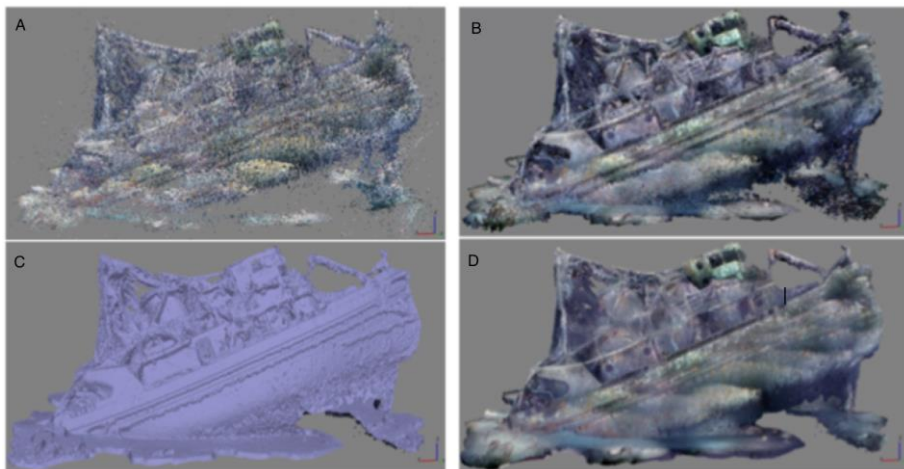


Figure 24: A) Sparse point cloud model. B) Dense point cloud model. C) Mesh model. D) Finished model (Nornes, Ludvigsen, Ødegård, & Sørensen, 2015).

8.6 Underwater Hyperspectral Imaging (UHI)

The seafloor is complex and dynamic, exhibiting large variability in biogeochemical composition over space and time. Obtaining high quality maps of features on the seafloor is limited by traditional methods such as in situ diver surveys, ship-based acoustics (echosounders), benthic box core or 'grab' samples, epibenthic sledge and beam trawl samples, underwater photography, and video towed from boat. These methods are often limited in spatial scale and generally qualitative, requiring considerable human interpretation. New techniques have been developed that rely on the spectral signature of various of the benthos. Different objects of interests (OOIs), from minerals to seagrass, absorb and reflect different portions of the visible spectrum giving them unique "optical

fingerprints". By measuring the color reflecting off the seafloor using hyperspectral imaging, these optical fingerprints can be used to develop qualitative and quantitative maps of benthic habitats, substrates, minerals, and organisms (Johnsen, et al., 2013).

Most of the seafloor is optically deep and cannot be imaged with passive techniques that rely on sunlight. For such situations, UHI can be deployed on underwater vehicles, such as ROV or AUV, and deployed in close proximity to the seafloor in order to systematically map the benthos over large areas. In contrast to passive remote sensors, underwater remote sensing requires active sensors using spectrally defined artificial light sources positioned close to the substrate for the benthic reflectance to be measured at high spatial and spectral resolution (Johnsen, et al., 2013).

By using UHI instead of the 3-color RGB-based pictures and video, one can move toward automated identification of OOI. To do so, the reflectance spectrum $R(\lambda)$ of an OOI is used to classify the habitat. If the UHI is deployed at ocean depths devoid of sunlight, the OOI must be illuminated by an artificial light source. The light from the source is directed along a narrow beam toward the OOI. Light reflected from the OOI is altered spectrally and detected by the UHI. However, the water and its optical constituents also affect the spectrum of the detected light. Light is absorbed and scattered along the direct and reflected beams in relationship to the optical properties of the water column. The reflectance spectrum from the OOI will be modified by particles and other substances in the water column and should be considered when spectrally classifying the OOI.

8.6.1 Benefits and resolutions of UHI

The benefit of placing hyperspectral imaging sensors on underwater platforms, in close proximity to the OOI, can be evaluated by considering four categories of resolution, namely:

1. Spatial (image pixel size)
2. Spectral (human eye vs broadband vs hyperspectral sensors)
3. Radiometric (bits per pixel and dynamic range)
4. Temporal (re-visit time).

8.6.2 Spatial Resolution

The spatial resolution available from an imager is related to the distance from the target and the signal-to-noise ratio of the sensor. A UHI mounted on underwater vehicles scanning OOI at a distance of 2 m above the seafloor will typically obtain a spatial resolution of approximately 2 mm. Different scales of mapping can be used to address different scientific and environmental questions and also be simultaneous and complementary to one another. The fine-scale features observable with UHI are ideal for mapping underwater habitats that comprise diverse mixtures of OOI varying on sub-meter scales. The technique is also useful for edge-detection and delineating changing ecotone boundaries over time (Johnsen, et al., 2013).

8.6.3 Spectral Resolution

The human eye utilizes so-called red, green, and blue (RGB) photoreceptor cells (cones with peak absorbance at 420, 534, and 564 nm), which is the basis of the human trichromatic

perception of colors. Artificial sensing systems, as well as colored image display systems such as television, computers, digital camera/video systems, and image scanners, have thus typically been based on the RGB color model. These RGB images are called ‘pseudo-true’ color because they use bands that are centered in the blue (450 nm), green (550 nm), and red (650 nm) portions of the visible spectrum and not the true spectral response of the human eye. While useful for human vision, however, spectral classification of standard RGB underwater imagery is often insufficient for distinguishing diverse bottom types.

Hyperspectral imagers, also called imaging spectrometers, typically detect light at approximately 1–5 nm spectral spacing and provide hundreds of wavebands across the visible spectrum, instead of only three afforded by the human eye. Each hyperspectral pixel thus contains information representing a continuous spectrum, even though the pictorial representation of the data is presented as a three band, RGB image. The great advantage for imaging and detection purposes is that each image pixel and its highly detailed spectrum has the potential to discriminate subtle differences in spectral features, thus providing a means of classifying different OOI.

8.6.4 Radiometric Resolution

The bit per pixel (= bit depth) denotes the number of digital levels determining the radiometric precision of the measurement (giving the dynamic range). A major advantage of higher bit rates is the ability to sample a greater range of intensity. More bits provide a given image with better exposure control and color intensity dynamics. A large dynamic range is especially important for marine targets, which include both bright and very dark targets. However, greater radiometric resolution results in larger data files, which can be difficult to process and manipulate with standard computer systems (Johnsen, et al., 2013).

8.6.5 Temporal Resolution

A UHI is not limited by orbital constraints, light, or cloud/ice cover, and can be deployed with a temporal frequency that is required for the question under investigation. The temporal resolution necessary for mineral mapping, for example, is far less than that required for algal distributions that can vary at daily to hourly time scales or even less. For a UHI sensor implemented on a given underwater platform, it is crucial to have high accuracy geolocalization to be able to re-visit a given site or OOI. Because of this, an ROV or AUV needs to use a dynamic position system to monitor and re-visit large areas and to give detailed time-series of habitat development.

8.6.6 UHI on Different Underwater Platforms

8.6.6.1 *UHI on Remotely Operated Vehicle*

An advantage of using an ROV as a UHI platform is the on-line control of the instrument and collection of the data stream. Any problems with the acquired data can be diagnosed rapidly, and controls can be sent to the platform to adjust the settings on the instrument package. Because power is provided through the tether, there are virtually no constraints regarding the power payload. This is particularly important when conducting active imaging that requires external light sources. Many different lamps with high power usage can be considered for deployment with the UHI mounted on an ROV. Moreover, ancillary sensors to measure water column optical properties, colored dissolved organic matter and total

suspended matter measurements of the water column and acoustic sensors to map bathymetry (multibeam echo sounder) or bottom

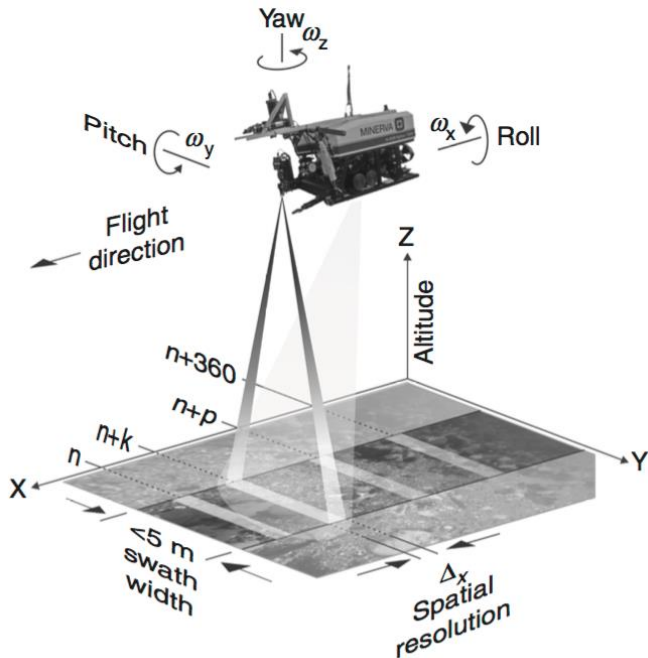


Figure 111 UHI deployed on ROV equipped with artificial light sources to illuminate OOI on seafloor (Johnsen, et al., 2013).

substrate (side scan sonar) can also be readily implemented on the package (Johnsen, et al., 2013). UHI deployed on an ROV is presented in Figure 11.

A major disadvantage of using ROVs for deployment of the sensor is that the tether, which is generally 500–1000 m long, limits the aerial coverage. In addition, considerable time and cost are associated with deploying a fully operational vessel to tether the ROV during the entire deployment time. From an operational perspective, the ROV contains external thruster motors that can interfere with imaging potential. For example, if the UHI is close to a soft-bottom seafloor (e.g., loose, unconsolidated sediments), the thrusters may suspend sediments and reduce image quality (Johnsen, et al., 2013).

8.6.6.2 UHI on Autonomous Underwater Vehicle

An AUV can either be a glider or propeller-driven system. Autonomous gliders change buoyancy internally and profile the water column by converting a fraction of their vertical motion into horizontal velocity. While useful for many oceanographic applications, gliders have very low power capacity and limited sustained sampling capabilities near the seafloor. As such, gliders are not ideal platforms for UHI and are not considered further here. Propeller-driven AUVs, in contrast, offer higher payloads than gliders and more systematic sampling capabilities that can be readily coupled with UHI. UHI deployed on an AUV is presented in Figure 12 (Johnsen, et al., 2013).

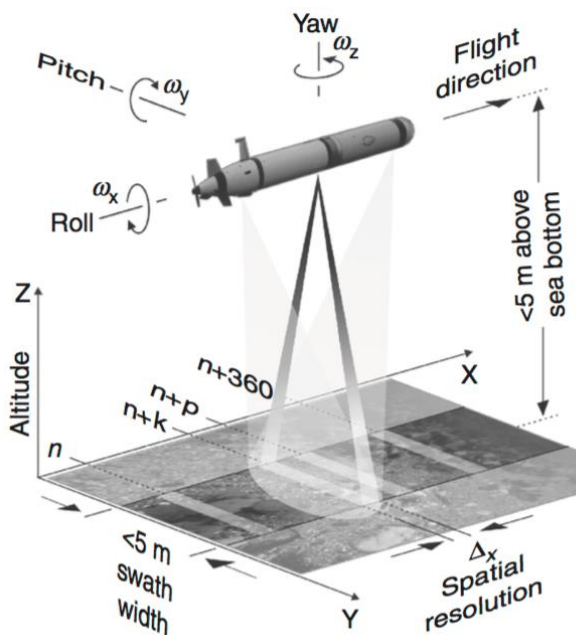


Figure 25: UHI deployed on AUV equipped with artificial light sources to illuminate OOI on seafloor (Johnsen, et al., 2013).

The AUV travels at speeds, typically between 1 and 5 knots, and samples over large distances without the constraints of a tether and ship-based crew. Propeller-driven AUVs are found in different sizes and range classes. Small AUVs are typically 1.5–2 m in length, about 20 cm diameter and weighing 40–100 kg with a range of 100 km with diving limits to 100–500 m depth. The small AUV system is hand deployable by two people from a small boat, requiring a lower operating cost compared to an ROV. Larger AUVs may be 3–5 m long, up to about 80 cm in diameter, weighing up to 900 kg, and can travel several hundred kilometers and to depths of 6000 m (e.g. REMUS 6000). With its high degree of speed/direction, altitude and pitch, roll, and yaw control, a large AUV may be the best

platform for UHI mapping over large areas of seafloor. Predefined flight patterns (i.e. horizontally, zigzag or terrain-following at predefined altitudes) are possible to achieve with high precision, as well as the possibility of adaptive sampling. Importantly, altitude control on AUVs makes mapping of the seafloor quite efficient (Johnsen, et al., 2013).

1 Bibliography

- Funk, C., Bryant, S., & Heckman, P. (1972). *Handbook of Underwater Imaging System Design*. Ocean Technology Department.
- Jaffe, J. S. (1990). *Computer Modeling and the Design of Optimal Underwater Imaging Systems*. IEEE JOURNAL OF OCEANIC ENGINEERING.
- Johnsen, G., Volent, Z., Dierssen, H., Pettersen, R., Van Ardelan, M., Søreide, F., et al. (2013). *Underwater Hyperspectral Imagery to Create Biogeochemical Maps of Seafloor Properties*. Woodhead Publishing Limited.
- Ludvigsen, M. (2010). *An ROV Toolbox for Optical and Acoustical Seabed Investigations*. Trondheim: Norwegian University of Science and Technology.
- Nornes, S. M., Ludvigsen, M., Ødegård, Ø., & Sørensen, A. (2015). *Underwater Photogrammetric Mapping of an Intact Standing Steel Wreck with ROV*. IFAC Workshop on Navigation, Guidance and Control of Underwater Vehicles.
- US Navy Office of Naval Research (ONR). (2014). *AUVSI Foundation and ONR Engineering Primer Document for RoboSub Competitions*.

1 Bibliography

- Bai, Y., & Bai, Q. (2012). *Subsea Engineering Handbook*. Gulf Professional Publishing.
- Chakrabarti, S. (2005). *Handbook of Offshore Engineering*. Elsevier Ltd.
- Hegrenæs, Ø., Sæbø, T. O., Hagen, P., & Jalving, B. (2010). *Horizontal Mapping Accuracy in Hydrographic AUV Surveys*.
- Lekkerkerk, H.-J., van der Velden, R., Roders, J., Haycock, T., de Vries, R., Jansen, P., et al. (2006). *Handbook of Offshore Surveying*. Clarkson Research Services Limited.
- SeaBeam Instruments . (2000). *Multibeam Sonar Theory of Operation*. Communications SeaBeam Instruments.

1 Bibliography

- Allmendinger, E. E. (1990). *Submersible Vehicle Systems Design*. Society of Naval Architects and Marine Engineers.
- Andresen, M., Ludvigsen, M., & Ødegaard, Ø. T. (2003). *Slepeforsøk av modell for å bestemme Cd -koeffisient*.
- Berg, T. E. (2014). *Marine Operations, Submarines, AUVs-UUVs and ROVs*. Department of Marine Technology.
- Christ, R. D., & Wernli Sr, R. L. (2007). *The ROV Manual: A User Guide for Observation-Class Remotely Operated Vehicles*. Oxford: Elsevier Ltd.
- Fossen, T. I. (2011). *Handbook of Marine Craft Hydrodynamics and Motion Control*. John Wiley & Sons Ltd.
- Griffiths, G. (2003). *Technology and Applications of Autonomous Underwater Vehicles*. London: Taylor & Francis.
- Hoerner, S. F. (1965). *Fluid-Dynamic Drag*.
- Ludvigsen, M. (2010). *An ROV toolbox for optical and acoustical seabed investigation*. Norwegian University of Science and Technology.
- Ludvigsen, M., & Ødegaard, Ø. T. (2003). *Slepeforsøk modell Cd-koeffisient i alle vinkler*.
- Ludvigsen, M., & Ødegaard, Ø. T. (2004). *Fullskala thrust-test av Minerva*.
- Ludvigsen, M., & Ødegaard, Ø. T. (2005). *Friprøveforsøk med ROV-thruster*.
- Ludvigsen, M., & Ødegaard, Ø. T. (2006). *Sammenfatning av hydrodynamiske forsøk med ROV-en Minerva*.
- Moore, S. W., Bohm, H., & Jensen, V. (2010). *Underwater Robotics Science, Design & Fabrication*. Monterey: Marine Advanced Technology Education (MATE) Center.

1 Bibliography

- Allmendinger, E. E. (1990). *Submersible vehicle systems design*. Society of Naval Architects and Marine Engineers.
- Bai, Y., & Bai, Q. (2010). *Subsea Engineering Handbook*. Oxford: Elsevier Inc.
- Christ, R. D., & Wernli Sr, R. L. (2007). *The ROV Manual: A User Guide for Observation-Class Remotely Operated Vehicles*. Oxford: Elsevier Inc.
- Hallset, J. O. (2006). *Artic Subsea Systems - IMR Tasks (WP1)*. Stavanger: Poseidon Group AS.
- IMCA. (2009). *Code of Practice for The Safe & Efficient Operation of Remotely Operated Vehicles*. IMCA.
- Ludvigsen, M. (2010). *Axiomatic Design*.
- More, S. W., Bohm, H., & Jensen, V. (2010). *Underwater Robotics Science, Design & Fabrication*. Monterey: Marine Advances Technology Education (MATE) Center.
- NORSOK . (2016). *U-102 Remotely operated vehicle (ROV) service*. Norsk Standard.
- Seto, M. L. (2013). *Marine Robot Autonomy*. New York: Springer.

Unmanned Vehicle Systems International (AUVSI) Foundation & US Navy Office of Naval Research (ONR) . (2014). *Engineering Primer Document for RoboSub Competitions* . AUVSI Foundation and ONR .

9 References

- Fossen, T. I. (2011). *Handbook of Marine Craft Hydrodynamics and Motion Control*. John Wiley & Sons Ltd.
- Jalving, B. (2007). *Depth Accuracy in Seabed Mapping with Underwater Vehicles*. Kjeller: Norwegian Defence Research Establishment (FFI).
- Kongsberg. (2014). Acoustic underwater positioning and navigation system HiPAP and HPR. Retrieved 16.07.2015:
<http://www.km.kongsberg.com/ks/web/nokbg0240.nsf/AllWeb/FF57C18363FAD917C1256A7E002B9F2F?OpenDocument>.
- Lekkerkerk, H.-J., van der Velden, R., Haycock, T., & Jansen, P. (2006). *Handbook of offshore surveying: Vol. 1 : Preparation & positioning*. London: Clarkson Research Services Limited.
- Ludvigsen, M. (2010). *An ROV toolbox for optical and acoustical seabed investigations (Vol. 2010:74)*. Trondheim: Norges teknisk naturvitenskaplige universitet.
- Milne, P. (1983). *Underwater acoustic positioning systems*. London: Spon.
- Paull, L., Saeedi, S., Seto, M., & Li, H. (2014). *AUV Navigation and Localization: A Review* *Oceanic Engineering, IEEE Journal of*, 39(1), 131-149. doi: 10.1109/JOE.2013.2278891.

- ALM Oceanographic. (u.d.). Multibeam System Overview. Retrieved 25.06.2015:
<http://www.amloceanographic.com/CTD-Sound-Velocity-Environmental-Instrumentation-Home/Multibeam-Overview>.
- Brechovskich, L. M. (2003). *Fundamentals of ocean acoustic*. New York: AIP Press.
- Diner, N. M. (n.d.). *Theory of Fish Detection. Fishing vessel Technology - 20th Graduate School Module 2 - Fishing Gear and Other Equipment*. French Research Institute for Exploration of the Sea.
- Hovem, J. (2012). *Marine Acoustics - The Physics of Sound in Underwater Environments*. Los Altos Hills, California: Peninsula Publishing.
- Jalving, B. (2007). *Depth Accuracy in Seabed Mapping with Underwater Vehicles*. Kjeller: Norwegian Defence Research Establishment (FFI).

- Kongsberg. (2014). GeoChirp 3D - high resolution sub-bottom profiler. Retrieved: 19.06.2015:
<http://www.km.kongsberg.com/ks/web/nokbg0240.nsf/AllWeb/E0788FD1BE34357FC1257C93004ABB49?OpenDocument>.
- Lekkerkerk, H.-J., van der Velden, R., Roders, J., Haycock, T., de Vries, R., Jansen, P., & Beemster, C. (2006). *Handbook of Offshore Surveying*. Clarkson Research Services Limited.
- Lurton, X. (2002). *An introduction to underwater acoustics: principles and applications*. London: Springer.
- Mazel, C. (1985). *Side Scan Sonar: Record Interpretation ; Training Manual*. Klein Associates Inc.
- RD Instruments. (1996). *Principle of Operation*. San Diego: RD Instruments.
- University of Southampton. (2011). Marine Seismic Reflection. Retrieved 01.07.2015:
<http://www.soes.soton.ac.uk/research/groups/3dchirp/background.htm>.
- Allmendinger, E. E. (1990). *Submersible vehicle systems design*. Jersey City, N.J.: Society of Naval Architects and Marine Engineers.
- AML Oceanographic. (2015). Multibeam System Overview. Retrieved from
<http://www.amloceanographic.com/CTD-Sound-Velocity-Environmental-Instrumentation-Home/Multibeam-Overview>
- Brechovskich, L. M., & Lysanov, J. (2003). *Fundamentals of ocean acoustics*. New York: AIP Press.
- Diner, N., Mr. . *Theory of Fish Detection*. Fishing Vessel Technology - 20th Graduate School Module 2 - Fishing Gear and Other Equipment. French Research Institute for Exploitation of the Sea.
- Funk, C. J., Bryant, S. B., Heckman, P. J., & Department, N. U. C. O. T. (1972). *Handbook of Underwater Imaging System Design*: Ocean Technology Department, Naval Undersea Center.
- Hovem, J. M. (2012). *Marine acoustics: the physics of sound in underwater environments*. Los Altos Hills, Calif.: Peninsula Publishing.
- Karlsen, L., Hamre, J., & Gjøsæter, H. (2001). *Fiskeriteknologi*. [Oslo]: Landbruksforl.
- Kongsberg. (2014). GeoChirp 3D - high resolution sub-bottom profiler. Retrieved from
<http://www.km.kongsberg.com/ks/web/nokbg0240.nsf/AllWeb/E0788FD1BE34357FC1257C93004ABB49?OpenDocument>
- Lurton, X. (2002). *An introduction to underwater acoustics: principles and applications*. London: Springer.
- Mazel, C. (1985). *Side Scan Sonar: Record Interpretation ; Training Manual*: Klein Associates Inc.
- National Snow & Ice Center. (2013). Factors Affecting Arctic Weather and Climate. Retrieved from
https://nsidc.org/cryosphere/arctic-meteorology/factors_affecting_climate_weather.html
- Unesco. (1989). *Unesco Technical Papers in Marine Science*: Division of Marine Sciences, UNESCO.
- Unesco. (1994). *Unesco Technical Papers in Marine Science*: Division of Marine Sciences, UNESCO.
- University of Southampton. (2011). Marine Seismic Reflection. Retrieved from
<http://www.soes.soton.ac.uk/research/groups/3dchirp/background.htm>
- Valiron, F. (2001). *Descriptive Physical Oceanography*: Taylor & Francis.